NOVEL APPROACHES TO THE MEASUREMENT OF COMPLEX ATMOSPHERIC VOC MIXTURES USING PROTON TRANSFER REACTION MASS SPECTROMETRY

by

DANIEL JOHN BLENKHORN

A thesis submitted to the University of Birmingham for the degree of

DOCTOR OF PHILOSOPHY

School of Geography, Earth and Environmental Sciences

College of Life and Environmental Sciences

University of Birmingham

May 2018

Abstract

Proton Transfer Reaction – Mass Spectrometry (PTR-MS) is a soft chemical ionisation mass spectrometry technique frequently applied to measurement of volatile organic compound (VOC) abundance.

The overarching aim of this thesis is to improve the quantification of compounds that have proved difficult or even impossible to separate or to quantify, through advanced understanding of the detection and ionisation mechanisms and developments in the instrumental design and operation of PTR-MS for deconvolution of mixtures.

A new method for the preparation and use of diffusion tube methods as gas standards is reported. Detailed investigation of the ion-molecule reactions with chloroalkanes, chloroalkenes and other atmospherically important molecules, such as isoprene / 2-methyl-3-buten-2-ol, benzene / ethylbenzene / *o,m,p*-xylene and methyl vinyl ketone / methacrolein were undertaken to determine the ion-molecule reaction mechanisms, allowing quantification of isomeric species through understanding of the reaction products and novel approaches to the switching of the reduced electric field strength (E/n).

The modification of instrumental parameters of PTR-MS were investigated further for the quantification of semi volatile compounds (SVOCs) and more specifically, polycyclic aromatic hydrocarbons (PAHs). Use of a radio frequency (RF) ion

funnel and high temperature instrumentation allowed for sub nanogram limits of detection for many PAHs, including Benzo[a]pyrene.

Acknowledgements

Although my name is on this thesis, without the help, support and encouragement from many colleagues, friends and family, this work wouldn't have been possible.

First and foremost, I would like to thank my supervisors, Bill Bloss, Chris Mayhew and Rob MacKenzie. In addition to the opportunity to study for a PhD, they provided support, encouragement and several laboratories to work on ideas and interesting science for 4 years. Managing the ideas and expectations of 3 supervisors was challenging, but after 4 years I got the hang of it! They have each contributed significantly to my development as a researcher for which I am grateful. Without a grant from funding organisations NERC and ATCF, this work would not have been explored.

I have been lucky enough to be part of several research groups at the University of Birmingham. I have to thank Raquel, Ramon, Prema, David, David and Peter Watts from the molecular physics group for putting up with me every day for 4 years! I'm incredibly proud of what we have collectively achieved as a research group and was lucky enough to make some great friends. A special mention goes to John Thompson for his advice and collaboration, his reassurance and insightful knowledge of so many areas of science proved invaluable to myself and the group. In the geography research group, I would like to pay particular thanks to Leigh, Louisa and Roberto for their help, support, practical experience and willingness to lend a hand whenever asked.

During my PhD, the opportunity to apply for money to develop industrial links came about through NERC, which allowed me to take a brief pause from my PhD in order to pursue interesting academic and industrial problems, working as a researcher at Kore Technology for 6 fantastic months. This would not have been possible without the support and guidance from Fraser Reich, to whom I am eternally grateful. Whilst at Kore I was made to feel part of the team straight away, and I have to thank Fraser, Barrie, Steve, Dave, Clive, David, Renaud, Jack, Caroline, Toby, Colin and Rachel for their companionship and advice. I learnt something interesting and unique from every member of the team and hopefully we will have many successful years together.

My family have continually supported me in my academic studies and I wouldn't be studying for a PhD if it wasn't for the support of my parents Keith and Julie along with Ross, Emma, Mary and Pauline.

Many of my friends have also studied for a PhD and have given me great advice and support. I would like to thank Rich, Goo, Tom, Sam, Lynch, Forster, Greg and Sarah.

Last but not least, I would like to show my appreciation to my fiancé Charley who supported me through the highs and lows of a PhD, including the internship when I moved away for 6 months! Without her unwavering support, I wouldn't have been able to produce this thesis.

Table of Contents

Table of Figures

Table of Tables

Abbreviations

APCI – Atmospheric Pressure Chemical Ionisation

CI – Chemical Ionisation

EI – Electron Ionisation

eV – Electron Volt

FFR – Field Free Region

FWHM – Full Width Half Maximum (resolution)

Inter – Intermediate electrode

IMS- Ion mobility spectrometry

PTR-MS – Proton Transfer Reaction – Mass Spectrometer

SCIMS – Soft Chemical Ionisation Mass Spectrometry

SD – Source Drift

SIFDT – Selected Ion Flow Drift Tube

SIFT – Selected Ion Flow Tube

SVOC – Semi volatile organic compound

STP – Standard temperature and pressure (273.15K and 101.325KPa)

Td – Townsend (unit)

TDC – Time to Digital Converter

ToF – Time of Flight

VOC – Volatile organic compound

1 - Introduction

1.1 Background

The detection and quantification of trace levels of volatile organic compounds (VOCs) in the atmosphere is a complex issue and many different instrumental approaches and methodologies have been developed with the aim of quantifying trace VOCs (in this context, VOCs at parts per billion (ppb, i.e. molecules of VOC per 10^9 molecules of air) and parts per trillion (ppt i.e. molecules of VOC per 10^{12} molecules of air) level). The aim is to have a sensitive instrument capable of measuring at the ppb and ppt level, which is selective enough to provide positive identification of important VOCs with a time resolution that can resolve biological, chemical and physical drivers of change in VOC mixing ratios.

The time resolution of an instrument is of importance for measurement of VOCs in rapidly changing environments, such as field sites where meteorological conditions can influence the transport of VOCs from sources and where sources of VOCs can physically move, such as vehicles. This is also important for measurement of VOCs that have a short atmospheric lifetime.

Mass spectrometric techniques have become commonly used for the measurement of ambient air for their rapid measurement capability and the ability to provide identification based on the mass of the compound. However, complex systems will produce a large number of peaks, confusing the situation and complicating the analysis. Furthermore, purely mass spectrometric techniques

have limited success in differentiating isomers or isobaric compounds (i.e. compounds having the same exact mass or same nominal (whole number) molecular mass), as they appear at the same nominal mass in a spectrum and dependant on the mass difference of the compounds may contribute to a single peak, partially resolved or completely resolved peaks, representing multiple compounds. The increase in mass resolution provided by time of flight mass spectrometers has assisted in the separation of isobars, but isomer separation continues to be an issue, as shown in figure 1.

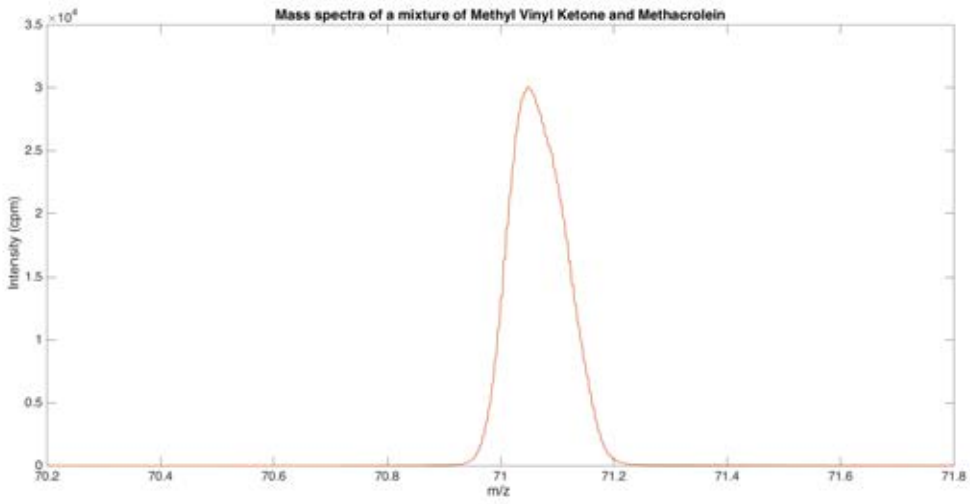

Figure 1 - PTR-MS mass spectrum showing a peak at 71.04 Da, corresponding to the ion $C_4H_7O^+$ produced by Methyl Vinyl Ketone and Methacrolein.

The alternative to mass spectrometry alone is to attach a hyphenated separation technique which has the capability of both isomer and isobar separation before the mass spectrometric analysis. Gas chromatography (GC) is a commonly used separation technique for gas phase molecules, physically separating compounds by their differential adsorption to a coated capillary column (figure 2). The capillary

column can be coated with a different polarity stationary phases which provide better separation for different types of molecules where a mobile phase of helium is often used. GC is commonly coupled to a mass spectrometer to give a retention time and mass spectrum for each eluted peak. This can be considered a ‘gold standard’ analysis, with many standard methods and conditions available to separate isomers and compounds, which can then be quantified from a single sample. For many environmental and industrial mixtures, a single GC separation before MS detection is not sufficient to resolve the mixture, so techniques involving multiple chromatographic steps have been developed, e.g GCxGC-MS [1].

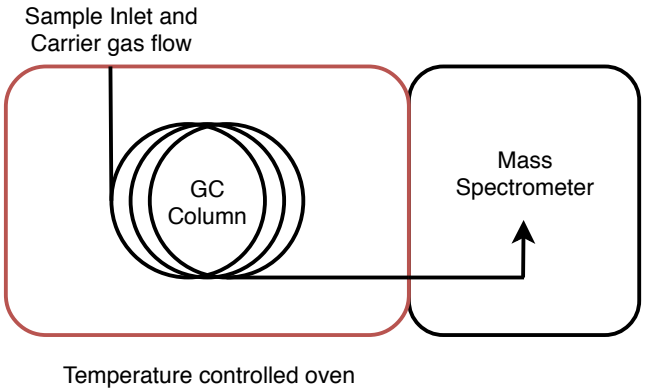

Figure 2 - Schematic of a typical GC-MS setup.

The drawback with GC-MS is that the technique is a non-real-time method. The sample often has to be desorbed onto a trap (which adsorbs VOCs) as a method of preconcentration before being transferred to the GC-MS where the contents of the trap can be desorbed onto the column. The time resolution of a measurement is also poor due to the time needed for chromatographic separation, with a typical GC-MS acquisition taking 30-40 minutes.

Because pre-concentration is often not necessary and transit times for analytes through the instrument to the detector are often of the order of 100 milliseconds, Proton Transfer Reaction – Mass Spectrometry (PTR-MS) provides real-time quantification of VOCs at the ppb/ppt level but suffers from the lack of a separation step that allows isomers to be resolved. As a result of this, PTR-MS and GC-MS are used extensively together to provide complementary analysis with PTR-MS providing the real-time, high time resolution measurement whilst GC-MS can quantify mixtures of isomers.

1.2 VOCs in atmospheric chemistry

VOCs play an important role in the composition of the troposphere [2] and understanding the sources and mixing ratios of these VOCs is imperative in determining the processes which release and consume VOCs. A challenge for atmospheric chemists is to quantify more accurately the compounds that are present in order to constrain emission sources for use in global emissions inventories [3, 4], to determine how the emissions of VOCs are changing in a more polluted and changing atmosphere, and to provide data for use in atmospheric chemical models [5-7]. Atmospheric chemical models rely on the ability to use source emission data as an input to chemical models. With changing land use and transport, VOCs may be detected far from the source.

VOCs can be categorised in the broadest sense by their origin, either emission from living organisms, i.e. biogenic, or as a result of human activity or production,

i.e. anthropogenic. Some general characteristics of biogenic and anthropogenic VOC emissions are given in sections 1.2.1 and 1.2.2. Compounds can be emitted by both biogenic and anthropogenic sources and in this case, they are usually described by the specific VOC emission source.

VOCs are reactive in the atmosphere, undergoing removal via chemical oxidants (primarily with OH radicals and (in the case of alkenes) tropospheric ozone during the day, and nitrate radicals (NO_3) during the night). Primary VOCs, emitted from biogenic and anthropogenic sources, can react in the atmosphere to form secondary products. The relative concentrations of secondary VOC products, combined with knowledge of the atmospheric reactivity and hence corresponding atmospheric lifetimes of their parent species are important for determining the sources, sinks and transport of VOCs. Many VOCs have atmospheric lifetimes on the order of hours to days in the presence of OH radicals, some examples are shown in table 1 [3].

Table 1 - Atmospheric lifetime of VOCs with respect to attack by OH radicals at a concentration of 1.6 x 10^6 molecule cm^{-3}. Data taken from ref [8]

VOC	**Atmospheric Lifetime**
Methane	3 years
2-Methyl-2-butene	2 hours
Isoprene	1.7 hours
Benzene	5.7 days
Toluene	1.2 days

VOCs are also involved in many other atmospheric processes including tropospheric ozone formation, semi volatile organic compound (SVOC) formation and secondary organic aerosol formation.

The formation of tropospheric ozone occurs through radical cycles initiated the reactions of VOCs with (usually) the OH radical. The resulting hydro and organic peroxy radicals can be interconverted by reaction of NO, forming NO_2, which can then be photolyzed to form NO and atomic oxygen. Atomic oxygen and O_2 then react rapidly in the troposphere to form ozone.

1.2.1 Biogenic VOC sources

Many thousands of different primary VOCs are released into the atmosphere from biogenic sources [9] and orders of magnitude more secondary compounds are produced from atmospheric chemical reactions [8]. The dominant biogenic VOC emission is the molecule isoprene (C_5H_8), a hemiterpene produced and emitted predominantly by trees. Isoprene is estimated to account for around 44% of the global biogenic non methane VOC emission, which equates to over 500Tg/year [3]. Isoprene is synthesised and released promptly by plants and trees [2, 10, 11]. Other classes of commonly released biogenic VOCs include monoterpenes ($C_{10}H_{16}$) and sesquiterpenes ($C_{15}H_{24}$), which comprise of different structural arrangements of 2 and 3 isoprene units respectively [8].

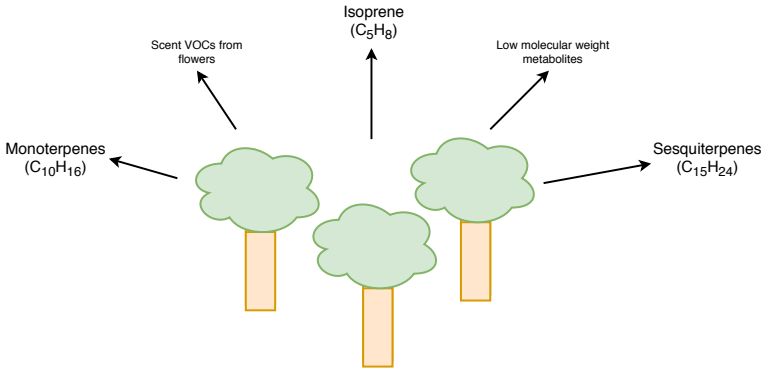

Figure 3 – Schematic of some common VOCs emitted from plants and trees

In addition to hydrocarbon-based VOCs, many oxygenated VOCs (OVOCs) are emitted into the troposphere from biogenic sources, evaporation of oxygen containing solvents and are also produced in the atmosphere as a result of oxidation [12]. The most common OVOCs in the atmosphere are alcohols, ketones and aldehydes, such as methanol, ethanol, acetone, acetaldehyde [13]. Oxidation of primary hydrocarbons, by H abstraction reaction with OH, followed by O_2 addition also leads to the formation of OVOCs as secondary species in the atmosphere.

The activity and reactivity of these compounds is important for atmospheric processes involving radical reactions and the cyclic processes that control and initiate them [14, 15].

1.2.2 Anthropogenic VOC sources

All anthropogenic VOC production relates ultimately to fossil fuel use and land use change. A wide range of human activity is subsequently responsible for the emission of anthropogenic VOCs into the atmosphere. VOCs can be emitted as by-products of combustion, produced as intermediates in the synthesis of consumer products, solvent use or due to land use change as a result of human interference. Individual anthropogenic VOC compounds may pose specific environmental and/or human health problems. Halogenated compounds can contribute to the depletion of stratospheric ozone [16]. Other aromatic compounds are persistent in the environment, accumulate in fatty tissue of top predator animals and cause immediate health effects by inhalation or absorption [17].

VOCs are volatile – they have vapour pressures that mean they exist exclusively in the gas phase in the atmosphere and are defined by the EU as organic compounds with a boiling point < 250 °C at standard pressure (101.3 kPa) [18]. In addition to VOCs, there are also semi volatile organic compounds (SVOCs), which are defined as compounds that elute after n-hexadecane in a 100% non-polar GC column [19, 20]. More commonly the definition is usually taken to mean a compound with a high molecular weight and boiling point such that it has a low vapour pressure at room temperature, resulting in partitioning between gas and particle phase in the atmosphere. Although SVOCs are less volatile than VOCs, they can be transported in the gas phase by the atmospheric and climatic conditions leading to inhalation by humans far from the source [21]. SVOCs therefore can be responsible for many adverse health effects [22, 23].

1.3 Measurement of VOCs using Proton Transfer Reaction – Mass Spectrometry

Many atmospheric research groups have employed PTR-MS as a technique for measuring VOCs, with several comprehensive reviews published, e.g. Lindinger et al [24], Blake et al [25] and as comprehensively summarised in a book by Ellis and Mayhew [26]. Laboratory based studies make up the bulk of the literature on the use of PTR-MS and range from sensitivity and compound detection advances [27] to the detection of compounds for the measurement of OH reactivity [28]. Several years after development of the PTR-MS, researchers started deployment of the PTR-MS to more challenging environments, such as forests [29-31], on board research ships [32-34] and research aircraft [35-38].

1.3.1 Isomer quantification

An issue with the detection of VOCs with PTR-MS alone is the inability to quantify isomers, which is practically overcome in the field by use of a complimentary technique with a chromatographic separation, such as GC-MS. In addition to this, under conditions where fragmentation is promoted, fragment ions can be formed that may be misinterpreted as other protonated parent molecules. This is the case for ethyl benzene (m/z 107) which can fragment to form an ion at m/z 79, which is the ion commonly used for quantification of benzene in PTR-MS. This causes issues when trying to calculate the concentration of the molecule in the sample gas. This problem has been identified by Rogers et al [39] who proposed a simple algorithm to correct benzene overestimation during a field campaign, however this

only provided a simple correction applicable for a specific set of conditions to the quantification of benzene.

The motivation for quantification of these compounds is that many VOC isomers have different atmospheric lifetimes and reaction products. Understanding the composition of a mixture of isomers (both in a controlled sample and real air), the quantity and atmospheric fate of these compounds is important to understand atmospheric processes.

Recent attempts have been made to interface fast GC systems with PTR-MS in order to provide basic separation for targeted isomers such as monoterpenes and have demonstrated limited success [40, 41]. Fast GC systems have to have either a shorter length or wider bore capillary GC column than traditional GC-MS systems in order to provide quick separation and a high time resolution measurement. In turn, this decreases the range of compounds for which this can be useful as the chromatographic separation is less comprehensive. In order to provide separation for different sets of isomers or multiple target compounds, more research needs to be done to optimise GC conditions including column selection and temperature control.

1.4 Measurement of SVOCs using Proton Transfer Reaction – Mass Spectrometry

As PTR-MS has shown its value in the measurement of VOCs, attention has also turned to the detection of less volatile compounds, both in the context of environmentally important molecules and security applications for fast, real time, positive identification [42]. Semi volatile organic compounds (SVOCs) are compounds that have a lower vapour pressures than VOCs and therefore mostly exist as a solid or condensed liquid (such as a droplet or aerosol) at room temperature. The equilibrium between the solid/liquid and vapour phase depends on the vapour pressure of a compound. For SVOCs, the vapour pressures are low and therefore increased temperatures are needed to shift the equilibrium to favour the vapour phase. This is essential for gas phase analysis, as a requirement is for the compound to be mostly partitioned in the vapour phase for efficient transport to the mass analyser (by reducing the adsorption onto the instrument surfaces). Without efficient transfer of the SVOCs to the mass analyser, adsorption on inlet lines and memory effects (observed as tailing of a peak or inefficient thermal desorption) will dominate and interfere in the analysis. Despite this, some higher volatility SVOCs are able to be detected by a PTR-MS at modest temperatures (≈100°C), such as naphthalene [43]. However, many SVOCs have much lower vapour pressures than naphthalene and for analysis of these compounds, a heated inlet and drift tube system is required to increase the proportion of the SVOCs in the vapour phase.

As SVOCs have lower vapour pressures than VOCs, they are more difficult to transport in the gas phase at atmospheric pressure. In order to measure these compounds, it is necessary to operate sections of instrumentation and analyte transfer lines at a higher temperature where the vapour pressure is comparable to the measurement of a VOC at modest temperatures. Significant modifications to instrumentation are required to allow for high temperature operation and these can be expensive and require regular maintenance. Commercial PTR-MS instruments are available which are configured to introduce semi volatile analytes into the mass spectrometer at high temperatures (up to 200°C) with the use of a high temperature oven and transfer line, allowing rapid measurement with minimal memory effects [42]. This allows a range of desorbers to be attached to the high temperature inlet, capable of heating swabs (of those types commonly used in security applications), desorption tubes and Solid Phase Micro Extraction (SPME) fibres to temperatures over 200°C.

The benefit of being able to measure both VOCs and SVOCs with the same instrument is seen in the initial capital cost saving, flexibility and high time resolution measurements, giving researchers the ability to measure a wider range of compounds with a single mass spectrometer.

1.5 Aims and Thesis outline

The thesis is broadly split in to 4 experimental sections, which aim to enhance the capability of PTR-MS by investigation of the ionisation, detection and quantification of compounds not previously reported, including the quantification of isomers. After chapters 1 and 2, which introduce the requirement for understanding the ionisation mechanisms and introduction of the analytical instrument used for these studies (PTR-MS), 4 chapters of methodology and results follow.

Chapter 3 investigates the way in which gas standards can be produced and used for experimental work, including static and dynamic calibration. This work forms the basis of the experimental design which is then utilised in the subsequent experimental chapters (4,5 and 6), to provide accurate standards for determination of ion-molecule reaction products and instrumental sensitivity. Although the dynamic generation of VOC standards is common within the PTR-MS measurement community, an investigation into storage of oxygen sensitive VOC storage is novel to this work. The generation of SVOC standards has not previously been reported for calibration of PTR-MS instrumentation, so as a result, the secondary aim was to develop a method and calibration equipment suitable for the generation of dynamic SVOC standards.

In chapter 4 there is a discussion of the fundamental ion-molecule reactions that give rise to the detection of saturated and unsaturated chlorocarbons. Many of the organochlorides investigated may be present in the air and are contained within

the EPA gas standard, TO-14. This gives rise to significant commercial interest in order to provide instrumentation capable of accurately implementing the methodology for the detection and quantification of these compounds.

Previous studies using the related soft chemical ionisation instrumentation SIFT-MS determine that unsaturated chlorocarbons are observed using the hydronium ion at the protonated molecular ion [44]. The ionisation mechanisms discovered here give rise to a predictive mechanism of ionisation, which is supported by theoretical ion energetics calculations.

Chapter 5 is concerned with the experimental and data processing methods to aid in the quantification of isomeric mixtures without separation. This chapter focusses on atmospherically important compounds that are known to produce significant interferences when measured by PTR-MS, such as BTEX (Benzene, Toluene, Ethylbenzene and *o,m,p*-Xylene) and isoprene and 2-methyl-3-buten-2-ol. The aim is to develop methods for quantification of these compounds which produce significant interference in a PTR-MS mass spectrum.

In chapter 6, the high temperature PTR-MS system has been applied to the measurement of polycyclic aromatic hydrocarbons (PAHs), which are large SVOCs with predominantly anthropogenic sources and are often produced or emitted as by-products of incomplete combustion [45]. Their abundance may be of particular concern in developing and emerging economies, such as China, where large scale combustion of ‘dirty’ fuels produces large quantities of SVOCs [46].

The aim of these experiments was to analyse a range of common PAHs whilst optimising the PTR-MS parameters, including the use of the RF ion funnel to allow further sensitivity enhancements. The secondary aim was to use the SVOC standards produced in chapter 3 in order to assess the ability to use PTR-MS for on-line, real-time SVOC analysis.

Chapter 7 suggests further work, which would build upon the studies contained within this thesis, with a view from both an academic and commercial position.

2 - Proton Transfer Reaction – Mass Spectrometry (PTR-MS)

2.1 Introduction

Proton Transfer Reaction – Mass Spectrometry (PTR-MS) was developed by Werner Lindinger and colleagues at the Institute for Ion Physics in Innsbruck, Austria, in the early 1990's for the detection of VOCs [47]. Until then other techniques, such as Gas Chromatography - Mass Spectrometry (GC-MS) and Electron Impact - Mass Spectrometry (EI-MS) were commonly used for the measurement of VOCs. Selected Ion Flow Tube - Mass Spectrometry (SIFT-MS), which was mainly a research tool during the development of PTR-MS, was also used for the measurement of VOCs in research laboratories. However, each technique has limitations depending on the sample.

GC-MS is often described as the 'gold standard' for VOC analysis, due to good instrument sensitivity (ppb/ppt) and ability to separate and quantify isomers. A drawback to GC-MS is that it is not capable of real-time analysis with a typical measurement taking ≈30 minutes, needed for compound separation through a column. Another limitation of GC-MS is the requirement for significant sample preconcentration before desorption onto the chromatographic column. This leads to time averaged samples where a single sample can represent air that has been collected for 30 minutes or more. In addition, the column stationary phase, length, temperature and flow settings have to be optimised for specific compounds, although standard methods are available which specify column types, flows and

temperature settings.

SIFT instruments were first designed and reported by Adams and Smith at the University of Birmingham in 1976 for the study of ion-molecule reactions in order to determine collisional rate coefficients and product ions for specific ion-molecule reactions [48]. Since then, the SIFT has been commercialised and used in a variety of analytical applications for the detection of VOCs [49]. SIFT employs a mass filter, usually a quadrupole, to select the reagent ions used for chemical ionisation. This allows a high purity, but often a lower current (compared to PTR-MS) reagent ion beam to be used in the flow tube, where the analyte is ionised. The use of a flow tube, with no electric field strength, also means that reagent cluster ions are common which reduces the reagent ion signal further. This lower current ion beam reduces the sensitivity of the SIFT in comparison to other techniques, such as PTR-MS.

PTR-MS was developed as an analytical instrument to address and improve upon the limitations of SIFT and as a result provides real time, sensitive analysis with the ability to control fragmentation by the manipulation of the reduced electric field strength in the drift tube.

In 2002, Kore Technology developed and commercialised a Time of Flight (ToF) system to attach to a PTR drift tube developed by researchers at the University of Leicester [50]. Kore Technology have since designed and built full PTR-ToF-MS instruments and these were used for the experimental work presented in this

thesis. The following information, descriptions and schematics in the PTR-MS chapter will be applicable to the series 1 range of PTR-MS instruments that were used.

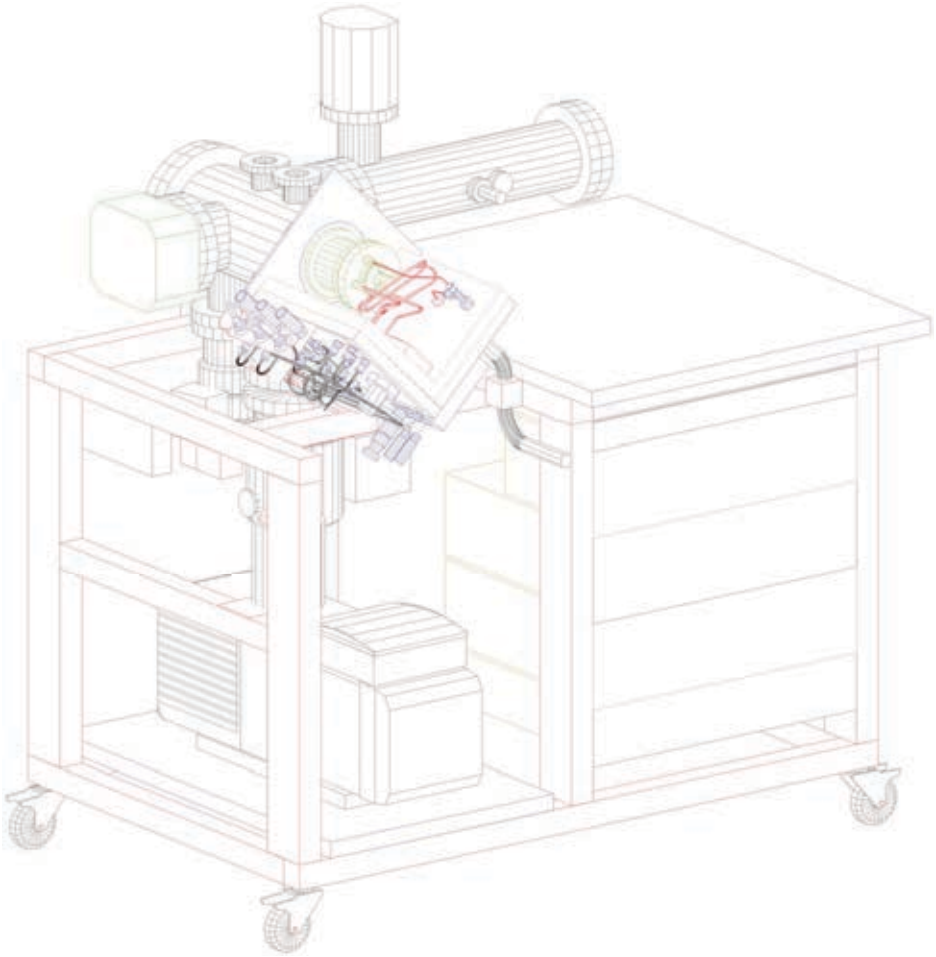

Figure 4 - 3D model of the PTR-MS instrumentation used in this thesis, reproduced with permission from Clive Corlett (Kore Technology Ltd).

A PTR-MS comprises of several main sections: an ion source for production of the reagent ions, a drift tube for the reaction of the reagent ions with the analyte gas containing VOCs, transfer optics for effective transmission of the ions from the drift tube into the mass selector, an ion detector and a pulse counting system. Each of these components of the PTR will be explained in depth in the following sections.

2.2 Principles of Ion chemistry

The most common form of ionisation in mass spectrometry is electron ionisation (EI), where the use of ≈ 70 eV electrons (usually produced as emission from a filament) collide with a molecule, ionising the molecule, resulting in a positive ion (equation 1).

$$e^- + M \rightarrow M^+ + 2e^- \quad (1)$$

Within this ionisation process, there is a significant amount of energy available, which often causes fragmentation of the ionised species. This of course is not desirable if the aim is to preserve the ionised species for identification and quantification e.g. within a complex mixture. Other ionisation mechanisms which reduce the energy difference involved in the ionisation process are required.

Chemical Ionisation (CI) is another common form of ionisation where an ionised chemical species is used to ionise an analyte molecule. There are several mechanisms of CI, which are shown in equations 2-5 [51].

$$XH^+ + M \rightarrow MH^+ + X \quad \text{Proton Transfer} \quad (2)$$

$$X^+ + M \rightarrow M^+ + X \quad \text{Charge Transfer} \quad (3)$$

$$X^+ + MH \rightarrow M^+ + HX \quad \text{Hydride Transfer} \quad (4)$$

$$X^+ + M + Z \rightarrow MX^+ + Z \quad \text{Adduct Formation} \quad (5)$$

The energy difference in these CI processes tends to be several eV rather than the 70eV in EI, which leads to considerably less fragmentation. Examples of some of the techniques that make use of CI include PTR-MS, SIFT-MS and atmospheric pressure chemical ionisation (APCI), where a solvent spray ion source produces the reagent ions. In PTR-MS and SIFT-MS, the reagent ion of choice is usually hydronium (H_3O^+), as it can easily be created from deionised water in a glow discharge ion source, producing a high purity reagent ion beam which can proton transfer to a range of VOCs (explained further in section 2.3.1).

2.3 Ion source

The ion source in most PTR-MS instruments is a hollow cathode glow discharge source, which produces reagent ions by applying an electrical potential between two electrodes, a hollow cathode and an anode, producing an electrical discharge which forms a self-sustaining plasma. The glow regions of the discharge are where excited neutral atoms decay, emitting photons that produce a visible glow [26, 52]. In the original instrumentation, radioactive ionisation sources were trialled, with alpha emitters such as ^{241}Am commonly used [50].

The glow discharge is formed by applying a DC electric current to a low-pressure gas between two electrodes, in the case of PTR-MS, an anode and a hollow cathode. Ions are formed initially by processes such as cosmic gamma ray absorption and thermal molecular collisions, which release an electron [26]. The electron migrates to the anode but because of the significant water vapour

pressure (1.3 mbar) in the hollow cathode, there is a low mean free path and the electron is likely to collide with water vapour molecules, ionising them in an EI mechanism, releasing an electron at each collision (equation 1). The propagation of this reaction forms a self-sustaining plasma, providing the voltage supplied between the cathode and anode does not fall below the breakdown voltage for the electrode spacing [52]. At voltages lower than the breakdown voltage, the gas/vapour is not electrically conductive and acts as an insulator. The breakdown voltage for a gas or vapour at a given pressure between electrodes of a certain spacing is determined by Paschens law and represented graphically as Paschen curves (figure 5) [53]. This determines the minimum voltage required to sustain a discharge in the ion source at a given pressure and distance between two electrodes. Paschen curves are available for most gases and vapours that are used in the PTR-MS ion source [54].

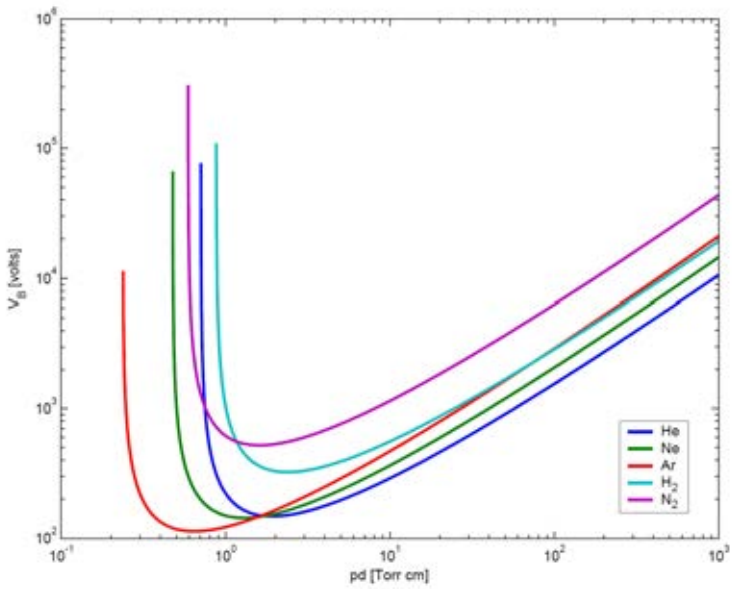

Figure 5 - Paschen curves for common gases in a glow discharge ion source [53]

The construction of the PTR-MS ion source consists of an anode and cathode, connected by a peek insulator and Viton o-rings. This gives a vacuum seal but provides electrical insulation between the anode and cathode. A high purity reagent ion feed gas is introduced whilst maintaining a low cathode pressure (≈1-2mbar), with a large voltage applied (up to 800 V).

Once a plasma has been started, typically a voltage difference of only 250-400V is required to maintain the glow discharge plasma.

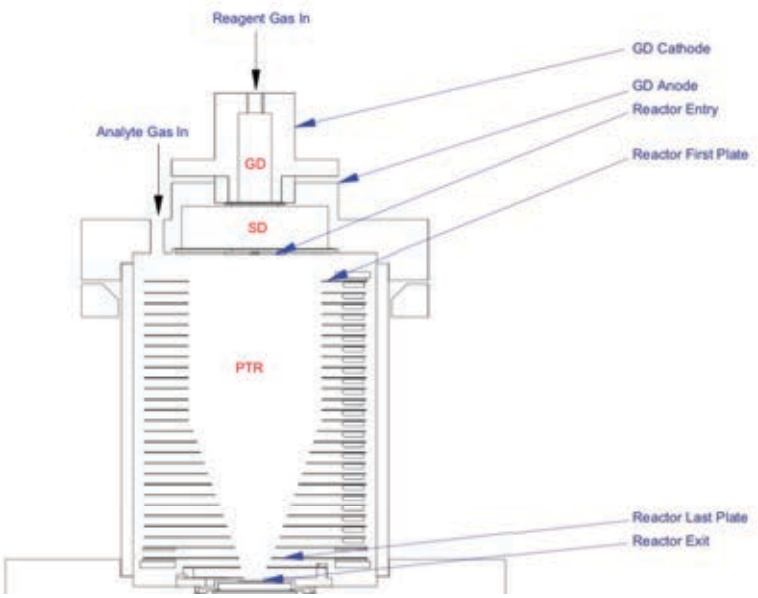

Figure 6 - Schematic of ion source assembly, reproduced with permission from Kore Technology, hardware reference manual z9831m1r0.

In the current generation of PTR-MS instrumentation, aluminium is used as the material for the anode and cathode. Along with the ability to easily machine the metal, aluminium forms a surface oxide (Al_2O_3), which has a high secondary electron emission coefficient, meaning that the incident collision of an ion or

electron with the metal oxide surface usually has enough energy to release secondary electrons and continue the propagation of the plasma [53]. The maximum secondary electron coefficient of aluminium oxide is 9, which means a maximum of 9 electrons can be released for every incident ion or electron collision, which allows the plasma to propagate efficiently once formed [55, 56].

2.3.1 Reagent Ions

Reagent ions are integral for effective soft ionisation of VOCs in a sample gas. In order to ensure that the VOC is ionised in such a way that the technique remains quantitative, the reagent ions must be in excess, not significantly depleted when the VOC-containing gas is measured and have the ability to ionise the sample by at least one of the CI processes in section 2.2.

2.3.1.1 Proton transfer

When using a PTR-MS with the aim of ionising by proton transfer, the reagent ion of choice is usually the hydronium ion, H_3O^+. This is created in the hollow cathode using water vapour as the feed gas and a high voltage discharge. The water vapour is supplied from a water bottle containing liquid water heated to 40°C. The water bottle is evacuated by the vacuum system to remove air and dissolved gases, leaving a pure water vapour at a pressure of 60mbar.

The initial step in the formation of the hydronium ion proceeds with electron impact of H_2O, leading to the formation of H_2O^+ and other fragment ions. H_2O^+ can then react further with water to produce H_3O^+ as shown in equation 6.

$$H_2O^+ + H_2O \rightarrow H_3O^+ + OH \qquad (k = 1.8 \times 10^{-9}\, cm^3\, s^{-1}) \qquad (6)$$

The fragment ions formed in the glow discharge can also be converted to hydronium by a fast reaction (often at the collisional rate), or formation of H_2O^+ which can react with water as shown in equations 7-12. Reaction rate coefficients for equations 6-12 taken from Ellis and Mayhew [26].

$$OH^+ + H_2O \rightarrow H_3O^+ + O \quad (k = 1.3 \times 10^{-9}\, cm^3\, s^{-1}) \qquad (7)$$

$$OH^+ + H_2O \rightarrow H_2O^+ + OH \quad (k = 1.8 \times 10^{-9}\, cm^3\, s^{-1}) \qquad (8)$$

$$O^+ + H_2O^+ \rightarrow H_2O^+ + O \quad (k = 2.6 \times 10^{-9}\, cm^3\, s^{-1}) \qquad (9)$$

$$H_2^+ + H_2O \rightarrow H_3O^+ + H \quad (k = 3.4 \times 10^{-9}\, cm^3\, s^{-1}) \qquad (10)$$

$$H_2^+ + H_2O \rightarrow H_2O^+ + H_2 \quad (k = 3.7 \times 10^{-9}\, cm^3\, s^{-1}) \qquad (11)$$

$$H^+ + H_2O \rightarrow H_2O^+ + H \quad (k = 8.2 \times 10^{-9}\, cm^3\, s^{-1}) \qquad (12)$$

The proton transfer from a hydronium ion to a VOC in the drift tube will efficiently occur during a collision if the proton affinity of the VOC molecule is higher than that of water (691 $\pm$ 3 kJ/mol). Most of the main constituents of air, nitrogen, oxygen and argon, have a lower proton affinity than water and therefore will not be ionised by the transfer of a proton from hydronium. This gives the advantage of removing the matrix effects when using air as the sample gas and only ionising

VOCs and compounds of interest, producing a much simpler mass spectrum. Some proton affinities of common gasses and VOCs are shown in table 1.

Table 2 - Proton affinity of common diatomic molecules and VOCs [57]

Molecule	**Proton affinity (kJ/mol)**
Oxygen	421
Nitrogen	494
Carbon dioxide	541
Water	691
Benzene	750
Ethylbenzene	788
p-Xylene	794
Water cluster ($H_3O^+.H_2O$)	808
Methacrolein	809
Acetone	812
Isoprene	826
Methyl Vinyl Ketone	835

In the case where low energy drift tube conditions, such as 80Td are used (see section 2.4.1 for a discussion of drift tube conditions), the hydronium ion can cluster to other neutral water molecules. The cluster ion ($H_3O^+.H_2O$) formed then has a higher affinity for the extra proton it has (808 $\pm$ 6 kJ/mol [58]) than

hydronium, reducing the variety of reactions that would result in a proton transfer from a cluster ion to a VOC. Multiple water cluster ions are possible with the formula $H_3O^+.(H_2O)_n$, however the ion source design and source drift voltage aim to minimise these clusters and maximise the hydronium reagent ion signal.

Other molecules have been used as proton transfer donors (discussed in next section), such as NH_4^+ [59, 60]. However, as yet these have found only niche applications for VOC ionisation and hydronium is most commonly used.

2.3.1.2 Alternate reagent ions

As the technique developed, researchers found that a variety of reagent ions can be created with commercial PTR-MS instruments using different reagent ion gases. However, in this case we should then refer to the technique as Soft Chemical Ionisation Mass Spectrometry (SCIMS) as the mode of chemical ionisation could be charge transfer rather than proton transfer. Many different reagent ions can be produced by using a different reagent ion gas, such as O_2^+ [60, 61] , NO^+ [60] and Kr^+ [62]. When using alternate reagent ions that do not have a proton to donate, the main mechanism of CI is charge transfer, which proceeds depending on the ionisation energy of the reagent ion and molecule.

2.3.2 Source Drift region

The source drift (SD) region is a section between the ion source and the drift tube, approximately 1 cm in length, where the purity of the reagent ion is increased through reactions to produce the terminal ion (equations 6-12). This is achieved through application of a voltage between the anode and the entry to the drift tube. The voltage difference between the anode and the drift tube entry (1st plate) is typically around 200 V, allowing the ions to be more efficiently extracted into the drift tube. The SD region also contains a SD electrode near the entry to the drift tube, which is set around 20 V higher than the collision energy voltage and acts as a 'funnel', preventing the analyte gas from back streaming into the glow discharge region (shown in figure 7).

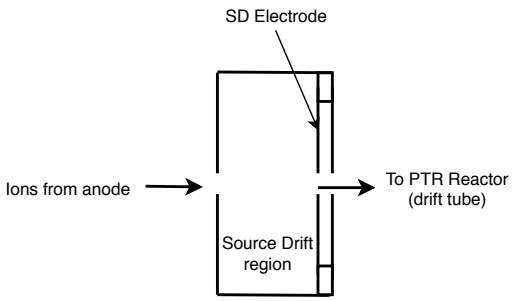

Figure 7 - Schematic representation of the source drift region in a PTR-MS

The analyte gas can often be air, which if allowed to backstream into the GD region can create ions such as O_2^+, NO^+ and N_2^+ (although N_2^+ rapidly charge exchanges to produce H_2O^+), which are undesirable when aiming to produce a high purity H_3O^+ reagent ion beam. The aim is to keep the O_2^+ count rate to less than 3% of the total reagent ion signal, which ensures a high purity hydronium

reagent ion beam. The SD electrode reduces the O_2^+ signal by around a factor of 4 and therefore helps to reduce back streaming.

2.4 Drift tube

The drift tube differs in design between PTR-MS instrumentation, however the basic principle is still the same. The idea is to apply an electric field of constant gradient along the length of the drift tube, from where the reagent ions and analyte gas enter, to the 400 μm orifice at the end where ions exit the drift tube.

The drift tube design used by Kore (and for all work contained within this thesis) is a reactor of 26 steel ring electrodes, connected to each other by way of a resistor chain, which are inserted into ceramic rods to give the reactor mechanical strength (figure 8). The reactor is mounted inside a glass drift tube, which is typically operated at 0.8-2 mbar, using push contacts to provide the electrical connections. The resistors are printed onto a ceramic plate that slots into a gap in the electrodes which allows each reactor plate to be supplied a voltage to give a constant reduced electric field along the reactor.

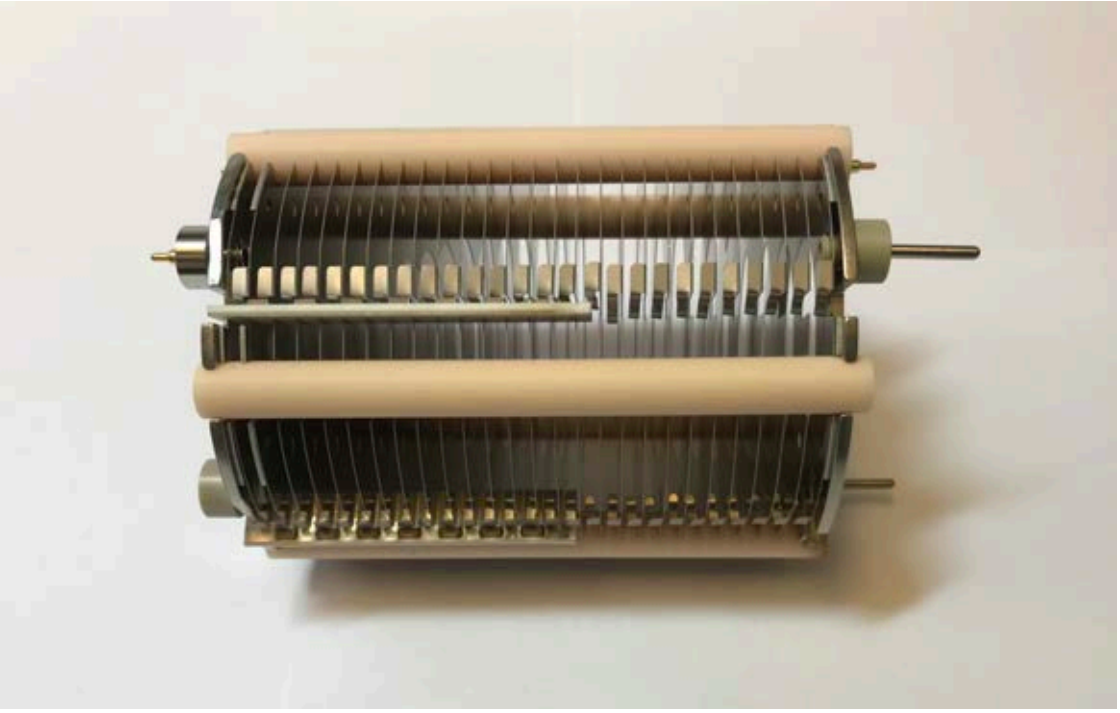

Figure 8 - Image of the PTR-MS reactor, taken from the drift tube of the PTR-MS used in this work. The electrode plates are inserted into the ceramic rods with resistors providing the electrical connection between the plates.

2.4.1 Reduced Electric Field - E/n

The reduced electric field, or more commonly referred to as E/n, is a ratio of the electric field applied (E) and the number density (n) of the gas in the drift tube. This ratio is crucial in PTR-MS to quantify the collisional energy of the ions with neutral species within the drift tube. The parameter E is simply calculated using equation 13.

$$\text{Electric field strength} = \frac{\text{Entry voltage} - \text{Exit voltage}}{\text{Length of drift tube}} \qquad (13)$$

The number density (n) can be calculated from the rearrangement of the ideal gas equation and a pressure and temperature measurement from the drift tube.

$$n = \frac{N_A}{V_M} \frac{273.15}{T_d} \frac{P_d}{101.325} \quad (14)$$

Where T_d is the temperature of the drift tube, P_d is the pressure in the drift tube, N_A is Avogadro's number and V_M is the volume of a mole of gas at STP (22.4 L). The reduced electric field is often for convenience referred to in units of Townsend (Td), where 1 Td = 10^{-17} V cm^2. A typical value used for the reduced electric field in a normal mode of operation for the PTR-MS may be 120-140 Td, but can often be in the range of 80-220Td dependent on the analysis. The reduced electric field strength in the drift tube can be changed through manipulation of the drift tube entry voltage (E) or the number density (n, drift tube pressure). The drift tube entry voltage is more convenient to change, with a quicker response time of < 0.1 seconds, compared to the drift tube pressure (> 10 seconds). Manipulating the electric field or switching between two different values may give more information about the compounds to be measured. This is further explored in chapter 5, during the investigations into the quantification of isomers without separation.

2.4.2 Ion Mobility in the drift tube

The ions in the drift tube (both reagent ions and ionised VOCs) are accelerated by the electric field applied through the ring electrode plates. At 1 mbar, the mean

free path is approximately 50 μm and as a result, multiple ion-molecule collisions occur as the ions move through the drift tube towards the most negative electrode (PTR exit = 3.8 V). This limits the maximum velocity of ions in the drift tube and a steady state velocity of the ions achieved. The drift velocity can be defined at low electric field strengths.

$$v_d = KE \tag{15}$$

Where v_d is the drift velocity and K is the ion mobility. The ion mobility K is dependent on many factors including the mass and structure of the ion, but also external factors such as temperature and pressure. For this reason, the reduced mobility (mobility for specific ion/molecule collisions) is used which refers to the value at STP and is given by.

$$K = \frac{760}{P}\frac{T}{273}K_O \tag{16}$$

The drift velocity can then be more accurately described using the reduced mobility term.

$$v_d = \frac{760}{P}\frac{T}{273}K_0E \tag{17}$$

The temperature and pressure term can be simplified by defining the number density N_0 at STP and reducing the pressure and temperature terms using N and N_0.

$$v_d = K_0 N_0 \frac{E}{N} \tag{18}$$

Equation 18 shows the drift velocity as a function of the reduced mobility, number density at STP, and the reduced electric field E/N parameter. Knowing the drift tube length, the drift time of an ion can be calculated for a specific temperature, pressure and reduced electric field.

$$t_d = \frac{L}{K_0 N_0} \frac{N}{E} \tag{19}$$

For an instrument which has a drift tube of length 9.7 cm and given an E/N of 140 Td, the drift time of a hydronium ion is t_d = 92 μs.

The drift time also has an effect on the sensitivity of instrument. The drift time is reduced at higher E/N as the ions have a higher average velocity and as a result, a shorter reaction time between reagent ions and VOCs, leading to a decrease in sensitivity.

2.4.3 RF Ion funnel drift tube

For some experiments detailed within this thesis, an upgraded instrument from Kore technology which features the radio frequency (RF) ion funnel system was used. Mechanically, the main modification from the standard drift tube is that ring electrodes in the second half of the ion funnel instrument have decreasing internal diameters, narrowing from 40 mm to 6 mm, giving the physical form of a funnel. The RF voltage is an oscillating voltage applied between pairs of alternating ring electrodes in the second half of the drift tube which have the decreasing internal diameter ring electrodes. Without the RF voltage applied, these plates provide the same electric field strength as a normal drift tube, allowing for normal direct current (DC) only operation.

When the ring electrodes in the second half of the drift tube are also supplied with an RF voltage in addition to the DC voltage that is normally applied during operation, ion funnelling takes effect. In this instrument, the RF voltage supplied to the ring electrodes has a peak-to-peak amplitude of 195 V at a 780 kHz frequency.

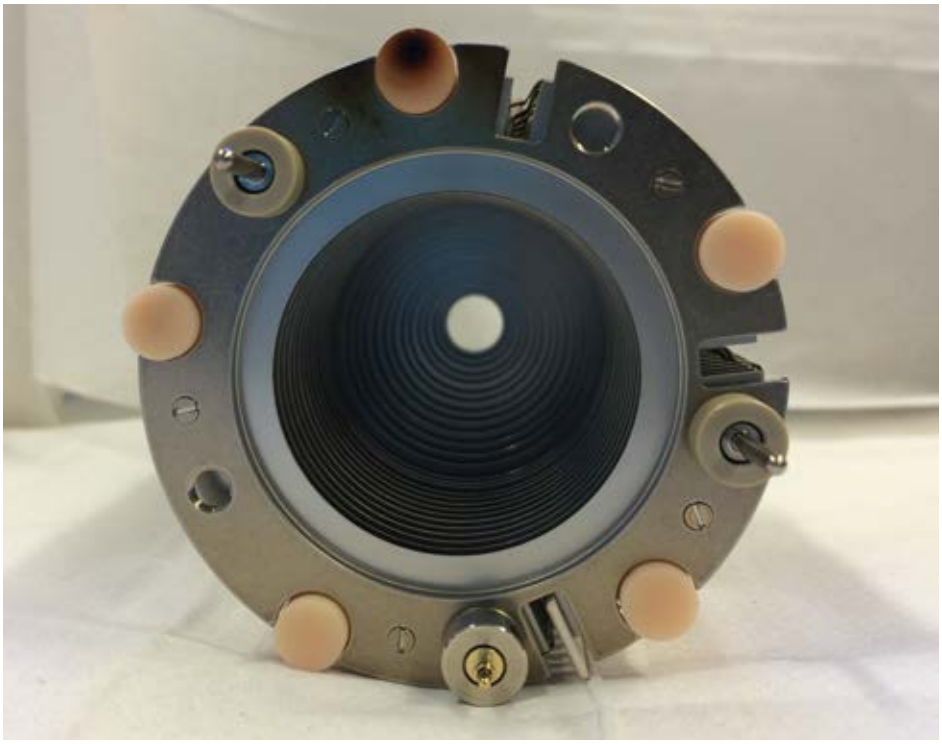

Figure 9 -An image showing the RF reactor (drift tube) used in this study, showing the decreasing internal diameter of the ring electrodes.

The effect of this RF voltage is that the ions are pushed towards the centre of the drift tube so that more ions are extracted through the exit aperture than in DC only operation. The RF field aims to overcome dispersion of ions in the drift tube through space charge effects and the result of Brownian motion of the ions as they collide with neutral molecules. This leads to an increase in the ion current leaving the drift tube and therefore an increase in sensitivity. To achieve the best sensitivity enhancement in the RF mode, the drift tube operating conditions have to be optimised. Typically for most VOCs, the best sensitivity is achieved when the drift tube pressure and voltage are reduced to 0.7-0.8 mbar and 70-100 V DC respectively (although actual instrument conditions will be detailed in each experimental chapter), where the reduced pressure and voltage allow VOC ions to penetrate deeper into the centre of the drift tube without collisions with neutral

molecules and therefore pass through the exit aperture. Sensitivity enhancements have been reported for this RF ion funnel design, with an increase of 1 or 2 orders of magnitude for some common VOCs [27]. In DC only operation, the optimum sensitivity for VOCs is 5 cps/ppb, however, using the RF ion funnel, the sensitivity is approximately 100 cps/ppb with a detection limit of <30ppt.

2.5 Ion optics

The ion optics in a PTR-MS have several functions and sit in the differential pumping region where the pressure is around 10^{-4} mbar, between the drift tube (≈1 mbar) and the time of flight mass analyser (≈10^{-7} mbar). The ion optical column is responsible for extracting the ions and producing a narrow ion beam, which can be 'sampled' by the extraction pulser of the time of flight (ToF) detector (explained in section 2.6). The narrow ion beam is generally achieved using a series of factory tuneable deflectors, which aim to steer the beam and allow it to pass into the ToF source perpendicular to the pulser plates.

The second function of the ion optics is to allow the ions to pass through the differential pumping region to the pulser region. The differential pumping region requires high capacity pumping from a 255 L s^{-1} turbomolecular pump backed with a rotary pump, to reduce the pressure in this region by 4-5 orders of magnitude. As a result of the pressure change, the flow changes from viscous flow in the drift tube to molecular flow in the transfer optics. The pressure decrease from drift tube

to time of flight detector is needed to keep the mean free path in the transfer optics and reflectron high to reduce ion scattering (explained further in 2.6). This requires the ions to be steered through a differential pumping aperture (1x4 mm slit) at the end of the ion optical column.

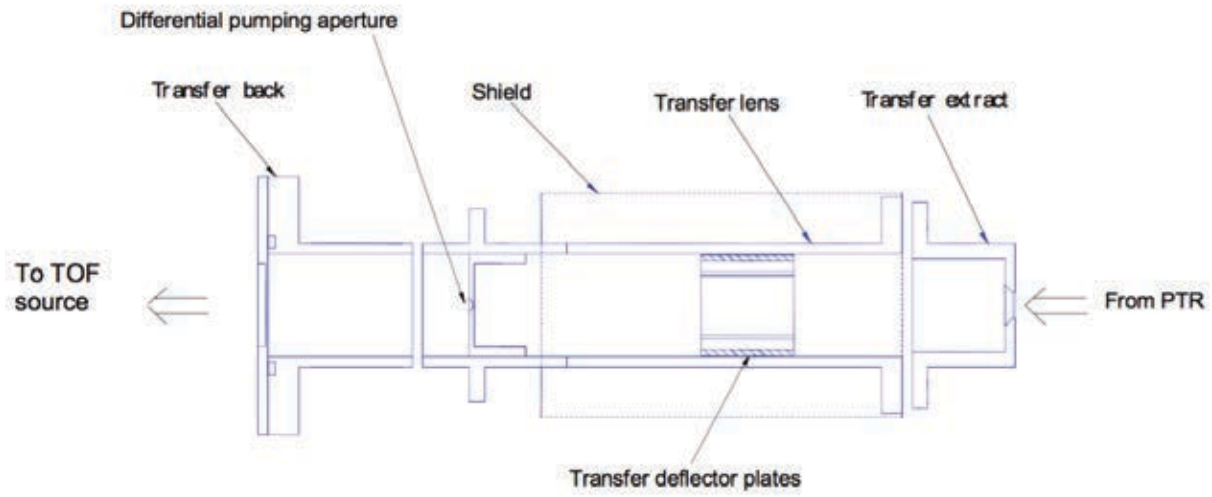

Figure 10 - Ion optics schematic (reproduced from Kore Technology Hardware reference z9831m1r0), showing the transfer lens electrodes that focus the ion beam.

2.6 Time of flight mass analyser

The time of flight (ToF) detector is a commonly used mass spectrometric analyser in many different mass spectrometric techniques. In more recent times, the ToF has been attached to PTR for the benefits of high mass resolution and ability to record a full spectrum without the need for a scanning mass analyser.

The ToF detector system comprises of 3 main parts:

1) Pulser unit – This is where a 'packet' of ions is pulsed down the flight tube
2) Flight tube and reflectron – This is the high vacuum region where the ions separate in space and time
3) Detector – Usually but not limited to multichannel plate detectors, where ions are counted and recorded electronically.

2.6.1 Principles of Time of Flight – Mass spectrometry

Within the pulser unit, the ions arrive as a narrow beam from the differential pumping region (10^{-4} mbar) into the high vacuum (10^{-7} mbar) region. Ions are pulsed into the flight tube where an ion extraction field is created by applying a voltage of around -350 V to the extract plate. This 3 μs pulse allows the ions to enter the ToF region, via an intermediate electrode (Inter) and a field free region (FFR) electrode where the final ion acceleration occurs. This FFR voltage specifies the energy with which the ions have during their time in the flight tube.

The extraction, flight and detection of a packet of ions is generally termed a cycle, with a typical acquisition containing around 30,000 cycles/sec for the length of flight tube used in this instrument.

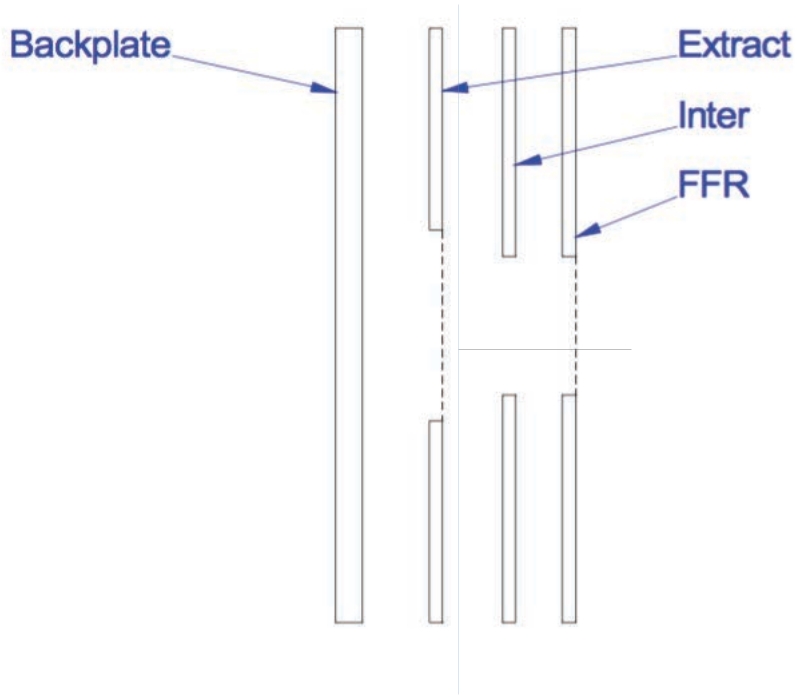

Once extracted, the ions travel towards the reflectron through a pair of electrodes (x and y deflectors) which can be used for ion steering to correct for any mechanical misalignment. The aim of the reflectron is to allow the ions to separate based on the ratio of mass to charge of the ion and then reverse the ions back down the flight tube at an angle of about 2.5° (towards the detector). This ‘V’ shape allows the ions to travel a greater distance in the flight tube and allow for a larger separation of the ions pulsed into the reflectron. The heavier ions will penetrate deeper into the reflectron and will therefore take longer to reach the

detector. By measuring the time taken from the pulse to the detection of each ion in a cycle, the time can be converted into a mass using mass conversion parameters. The mass conversion parameters are based on the equation which converts a time of flight to a mass (equation 20), where m is the m/z of the ion, t is the time of flight of the ion and t_0 and C_b are calibration factors defined by the calibration software program.

$$m = \left(\frac{t - t0}{C_b}\right)^2 \qquad (20)$$

In the calibration procedure, the software takes the definition of the centre of a peak from the user and an accurate mass for the peak and calculates the calibration factors t_0 and C_b. The quality of the ion optics and the effective length of the reflectron are the main parameters that determine the maximum mass resolution possible for a time of flight system. The benefit of increased mass resolution is seen for the separation of isobaric species, such as in the case of

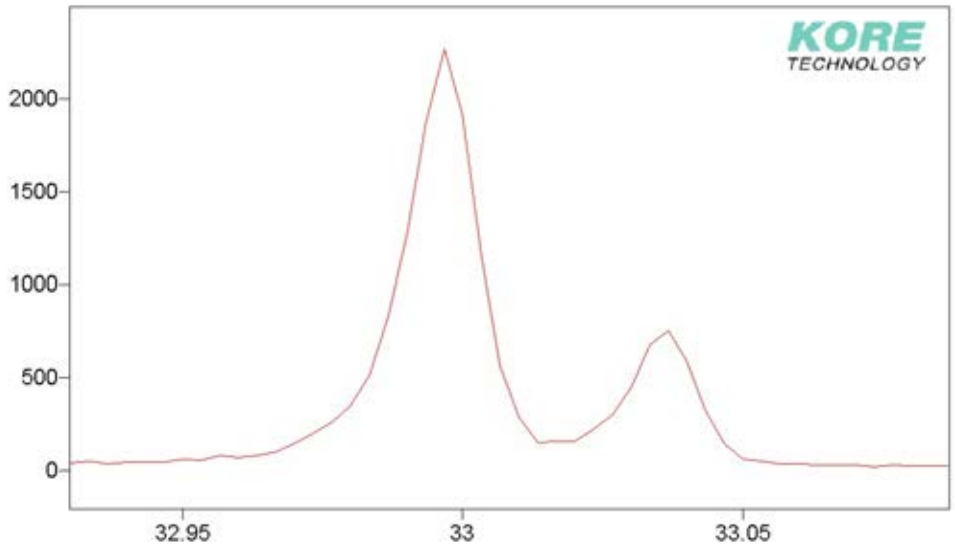

Figure 12 - Mass spectrum showing separation of O+ ^{17}O (32.994 Da) and protonated methanol, CH_3OH_2 (33.034 Da)

methanol and an O_2^+ isotope which have a mass difference of 0.04 amu and can be separated by a time of flight system with a measured resolution of 2300 FWHM (figure 12).

2.6.2 Ion Detectors and counting systems

After the mass analyser, it is important to have a device capable of counting the ions produced in the PTR-MS. As the ion current that reaches a detector for a single ion arrival is low, a requirement is to have a detector sensitive enough to register the arrival of an ion and amplify the signal to a level that can be recorded. There are several types of detector that can be used, including discrete dynode, channel electron multiplier and microchannel plate detectors. Discrete dynode and channel electron multipliers both rely on a similar design and concept, of an ion arrival at a conversion dynode that releases an electron. The electron continues to collide with multiple dynodes in order to cascade electrons and amplify the signal by 4-5 orders of magnitude. The microchannel plate detector works in a similar way and is popular in TOF instruments because it has a significantly higher time resolution due to the design and construction.

2.6.2.1 MCP Detector

The detector in a Kore Technology PTR-MS is a microchannel plate (MCP) detector. The MCP comprises of a series of small tubular channels which are offset at an angle to the incoming ion beam. Providing the ion beam is correctly aligned to strike the MCP, as an ion travels through the channel, it will collide with the channel surface and release electrons as a function of the electric field applied

to the plates. MCP detectors usually operate with strong electric fields to provide amplification of the ion arrival by a few orders of magnitude. The amplification can be adjusted by stacking the MCPs or modifying the electric field strength. The electron signal is then collected on an anode at the rear of the MCP and the analogue signal processed.

The detector is mounted on a flange inside the reflectron and adjusted to ensure the MCP is perpendicular to the incoming ion beam and not necessarily perpendicular to the flange itself. The ion beam in the reflectron has a physical diameter associated with it, depending on the flight path of the ion. If the ion flight path is not perpendicular to the MCP surface, then ions that have the same m/z will have a slightly different flight time and this can increase the spectral peak width, reducing the resolution of the mass analyser (shown in figure 13).

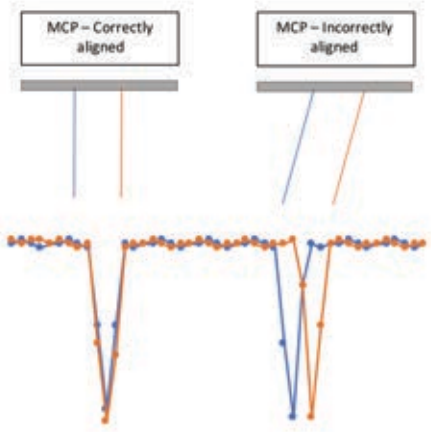

Figure 13 - Schematic showing the effect of peak broadening due to incorrect MCP alignment with the blue and orange lines showing the spatial distribution of the ion beam, the correct alignment is with the incoming ion beam perpendicular to the MCP surface.

The anode signal from the MCP is amplified by a pre-amplifier if the signal is above a certain threshold. In order for the ion arrival signal to be above the

threshold set at the pre-amplifier (to further amplify the signal for digital ion counting), the gain (electric field applied to the MCP) must be optimised and correctly set to account for the detector degradation.

On the instrument used in this thesis, the gain was adjusted to account for detector degradation if a 0.2 potentiometer turn (60 V) increase in detector voltage provided a 60% increase in signal, in line with guidance from Kore Technology. During experimental work the detector gain was checked for MCP degradation monthly but adjustment was typically only required every 6 months.

The ion arrival time is counted by a 4 GHz time to digital converter (TDC), which can record the arrival time of the signal with a resolution of 0.25 nsec and provide a digital signal for storage and interpretation by software.

2.6.2.2 Saturation in pulse counting systems

Saturation in any ion counting system is an important issue for the accurate detection and counting of ions and one which is generally taken for granted. At high ion signal intensities, the detector gives a non-linear response to ion signal and subsequently causes an underestimation of the ion signal, shown in figure 14 with a benzene calibration standard.

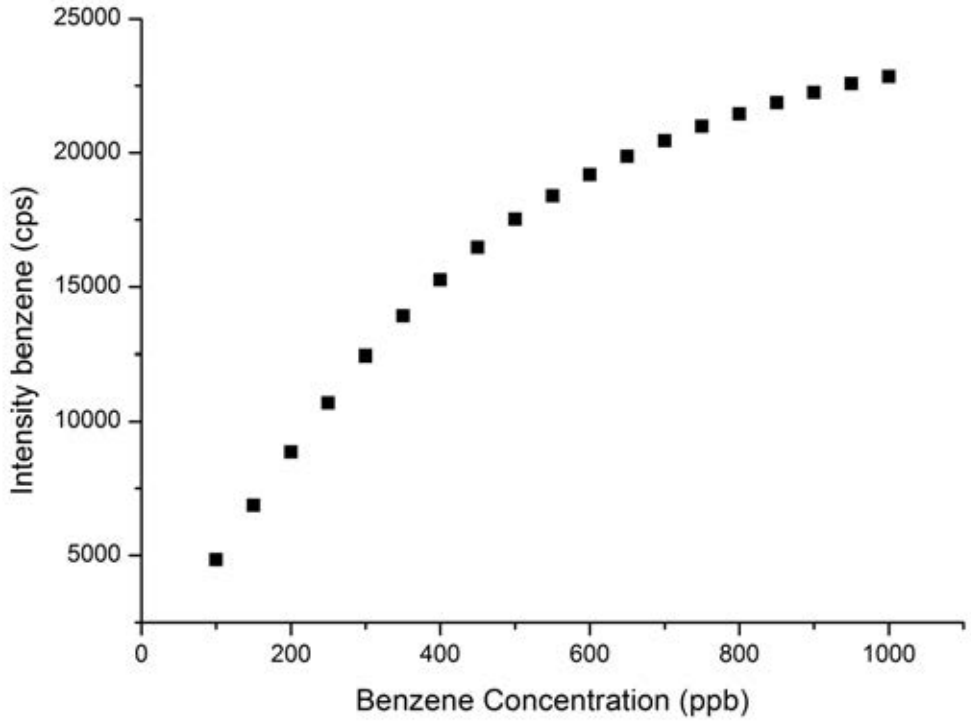

Figure 14 – Detector response in counts per second (cps) to a benzene calibration standard measured using a drift tube pressure of 0.75mbar, 100v DC entry voltage and the RF ion funnel on.

Saturation is not always obvious from features such as peak shape (saturation of a peak in a mass spectrum often shows a 'double peak' as shown in figure 15). Within a pulse counting system, saturation is dependent on the ability of the ion counting system (detector, TDC and counting electronics) to register the arrival of an ion and to be ready for a subsequent ion arrival. The time taken for this process to occur is often termed the 'dead time' of the detector, the time for which the system cannot count another arriving ion. If during a cycle, several ions at each mass are reaching the detector, then only one can be recorded and this leads to an underestimation of the ion signal reaching the detector.

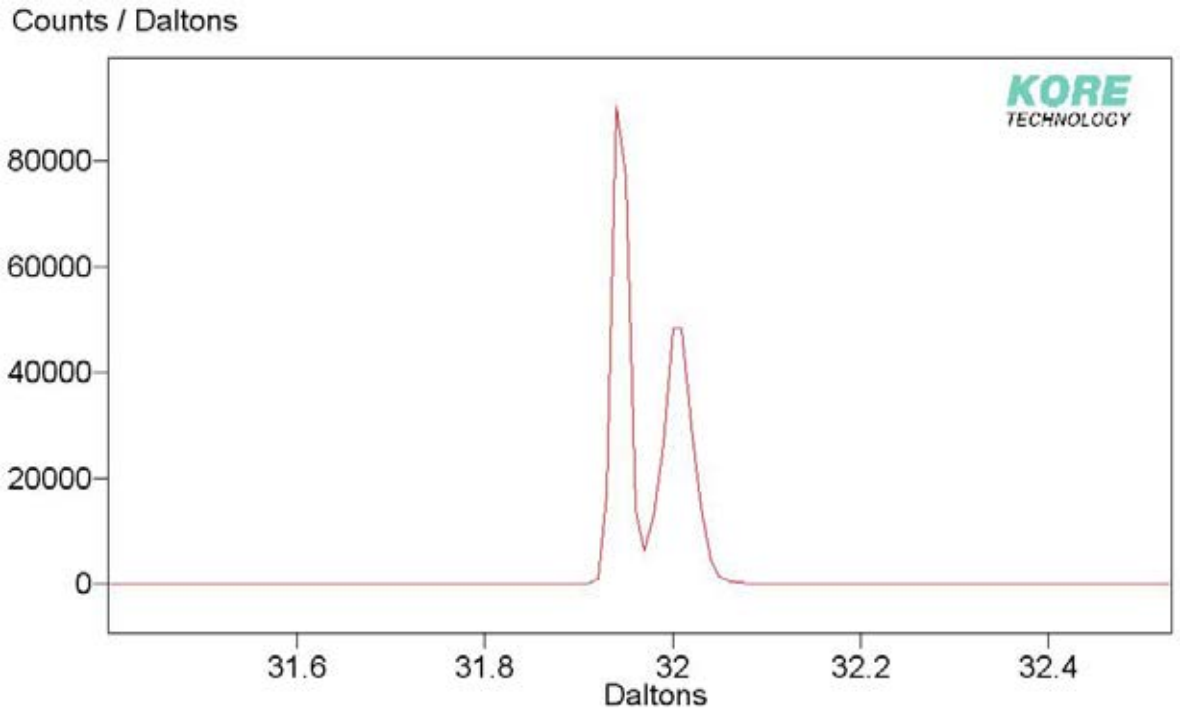

Figure 15 - Mass spectrum showing saturated double peak at m/z 32 (oxygen). This spectrum was verified as saturated by calculation of the actual count rate from the ^{18}O isotope of O_2^+ at m/z 34.

During an acquisition, it is impossible to work out if a second ion arrives while the detector is recovering from the previous ion arrival. For this reason, a threshold needs to be established where the dead time effects are significant and the count rate cannot be reliable. For Kore technology instruments, if the measured count rate for any m/z is more than 60% of the number of cycles in the acquisition, then the dead time effects mean that the measured intensity cannot be used for qualitative or quantitative measurement.

For some ions, such as reagent ions, the count rate is very unreliable (and often the same as the number of cycles in the acquisition) due to saturation and for this reason, isotopologues containing the minor isotope of oxygen (^{18}O which is stable but has a lower natural abundance due to 2 additional neutrons in the atomic

structure), are measured to give a calculated value for the actual count rate of the reagent ion. The isotope signal can be multiplied by the appropriate factor to estimate the ion signal at the saturated mass. This is a commonly used method of calculating reagent ion intensities, or by using other minor isotopes, the actual ion signals from concentrated species.

2.7 Data acquisition and storage

The acquisition and storage of PTR-MS data is crucial to the efficient performance of the system as a whole. Software packages are used to provide commands to start measurements, store data, mass calibration and analysis. The data acquisition system is linked to the 4 GHz TDC by a USB connection which allows for fast data transfer.

The instrument used in this thesis was controlled using a variant of a Thermo fisher GRAMS software, with a Kore Technology specific workbook which gives the functionality to acquire mass spectra in multiple modes, save the data and analyse the spectra. Several other standalone programs allowed physical parameters such as temperature, pressure and voltages to be displayed and controlled.

2.8 Quantification of water clusters in DC and RF operation

The degree to which the reagent ion signal is a pure H_3O^+ beam is important in the quantification of analytes using multiple E/N values, including those which are isomeric or that have a proton affinity less than the hydronium cluster ions (and therefore are not ionised at low E/N where the cluster ions dominate).

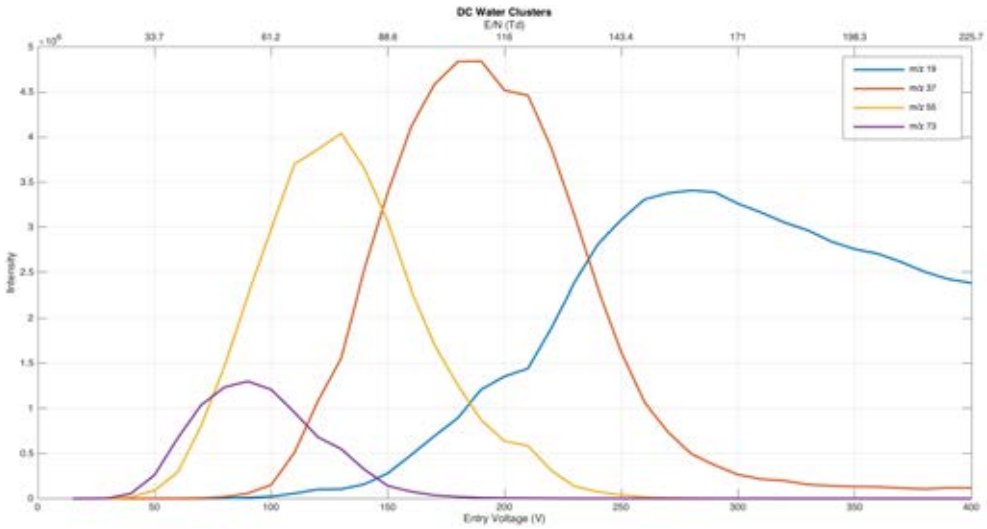

Figure 16 - Distribution of reagent ion clusters using water vapour as the hollow cathode feed gas in DC operation. The PTR drift tube pressure was 1.0 mbar, with the hollow cathode pressure 1.3 mbar and the drift tube at 100°C.

As the reduced electric field strength increases, the reagent ion clusters dehydrate/fragment on collision with neutral molecules to produce lower mass cluster ions and ultimately, the hydronium ion. The reagent ion clustering can be controlled by both changing the E/N (reduced electric field) or the pressure in the hollow cathode. A reduction in the hollow cathode pressure would decrease the clustering of hydronium ions but would result in a larger proportion of air in the drift tube able to backstream into the cathode forming ions such as O_2^+. Experimentally

the glow becomes harder to start and maintain at low HC pressures and as a result, 1.3 mbar is chosen as a compromise.

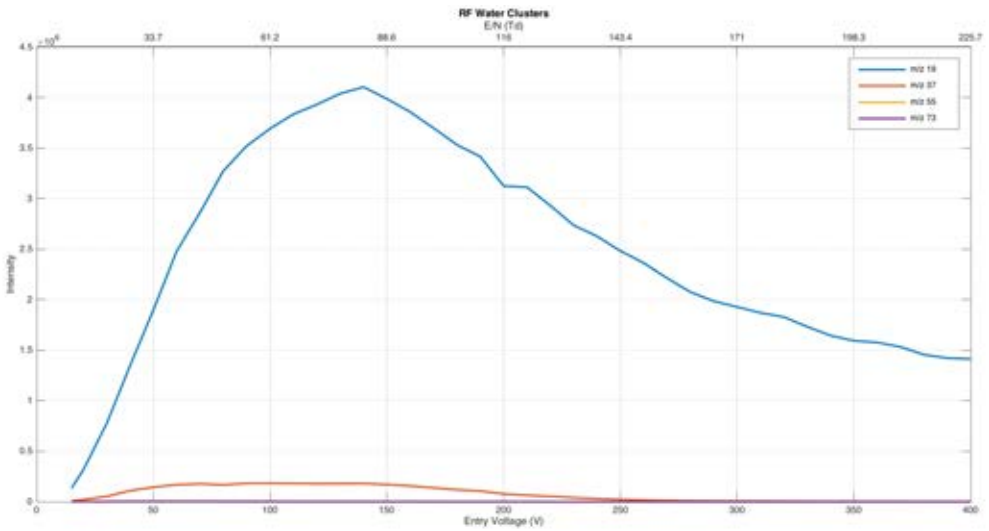

Figure 17 - Distribution of reagent ion clusters using water vapour as the hollow cathode feed gas in RF ion funnel operation. The PTR drift tube pressure was 1.0 mbar, with the hollow cathode pressure 1.3 mbar and the drift tube at 100°C.

Although when using the RF field, the clustering is minimised at all entry voltages investigated, the RF field provides additional energy to the molecules which causes unpredictable behaviour with respect to the fragmentation/transmission of ions (reagent ions and analyte ions). The phenomenon is most pronounced at low DC voltages, where the reagent ion transmission is low (m/z 21) however the sensitivity for many compounds, particularly those of high mass, is exceptionally high. This infers a mass dependent transmission as real reagent ion concentration in the drift tube must be much higher. When measuring ion current at PTR exit, the ion beam is around 10 nA, of which >99% is expected to be hydronium. As a result, the use of the term ‘E/n’ is not applicable when using the RF ion funnel as the additional energy contribution to the ions is greater than the amount measured

by the reduced electric field.

For this reason, the work on isomer separation is investigated in DC mode, as the ion transmission and fragmentation is purely a function of the reduced electric field (E/N) rather than this term and an unknown fragmentation contribution from the RF field.

2.8.1 Effect of Humidity on samples

The humidity of a sample gas will alter the conditions inside the PTR-MS drift tube. For a given reduced electric field strength, the increase in water molecules in the drift tube generally leads to more reagent ion clustering $H_3O^+(H_2O)_n$. Some compounds, which have a higher proton affinity than the water cluster, will continue to accept a proton from the cluster ion on collision. For those compounds with a lower proton affinity than the water cluster ion, the increase in humidity decreases the H_3O^+ available for proton transfer and the instrumental sensitivity will decrease [26]. Some researchers have aimed to derive corrections for humidity effects in PTR-MS, but generally these require instrument specific calibration factors.

Within the experimental sections of this thesis, dry gas standards with 0% humidity were used for method development as this simplifies the analysis. However, the humidity of the sample is not expected to make a large difference in either the product ions or sensitivity of the instrument.

2.9 Data analysis protocols

For all of the sample measurements taken in the experimental sections of this thesis, background mass spectra, those measured without the analyte of interest, were analysed and subtracted from the sample mass spectra in order to provide a signal from the sample of interest.

Background measurements were taken before and after each sample measurement, for each setting of the reduced electric field strength investigated. The reagent ion signal from background to measurement was within 5%. To background subtract, both the background spectra and sample spectra were normalised, with the resulting background spectra subtracted from the sample spectra.

The background subtraction removes any influence on the sample mass spectra that comes from within instrument contamination which exists in all PTR-MS systems. Common ions that are present in a PTR-MS drift tube include $C_3H_3^+$, $C_3H_5^+$ and $C_3H_7^+$ and are produced from hydrocarbons.

3 - Calibration and generation of VOC standards

3.1 Importance of calibration techniques

Calibration of VOCs is important for many instruments, including the PTR-MS, in order to allow the end user or instrument software to report a concentration for a measured compound. However, in this work calibration equipment has also be used to provide single or multi component gas mixtures to use within the experimental methodology. It allows the researcher to accurately prepare a gas standard for PTR studies and can be much more flexible than the static standards discussed in section 3.2. For example, much of the experimental work in chapters 4, 5 and 6 used either static or dynamic standards generated using the methods discussed in this chapter to allow the determination of fragmentation patterns or concentration for the compounds discussed.

3.1.1 Calculation of concentration using rate coefficients

The concentration of an analyte in a gas sample to be measured using PTR-MS is often expressed as the volume mixing ratio (VMR), the number of analyte molecules per million or billion by volume (ppmv, ppbv respectively). The benefit of using the VMR is that the VMR of the gas inside the drift tube is the same as the VMR of the gas sampled, with the measurement of the sample temperature independent. The VMR of an analyte in a PTR-MS drift tube can be calculated theoretically from the ratio of analyte to reagent ion signals using the following equation.

$$VMR_M = \frac{i\,MH^+}{i\,H_3O^+}\,\frac{1}{kt}\,\frac{10^9}{N_d} \qquad (21)$$

Where VMR_M is the volume mixing ratio (in ppbv) for compound M, k is the reaction rate coefficient of compound M with H_3O^+, t is the reaction time (or drift time), N_d is the total number density of gas in the PTR drift tube (in cm^{-3}) and the measured intensity of the protonated analyte and the calculated hydronium ion signal (iMH^+ and iH_3O^+ respectively). This calculation is often used by commercial instrument manufacturers and researchers to provide an on-line VMR and for reporting in peer reviewed publications [63]. Although this is useful in certain circumstances, some of the terms contain significant uncertainties and therefore the calculated VMR must be reported with significant uncertainty.

The rate coefficients for proton transfer reactions with hydronium are often known through theoretical calculation or measured using SIFT with typical uncertainties of $\pm$ 25% (and can be as large as 50% [26, 64]), which is a significant source of error in the calculation of the VMR. The extraction and transmission efficiency of the ions from the drift tube to the detector can also be a function of their mass and the response of detectors of the type commonly used in mass spectrometry can be mass and structure dependant [65]. As a result, corrections should be made for the extraction, transmission and detection efficiency if using a theoretical approach for the calculation of VMRs.

In the case of using the RF ion funnel, this is difficult to correct for as for specific conditions (used in chapter 6), the transmission effects are significant, the count

rate of hydronium and analyte are often the same (when we know their abundance to be very different in the drift tube). This difference in transmission efficiency of the hydronium ion is assumed to be the differential ion extraction efficiencies from the drift tube due to the RF field causing the more efficient extraction of heavier ions.

For the reasons stated here, the use of calibration standards is required in order to reduce the measurement error and therefore be able to determine the error in the method of analysis (for quantification of isomers).

3.2 Static methods

Several static methods of VOC calibration exist, but by far the most popular is the gas cylinder calibration standard. Usually prepared by a gas handling company, this involves gravimetric addition of a VOC of interest (usually in liquid form), with the cylinder then filled to a given pressure with a balance gas, such as nitrogen or zero air to create a gas mixture of a known concentration.

Static gas standards usually provide the simplest solution for VOC instrument calibration and VOC instrument investigation as they can be certified for several years and require little user skill or input. For these reasons, static methods such as gas cylinders have become very popular in labs and fieldwork locations.

However, gas cylinders are not perfect and can be inflexible for investigation into single component VOCs, reactive mixtures or unstable target compounds. There are other issues to bear in mind with static gas mixtures, many compounds will adsorb to the untreated surfaces of the inside of the canister, reducing the output concentration from the certified value and the gas mixtures are usually expensive to prepare and purchase. Gas standards can often have minimum concentrations (to avoid the previously mentioned surface effects) which may not be suitable for ppb calibration or experimental applications without methods of dilution. In addition, some chemical species readily decompose thermally or on contact with surfaces, are not available commercially or are toxic and not available as gas standards.

Static gas standards can also be made in Tedlar® or FEP bags, usually by injecting a known volume of compound into the bag and filling with a known volume of dry gas, such as nitrogen or zero air. This is useful if the application is not highly dependent on the concentration of the calibration gas, such as in the determination of branching ratios, as Tedlar® and FEP bags suffer from significant surface adsorption within minutes of preparation, reducing the concentration of the analyte in the gas phase. Teflon bags are best used when the molecular or fragment ions do not interfere with the contamination peaks from a ‘clean’ Tedlar® bag and provide a quick, simple and cheap method of producing a gas mixture. Tedlar® bags are particularly prone to surface effects and contaminants given off from the polymer, meaning that blank bag samples to check for contaminants are essential.

3.3 Dynamic calibration

An alternative to the static gas standard is a dynamically produced standard, where the calibration gas is produced when needed by means of a gas calibration unit. These have been available commercially for over 25 years and have been adopted as a method of gas standard preparation by research laboratories worldwide [66]. The ISO/British standard maintains the minimum standard for manufacturers and end users to follow [67].

The principle of a dynamic calibration system is that with a constant temperature and a stable gas flow, that either a permeation or diffusion device will 'emit' a VOC at a constant rate. Gravimetric calibration allows the user to work out the mass of compound released from the device over a suitable time period and with a known flow rate, work out the concentration of VOC in the output gas. The concentration of a compound created by this method can be calculated from the following equation.

$$C = \frac{P \times \left(\frac{V_m}{mw}\right)}{F_C} \qquad (22)$$

Where C is the concentration (in ppmv) of the compound in the gas mixture created, P is the permeation rate (ng/min) at a given temperature, V_m is the molar volume (24.46 L mol^{-1} for an ideal gas at 1013.2 mbar and 25°C), mw is the molecular weight of the compound and F_c is the flow rate in ml/min at standard reference conditions (1013.2 mbar and 25°C) [68]. Should the flow rate be

measured at conditions other than the standard reference conditions (1013.2 mbar and 25°C), corrections can be made to adjust the flow rate [68]. This equation can be applied to both permeation and diffusion tubes to calculate output concentration of a dynamic standard.

The dynamic calibration system usually comprises of a temperature-controlled oven module (usually controlled to ± 0.1°C) to maintain a constant vapour pressure for the compound in the diffusion tube and a method of delivering a flow of carrier gas, such as a gas cylinder attached to a mass flow controller (MFC), pressure regulator or pump. Being able to control the temperature and flow accurately is crucial when reporting the output VOC concentration as the vapour pressure increases exponentially. For isoprene, using the same ΔT (5 K) marked at points 1 and 2 on figure 18, the Δ vapour pressure is 3000 Pa and 17000 Pa respectively. For this reason, accurate temperature control reduces the vapour pressure fluctuations and the error in the output concentration. As a result of this, it is desirable to operate a permeation/diffusion tube thermostat at a temperature where the gradient of the vapour pressure curve is shallow (for isoprene, <280 K) in order to reduce the rate of change in vapour pressure with temperature. For volatile compounds such as isoprene, this means operating sub ambient (<293 K), for less volatile compounds, such as the PAH fluoranthene, a much higher temperature is required (>400 K).

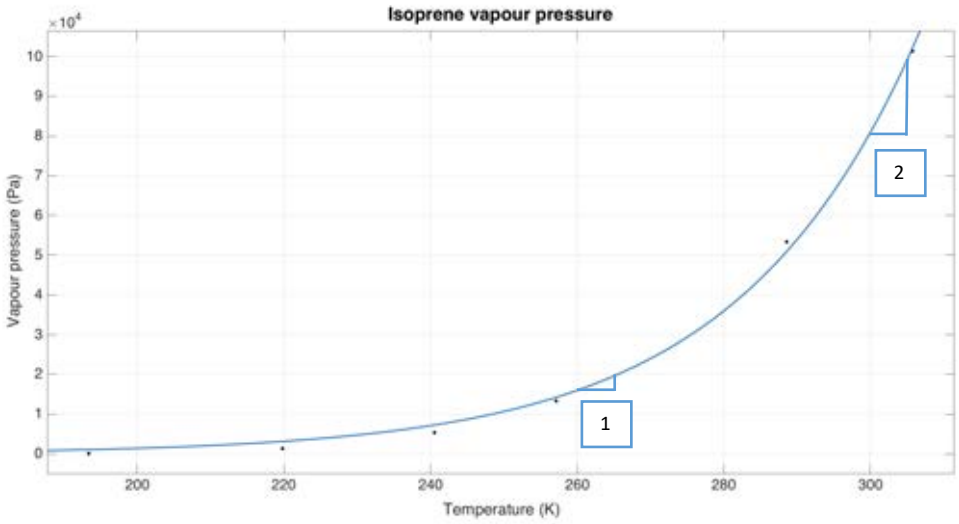

Figure 18 - Isoprene vapour pressure curve, data taken from CRC handbook of Chemistry and Physics [55].

Dynamic calibration systems are often constructed in such a way that they will be able to take both permeation and diffusion devices; however, this relies upon the oven module being vertical to avoid liquid touching the capillary bore section of the diffusion devices.

3.3.1 Permeation tubes

Permeation devices have become the most common method of choice for dynamic gas standard preparation in the last 25 years. The principle is to enclose the VOC in its pure form in a membrane that is semi permeable to the VOC, so that the VOC can pass through the membrane at a constant rate at a given temperature. The VOC forms a two-phase equilibrium, so provided liquid is visible in the tube, the internal vapour pressure will be constant and therefore a constant emission is achieved (for a well-controlled temperature). Commercial and homemade devices are usually made from Teflon tube, sealed at either end with

crimped Teflon inserts or gas tight fittings. A wide range of compounds, such as alcohols, ketones, esters, terpenes and hydrocarbons can be used with Teflon permeation devices, with companies offering tubes pre-calibrated for a given temperature [69].

One of the disadvantages of this technique is that as the tubes emit the compound, they also become permeable to gasses in the other direction [66]. Depending on how rigorous the storage procedure is, oxygen can pass into the tube and if the compound is oxygen sensitive, can be responsible for degradation of the compound and ultimately a tube that has uncalibrated itself.

During this work, it was discovered that this was an issue due to the discolouration of the liquid MVK in the permeation tube. This was then confirmed by analysis of a headspace analysis of the liquid MVK.

Initially permeation tubes were constructed for the compounds of interest, stored with food grade oxygen absorbers which consist of packets of ultrafine iron powder that oxidise to form iron oxide, removing oxygen from the local atmosphere. However, they quickly degraded, which was confirmed visually from the discolouration of the liquid and by checking for degradation products in the PTR-MS spectra, shown in figure 20. After 2 years of storage (using ultrafine iron powder oxygen absorbers), the major product ions observed are from the degradation products in figure 21.

Figure 19 – Image of the oxidised MVK 181 days after receipt of the compound. The MVK arrived as a colourless liquid but oxidised over 180 days to a yellow/brown liquid.

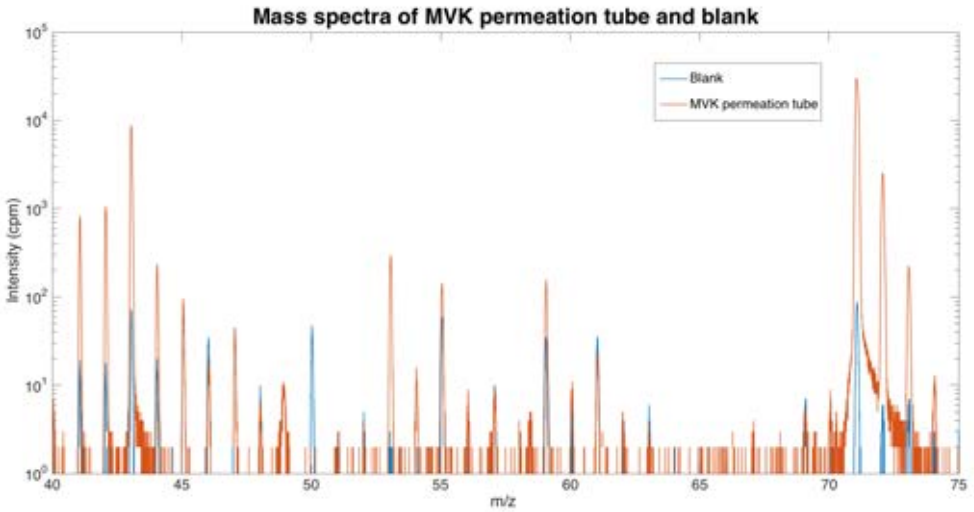

Figure 20 – Mass spectra of MVK permeation tube (orange) and zero air blank (blue) plotted on a log intensity scale, measured 181 days after production of the permeation tube. Mass spectra measured for 60 seconds, at 1 mbar drift tube pressure and 1.3 mbar hollow cathode pressure with an E/n of 140 Td. Large peak at m/z 71 is the protonated MVK molecular ion, other peaks from oxidised contaminants include m/z 43 (glycolaldehyde and $C_3H_7^+$ from MVK fragmentation), m/z 59 (glyoxal) and m/z 73 (methylglyoxal and ^{18}O isotope of MVK).

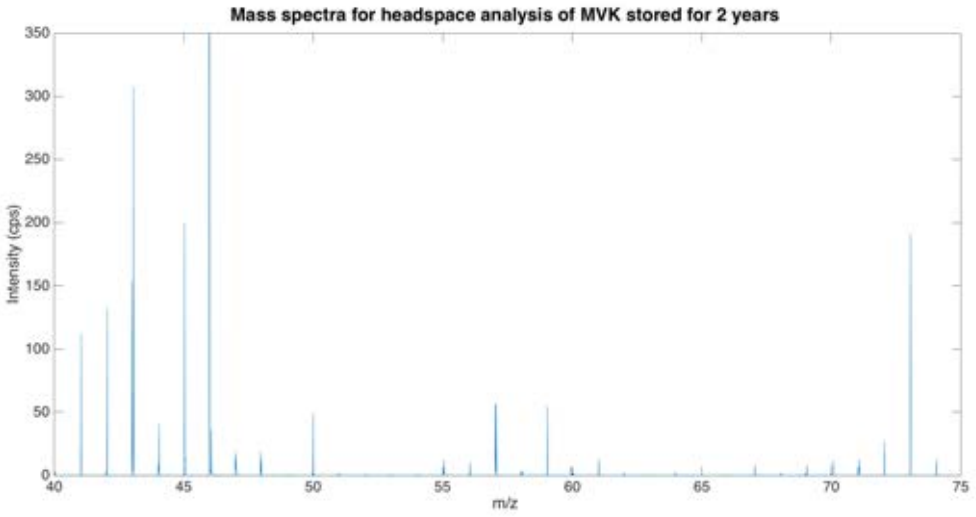

Figure 21 - Mass spectra of liquid from the MVK permeation tube (blue), measured 2 years after production of the permeation tube. Mass spectra measured at 1 mbar drift tube pressure and 1.3 mbar hollow cathode pressure with an E/n of 140 Td. The small peak at m/z 71 is the protonated MVK molecular ion which is of a much lower intensity than the other peaks from oxidised contaminants including m/z 43 (glycolaldehyde and $C_3H_7^+$ from MVK fragmentation), m/z 59 (glyoxal) and m/z 73 (methylglyoxal and ^{18}O isotope of MVK).

As a result of the degradation of MVK in permeation tubes, diffusion tubes were employed rather than permeation tubes for the experimental sections of the thesis which required them, allowing a more appropriate method of storing oxygen sensitive compounds to be used.

3.3.2 Diffusion tubes

Diffusion tubes are the main alternative for dynamic VOC generation and consist of a precision capillary bore section attached to a reservoir. The construction of diffusion tubes is generally achieved with a borosilicate glass, some with a sealed end and others with a cap for cleaning and refilling. Diffusion tubes work on the principle that at a given controlled temperature, with a capillary bore length, that a compound will diffuse out of the end at a constant rate.

Figure 22 - Image showing diffusion tube used in this work with PTFE cap and capillary bore of 0.1mm diameter and 8cm length

The diffusion method provided a solution for making low cost but high accuracy standards for the development of the isomeric separation work presented as part of this thesis. Diffusion tubes were also used in the preparation of a PAH standard to determine if on-line, real time air sampling for PAHs would be possible using PTR-MS.

3.4 Generating diffusion tube mixtures of oxygen sensitive VOCs

The motivation behind this work was to develop a way of using the existing technology of permeation and diffusion methods to prepare different oxygen sensitive VOC mixtures to allow experimentation for the isomeric separation experiments. This was important as different gas mixtures needed to be created, including single component and multi component mixtures.

It was clear that the development of a method of storage appropriate for oxygen sensitive VOCs was required. The obvious choice was to store the compound in an inert gas, limiting the exposure to oxygen and therefore limiting any possible oxidation. As a result, the consequence of storage and calibration of methyl vinyl ketone (MVK) as a function of time was investigated. A deoxygenation process for

oxygen sensitive compounds was devised, using a nitrogen flushed desiccator and then evaluated using the change in emission rates for refillable diffusion tubes over a 4-month storage period.

3.4.1 Methyl Vinyl Ketone (MVK)

MVK is an important compound in atmospheric chemistry as a main product in the oxidation of isoprene. In experiments detailed in chapter 5, it was important to be able to generate standard mixtures of MVK in order to assess the fragmentation in an attempt to differentiate MVK from its structural isomer, methacrolein (MACR).

From the knowledge acquired through creating permeation tubes, it was known that the degradation of MVK was significant over the time period that the sample would be used (150 days) and therefore motivated the work on the deoxygenated storage of MVK to ensure accurate calibration. Unfortunately, the storage procedure and duration of storage while the compound was with the manufacturers was unknown (Sigma Aldrich, UK). It was assumed that at day 1 of the study (the moment the compound arrived) that the compound was the stated purity provided by Sigma Aldrich.

3.4.1.1 Experimental details

To determine if the compound had degraded to other products we used the approach that the same compound in the same tube should have the same

emission rate. Any significant deviation from this emission rate would be attributed to formation of a more or less volatile compound.

On receipt of the MVK, the 5ml sample was split into 2 separate 2.5ml samples in amber vials. One was stored in a vial which was stored exposed to air and the other vial went through a de oxygenation procedure, which involved flushing the vial with ultra-pure nitrogen for 5 minutes to remove oxygen in the vial. The deoxygenated vial was placed in a vacuum desiccator and flushed with ultra-pure nitrogen for 10 minutes in order to remove as much oxygen as possible. The desiccator was swiftly sealed with oxygen absorbers (ultrafine iron powder, Fresherpack, UK) and a molecular sieve (5A, Sigma Aldrich, UK) to ensure, as much as possible, an oxygen free, dry atmosphere. Both samples were refrigerated at 4°C for the duration of the experiment and the storage procedure repeated when MVK was removed for experiments. The calibration was performed using a Kintek 491M thermostat, set at 40°C $\pm$ 0.1°C with a 100 ml/min flow of oxygen free nitrogen of purity 99.998% (BOC, UK).

For this experiment, a diffusion tube of 0.2 mm capillary bore diameter and 2 cm capillary tube length (0.2 mm/2 cm) was used for the deoxygenated MVK and a 0.5 mm capillary bore diameter and 2cm capillary tube length (0.5 mm/ 2cm) for the MVK stored in the presence of oxygen. Gravimetric calibration of the tubes was performed by briefly removing the tube from the thermostat in order to weigh the tube on a Cole Parmer PA120 digital balance (120 g x 0.0001 g).

3.4.1.2 Results

A calibration was attempted at 3 different start times (14, 35 and 127 days) from the delivery of the MVK to observe the effect of oxygenation on the sample. The weighing data for each calibration experiment was plot, with a linear regression line fit to the data for each calibration. As a different capillary bore tube was used for oxygenated vs deoxygenated, it would be the relative changes in emission rate that would show the effect of oxygenation of the sample rather than the comparison of the emission rate between the 2 samples.

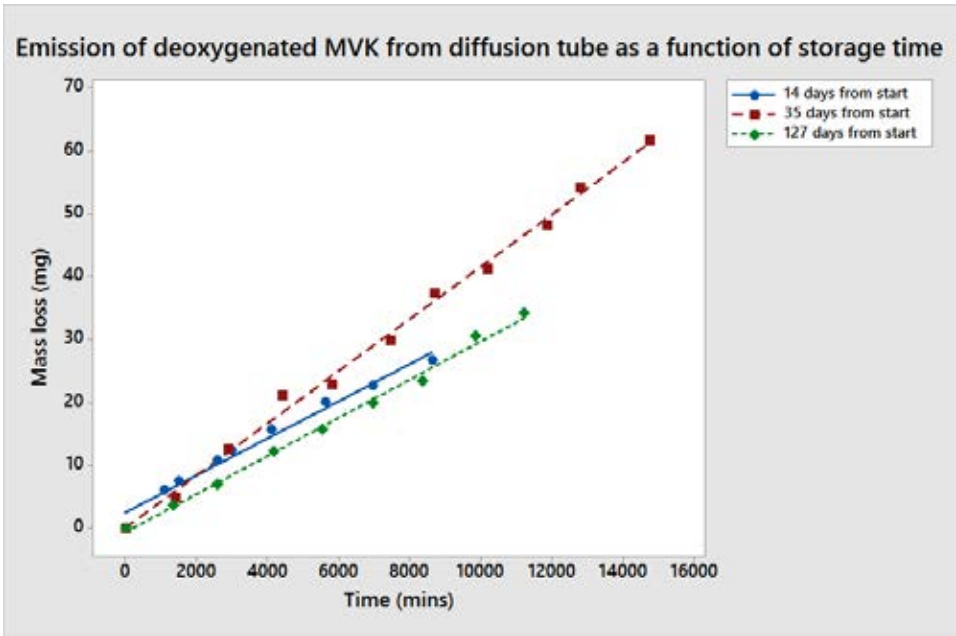

Figure 23 – Three calibration experiments showing the emission of a 0.5mm bore, 2cm length diffusion tube containing deoxygenated MVK at 40°C with a 100ml/min N_2 gas flow. The calibration experiments were started at 14, 35 and 127 days from receipt of the MVK and the initial deoxygenation procedure, showing the effect of storage of the sample on the emission output of the diffusion tube.

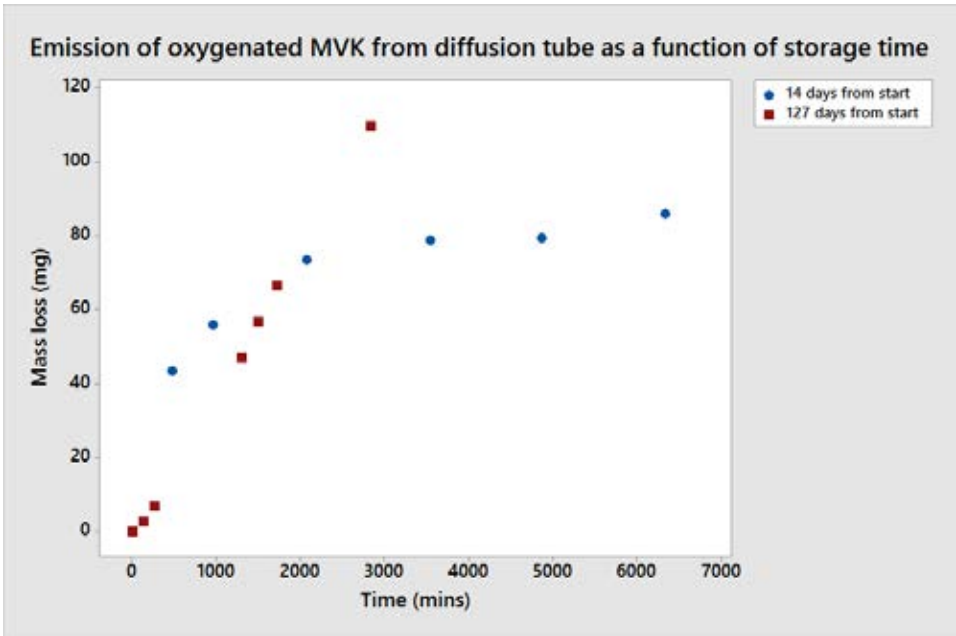

Figure 24 - Two calibration experiments showing the emission of a 0.2mm bore, 2cm length diffusion tube containing oxygenated MVK at 40℃ with a 100ml/min N_2 gas flow. The calibration experiments were started at 14 and 127 days from receipt of the MVK and the initial storage procedure, showing the effect of storing the sample in air on the emission output of the diffusion tube.

For the 3 scatter plots of the deoxygenated MVK in figure 23, the weight loss rates are similar for 14 days and 127 days and well within expected error of the balance and other physical parameters such as the temperature control etc. (lower 95% confidence interval calculated as 0.00281 and 0.00282, upper 95% confidence interval calculated as 0.00318 and 0.00316 for 14 and 127 days respectively). Full details of the error analysis and confidence intervals discussed in section 3.4.1.2.1. However, the 2 scatter plots in figure 24 for the MVK stored in oxygen show significant changes in emission behaviour of the diffusion tube at 14 and 127 days.

The deoxygenated MVK liquid which was used in this study was used to produce a suitable diffusion tube for the study detailed in chapter 5.4. The mass spectrum of the MVK used in the production of these diffusion tubes (180 days from receipt

and deoxygenation of the MVK) is shown in figure 25, with the major product ion from MVK and no apparent contamination from the degradation products.

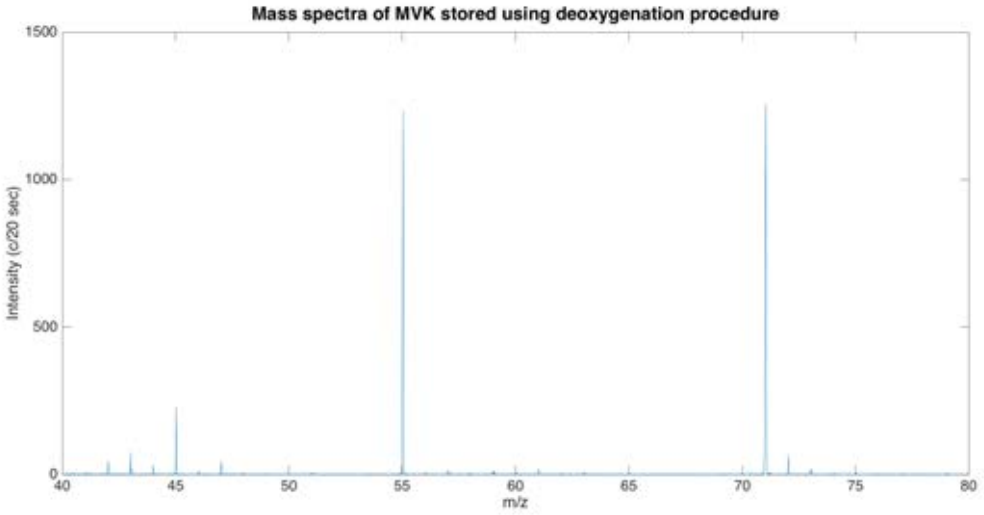

Figure 25 - Mass spectra of the MVK used in the deoxygenated storage procedure measured for 20 seconds using a drift tube of pressure of 1 mbar, a hollow cathode pressure of 1.3 mbar and an E/n of 140 Td, showing the protonated parent ion for MVK at m/z 71. The other major peak in this section of the mass spectrum was a water cluster ion at m/z 55 ($(H_2O)_2.H_3O^+$). The mass spectra were taken 180 days from receipt and deoxygenation of the MVK.

3.4.1.2.1 Error in the measurement

In order to determine that the differences between the oxygenated and deoxygenated MVK samples are significant, the uncertainties that may affect the generation of the diffusion tube standard must be quantified. In this system for generation of gas standards, there are multiple factors to consider which are summarised in table 3 as an error budget.

Table 3 - Sources of error in the generation of diffusion tube gas standards.

Source of Error	**Quantity**
Weighing diffusion tube	± 0.1 mg
Flow of carrier gas (Mass flow controller)	0.8 % of reading or 0.2 % of full scale range (100 ml/min ± 0.8 ml/min)
Temperature control	± 0.1°C
Diffusion tube capillary length	± 0.1 mm
Diffusion tube capillary diameter	± 3 μm
Change in diffusion tube capillary bore size (length and diameter) as a function of temperature	Unknown

Several of the errors would be easy to propagate in a bottom up approach, combining the errors to give an uncertainty in the measurement of each weight loss, or the emission from the diffusion tube. Some of the sources of errors are constant for the experiment, such as any systematic error in the diffusion tube diameter and length, although the effect of these uncertainties were reduced by using the same tubes for each set of measurements for a given storage procedure.

Some of the errors contained with the error budget in table 3 would be difficult to propagate in a bottom up approach to determine the change in emission rate from an uncertainty, such as the diffusion tube capillary bore and for this reason, a top down approach, using the uncertainty on the measurements is employed. The top

down approach encompasses the errors within a set of measurements, so the 95% confidence interval (the confidence on the measurements taken).

The top down uncertainty analysis uses the 95% confidence interval for each set of measurements to give an estimate of the error in the calculated emission. The 95% confidence interval can be calculated from the sample mean $\pm$ (2σ x Standard Error). This can then be propagated though to determine the uncertainty in the output concentration. The disadvantage to a top down uncertainty analysis is that it does not give details about the size of each component of the error or which sources of error dominate but does indicate the total uncertainty on the measurement.

The final consideration when representing the data is to determine which regression analysis to use. A single regression analysis is not suitable for all experiments and for some experiments, a least squares fitting analysis will suffice. However, for data with outliers (which shouldn't not be excluded from the fit), reducing their leverage effect on the regression fit is desirable. For each calibration, a suitable regression (either ordinary least squares linear fit, or robust regression) has been selected.

Table 4 - Confidence interval on the fitted line from the robust regression for the deoxygenated MVK diffusion tube weight loss measurements. The confidence interval was calculated as the sample mean plus (SE x 1.96) and the sample mean minus (SE x 1.96).

	14 days	35 days	127 days
95% Lower CI	0.00281	0.00407	0.00282
95% Upper CI	0.00318	0.00424	0.00316

The 95% confidence limits for the deoxygenated MVK diffusion tube experiments in table 4 show excellent agreement between the calibration experiments at 14 and 127 days from receipt of the MVK. The reading for 35 days deviates from the consistent readings at 14 and 127 days and it is suggested that this may be as a result of experimental error, such as a loose-fitting cap on the diffusion tube or slightly higher ambient temperature in the laboratory. This can be observed as OLS fitted line plots in figure 23. The scatter plots in figure 24 for the oxygenated MVK at 14 and 127 days show significant differences in emission behaviour between the two experiments.

3.4.1.3 Discussion

During the course of the storage experiment, there was a discolouration of the liquid MVK which was stored in an oxygenated environment compared to that which was stored in a dry N_2 environment. The discolouration of the liquid in the diffusion tube was as a result of the degradation of MVK producing the oxidation products glyoxal, methyl glyoxal and glycoaldehyde [70-72], which are a clear yellow liquid. Although methyl glyoxal and glycoaldehyde have lower vapour pressures than MVK, glyoxal has a much higher vapour pressure and therefore

would result in a much higher emission rate (and therefore mass loss) from the oxygenated diffusion tube (vapour pressure data shown in table 5).

Table 5 - Physical properties of compounds produced as a result of MVK oxidation. Est denotes an estimated value from experimental data.

Compound	Molecular weight (g/mol)	Product ion (PTR-MS, H_3O^+)	Vapour pressure (Pa at 25°C)
Glyoxal	58.04	59	34 kPa [73]
Methyl Vinyl Ketone (MVK)	70.09	71	11kPa [74]
Methyl glyoxal	72.06	73	3.5 kPa Est [75]
Glycolaldehyde	60.05	43	5 Pa [76]

The results of this study show that diffusion tubes are a much more suitable way of preparing a dynamic gas standard than permeation tubes, and that the storage and purity of the starting compound is crucial to the emission rate.

3.5 Generating diffusion tube standards of PAHs

For the experimental work in chapter 6, it was crucial to be able to measure both static standards and to create PAH standards in a gas simulating real world air in order to demonstrate the capability of PTR-MS as a tool for measuring PAHs at high time resolution and in real time. The low vapour pressure of PAHs means that static calibration methods such as gas cylinders are unlikely to be successful due to significant wall effects and the inability to use increased temperatures with high pressure gas standards. The low vapour pressure also creates difficulties in producing PAH samples in air using dynamic methods also. For this reason, super ambient thermostat systems (which operate at T > 130°C) and heated transfer lines are needed in order to produce and transfer the air samples successfully to the detection system, the PTR-MS.

3.5.1 Experimental Details

Fluoranthene (Sigma Aldrich, UK) of purity >97% was purchased and used without further purification, although some purification may occur during calibration. As PAH samples are solid at room temperature, the handling of these compounds was much simpler than for liquid VOCs. 500mg of a solid PAH was placed into the diffusion tube and incubated at 177°C, a temperature selected in order to provide an emission rate suitable for detection/calibration using the PTR-MS. Diffusion tube sizes and thermostat temperatures used for the study are shown in table 6.

Table 6 - Conditions used in the calibration of fluoranthene diffusion tubes for the experiments detailed in chapter 6.7.2

PAH	Fluoranthene
Tube dimensions	Tracer Measurement systems tube 2mm/2cm and 0.1mm/8cm
Thermostat Temperature	177°C
Emission Rate	3570 ng/min and 2.23 ng/min
Flow rate of N_2 during calibration	100 ml/min

From gravimetric calibration of the diffusion tube, regression analysis on the mass loss data can be used to extract the emission rate of the diffusion tube, shown in figure 26.

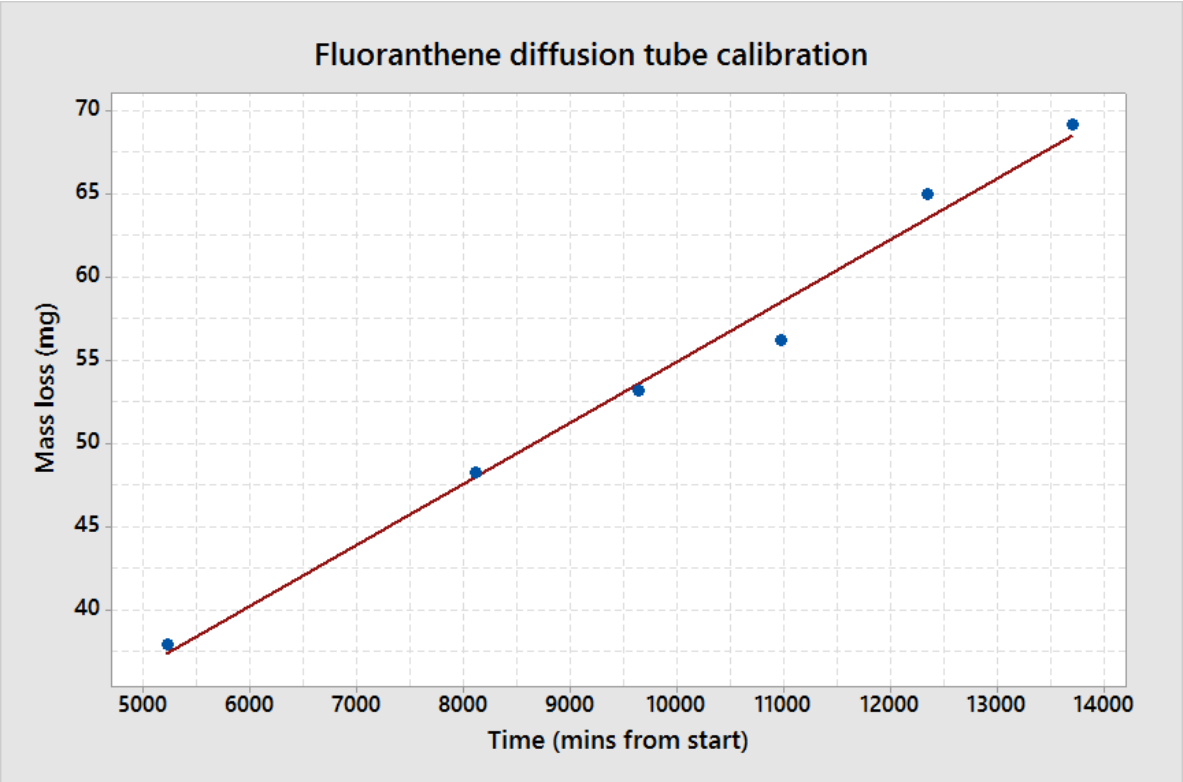

Figure 26 – Linear regression analysis of fluoranthene diffusion tube calibration, using a 2mm diameter and 2cm length capillary bore diffusion tube

The emission rate for the 2mm/2cm tube is 3570 ng/min, which would saturate the signal at a protonated single mass unit during calibration of a PTR-MS, even diluted in the largest carrier gas flow that the thermostat can conveniently manage (4 LPM). The calibration of a wide bore tube is the ideal way to start, as the time between significant mass loss measurements is reduced. A narrower bore tube can be used to produce a lower emission rate based on the calibration of the 2mm/2cm diffusion tube. The emission rate of the narrow bore tube can be calculated from the calibration of the larger bore tube by scaling the reduction based on the new dimensions of the capillary bore.

For the measurements on the PTR-MS, a 0.1mm/8cm capillary bore diffusion tube was used, with a 4-fold reduction in the length and 400-fold reduction in the cross-sectional area of the capillary bore section compared with the 2mm/2cm tube which was calibrated. From this, the emission rate of the 0.1mm/8cm diffusion tube used in chapter 6.7.2 can be calculated to be 2.23 ng/min.

3.5.2 Discussion

The method of generating standard atmospheres of low volatility compounds has been demonstrated with diffusion tube methodology, using high temperature thermostats and transfer lines. This methodology is the basis of the experiment detailed in chapter 6.7.2, where the output of this thermostat is used to assess the ability of the PTR-MS to detect a PAH in ‘ambient’ air (in this case generated in a

standard atmosphere) and to determine linear response of the PTR-MS to the supplied fluoranthene concentration.

Although this method can be used to generate a standard of the PAH used for calibration, it is reasonable to assume that given the low volatility of fluoranthene ($1x10^{-3}$ Pa [45]), there will be an equilibrium between the PAH in the gas phase and the PAH which is moving with the flow down the transfer lines. This is not an issue provided the sample (air, standard etc.) is able to reach the instrument via a heated transfer line, with no cold spots in the transfer of the sample to the instrument. The conditions used for the generation of the dynamic fluoranthene standard which is used for calibration of the PTR-MS in chapter 6 are specific to fluoranthene, but can be optimised for other PAHs.

In chapter 6.7.2 the output of this calibrated tube is used for calibration of a high temperature PTR-MS and to demonstrate the capability of PTR-MS for on-line measurements of fluoranthene.

4 – Detection and Ionisation Mechanisms of Halogenated Compounds - Organochlorides

4.1 Introduction

Halocarbons are defined as compounds containing at least one halogen atom (F, Cl, Br or I), covalently bonded to a hydrocarbon. Halocarbons in the atmosphere are important for many reasons, some have potential for stratospheric ozone depletion [77], others are toxic to humans and other organisms [78] and as greenhouse gases, halocarbons contribute significantly to surface climate change, with an increase in warming of 0.4 K in the last 50 years through halocarbon emission and reactions [79]. Some halocarbons are derived from exclusively anthropogenic origins and others have both anthropogenic and biogenic sources, such as methyl chloride [80].

Atmospheric concentrations of the anthropogenic halocarbons responsible for stratospheric ozone depletion have recently been declining with the introduction and subsequent amendments of the Montreal protocol [81, 82]. Measuring the decline of these compounds in the troposphere and the subsequent reduction in the size of the annual stratospheric ozone holes is important in monitoring the anthropogenic effect on the atmosphere caused by rapid industrialisation of many developed countries. Even 28 years after the agreement first came into force, atmospheric measurement of these compounds is still imperative to monitor the decreasing atmospheric mixing ratios, ensuring the safe disposal of existing stockpiles and to confirm that all countries are abiding by the protocol and its amendments. Despite the introduction of the Montreal protocol, there is evidence

for continued emission for some of these banned compounds, although at a much lower emission rate than before than ban came into force [83].

The Montreal protocol and the subsequent amendments place controls on the most destructive of the ozone depleting halocarbons, which includes many chlorofluorocarbons and organochlorides, such as carbon tetrachloride and 1,1,1-trichloroethane (methyl chloroform). However, regardless of the ability of a compound or its oxidation products to deplete stratospheric ozone, chlorine containing compounds can be toxic, harmful and in some cases, carcinogenic to humans and animals. Many organochlorides that are not controlled by the Montreal protocol have important commercial applications and are produced in vast quantities, such as vinyl chloride for the production of PVC [78]. Other organochlorides with commercial applications include tetrachloroethene, which until recently was commonly used in dry cleaning and as a general solvent [78], trichloroethene which was used as a solvent and degreaser [78] and dichlorodiphenyltrichloroethane which, although currently a controlled pesticide, continues to be used for vector control, limiting the transmission of disease causing pathogens [84]. As a result, monitoring the production, any potential release and atmospheric concentrations are important in both industrial and rural locations.

Some organochlorides such as chloromethane, chloroform and chlorinated ethenes (C_2HCl_3 and C_2Cl_4) are particularly reactive and have an atmospheric lifetime of less than 2 years in the presence of OH radicals [85, 86]. Others are

less reactive and have a longer lifetime (up to 10 years with respect to OH radicals). Regardless of reactivity, these compounds still contribute to the overall atmospheric chlorine compound budget. Although all of the organochlorides have anthropogenic sources, only the most reactive organochlorides appear to have natural sources [86].

4.2 Motivation

Halogenated compounds, such as chlorobenzene and dichlorobenzene, are often used in calibration gases to assist in accurate mass calibration for chemical ionisation mass spectrometers across a large mass range due to their high molecular mass, minimal fragmentation and chlorine isotope pattern, providing multiple peaks to mass calibrate on, which is especially useful in the detection of high mass compounds (m/z > 150). An extensive literature search revealed that publications based on the detection of organochlorides using PTR-MS are limited to the detection of unsaturated organochlorides [87, 88]. Peer reviewed publications on the ion-molecule reactions of hydronium with saturated chlorine containing compounds using PTR-MS could not be found, either as laboratory-based studies, or on field campaigns. In fact, some literature claims that no reaction occurs between the hydronium ion and saturated organochlorides, such as chloroform [89]. This is in contrast to using O_2^+ as a reagent ion, where CCl_2^+ is observed as the product of a charge exchange reaction followed by hydrogen halide elimination of HCl [89].

There has been a significant amount of research on the ionisation of organohalides using the closely related technique SIFT-MS, by Spanel and Smith [44, 90]. As the collisional energy of the ions in the SIFT-MS flow tube (thermal) is less than in a drift tube of a PTR-MS at the standard reduced electric fields, then the product ions in SIFT can be observed as not only the molecular ion, but the molecular ion clustered to hydronium, $M.H_3O^+$. The results from SIFT-MS studies are invaluable in determining rate coefficients that can be used for PTR-MS; however due to the differing energies of the flow vs drift tube, differences in product ions are common (branching ratios and type).

The initial motivation behind this work was to investigate the fragmentation of the chlorinated structural isomers of small halocarbons, to determine if there was any way to quantify isomers without separation. After experiments with the analytical standard TO-15 (detailed in 4.3) and the literature search, it also became apparent that investigating the ion-molecule reactions of hydronium with saturated and unsaturated organochlorides would contribute to our understanding of the ionisation mechanism and hence assist in quantifying structural isomers.

4.3 Initial results with TO-15

The investigation into the ion-molecule reactions of organochlorides started by measuring an environmental gas standard, TO-15, for which standard methods of analysis are detailed and approved by environmental governing bodies such as the US EPA. TO-15 is commonly used to ensure compliance of an instrument and laboratory with the standard method protocols but is also used for determining instrument response (sensitivity) for techniques such as GC-MS using these standard operating procedures.

The TO-15 standard was purchased from Sigma Aldrich and contained 64 compounds, each at a concentration of 1ppm in a balance gas of nitrogen (Full compound list in appendix A). The compounds contained within the TO-15 standard are a mixture of hydrocarbons, organochlorides, halocarbons, structural isomers and isobaric compounds. For analysis using PTR-MS, the mixture was diluted using mass flow controllers to provide a concentration of 200ppb of each compound.

4.3.1 Experimental conditions (TO-15)

For the initial investigation, a general set of PTR-MS conditions were used to gather mass spectra for the TO-15 standard mixture, recording data with both H_3O^+ and O_2^+ reagent ion beams. A drift tube pressure of 1 mbar and a hollow cathode pressure of 1.3 mbar was used, with a drift tube oven temperature of

100°C (which was chosen to minimise any effect on the E/n value due to changes in drift tube temperature from ambient temperature fluctuations). The voltage gradient applied resulted in an E/n of 140 Td (where 1 Td = 10^{-17} V/cm^2). Data was recorded for an experiment time of 60 seconds.

Owing to the large number of compounds in the gas standard, the spectra contained a peak at almost every nominal mass, with some m/z containing several isobaric and isomeric peaks. This complicated the data analysis and as a result, the ions identified could only be tentatively assigned. An example of the spectra used for determination of the product ions and ionisation mechanisms can be seen in figure 27, which demonstrates that the ionisation mechanisms for each of the compounds can only be tentatively inferred from the multi-component gas standard.

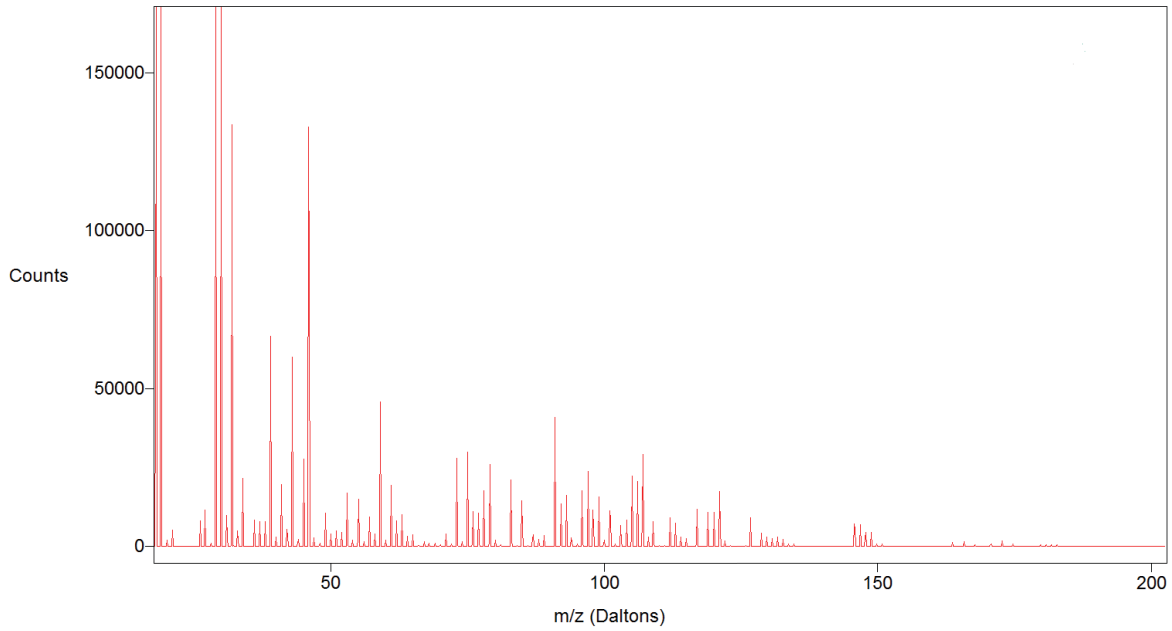

Figure 27 - Spectra of TO-15 (200ppb in nitrogen) using hydronium as the reagent ion, measured for 60 seconds

4.3.2 Results of TO-15 standard

4.3.2.1 Hydronium ionisation of TO-15

The data were analysed and tabulated by increasing number of carbons/halogens, at which point is was observed that some organochlorine species are not detected as the protonated parent ion, but instead protonate and then eliminate HCl (without any observation of the protonated parent ion).

A trend was observed where depending on the location of the chlorine on the molecule and the bonding regime of the nearest carbon, there appeared to be a defined and predictable ionisation relationship whereby the protonated parent molecule or the loss of HCl from the protonated molecule occurs (the full list of tentatively assigned ionisation mechanisms is shown in table 6). This data was extracted from the mass spectrum in figure 27, determining the potential product ions for each compound (MH^+ or $M\text{-}Cl^+$) and whether they were observed in the mass spectrum. Within this study it was hypothesised that in an organochloride, where the chlorine atom is directly attached to a saturated carbon, the chlorine is lost as HCl, whereas when the chlorine is attached to an unsaturated carbon the molecule appears to protonate.

The tentative identification of the method of ionisation of the compounds in the TO-15 mix are shown in table 7.

Table 7 - Tentative identification of ionisation method for compounds in the gas standard TO-15 using hydronium as the reagent ion, ordered by increasing number of carbons.

Compound	Structure	Tentatively assigned method of Ionisation ($+H^+$ or –HCl)
Trichloro methane		M-HCl
Carbon Tetrachloride		M-HCl
Dichlorobromo methane		M-HCl
Dibromochloro methane		M-HCl
1,1 – Dichloro ethene	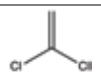	MH^+
1,1,1-Trichloro ethane		M-HCl
Trichloro ethylene	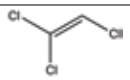	MH^+
Tetrachloro ethene		MH^+
1,1,2,2-Tetrachloro ethane	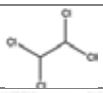	M-HCl
Trans-1,3-dichloro propene		M-HCl
1,2-Dichloro propane	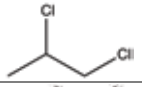	M-HCl
Hexachloro1,3-Butadiene	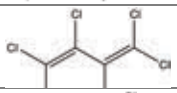	MH^+
Chlorobenzene	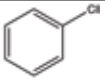	MH^+
1,2-Dichlorobenzene	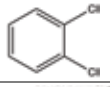	MH^+
1,2,4-Trichlorobenzene	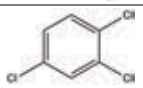	MH^+
Benzyl Chloride	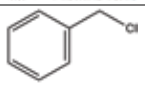	M-HCl

In TO-15, this difference is perhaps best demonstrated with the molecule benzyl chloride (shown in figure 28); in which the loss of HCl is observed. Despite the unsaturated, aromatic nature of the benzene ring, on ionisation the chlorine is lost, which suggests that the bonding regime of the atom that is directly bonded to the chlorine is an important factor in the ionisation relationship.

Furthermore, this mechanism seems to proceed for many molecules in the TO-15 mixture as either 100% protonation or 100% HCl loss. The number of isobaric and isomeric compounds in TO-15 made this analysis difficult and therefore these ionisation mechanisms are only assigned tentatively. Equations 23 and 24 show the proposed overall mechanisms for ionisation of saturated and unsaturated organochlorines with hydronium as the reagent ion.

$$\mathrm{H_3O^+} + \mathrm{Sat\ Organochloride} \rightarrow \mathrm{MH^+} + \mathrm{H_2O} \quad (23)$$

$$\mathrm{H_3O^+} + Unsat\ Organochloride \rightarrow [M - Cl]^+ + HCl + \mathrm{H_2O} \quad (24)$$

The literature on the detection of chlorinated compounds by PTR-MS gives mixed information on which compounds are protonated or lose HCl or whether these ionisation mechanisms had been observed before in PTR-MS [44, 89-91]. This was supported by the lack of and inconclusive literature of protonation of saturated chlorinated compounds, such as chloroform and carbon tetrachloride [89, 92].

However, other sources such as “Ion/Molecule Attachment Reactions: Mass Spectrometry” by Fujii (2015) demonstrate the loss of HCl from chloroform using hydronium as the reagent ion in PTR-MS, in order to compare the energy difference in flow vs drift tube [91].

4.3.2.2 O_2^+ Ionisation of TO-15

As for the hydronium ionisation, the data for the reaction of O_2^+ with TO-15 were analysed through predicting the possible product ions, predominantly M^+ or $M\text{-}Cl^+$ and examining the mass spectrum shown in figure 29 for the possible ion species for each compound.

The mass spectrum was complex as was the case with hydronium, so identification of the ionisation mechanism was tentative again. An example spectrum of TO-15 ionised with O_2^+ is shown in figure 29, showing a peak at almost every nominal mass.

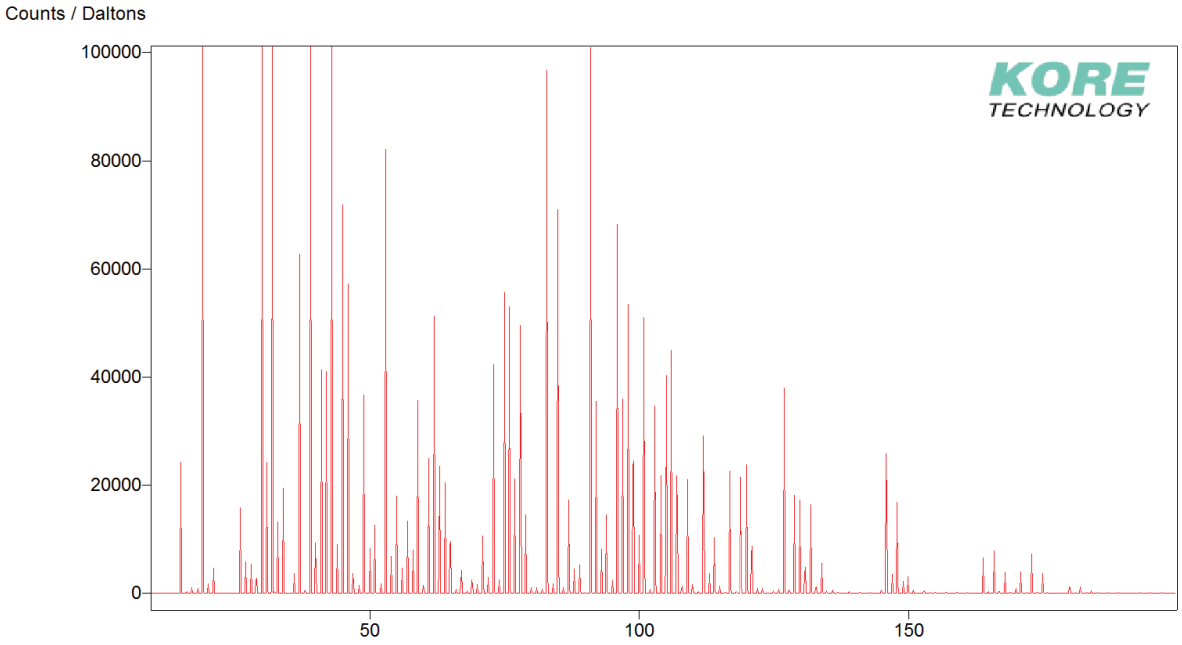

Figure 29 - Spectra of TO-15 (200ppb in nitrogen) using O_2^+ as the reagent ion, measured for 60 seconds

The tentative identification of the ionisation mechanisms are shown in table 8, with the structure of each compound.

Table 8 - Tentative identification of ionisation method for compounds in the gas standard TO-15 using O_2^+ as the reagent ion, ordered by increasing number of carbons.

Compound	Structure	Method of ionisation (Cl loss or charge exchange)
Dichloromethane		Cl loss
Chloroform	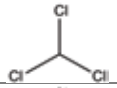	Cl loss
Carbon Tetrachloride	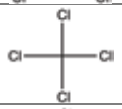	Cl loss
Dichlorodifluoromethane	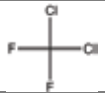	Cl loss
Dichlorobromomethane	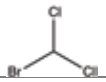	Cl loss
1,1 and 1,2 Dichloroethane		Cl loss
1,1 1,2 cis and 1,2 trans Dichloroethene		Charge exchange
Tetrachloroethene	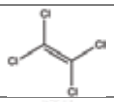	Charge exchange
Cis and trans 1,3 Dichloropropene	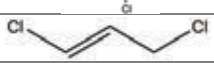	Cl loss
Chlorobenzene	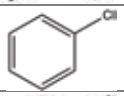	Charge exchange
1,2,4 Trichlorobenzene	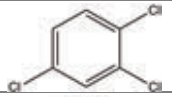	Charge exchange
Benzyl Chloride	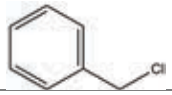	Cl loss

Several curious results have arisen from the tentative identification, including the loss of chlorine from compounds containing chlorine and other halogens (fluorine or bromine). To make sense of the initial identification of the ions in the gas mixture, single compounds from the TO-15 toxic environmental gas standards were analysed to determine product ion distributions and ionisation mechanisms for the individual compounds.

4.4 Single compound analysis

Following on from the tentative identification of the ionisation method of organochlorides in the TO-15 mixture (full compound list in Appendix A) using both hydronium and O_2^+ as the reagent ion, a selection of organochlorides were investigated individually in an attempt to provide evidence to support the hypothesis and quantify the different ionisation methods, including several isomeric compounds.

The compounds chosen for this single compound analysis study were in the TO-15 mixture originally investigated, isomeric compounds that may fragment or ionise differently, compounds that have been investigated by other similar techniques to PTR-MS [93] or those which were strictly relevant to air pollution chemistry (such as the restrictions by the Montreal protocol) [82].

4.4.1 Experimental

For the single compound analysis, Teflon bags were used to produce individual gas standards. Although Teflon bags can suffer from contamination at certain masses (usually m/z 88 and 95, dimethyl acetamide and phenol respectively), for the purposes of these tests, they provided a suitable, easy way of preparing a gas standard. For these experiments, the concentration of the organochloride in the standard was unimportant, provided the concentration in the bag was high enough to be detected but low enough to not saturate the ion counting system. Significant

care was taken to ensure that the Teflon bag chosen for each compound had no contamination at the masses expected for protonation or HCl loss. In the case where there was contamination at m/z 88 or 95 that could interfere with an expected peak, an alternative method of gas standard generation was used by creating a gas standard with a diffusion tube (see section 3.3.2).

Prior to measurement of the organochloride gas sample, a background (nitrogen only) E/n study was measured to provide a measurement at each E/n for subtraction and to ensure that the bag was not contaminated at the expected masses. This is important during the data analysis, when subtraction of the nitrogen background signal removes any significant interferences from bag contaminants.

4.4.1.1 Preparation of gas standards

To prepare the standard, 0.1 μL of the pure compound was added to a 10 L Teflon bag filled with oxygen free nitrogen (99.999%, BOC, UK) and further diluted to achieve an approximate concentration of 1ppm. This was connected to the PTR-MS via a PTFE tube to check for saturation by monitoring the peak integrals for the protonation and HCl loss peaks against the number of cycles. In cases where any of the product ion peaks were saturated (count rate per second > 60% of the number of cycles/second), 200ml of gas was removed from the Teflon bag and refilled with ultrapure nitrogen. This process was repeated until the compound was not saturated with respect to the pulse counting system.

4.4.1.2 Organochlorides Investigated

Some common small organochlorides, selected aromatic organochlorides, isomeric organochlorides and organochlorides from the Montreal protocol were investigated individually to determine the mechanism of ion molecule reaction for each compound and any additional fragmentation of each compound (for example protonation followed by loss of HCl etc.). A full list of compounds investigated is shown in table 9, with the predicted ionisation mode, formatted by increasing carbon number.

A key set of isomers were chosen that would provide key information on the ionisation mechanism, 2-chloropropene and 3-chloropropene. Despite being isomers, if the results observed in the preliminary investigation apply to all organochlorides, then the ions produced from these isomers will be at different m/z, providing a method of quantifying organochloride isomers without chromatographic separation.

Table 9 – Compounds investigated in the single bag analysis study, ordered by increasing carbon number. All compounds supplied by Sigma Aldrich (UK).

Name	Structure	Predicted Ionisation mode H_3O^+ O_2^+	Compound Purity
Chloroform-d	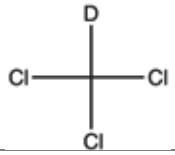	Loss of HCl/DCl Loss of Cl	99.8 atom % D
Carbon tetrachloride	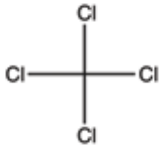	Loss of HCl Loss of Cl	99.5+%
Pentachloroethane	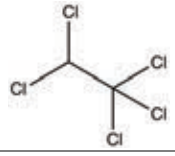	Loss of HCl Loss of Cl	95%
2-Chloropropene	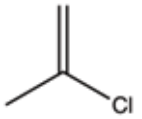	Protonation Charge exchange	98%
3-Chloropropene	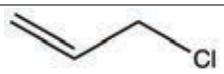	Loss of HCl Loss of Cl	(Analytical standard)
2,2-Dichloropropane		Loss of HCl Loss of Cl	98%
Chlorobenzene	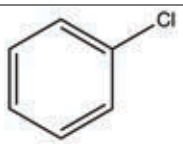	Protonation Charge exchange	99.8%
1,2-Dichlorobenzene	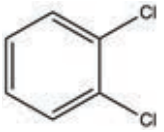	Protonation Charge exchange	99.9%

4.4.1.3 Experimental procedure

An E/n study was run for each of the individual organochlorides chosen, taking a mass spectrum in 10 Td steps from 80-200 Td (where PTR entry voltage allowed) with a drift tube pressure of 1mbar, a hollow cathode pressure of 1.3 mbar and an oven temperature of 100 °C. At each E/n, a 10 second measurement (equivalent to 300,000 cycles) was taken for background and sample giving a measurement per setting of electric field strength.

The data were extracted for the bag background spectra and the sample bag spectra, which was normalised and background subtracted. The ions produced for each organochloride were identified and a branching ratio graph plotted for each compound, which shows the percentage of parent ion and fragment ions at different E/n values, with the sum of the parent ion and fragment ions totalling 100%. This is represented schematically in figure 30.

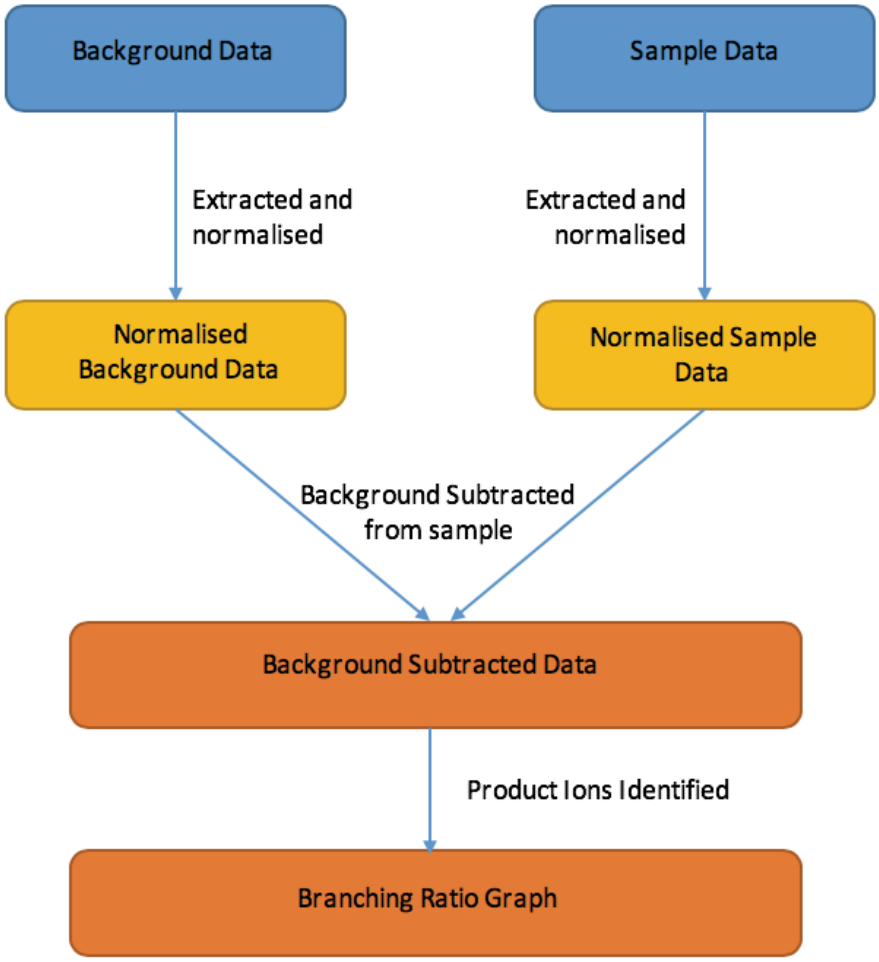

30 - Flow chart showing the data processing steps

4.4.2 Branching ratio results

The product ion graphs for the individual compounds analysed are contained within appendix B. The structure of the molecule and the corresponding product ion branching ratio results have been summarised for a low-moderate electric field setting (120 Td) and a high electric field setting (200 Td) using H_3O^+ (table 10) and O_2^+ (table 11) as the reagent ion in PTR-MS.

Table 10 – Product ion distributions of individual chlorocarbons for the reaction with H_3O^+ at low (120Td) and high (200Td) E/n. The percentage of product ion is given in brackets; the assumed neutral loss is given in square brackets. The DFT calculations shown here in columns 5 and 6 were performed by Peter Watts.

Compound	Structure	H_3O^+ Product ions (120Td)	H_3O^+ Product ions (200Td)	Calcs protonation (kJ mol^{-1})	Calcs HCl loss (kJ mol^{-1})	Expected observation	Comment on structure following protonation
Chloroform-d $CDCl_3$		**$CDCl_2^+$** (100) [HCl + H_2O]	**$CDCl_2^+$** (100) [HCl + H_2O]	ΔH = +25 ΔG = +8	ΔH = +46 ΔG = +2	$CDCl_2^+$	Formation of HCl almost complete
Carbon Tetrachloride CCl_4		**CCl_3^+** (100) [HCl + H_2O]	**CCl_3^+** (100) [HCl + H_2O]	-	-	-	-
1,1,2-Trichloroethane $CHCl_2CH_2Cl$	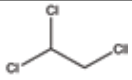	**$CHCl_2CH_2Cl.H^+$** (4) [H_2O] **$CHCl_2CH_2OH_2^+$** (2) [HCl] **$CHCl_2CH_2^+$** (16) [HCl + H_2O] **$CHClCHOH_2^+$** (78) [2HCl]	**$CHCl_2CH_2OH_2^+$** (2) [HCl] **$CHCl_2CH_2^+$** (12) [HCl + H_2O] **$CHClCHOH_2^+$** (64) [2HCl] **$CHClCH^+$** (3) [2HCl + H_2O] **$CHCOH_2^+$** (20) [3HCl]	-	-	-	-
Pentachloroethane $CHCl_2CCl_3$	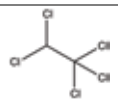	**$CCl_2CHCl_2^+$** (95) [HCl + H_2O] **CCl_2CCl^+** (5) [2HCl + H_2O]	**$CCl_2CHCl_2^+$** (32) [HCl + H_2O] **CCl_2CHCl^+** (40) [HCl + Cl + H_2O] **CCl_2CCl^+** (23) [2HCl + H_2O] **$C_2Cl_2^+$** (5) [2HCl + Cl + H_2O]	-	-	-	-
Hexachloroethane CCl_3CCl_3	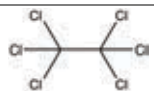	**$CCl_3CCl_2^+$** (39) [HCl + H_2O] **CCl_3CClOH^+** (5) [2HCl + H_2O + H_2] **CCl_2ClO^+** (2) [3HCl] **$CHClCClO_2^+$** (1) [4HCl] **CCl_3^+** (53) [$CHCl_3$ + H_2O]	**$CCl_3CCl_2^+$** (52) [HCl + H_2O] **CCl_3CClOH^+** (1) [2HCl + H_2O + H_2] **$CCl_2CCl_2^+$** (15) [2HCl + 2H_2O] **CCl_2CClO^+** (1) [3HCl] **$CHClCClO_2^+$** (1) [4HCl] **CCl_3^+** (30) [$CHCl_3$ + H_2O]	-	-	-	-
1,2-Dichloropropane $CH_3CHClCH_2Cl$	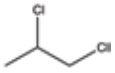	**$CH_3CHClCH_2^+$** (17) [HCl + H_2O] **$CH_2CHCH_2^+$** (83) [2HCl + H_2O]	**$CH_3CHClCH_2^+$** (9) [HCl + H_2O] **$CH_2CHCH_2^+$** (45) [2HCl + H_2O] **CH_2CHC^+** (46) [2HCl + H_2O + H_2]	-	-	-	-
2,2-Dichloropropane $CH_3CCl_2CH_3$		**$CH_3CClCH_3^+$** (100) [HCl + H_2O]	**$CH_3CClCH_3^+$** (57) [HCl + H_2O] **$CH_3CCH_2^+$** (28) [2HCl + H_2O] **$CHCCH_2^+$** (15) [2HCl + H_2O + H_2]	ΔH = -60 ΔG = -88	ΔH = -47 ΔG = -96	$CH_3C^+ClCH_3$	Formation of HCl almost complete
1-Chloropentane $C_5H_{11}Cl$		**$C_5H_{11}^+$** (100) [HCl + H_2O]	**$C_5H_{11}Cl.H^+$** (2) [H_2O] **$C_5H_{11}^+$** (98) [HCl + H_2O]	-	-	-	-
Benzyl Chloride $C_6H_5CH_2Cl$	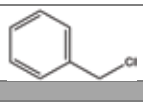	**$C_6H_5CH_2ClH^+$** (1) [H_2O] **$C_6H_5CH_2^+$** (99) HCl + H_2O)	**$C_6H_5CH_2ClH^+$** (1) [H_2O] **$C_6H_5CH_2^+$** (99) HCl + H_2O)	-	-	-	-
Trans-1,2-dichloroethene CHClCHCl		**$CHClCHCl.H^+$** (18) [H_2O] **$CHClCHOH_2^+$** (82) [HCl]	**$CHClCHCl.H^+$** (68) [H_2O] **$CHClCHOH_2^+$** (17) [HCl] **$CHClCH^+$** (15) [HCl + H_2O]	ΔH = +1 ΔG = +1	-	-	$CH_2ClCHCl^+$ - same result from cis isomer
2-Chloropropene $CH_3CCl{=}CH_2$		**$CH_3CCl{=}CH_2.H^+$** (92) [H_2O] **$CH_3C{=}CH_2OH_2^+$** (8) [HCl]	**$CH_3CCl{=}CH_2.H^+$** (58) [H_2O] **$CH_3C{=}CH_2OH_2^+$** (3) [HCl] **$CH_3C{=}CH_2^+$** (39) [HCl + H_2O]	ΔH = -97 ΔG = -101	-	MH^+	Protonation of Cl not favoured so less HCl loss observed than 3-chloropropene
3-Chloropropene $CH_2{=}CHCH_2Cl$	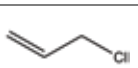	**$CH_2{=}CHCH_2Cl.H^+$** (3) [H_2O] **$CH_2{=}CHCH_2^+$** (97) [HCl + H_2O]	**$CH_2{=}CHCH_2Cl.H^+$** (4) [H_2O] **$CH_2{=}CHCH_2^+$** (96) [HCl + H_2O]	ΔH = -31 ΔG = -34	-	$CH_2CHCH_2^+$	Protonation on Cl and C1 favourable leading to HCl loss
Chlorobenzene C_6H_5Cl	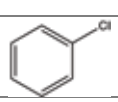	**$C_6H_5Cl.H^+$** (99) [H_2O] **$C_6H_5OH_2^+$** (1) [HCl]	**$C_6H_5Cl.H^+$** (59) [H_2O] **$C_6H_5^+$** (35) [H_2O + HCl] **$C_6H_5OH_2^+$** (6) [HCl]	-	-	-	-
1,2-Dichlorobenzene $C_6H_4Cl_2$	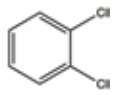	**$C_6H_4Cl_2.H^+$** (99) [H_2O] **$C_6H_4Cl^+$** (1) [HCl + H_2O]	**$C_6H_4Cl_2.H^+$** (21) [H_2O] **$C_6H_4Cl^+$** (67) [H_2O + HCl] **$C_6H_4^+$** (12) [H_2O + HCl + Cl]	ΔH = -62 ΔG = -63	-	MH^+	Protonation on both 3 and 4 ring carbons similar
1,2,4-Trichlorobenzene $C_6H_3Cl_3$	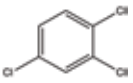	**$C_6H_3Cl_3.H^+$** (100) [H_2O]	**$C_6H_3Cl_3.H^+$** (51) [H_2O] **$C_6H_4Cl_2^+$** (19) [Cl + H_2O] **$C_6H_3Cl_2^+$** (27) [HCl + H_2O] **$C_6H_2Cl^+$** (3) [2HCl + H_2O]	-	-	-	-

Table 11 - Product ion distributions of individual chlorocarbons for the reaction with O_2^+ at low (120Td) and high (200Td) E/n. The percentage of product ion is given in brackets; the assumed neutral loss is given in square brackets.

Compound	Structure	O_2^+ Product ions (120Td)	O_2^+ Product ions (200Td)
Chloroform-d **$CDCl_3$**	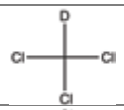	**$CDCl_2^+$** (100) [ClO_2]	**$CDCl_2^+$** (100) [ClO_2]
Carbon Tetrachloride **CCl_4**	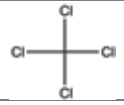	**CCl_3^+** (100) [ClO_2]	**CCl_3^+** (100) [ClO_2]
1,1,2-Trichloroethane **$CHCl_2CH_2Cl$**	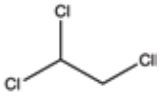	**$CHClCClH_2^+$** (12) [ClO_2] **$CHClCHCl^+$** (46) [HCl + O_2] **$CHCl_2^+$** (38) [$CH_2Cl + O_2$] **$CClO_2^+$** (4) [CCl_2H_3]	**$CHClCClH_2^+$** (30) [ClO_2] **$CHClCHCl^+$** (30) [HCl + O_2] **$CHCl_2^+$** (40) [$CH_2Cl + O_2$]
Pentachloroethane **$CHCl_2CCl_3$**	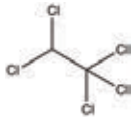	**$CCl_2CHCl_2^+$** (41) [ClO_2] **CCl_3^+** (52) [$CHCl_2 + O_2$] **$CHCl_2^+$** (6) [$CCl_3 + O_2$]	**$CCl_2CHCl_2^+$** (37) [ClO_2] **CCl_2CHCl^+** (4) [Cl_2O_2] **CCl_2CCl^+** (3) [HCl + ClO_2] **CCl_3^+** (49) [$CHCl_2 + O_2$] **$CHCl_2^+$** (7) [$CCl_3 + O_2$]
Hexachloroethane **CCl_3CCl_3**	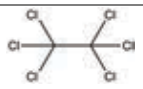	**$CCl_3CCl_2^+$** (55) [ClO_2] **CCl_3^+** (45) [$CCl_3 + O_2$]	**$CCl_3CCl_2^+$** (39) [ClO_2] **$CCl_2CCl_2^+$** (20) [$2ClO_2$] **CCl_3^+** (41) [$CCl_3 + O_2$]
1,2-Dichloropropane **$CH_3CHClCH_2Cl$**	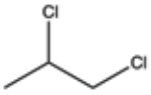	**$CH_3CHClCH_2Cl^+$** (1) [O_2] **$CH_3CHClCH_2^+$** (6) [ClO_2] **$CH_3CHClCH^+$** (29) [HCl + O_2] **CH_3CHCCl^+** (32) [$CH_2Cl + O_2$] **CH_2CHCCl^+** (32) [$CH_3Cl + O_2$]	**$CH_3CHClCH_2^+$** (5) [ClO_2] **$CH_3CHClCH^+$** (19) [HCl + O_2] **CH_3CHCCl^+** (32) [$CH_2Cl + O_2$] **CH_2CHCCl^+** (44) [$CH_3Cl + O_2$]
2,2-Dichloropropane **$CH_3CCl_2CH_3$**		**$CH_3CHClCH_2Cl^+$** (1) [O_2] **$CH_3CHClCH_2^+$** (99) [ClO_2]	**$CH_3CHClCH_2^+$** (66) [ClO_2] **CH_3CHCH^+** (44) [HCl + ClO_2]
Trans-1,2-dichloroethene **CHClCHCl**		**CHClCHCl$^+$** (99) [O_2] **CHClCH$^+$** (1) [ClO_2]	**CHClCHCl$^+$** (92) [O_2] **CHClCH$^+$** (8) [ClO_2]
2-Chloropropene **$CH_3CCl{=}CH_2$**	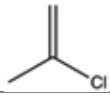	**$CH_3CCl{=}CH_2^+$** (85) [O_2] **$CH_3C{=}CH_2^+$** (15) [ClO_2]	**$CH_3CCl{=}CH_2^+$** (22) [O_2] **$CH_3C{=}CH_2^+$** (26) [ClO_2] **$CH_3C{=}C^+$** (52) [$ClO_2 + H_2$]
3-Chloropropene **$CH_2{=}CHCH_2Cl$**	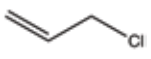	**$CH_2{=}CHCH_2Cl^+$** (52) [O_2] **$CH_2{=}CHCH_2^+$** (47) [Cl + O_2] **$CH_2{=}CHC^+$** (1) [$ClO_2 + H_2$]	**$CH_2{=}CHCH_2Cl^+$** (6) [O_2] **$CH_2{=}CHCH_2^+$** (20) [Cl + O_2] **$CH_2{=}CHC^+$** (74) [$ClO_2 + H_2$]
Chlorobenzene **C_6H_5Cl**	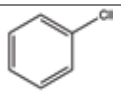	**$C_6H_5Cl.H^+$** (99) [O_2] **$C_6H_5OH_2^+$** (1) [HCl]	**$C_6H_5Cl.H^+$** (59) [O_2] **$C_6H_5^+$** (35) [ClO_2] **$C_6H_5OH_2^+$** (6) [ClO_2]
1,2-Dichlorobenzene **$C_6H_4Cl_2$**	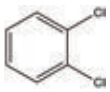	**$C_6H_4Cl_2.H^+$** (99) [O_2] **$C_6H_4Cl^+$** (1) [ClO_2]	**$C_6H_4Cl_2.H^+$** (21) [O_2] **$C_6H_4Cl^+$** (67) [ClO_2] **$C_6H_4^+$** (12) [ClO_2 + Cl]
1,2,4-Trichlorobenzene **$C_6H_3Cl_3$**	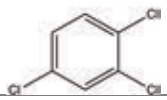	**$C_6H_3Cl_3^+$** (100) [O_2]	**$C_6H_3Cl_3^+$** (100) [O_2]

The individual compound results shown in tables 10 and 11 agree with the data extracted from TO-15 and indicate that for 93% compounds investigated here, the predicted ionisation mechanism is applicable. At higher E/n some of the compounds that protonate (unsaturated organochlorides) also fragment to lose HCl. This follows the understanding that the excess energy involved in ionisation must be dissipated, with a higher degree of fragmentation at increasing reduced electric field strength and therefore the increasing collisional energy.

4.5 Discussion

The results from tables 10 and 11 show the product ions for the reactions of H_3O^+ and O_2^+ with organochlorides. From the product ion branching ratios and the ions produced, the ionisation mechanism can be inferred. There are 3 main ionisation mechanisms that occur with organochlorides, dependent on the structure of the compound.

Many of the organochlorides undergo protonation or charge exchange similar to VOCs, producing MH^+ or M^+. Some of the organochlorides investigated undergo loss of Cl following protonation, leaving $[M\text{-}Cl]^+$. The results from the single compound analysis demonstrate that a third mechanism also occurs, where the substitution of Cl for OH_2^+ is observed in the presence of H_3O^+. The third mechanism is not observed when using O_2^+ as the reagent ion (due to the lack of H_2O). In these conditions, O_2 is not incorporated into the molecule.

Literature on the ionisation of organochlorides using similar techniques such as SIFT-MS have reported some of the mechanisms observed here, on a limited study of organochlorides, such as chloromethanes, chloroethane and chloroethenes [44, 90]. However, when comparing the ionisation mechanisms of organochlorides in the literature for SIFT and PTR-MS in this study, there are discrepancies between the ions produced for a given molecule, where the energy difference from the reduced electric field applied to the drift tube vs flow tube is influential in the ionisation mechanisms that occur.

An example of this is the molecule chloroform, which in SIFT produces the protonated cluster ion ($H_3O^+.CHCl_3$), whereas in PTR-MS, produces a product ion from the loss of Cl, $CHCl_2^+$. For this reason, it is useful to understand the product ions formed from these compounds within the PTR-MS (which is more commonly deployed for atmospheric science measurements than SIFT).

4.5.1 Ionisation mechanisms

Although some of the ionisation mechanisms have previously been reported using SIFT, an explanation of each mechanism will be given, including experimental and theoretical evidence for why the mechanism is observed in PTR-MS, for which compounds these mechanisms apply and why the product ions may be different to the observed product ions in SIFT-MS.

4.5.2 Protonation / Charge Exchange

As expected, some organochlorides undergo proton transfer (with H_3O^+) and charge exchange (with O_2^+). The compounds that tend to protonate are those with a chlorine atom bonded to a carbon which has a double bond (sp^2 hybridised), such as chlorobenzene (figure 31) and 2-chloropropene. The expected mechanism for this ionisation is protonation onto the carbon atom.

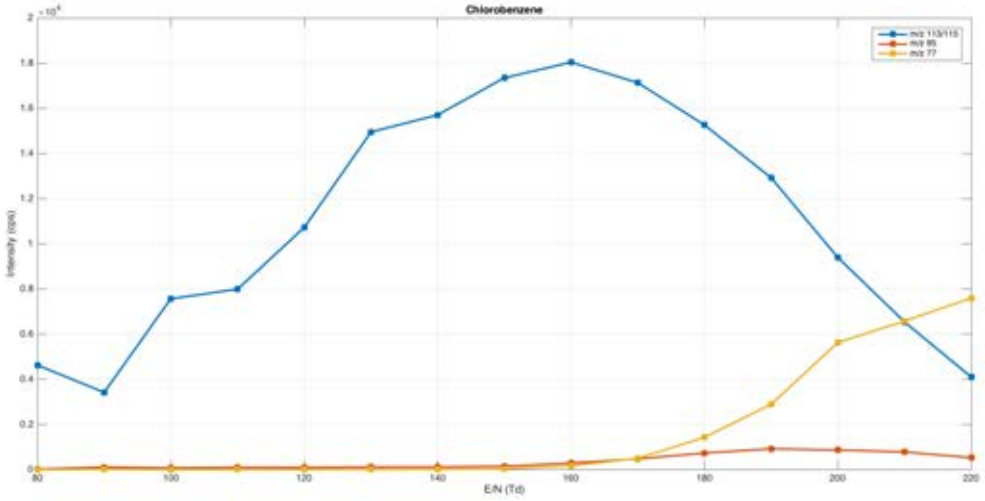

Figure 31 - Chlorobenzene intensity as a function of electric field strength (E/n), data normalised and background subtracted. The ions at m/z 113/115 are the result of protonation of chlorobenzene and is dominant between 80-200Td.

The bond dissociation energy of the C=**C-Cl** bond is high (≈ 400 kJ mol^{-1}, 399.6 kJ mol^{-1} for chlorobenzene) for the compounds where protonation is observed as the dominant product ion. For this reason, these molecules only tend to produce fragment ions showing the loss of HCl at high E/n, where the average collisional energy in the PTR-MS system is greater and the energy available is sufficient to break the C-Cl bond causing fragmentation of the parent ion.

For organochlorides that protonate such as chlorobenzene and 1,2-dichlorobenzene, a shift in dominant ionisation mechanism observed from protonation to HCl loss as the reduced electric field strength is increased.

4.5.3 Loss of HCl / ClO_2

Some of the organochlorides investigated lose HCl on ionisation during reaction with H_3O^+ or O_2^+. Some of these product ions have been reported before using SIFT [44]; however for some compounds such as chloroform, the product ions produced in SIFT and PTR-MS are different. For this reason, it is important to establish the product ions produced in PTR-MS, the mechanism and a theoretical understanding of the product ions produced.

Determination of the predicted ionisation mechanism can be aided by measurement of deuterated compounds. When investigating chloroform-d with H_3O^+ as the reagent ion, the product observed is the loss of HCl, rather than the loss of DCl. This shows that the proton from the hydronium is the one that is lost as HCl, rather than a proton from the molecule.

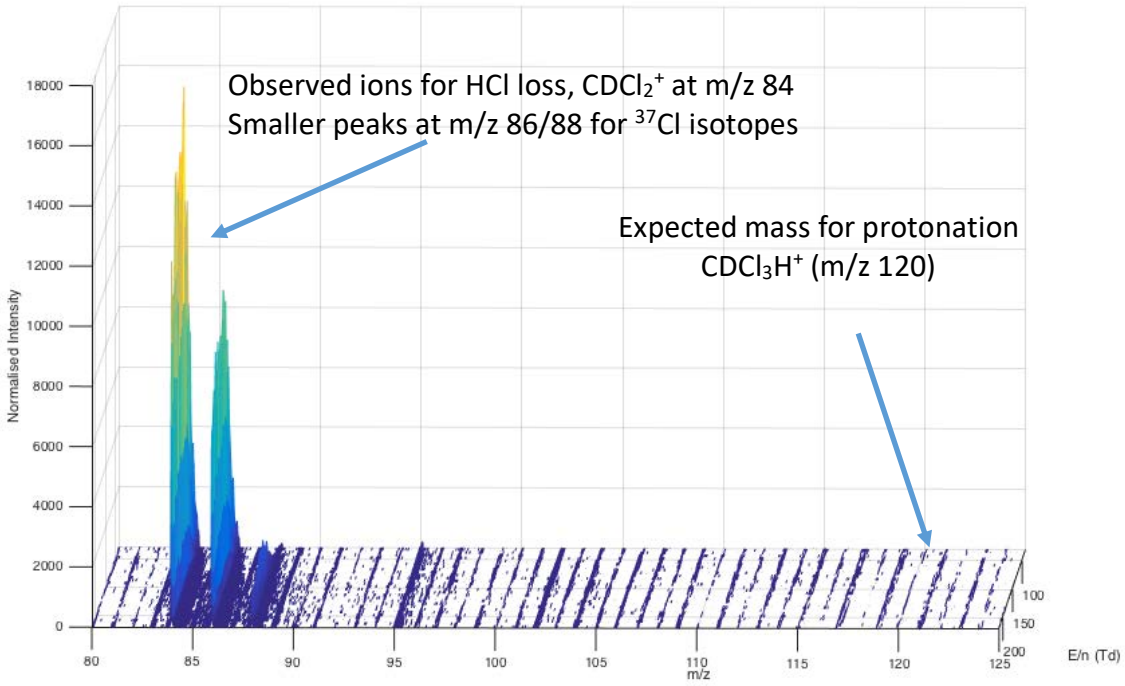

Figure 32 - Mass spectra at multiple E/n values for the ionisation of chloroform-d. The $CDCl_2^+$ ion (including isomers are formed from the ionisation of chloroform-d using hydronium as the reagent ion. Protonation of this molecule would result in ions at m/z 120 which are not observed.

The mass spectra showing chloroform-d at different E/n values (figure 32) demonstrates that for chloroform-d regardless of E/n (within the range investigated), the production of the ion $CDCl_2^+$ is dominant. This is similar for many of the organochlorides that undergo hydrogen halide elimination, with the loss of HCl on protonation.

This suggests that the reaction proceeds via protonation onto an electronegative atom (in this case chlorine), forming a [R-C-Cl^+-H] ion which can then fragment, forming an ion and the neutral molecule HCl. If the protonation was on the carbon atom of chloroform with subsequent elimination of Cl, a mixture of HCl and DCl loss would be expected with a mixture of product ions detected.

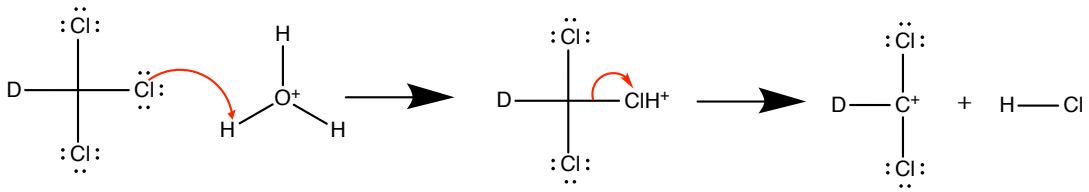

Figure 33 - Proposed mechanism of ionisation for saturated organochlorides when using hydronium as the reagent ion, example shown using Chloroform-d.

This mechanism allows exclusive elimination of HCl rather than DCl or a mixture of the two. The suggestion is that this mechanism of ionisation occurs in both saturated and unsaturated organochlorides and the difference in the product ions observed is due to the bond dissociation energy of C-Cl in the specific molecule, which would determine if the molecule is detected as the protonated ion, or fragments on ionisation losing HCl.

The bond dissociation energy for the C-Cl bond for those compounds that efficiently lose HCl on ionisation is much lower (BDE C-**C-Cl** ≈ 300 kJ Mol^{-1}) than the BDE for compounds that protonate (BDE C=**C-Cl** ≈ 400 kJ Mol^{-1}). A comprehensive list of BDEs taken from the literature for the compounds examined in this study is given in table 12. This suggests that even with low reduced electric fields, the energy in the PTR-MS drift tube is sufficient to cause the C-Cl bond to break, resulting in only product ions from the loss of HCl.

When using O_2^+ as the reagent ion, a similar ionisation mechanism to using hydronium is observed, with the loss of ClO_2 (or some association of Cl and O_2), rather than HCl. This was determined using chloroform-d, which produces ions at

m/z 84/86/88, corresponding to $CDCl_2^+$ and the ^{37}Cl isotopes. It cannot be determined if the Cl and O_2 are bonded, associated or non-covalently bonded using this method.

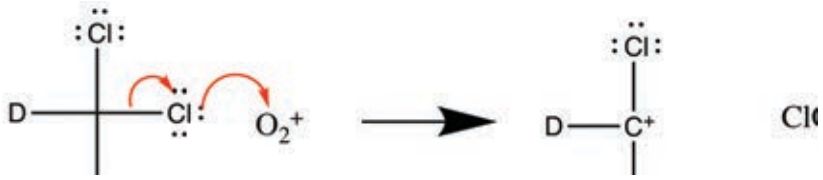

Figure 34 - Proposed mechanism of ionisation for saturated organochlorides when using O_2^+ as the reagent ion, example shown using chloroform-d.

Some of the compounds that lose HCl upon ionisation also display the loss of a second HCl from the molecule at higher E/n values. This behaviour is observed with 2,2-dichloropropane at reduced electric field strengths > 140 Td. At 200 Td, the product ion $[M\text{-}Cl]^+$ ion is most abundant (57%), but also loses a second HCl (28%) and subsequently H_2 (15%) which is common in mass spectrometry. However, the loss of a second molecule of HCl is only observed with compounds that have hydrogen atoms in the molecule as expected. The fragmentation of the molecule is derived from the structure and the initial ionisation reaction with organochloride compounds such as carbon tetrachloride not able to exhibit this additional ionisation/rearrangement.

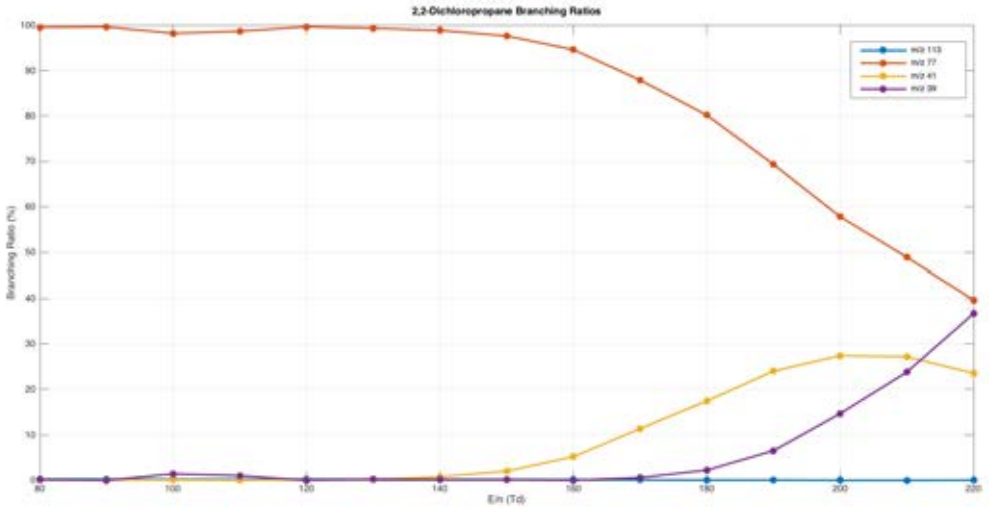

Figure 35 - Branching ratios of ions associated with 2,2-dichloropropane, showing the loss of Cl (m/z 77), loss of 2HCl (m/z 41) and the loss of 2HCl and H_2 (m/z 39).

4.5.4 Addition of H_2O and elimination of HCl

The exact mechanism for the addition of H_2O whilst losing HCl cannot yet be determined however, from experimental data some interesting mechanistic data can be extracted. Trans-1,2-dichloroethene is a compound studied here for which the addition of H_2O and elimination of HCl is a major product ion over the E/n range investigated. A discussion of the ions produced, the mechanism of production and how the reduced electric field allowed the extraction of mechanistic data.

4.5.4.1 Trans-1,2-Dichloroethene

Trans-1,2-dichloroethene has limited uses in industry but is often produced as by-product in the manufacture of organochlorides, although this can be used for production of trichloroethene and tetrachloroethene [78]. Previous work using SIFT-MS has shown that when ionised using the hydronium ion, trans-1,2-chloroethene produces a mixture of product ions [93].

Initial results of this work pointed towards a mixture of protonation and loss of HCl. On analysing the mass spectra, there were additional ions observed at m/z 79 and 81 in a 3:1 ratio, characteristic of an ion containing a single chlorine atom. The branching ratios of the product ions were plotted for a range of E/n values.

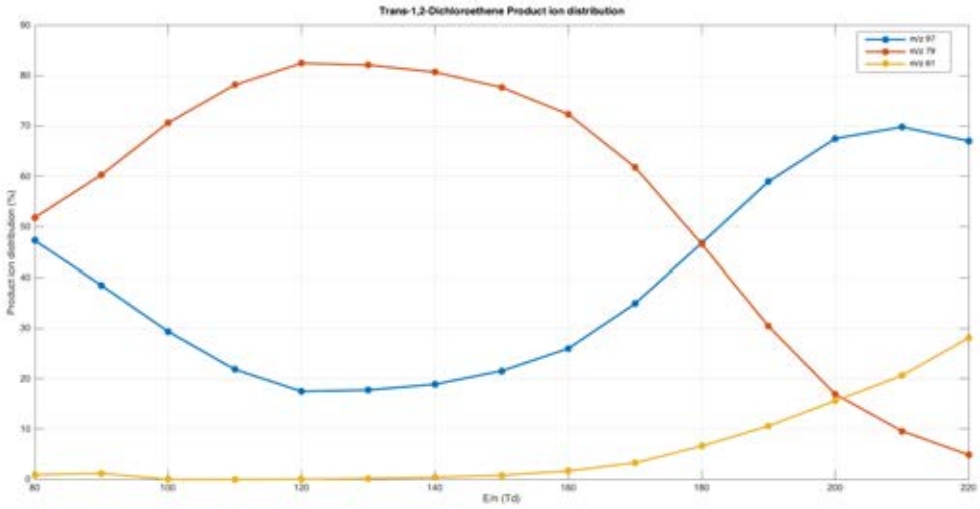

Figure 36 - Branching ratios of ions associated with trans-1,2-dichloroethene for a range of E/n values. Ions containing chlorine which have multiple isotopes been summed.

The ion at m/z 79/81 was identified as protonated 1-hydroxy-2-chloroethene ($C_2H_2ClOH_2^+$) which is shown in figure 37. This identification was based on the

accurate mass of the peak using a well calibrated mass spectrum, the presence of one chlorine atom (based on isotopic ratio of the 79/81 ions) and high mass resolution of the instrument. This ion was also identified and reported in the study using SIFT-MS by Mikhailov et al. [93].

Figure 37 - Proposed structure of protonated 1-hydroxy-2-chloroethene, a proposed fragment ion from protonation of trans-1,2-dichloroethene

To ensure that the ion at m/z 79 was not a result from a contaminant from the chemical as purchased, GC-MS was used to verify the purity of the sample. The chromatographic analysis shows only a single peak, with the mass spectra showing ions associated with trans-1,2-dichloroethene (m/z 61/63 and m/z 96/98). This suggests that there was no contamination of the pure sample, as a result it is concluded that the ion at m/z 79 is formed in the drift tube.

The normalised, background subtracted E/n data was plotted to determine the ion intensity as a function of electric field strength (E/n).

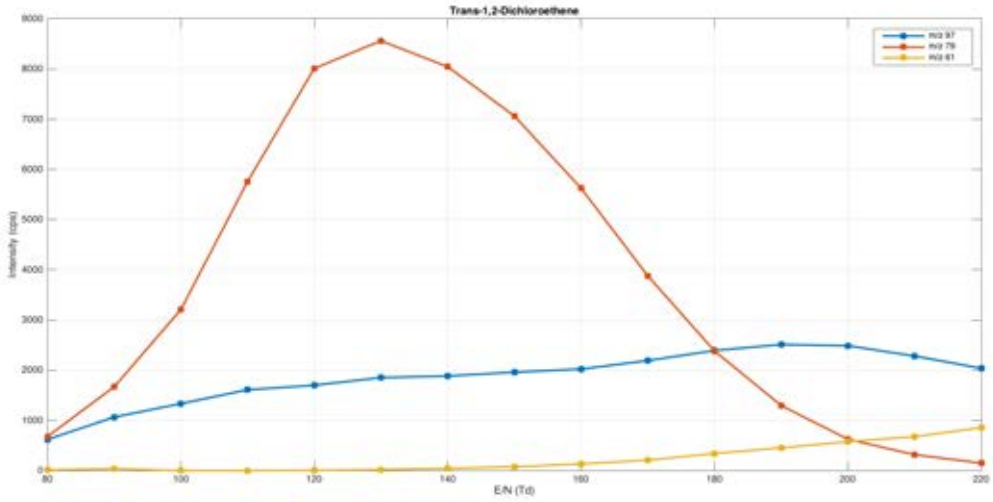

Figure 38 - Trans-1,2-Dichloroethene intensity as a function of electric field strength (E/n). Data normalised and background subtracted.

The formation of the ion $C_2H_2ClOH_2^+$ (1-hydroxy-2-chloroethene) at m/z 79 shown in figure 37 occurs over the E/n range investigated (80-220 Td). The molecule lost when forming $C_2H_2ClOH_2^+$ is HCl, which as a neutral molecule cannot be detected. Dehydration of this ion at E/n >130 Td (leading to a loss of H_2O) provides a feasible route for the loss of HCl from the starting molecule.

There appears to be 3 ionisation mechanisms forming the ions observed in the reaction of hydronium with trans-1,2-dichloroethene.

The ions at m/z 97/99/101 are formed from the non-dissociative proton transfer from hydronium to trans-1,2-dichloroethene. The proton affinity of trans-1,2-dichloroethene is less than that of water (608 kJ/mol [94]), and therefore proton transfer is inefficient due to significant reverse reaction with water ($MH^+ + H_2O \rightarrow M + H_3O^+$), but will still occur due to the energy distribution of the hydronium ions

(for the same reason that protonated CO_2 is observed at high CO_2 mixing ratios [95, 96]). The increasing signal intensity for MH^+ with increasing E/n is explained by the energy distribution of the H_3O^+ ion, represented as a normal distribution in figure 39.

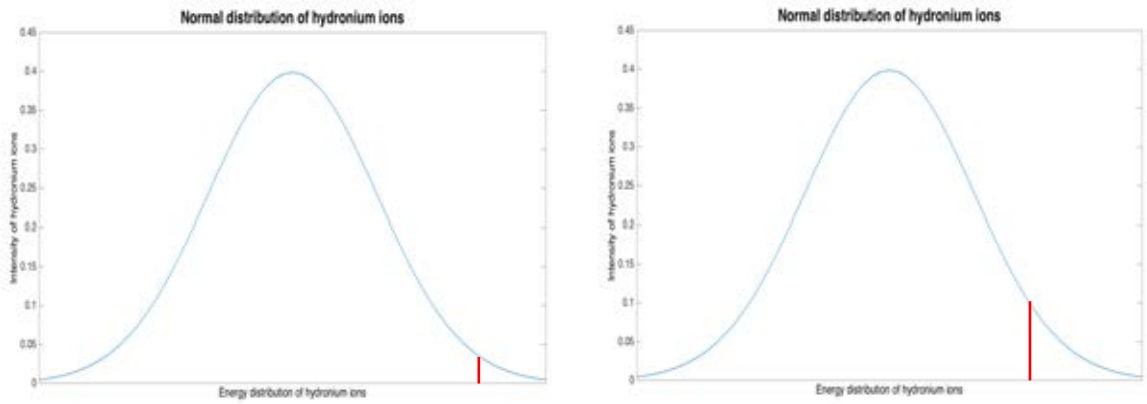

Figure 39 - Normal distribution of the hydronium ion energy. Left panel shows the proportion of the ions at low reduced electric field strength (E/n) which have sufficient energy to cause a proton transfer reaction with trans-1,2-dichloroethene (area under the curve to the right of the red line). Right panel shows the proportion of the ions at high reduced electric field strength (E/n) which have sufficient energy to cause a proton transfer reaction with trans-1,2-dichloroethene (area under the curve to the right of the red line). Figure not accurate (the proportions of ions that can cause a protonation reaction is not known but represented generally to show the principle of increasing MH^+ with increasing E/n).

Increasing the reduced electric field increases the proportion of the ions that have sufficient energy to protonate trans-1,2-dichloroethene, leading to an increase in MH^+ signal intensity as shown in figure 39. At E/n values > 190Td, fragmentation of the MH^+ is sufficient to cause a reduction on the MH^+ signal intensity, which is supported by the corresponding increase in the $[M\text{-}Cl]^+$ ion.

The hydrogen halide elimination suggested in the SIFT work (42% production of $C_2H_2ClOH_2^+$) is supported by this work [93]. In this study the resulting ion from hydrogen halide elimination, $C_2H_2Cl^+$, is not observed until higher E/n values

>150Td and is not observed at all in the SIFT study [93]. This is in spite of a significant protonated parent ion signal intensity at E/n<150Td. This is in agreement with the other unsaturated organochlorides studied in this chapter which do not undergo significant hydrogen halide elimination following protonation.

Instead it is suggested that the ion $C_2H_2Cl^+$ is produced by two mechanisms, the association of the hydronium ion to trans-1,2-dichloroethene, with the immediate elimination of the hydrogen halide, leaving the ion $C_2H_2ClOH_2^+$ at m/z 79/81. Figures 36 and 38 suggest that $C_2H_2ClOH_2^+$ formed in the drift tube is relatively stable in low-moderate energy conditions (80-140 Td). As shown in figure 38, at E/n values > 140Td, the $C_2H_2ClOH_2^+$ ion dehydrates and the ion intensity reduces with increasing E/n, as the ion signal for the formation of $C_2H_2Cl^+$ increases. The dehydration of the ion $C_2H_2ClOH_2^+$ is not surprising, due to the neutral loss of H_2O, based on the work by Brown et al on the fragmentation of alcohols in PTR-MS [97]. The second mechanism is the fragmentation of trans-1,2-dichloroethene on proton transfer at high E/n. This is due to the higher energy in the proton transfer with increasing reduced electric field strengths, causing hydrogen halide elimination. The proposed individual ionisation mechanisms explained in this section showing the formation of ions observed experimentally are shown in figure 40. The ions here have been reported by Mikhailov [93], but the suggestion of the dehydration mechanism for formation of the M-Cl ions is unique to this work.

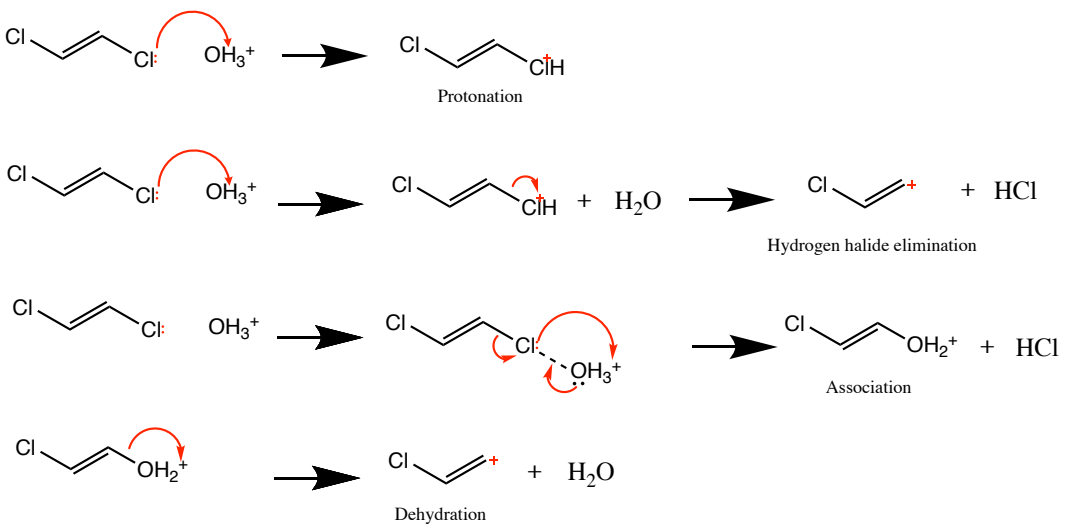

Figure 40 - Proposed ionisation mechanisms for the reactions between hydronium ion and trans-1,2-dichloroethene.

For trans-1,2-dichloroethene with O_2^+ as the reagent ion, the major ion at all E/n values is the charge exchange molecular ion, as expected based on the structure. In the SIFT work by Mikhailov (2006), significant $C_2H_2Cl^+$ was observed from the loss of ClO_2 (or some combination of Cl + O_2) [93].

4.5.5 Effect of Bond dissociation energy on product ion distribution

During chemical ionisation, either the proton affinity for proton transfer or ionisation energy for charge transfer of an analyte are the main drivers for whether the compound will ionise efficiently. The product ions are more difficult to predict than whether a compound will ionise, although common fragment ions and species can be determined from experiments and some knowledge of the chemical system. Computational methods, such as DFT calculations can allow the

energies of the molecule in the system to be modelled and computed, for confirmation or predictive analysis.

In the case of PTR-MS, where there is a combination of the chemical effects from chemical ionisation and energy provided from the electric field which may induce fragmentation, predicting the fragment ions can be difficult. Having observed the effect of the bonding regime on the ionisation and fragmentation of organochlorides, the logical parameter to investigate would be the strength of the chemical bonds in a molecule.

The bond dissociation energy of many C-Cl bonds have been determined experimentally and theoretically and are presented in the literature [55, 98]. The bond dissociation energy D^0_{298}, is the enthalpy change for the homolytic fission of 1 mole of a specific chemical bond [98], however in this case can be considered as the strength of the specified C-Cl bond for a given compound. For organochlorides with multiple C-Cl bonds which have different BDEs, the value given is the average value for cleavage of all C-Cl bonds (unless the bond is specified).

Table 12 - Literature values for the Bond Dissociation Energy (BDE) for the C-Cl bond in each compound shown, taken from literature sources [55, 98].

Name	Structure	Literature values for Bond Dissociation Energy, C-Cl bond ($kJ\ mol^{-1}$)
Chloroform-d $CDCl_3$	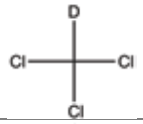	311.1 ± 2.0
Carbon Tetrachloride CCl_4	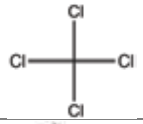	296.6
Pentachloroethane $CHCl_2CCl_3$	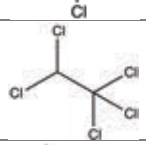	**Cl-C**$HClCCl_3$ 330.5 ± 4.2 **Cl-C**Cl_2CHCl_2 311.7
1,2-Dichloropropane $CH_3CHClCH_2Cl$	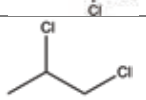	-
2,2-Dichloropropane $CH_3CCl_2CH_3$	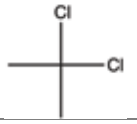	-
Trans-1,2-dichloroethene CHClCHCl		369.9
2-Chloropropene $CH_3CCl=CH_2$	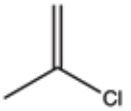	-
3-Chloropropene $CH_2=CHCH_2Cl$		298.3 ± 5.0
Chlorobenzene C_6H_5Cl	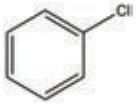	406.4 ± 0.8 399.6 ± 6.3
1,2-Dichlorobenzene $C_6H_4Cl_2$	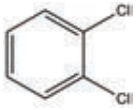	385.8

4.5.5.1 Loss of HCl

The bond dissociation energy for those compounds investigated that lose HCl at all E/n are around 300kJ mol^{-1} (BDE values specified in table 12, this includes compounds that have aromatic or unsaturated nature (such as 3-chloropropene and benzyl chloride). The nature of the bond that is connected to the C-Cl is the key in determining the fragmentation pattern and BDE.

For the organochlorides that lose HCl, such as 1,2-dichloropropane, the BDE of the C-C bond is much higher than the C-Cl bond, suggesting that in this case the C-Cl bonds are the first to break. From experimental determination, hexachloroethane (figure 41) loses HCl but also produces a fragment ion from the cleavage of the C-C bond. The fragment ions produced as a result of the C-C bond breaking arise from the weak C-C bond. This is due to the large number of electronegative chlorine atoms on each carbon, pulling electron density from the carbon – carbon bond in a roughly equal amount, causing the lengthening and weakening of the C-C bond.

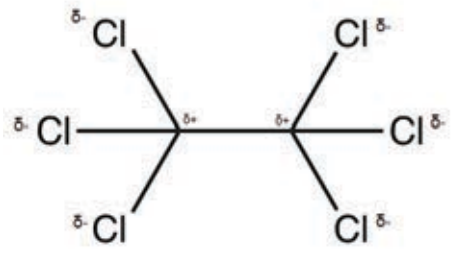

Figure 41 – Structure of hexachloroethane, showing the electronegativity of each of the atoms and the weakening of the C-C bond

In this case, the hexachloroethane C-C bond is weaker than the C-Cl bond and although significant HCl loss is observed (as a result of chemical effects), the energy of the PTR-MS system allows the formation of fragment ions as a result of the C-C bond breaking.

Table 13 - Literature values for the bond dissociation energies of C-C and C-Cl bonds in pentachloroethane and hexachloroethane, with the percentage production of fragment ions showing the breaking of the C-C bond.

	BDE C-C (kJ mol^{-1})	**BDE C-Cl (kJ mol^{-1})**	**Hydronium C-C bond breaking at 120Td (%)**	**O_2^+ C-C bond breaking at 120Td (%)**
Pentachloroethane	306.3 ± 8.4	**Cl-C**Cl_2CHCl_2 311.7	4	58
Hexachloroethane	285.8 ± 6.3	303.8	53	45

It is clear that the chemically favoured loss of HCl molecules is dominant for pentachloroethane. As the loss of HCl progresses, the strength of the C-C bond will increase as the number of electronegative atoms attached to it decreases. This results in the reduction of fragment ions as a result of the C-C bond breaking in pentachloroethane.

4.5.5.2 Protonation

The compounds that predominantly protonate (as they have C=C-Cl), such as 1,2-dichlorobenzene (figure 42), have bond dissociation energies of around 400 kJ mol^{-1}. At higher E/n values, the energy in the PTR-MS system is sufficient to cause some fragmentation, and these compounds then lose HCl as the energy in the system through collisions and the electric field is sufficient to break the bonds.

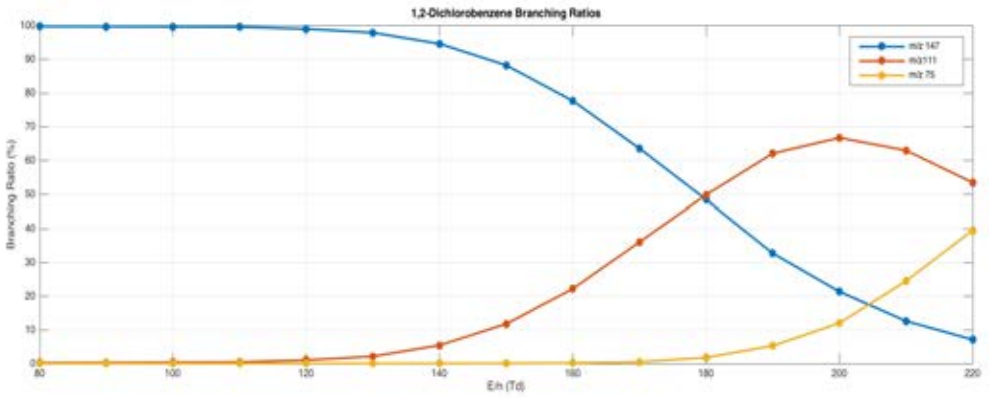

Figure 42 - 1,2-Dichlorobenzene branching ratios with the protonation across a range of E/n, with fragmentation (loss of HCl) under influence of stronger electric fields (>160Td).

4.5.5.3 Trans-1,2-dichloroethene

Trans-1,2-dichloroethene has a C-Cl BDE of 369.9 kJ mol^{-1}, which does not follow the trend of BDEs seen for the other small organochlorides investigated in this study. Trans-1,2-dichloroethene is the only molecule for which any significant H_2O addition is observed, which appears to be driven by chemical processes.

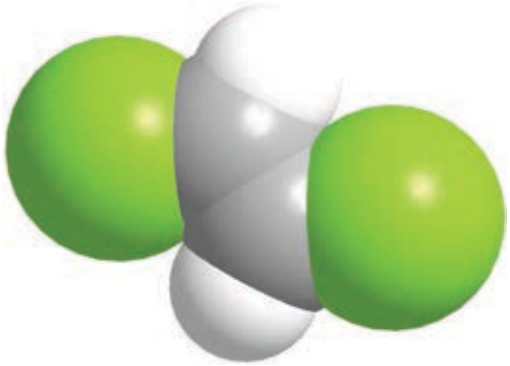

Figure 43 - Space filling model of trans-1,2-dichloroethene, carbon atoms (grey), hydrogen atoms (white) and chlorine atoms (green) are shown.

Other studies using SIFT have suggested that the atomic hydrogen attached to the central C=C bond may result in a potential energy barrier to reaction [93].

4.5.6 DFT calculations for organochlorides

Experimental data provides the most certainty on product ion distributions for compounds at given conditions in PTR-MS, however the use of theoretical calculations can provide information on the relative energies of the molecules, transition states and products in order to determine mechanistic information on ionisation and fragmentation.

DFT calculations performed by Peter Watts for several of the compounds in this study, support the ion-molecule reaction products determined experimentally in this study. For the compounds chloroform-d and 2,2-dichloropropane, the formation of HCl is complete and this is mirrored in the product ions observed. For 1,2-dichlorobenzene, the result of the DFT calculation, protonation on the ring

carbons 3 and 4 is demonstrated in the product ions observed at 120 Td, with some M-Cl observed at higher E/n values, such as 200 Td.

4.6 Generic fragmentation rules for organochlorides

From the individual organochloride analysis results shown in tables 10 and 11 with the predicted ionisation mechanism for organochlorides, several generic fragmentation rules can be conceived. The rules have some exceptions, which will be discussed in more detail individually with a discussion of the reason for the exception.

4.6.1 Structure relationship with ionisation method

The structure of the compound and more specifically, the position of the chlorine atoms on the compound have a major effect on the mechanism of ionisation. The following points describe the general ionisation mechanisms for an organochloride when using hydronium as the reagent ion.

1) If the chlorine is attached to a saturated carbon, then the molecule loses HCl as the ionisation mechanism, leaving $[M\text{-}Cl]^+$.

2) If the chlorine is attached to an unsaturated carbon, then the molecule protonates, forming MH^+.

3) In cases where the molecule has a chlorine atom attached to a saturated carbon and a second chlorine atom attached to an unsaturated carbon, the molecule loses HCl, leaving $[M\text{-}Cl]^+$ without any production of MH^+. This presumably proceeds via loss of the Cl bonded to the saturated carbon as shown in the mechanism in figure 33. This appears to be energetically favoured, as shown by the DFT calculations for compounds of interest.

4) Some organochlorides can lose HCl through addition of OH_2^+ which is present on collision with reagent ion (hydronium reagent only). The product ion of this reaction can then dehydrate at higher reduced electric field strengths, giving the product ion M-Cl from the original molecule.

5) The structure of the molecule and C-Cl bond dissociation energy are related (C-C-Cl BDE ≈ 300 kJ/mol, C=C-Cl BDE ≈ 400 kJ/mol) and this can act as a predictor for the ionisation mechanism observed as detailed in section 4.5.5. The organochlorides which have a C-Cl BDE of 300 kJ/mol undergo the loss of HCl at all reduced electric field strengths, whereas the organochlorides with a C-Cl BDE of 400 kJ/mol protonate at low-moderate electric field strengths.

Similarly, when using O_2^+ as the reagent ion, points 1-3 are still valid but are observed as the charge exchange products M^+, rather than MH^+ and the ionisation mechanism in point 4 is not possible.

4.7 Application of generic fragmentation rules for quantification of isomers without separation - Organochlorines

The generic fragmentation rules proposed, along with the specific individual samples investigated, allow a PTR-MS user to identify and quantify organochloride isomers without separation, based purely as a function of their predicted ionisation mechanism and subsequent fragmentation. This knowledge could be used within current and historic atmospheric measurements of environments which contain these isomers. Although one pair of isomers were investigated in this work, the method could be applied to other pairs of unsaturated isomers where the position of the chlorine with respect to the double bond is different.

4.7.1 2-Chloropropene and 3-Chloropropene

The two isomers, 2-chloropropene and 3-chloropropene provide an example of how the ionisation mechanism can be used for quantifying isomeric compounds without the need for chromatographic separation. Due to the position of the chlorine atom on the molecule with respect to the unsaturated carbon, the 2-chloropropene protonates at low E/n values, forming ions at m/z 77+79 (corresponding to the isotopes ^{35}Cl/ ^{37}Cl). In contrast, the other isomer, 3-Chloropropene loses an HCl molecule after ionisation and produces a single product ion at m/z 41 (no chlorine present).

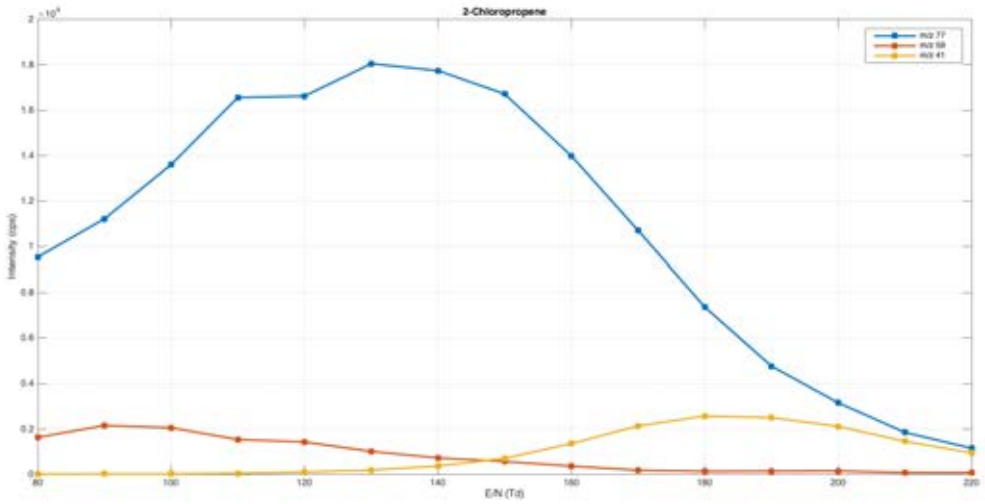

Figure 44 - 2-Chloropropene product ion intensity as a function of electric field strength (80-220Td). The dominant ion is the protonation of the molecule (MH^+) at m/z 77.

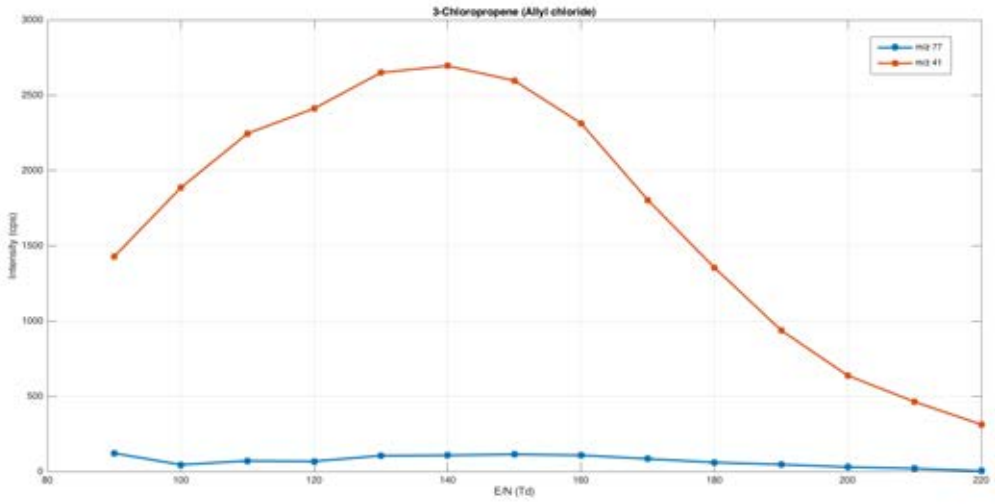

Figure 45 - 3-Chloropropene product ion intensity as a function of electric field strength (80-220Td). The dominant ion is the loss of HCl from the molecule ($M\text{-}Cl^+$) at m/z 41.

In order to quantify these isomers without separation, one should run the PTR-MS at a moderate E/n such as 140 Td (where the fragmentation in 2-Chloropropene is not promoted) and look for the ions produced at the two different m/z. This can easily be converted into a concentration using a relative sensitivity factor (RSF) derived from a suitable calibration technique (described in chapter 3).

4.7.2 Incorrect assignment of peaks

When an organochloride loses a Cl in the form of HCl, it leaves behind an ion, which is detected in PTR-MS. In the case of 3-chloropropene, the ion produced after loss of HCl is $C_3H_5^+$, a common ion produced by many compounds as a result of fragmentation. The detected ion may have been incorrectly assigned as a fragment from another molecule, when in fact there is a contribution from 3-chloropropene, causing issues with misidentification or inaccurate quantification.

In the example of 3-chloropropene, the ion produced has a low mass, which ordinarily would not be used for quantification as it is common to many compounds. However, this may be more of an issue for compounds that produce a higher mass ion, either by protonation or fragmentation, which are used for quantification.

4.7.2.1 1-Chloropentane

One such example where the ionisation mechanism can provide information on the interferences with VOC product ions is in the ionisation of 1-chloropentane, which ionises to produce $CH_3(CH_2)_4^+$ at m/z 71. There are other atmospherically important compounds that produce an ion at m/z 71, such as the protonation of Methyl Vinyl Ketone (MVK) and Methacrolein (MACR), which have been mentioned in chapters 3 and 5. The ion produced from 1-chloropentane is isobaric with MVK and MACR and has a mass difference of 0.036 amu, which may interfere in PTR-MS instrumentation with insufficient mass resolution to separate.

For a general case of a saturated organochloride that has only 1 chlorine atom, the single chlorine atom is lost as HCl, and as a result, the characteristic chlorine 3:1 ratio isn't observed for the remaining major fragment ion and cannot be used to help distinguish between isobaric ions. In this case, there is no evidence to connect the ion produced to the original chlorine containing molecule. This will make identification of these species very difficult, especially if the ion produced is isomeric or isobaric with other common compounds. In the general case of an organochloride with a chlorine atom attached to an unsaturated carbon, then the molecule protonates and can be identified and quantified using the protonated or charge exchange parent ion (MH^+ or M^+).

4.7.3 Development of an 'algorithm' for quantification

Although not within the scope of the thesis, it would be feasible to develop an algorithm based on peak finding/fitting using the fundamental knowledge of the ion-molecule reactions presented in this chapter in order to identify and attempt to quantify peaks in a mass spectrum. For organochlorides, this could consider the experimentally determined ionisation method (protonation/charge exchange, hydrogen halide elimination or association of H_2O). If this is not known experimentally, the 'predicted' ionisation method could be used to calculate the expected accurate mass for organochlorides and therefore allow quantitative data to be extracted.

This may be especially useful in the case of isobaric interferences or determining the presence of a selection of important molecules in a sample whether already known, or for compound discovery. This information is being used in the development of an algorithm for quantification of isomeric and isobaric interferences by Kore Technology, which is discussed further in section 7.2.

4.8 Conclusion

The work discussed in this chapter shows the evolution of an interesting measurement into a unique insight into the ionisation mechanisms, detection and quantification of saturated and unsaturated organochlorides using PTR-MS.

The measurement of an environmental standard often used for GC-MS has inadvertently uncovered a generic ionisation/fragmentation rule for organochlorines in soft chemical ionisation. This has provided a method to measure some organochlorides which were previously unreported by PTR-MS and also to quantify some organochlorides without separation.

The key findings of this chapter are:

1) Compounds containing a chlorine molecule either protonate, lose HCl (this has been demonstrated previously in the literature on a much smaller set of

compounds) or incorporate the reagent ion into the molecular structure, with the elimination of HCl.

2) The protonation or loss of HCl (or ClO_2) is dependent on the structure of the compound and the bonding of the carbon which the chlorine atoms are bonded to (C-C-Cl, loss of HCl, C=C-Cl, protonation), an observation novel to this work. The bond dissociation energy of the C-C-Cl (300kJ/mol) and C=C-Cl (400kJ/mol) provide evidence that the collisional energy in the PTR-MS drift tube is sufficient to cause fragmentation of the C-**C-Cl** bond at all reduced electric field strengths, whilst fragmentation of the C=**C-Cl** is observed only at higher reduced electric field strengths > 160 Td.

3) If a compound loses HCl, this may have been measured but incorrectly assigned to another compound in the case the resulting ion interferes with an ion of a protonated compound, e.g. 1-chloropentane creating an isobaric interference with MVK+MACR.

4) The ionisation mechanisms allow quantification of some organochloride structural isomers in cases where the position of the chlorine with respect to the double bond is different eg 2-chloropropene and 3-chloropropene. 2-chloropropene protonates to form ions at m/z 77/79, however the isomer 3-chloropropene loses HCl, forming an ion at m/z 41.

5) The detection of small saturated organochlorides proceeds exclusively via the mechanism of losing HCl rather than protonation when using a reagent ion such as hydronium. Limited data for organochlorides has been reported for the ion molecule reactions of hydronium and saturated organochlorides, apart from studies to determine proton transfer rate coefficients using SIFT [44]. Previous studies with SIFT report product ions for small organochlorides, such as chloroform) clustered to water ($H_3O^+.CHCl_3$), whereas the loss of HCl is observed with PTR-MS ($CHCl_2^+$).

5 - Quantification of isomeric species without chromatographic separation

5.1 Introduction

When analysing VOC mixtures, the technique selected for use is very much dependent on the compounds to be analysed, whether there are any isobaric or isomeric interferences which would complicate the analysis or simply single compounds at each m/z. In most complex matrices, such as air, there are usually multiple compounds that may be present at each m/z and therefore separation and quantification of these compounds is difficult.

GC-MS is a 'gold standard' analytical technique and is able to provide chromatographic separation of VOCs with the mass spectrometric capability, which enables isomers and isobars to be efficiently separated and quantified. Furthermore, 2D GC (GC x GC) has also been developed to give greater separation for VOCs in a complex matrix than GC alone, but is still imperfect when analysing mixtures of VOCs in ambient air [1]. GC-MS suffers from a low time resolution measurement, with a typical GC-MS run taking 40 minutes [99].

The time taken for a GC-MS run is one of the reasons why PTR-MS has become widely used for the measurement of VOCs, due to the real-time analysis capability and soft chemical ionisation of the VOC molecules, preserving the molecular ion on ionisation. However, the trade-off is the lack of a separation step and therefore the inability to quantify isomers. In some cases, depending on the research

objectives being addressed, this chemical non-specificity can be accommodated and the results can be presented as a sum of the isomers. For other studies, it is desirable to quantify isomers separately, to determine their presence for health effects or to understand their transport and reactions in the atmosphere.

Efforts have been made to reduce the run time of GC-MS with the introduction of the fast GC, which has the ability to separate isomers in less than 90 seconds [100], but the compromise in reduction of column length impacts on the ability to separate a wide range of isomers. For most of the research in this area, targeted isomers, such as monoterpenes, can be separated on the order of several minutes [40] rather than the more traditional 30-40 minutes for GC-MS. Some progress has been made in the selectivity of structural isomers, including for monoterpenes [101].

A solution to this problem would be to develop a method of isomer independent quantification in near real time for PTR-MS, rather than relying on a time-consuming separation step. This method could also be applied to mixtures of compounds, where a fragment ion from one compound interferes with a protonated molecular ion or fragment of a different chemical species.

In mass spectrometry, the standard method for compound identification is to compare fragmentation patterns to that of an individual compound. As a result, extensive databases of chemical fragmentation patterns (such as NIST) have

been constructed in order to provide compound identification. Using deconvolution software can allow mixtures of compounds to be identified and quantified.
The standard approach to the identification of compound in a sample using PTR-MS is slightly different owing to the limited fragmentation from the soft chemical ionisation of the sample. Many compounds ionise producing the protonated parent ion, allowing identification of the compound (or at least chemical formula in the case of isomers) which can be further confirmed by using a PTR-MS with high mass resolution (>4000 FWHM) and high mass accuracy (<3 ppm). The other approach to chemical identification in PTR-MS is to use *a priori* knowledge of chemical fragmentation or products of specific ion-molecule collisions to allow identification. For example, research on the ionisation of alcohols using PTR-MS has shown that the product ion resulting from proton transfer is the loss of OH from the alcohol [97] and from the work in chapter 4 of this thesis, the ionisation mechanism for some groups of chlorocarbons proceeds via the loss of HCl rather than protonation, regardless of the electric field strength.

Many VOCs commonly analysed by PTR-MS are often protonated with minimal fragmentation at low E/n values (<120Td). However, increasing the collisional energy by modifying the reduced electric field can induce fragmentation of the parent ion[102]. An example of this behaviour is observed for isoprene in figure 46.

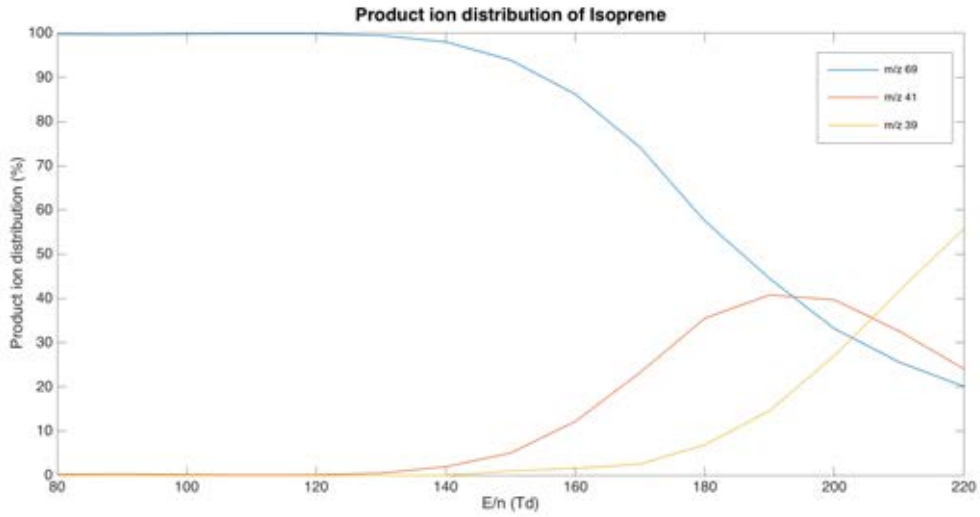

Figure 46 - Product ion distribution of isoprene between 80-220 Td, demonstrating the fragmentation that occurs at E/n > 120 Td.

This pattern – of fragmentation as a function of field strength – varies between molecules, including between isobaric species – offering the potential to separate and discriminate between otherwise "overlapping" compounds within PTR-MS analyses. To give more discriminating power, multiple electric field strengths can be used to provide more information on the mixture, using the change in product ion distributions at different electric field strengths in order to provide more discriminating power. For example, by using multiple electric field strengths the fragmentation observed by Rogers (2006) [39] for the BTEX isomers can be used to form an 'algorithm' for quantification.

In mathematical terms, using the changing peak intensities to solve simultaneous equations with multiple unknowns, which is possible with the use of multiple E/n values, would allow quantification of compounds. A general explanation of solving

unknowns can be thought of by solving 2 equations for 2 unknowns as shown in equations 25 and 26.

$$x_1 = Y + Z \tag{25}$$

$$x_2 = A\,Y + B\,Z \tag{26}$$

Where x_1 and x_2 are the two measured signal intensities at 2 different E/n values, Y and Z are the unknowns (in this case, the concentration/signal intensity of a pair of compounds) and A and B are experimentally determined factors that describe the relationship of Y and Z at the 2 different E/n values. The factors A and B can be determined experimentally and therefore the unknowns, Y and Z can be determined by solving the equations. More generally, this could then be expanded to improve the accuracy of species quantification from a baseline of other species and/or to separate larger numbers of isobaric species, from larger numbers of reduced electric field strength-dependent measurements of fragmentation.

To vary the E/n, either E (reduced electric field strength) or n (number density) can be changed. It is much simpler and more common in the PTR-MS community to change E (response time ≈ 10 ms) than n (response time >10 seconds) so for these experiments, E was modified to produce a different E/n. In order for any quantification tool to be of use to the measurement community, it should follow similar experimental methods already employed in field measurements, such as

using H_3O^+ as the reagent ion and reduced electric field strengths between 80-240Td.

By using different electric field strengths (low and moderate) to induce fragmentation in PTR-MS, the soft chemical ionisation principle could be retained whilst yielding molecule-specific information providing disambiguation of isomeric and interfering molecular ions. An important application of this would be in the measurement of simple synthetic mixtures of VOCs, such as biogenic VOC chambers which are dominated by a finite number of chemical species and where high time resolution measurements are required.

The fragmentation of a chemical species is a function of the electric field strength and within this work, the use of multiple electric field strength values were investigated (through switched E/n) in order to provide information potentially useful for the quantification of isomers. As part of this work, some of the data presented is using a fast switching E/n unit, a secondary power supply capable of switching the electric field strength in the drift tube at a frequency of 1Hz in order to change the E/n.

The principles discussed in the introduction are applied to three specific examples of isobaric and isomeric mixtures, isoprene and 2-methyl-3-buten-2-ol (232MBO), methyl vinyl ketone (MVK) and methacrolein (MACR) and benzene, toluene, ethylbenzene and xylene (BTEX) in order to determine the accuracy and precision in the measurement of a gas mixture.

5.2 Experimental

Acquiring mass spectra at different E/n values allows the determination of the product ion distribution as a function of the E/n value. Differences in the product ion distribution between compounds or changes in the product ion distribution as a function of E/n can be used to develop methods to quantify mixtures of compounds. For the mixtures discussed in this chapter, a similar experimental design was used for determining the differences between the ion-molecule products of isomers. For each set of isomeric overlaps, specific methods have to be developed to meet the challenges posed by these isomers.

Measurements of individual pure compounds were used to determine the product ion distributions and the differences in the instrumental response to the isomers. Initially experiments were crude, but suitable for determining the product ion distributions, by injecting a small amount of the liquid compound (<1μl) into a Teflon bag and diluting to a suitable concentration for measurement in DC mode (<2ppm), measured at 10Td steps over the E/n range 80-220Td. For this work, the PTR reactor was operated in DC mode rather than RF mode. Following from this, the diffusion tube methodology used in chapter 3 was utilised to create accurate standards, in order to quantify the methods developed.

5.3 Isoprene and 2-Methyl-3-buten-2-ol

Isoprene is the dominant biogenic emission globally, with over 500Tg of emission per year [4, 103]. This currently measured in PTR-MS as an ion at m/z 69, the result of non-dissociative proton transfer from hydronium (equation 28). However, another biogenic VOC 2-Methyl-3-buten-2-ol (232MBO, figure 48), which is abundant in the atmosphere in the US [104] and a degradation product of isoprene (figure 47) [105], can also undergo a proton transfer reaction, resulting in dissociation to produce an ion at m/z 69, which is an isomeric interference with that of isoprene (equation 28) [104]. Other compounds in the atmosphere may produce an ion at m/z 69, but are minor in comparison to isoprene and 232MBO.

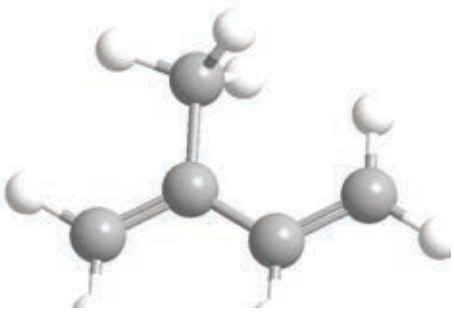

Figure 47 - Ball and stick structure of Isopr

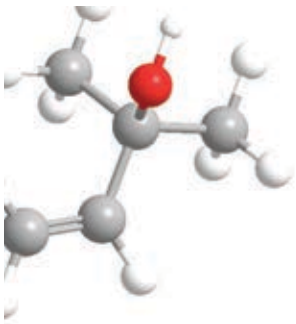

Figure 48 - Ball and stick structure of 232MBO

The major ions produced as a result of proton transfer for isoprene and 232 MBO are shown in equations 27 and 28, with the common ion to both compounds produced shown in red.

$$C_5H_8 + H_3O^+ \rightarrow C_5H_9^+ + H_2O \quad (27)$$

$$C_5H_{10}O + H_3O^+ \rightarrow x\, C_5H_{11}O^+ + y\, C_5H_9^+ + H_2O \quad (28)$$

The differences in the ion-molecule reactions of these compounds was investigated by determining the product ion distributions for both compounds, identifying the ions produced by each compound from a background subtracted spectra and representing them as a percentage of the total product ions from the compound, where the sum of the product ion distribution at each E/n is equal to 100%. Minor ions, which are in this case defined as an ion which contributes less than 1% when included in the product ion distribution, are not included. Exclusion of these ions does not contribute to a significant difference to the relative intensities of the other ions reported.

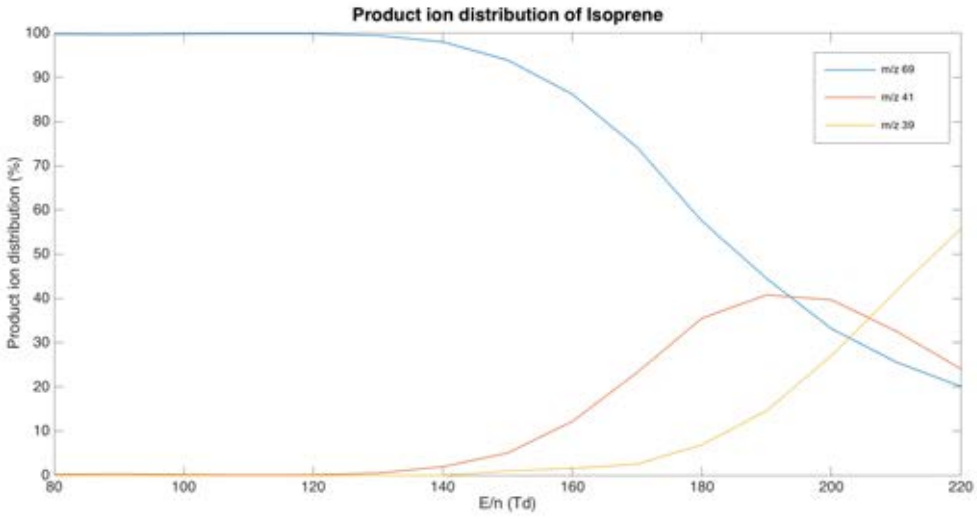

Figure 49 - Product ion distribution of Isoprene in the range of 80-220Td.

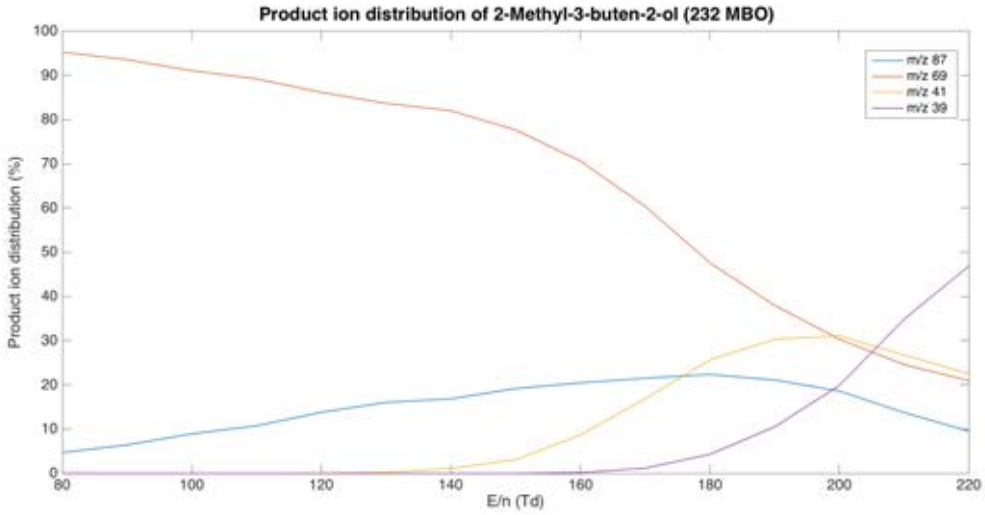

Figure 50 - Product ion distribution of 2-Methyl-3-buten-2-ol (232 MBO) in the range of 80-220 Td.

The dominant ion produced by both isoprene and 232 MBO is the ion at m/z 69 ($C_5H_9^+$) across most of the E/n range investigated. The product ions at m/z 41 and 39 represent the ions $C_3H_5^+$ and $C_3H_3^+$ respectively, with the latter formed as a result of loss of H_2 at high E/n values. These ions are ubiquitous in air samples of PTR-MS and often are present and detected whilst analysing zero air (as a result of zero air/instrument contamination) so cannot be used for any meaningful quantification or interpretation of the interferences.

At 100Td, where the signal intensity for the ion produced at m/z 69 for both isoprene and 232 MBO is around the maximum, the protonated parent ion of 232 MBO makes up 8% of the total product ion signal of 232MBO (the other 92% is the fragment $C_5H_9^+$ at m/z 69). Knowing this information, it would be feasible to determine the contribution of 232 MBO to the signal intensity recorded at m/z 69 and therefore allow a subtraction to be used in order to determine the isoprene

signal from a mixture as shown in equation 29. The intensity of isoprene calculated from equation 29 is applicable for any mixtures of isoprene and 232 MBO.

$$I_{Isop} = I_{69} - 92\left(\frac{I_{87}}{8}\right) \quad (29)$$

Where I_{Isop} is the isoprene intensity at m/z 69, I_{69} is the measured intensity at m/z 69 (contribution from both isoprene and 232MBO) and I_{87} is the measured intensity at m/z 87 (contribution from 232MBO only). The isoprene intensity calculated in equation 30 can then be converted into a concentration with use of an appropriate RSF. The correction derived in equation 29 applies to measurement of a system in which there are 2 components (isoprene and 232MBO), or a system where there are no other compounds that interfere at the masses used for quantification (m/z 69 and 87) for the specific set of conditions measured here. For different conditions such as changes in relative humidity, the relative contributions from Isoprene and MBO to the different product ions can be easily remeasured.

5.3.1 Mixture analysis

In order to determine if the correction derived in equation 29 can be used practically, a mixture was prepared using diffusion tube standards in order to assess the accuracy of the method.

Due to the relative differences in the vapour pressure of isoprene and 232 MBO, 2 different thermostat methods were used for generation of the standards. A diffusion tube of active length 2cm and 0.1mm diameter capillary bore was calibrated for isoprene and used with an N_2 gas flow at a temperature of 0°C in an ice/water bath whilst a 2cm length, 0.5mm diameter bore diffusion tube for 232 MBO was thermostatted at 35°C in a Kintek thermostat with a N_2 gas flow. The standard gas flows were analysed separately and combined by attaching them in series to give a mixed gas standard. The calibration graphs of isoprene and 232 MBO are shown in figures 51 and 52.

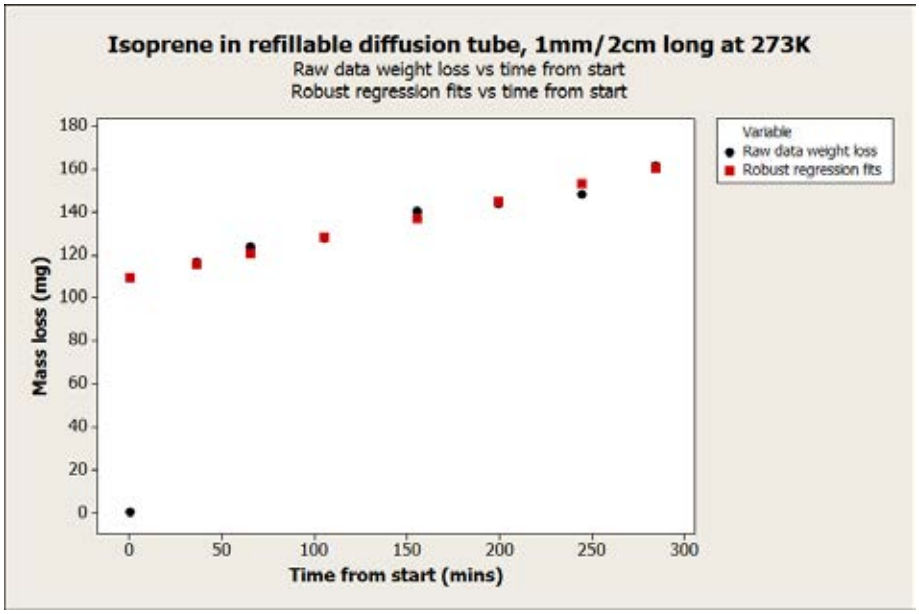

Figure 51 - Calibration graph of 1mm/2cm Isoprene diffusion tube at 0℃ incubated in a salt-ice bath. The robust regression fit reduces the influence of the point of leverage at 0,0 where the loss of volatile impurities is expected to occur.

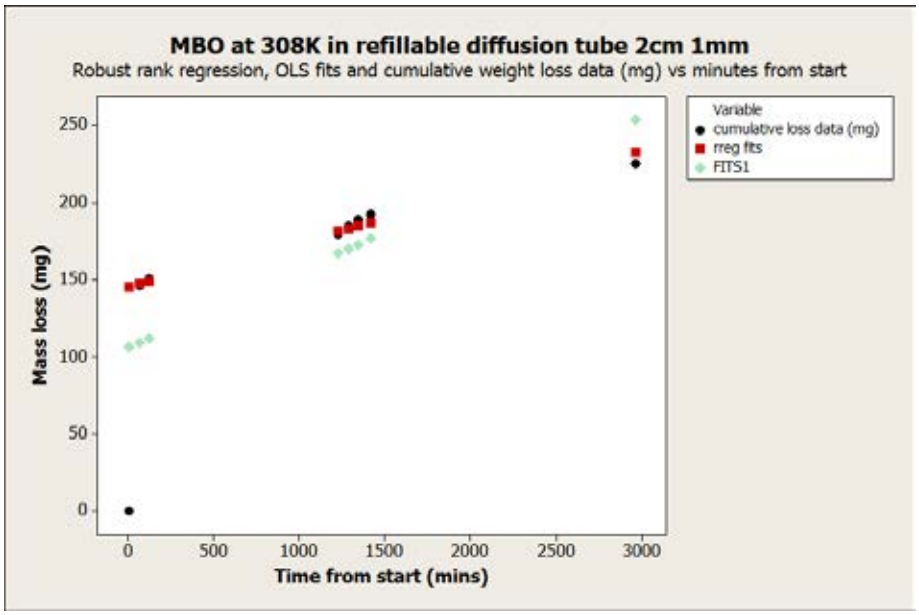

Figure 52 - Calibration graph of 232MBO diffusion tube at 35℃, with the cumulative mass loss raw data in blue, the robust regression fits in red and the ordinary least squares linear regression in green. The robust regression fit reduces the influence from the point of leverage at 0,0 where the loss of volatile impurities occurs.

A mixture was analysed, by using a dilution flow rate through the thermostat units in series to give a fixed concentration of the analyte in the gas stream. The experimental setup for creating the standard mixtures is shown in figure 53.

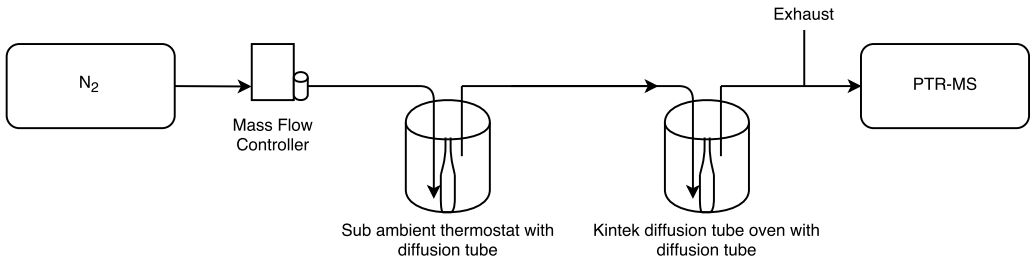

Figure 53 - Experimental setup for the analysis of mixtures of isoprene and 232MBO. The isoprene tube was thermostatted at 0℃ where it was mixed into a N_2 gas stream, controlled by a 0-4 Lpm mass flow controller. The isoprene standard atmosphere was then routed through the 232 MBO diffusion tube oven at 35℃ to avoid loss of the compound. The excess gas was exhausted before PTR-MS analysis of the mixture.

By applying equation 29 to the data acquired using the experimental setup in figure 53, the concentration of the isoprene and 232MBO can be calculated and compared to the calibrated process gas concentrations for isoprene and 232MBO from the diffusion tube setup.

Table 14 - Results of the analysis of mixtures of Isoprene and 232MBO using the method described.

Mixture	Isoprene conc from thermostat (ppbv)	232 MBO conc (ppbv)	232 MBO count at m/z 87	232 MBO count at m/z 69	Isoprene count at m/z 69	Calculated Isoprene conc (ppbv)	Calculated MBO conc (ppbv)
1	392 ± 101	592 ± 38	28682	326378	127106	432	521

The mixture analysed shows that the mixing ratios for isoprene and 232MBO in a mixture can be extracted within a 10% uncertainty using a subtraction method for a given set of instrumental conditions. The subtraction relies on statistically significant peak intensities for both 232 MBO at m/z 87 and isoprene at m/z 69 in order for the subtraction to work effectively.

5.4 Methyl Vinyl Ketone and Methacrolein

Methyl vinyl ketone (MVK) and Methacrolein (MACR) (both C_4H_6O) are products of the reaction of isoprene (the dominant biogenic VOC emission globally [3]) with OH radicals and NO [14, 106]. The relative abundances of MVK and MACR in the atmosphere can act as probes for the oxidative capacity of the atmosphere. As isomers, MVK and MACR cannot be quantified individually by PTR-MS and are usually reported as a sum of the two isomers. It is important to quantify these compounds in order to determine the photochemical age of isoprene from its sources as it reacts in the atmosphere [104].

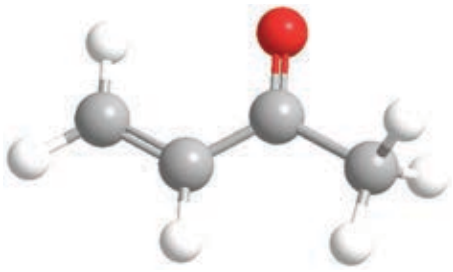

Figure 54 - Ball and stick structure of MVK

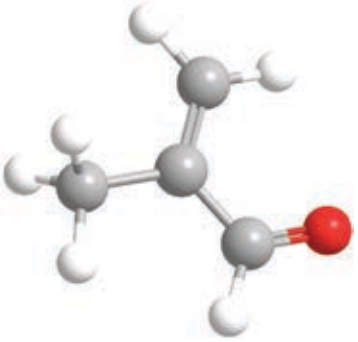

Figure 55 - Ball and stick structure of MACR

In order to develop an approach to the quantification of isomers, the isomeric pair of MVK and MACR were studied as an exemplar system using PTR-MS. Initially it is important to characterise the fragmentation behaviour of MVK and MACR as a function of drift tube voltage, to understand if the fragments produced can be manipulated to give information useful to the quantification of the isomers.

5.4.1 GC-MS verification of isomeric purity

Although the compounds purchased were stated as >99% purity, before the PTR-MS measurements we verified that by analysis using GC-MS. MVK is known to be unstable in air and undergo rapid polymerisation, so is supplied with hydroquinone (0.5%) and acetic acid (0.1%) as inhibitors to polymerisation.

Table 15 - Conditions for analysis of MVK, MACR and mixture of both compounds using GC-MS

Dilution of MVK/MACR	100:1 dilution in HPLC grade acetone (Sigma Aldrich)
Column type	HP5-MS 30m column (0.25mm, 0.25µm)
Split injection	50:1
Start temp	40ºC
Temperature ramp	1ºC/min
Run time	15 min

Using the parameters specified in table 15, single compound mixtures diluted in acetone were analysed, along with a mixture of MVK and MACR.

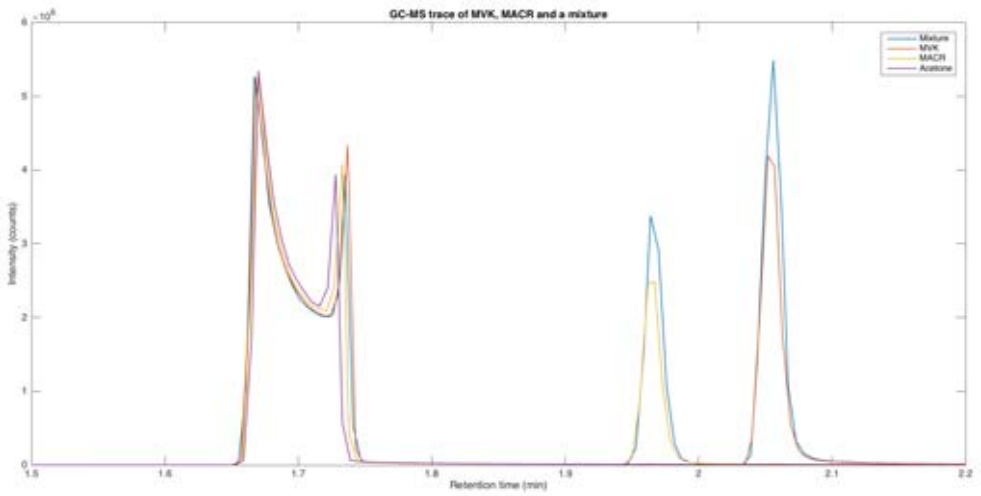

Figure 56 - Chromatographic trace of MVK (red), MACR (yellow) and a mixture of the two compounds (blue) and an acetone blank (purple). Acetone elutes between 1.66 and 1.74 min, MACR elutes at 1.97 min and MVK elutes at 2.06 min. These assignments were verified using the mass spectra.

The elution of the single component standards gives a retention time of 1.97min for MACR and 2.06min for MVK. This agrees with the mixture of MVK and MACR analysed (where there is clear separation of the two isomers). On closer inspection of the single compound chromatographs (figure 57), there is no evidence of significant contamination between the individual isomers (i.e. they are isomerically pure).

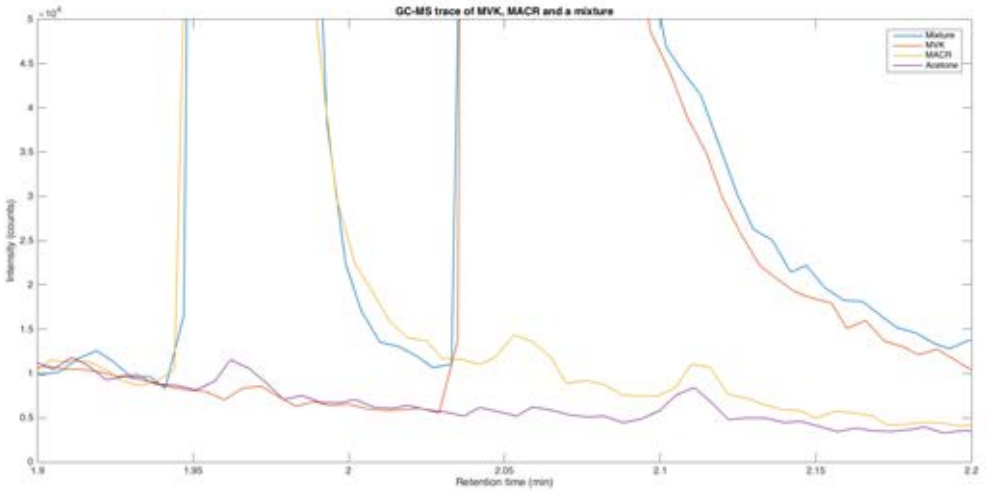

Figure 57 - Chromatograph from figure 56 magnified to show minimal contamination in the individual samples. Colours as in figure 56.

5.4.2 Product ion distributions of MVK and MACR

For the analysis of the individual isomers with PTR-MS, MVK and MACR were analysed at different E/n values and the fragment ions identified. These are then used to plot the product ion distribution (branching ratios) for each compound at different E/n (usually from 80-180Td).

The product ion branching ratios for MVK and MACR are shown in figures 58 and 59. As isomers, MVK and MACR produce the parent ion at m/z 71 and with increasing E/n, a fragment ion at m/z 43.

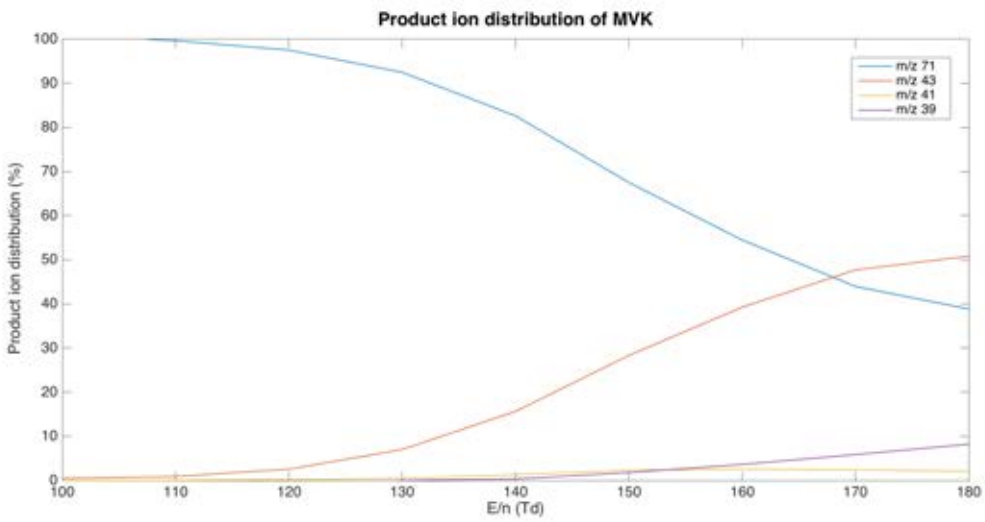

Figure 58 – Product ion distribution for Methyl Vinyl Ketone (MVK) in the range 100-180Td. Mass 43 produced by MVK is the ion CH3CO⁺.

MVK starts to undergo significant fragmentation at E/n >120Td, predominantly producing the fragment ion at m/z 43, which can be positively identified using the accurate mass of the peak as CH_3CO^+.

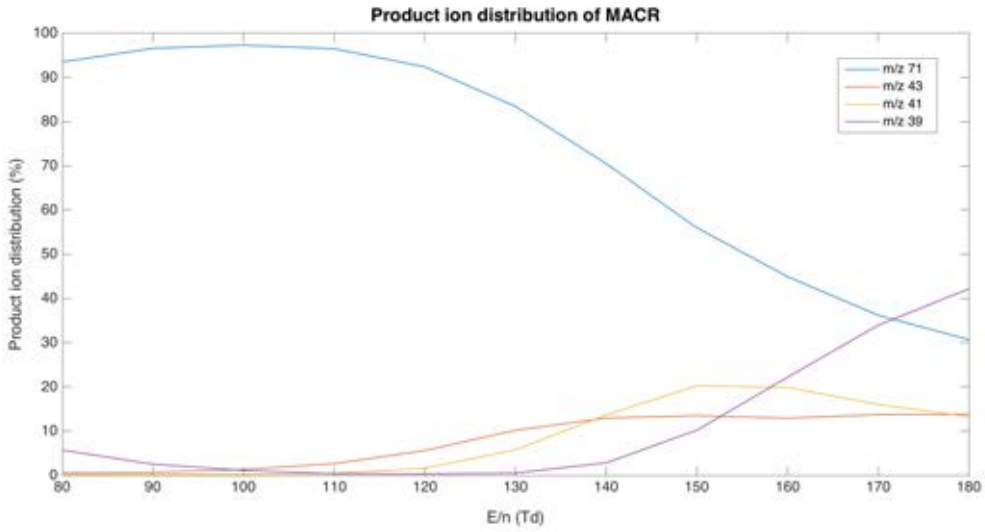

Figure 59 - Product ion distribution (branching ratios) of Methacrolein (MACR) over the range of 80-180Td. The increase of m/z 71 between 80-90Td is probably due to the difficulty in subtracting the background of m/z 39 from the ion $H_2O.H_3{}^{18}O$ at low drift tube energies.

The product ion distribution of methacrolein (MACR) differs from MVK in the fact the main fragment ion is at m/z 39, the ion $C_3H_3^+$ which is formed from subsequent loss of H_2 from $C_3H_7^+$ (m/z 43) and $C_3H_5^+$ (m/z 41). The fragment ions were confirmed by use of a high-resolution PTR-MS instrument, with a measured resolution of >4000 FWHM. The product ions produced are described in table 16.

Table 16 - Product ions from the ionisation of MVK and MACR using the hydronium ion, shown with the nominal mass in brackets.

Compound	Product ions
MVK	$C_4H_6OH^+$ (71), CH_3CO^+ (43)
MACR	$C_4H_6OH^+$ (71), $C_3H_7^+$ (43), $C_3H_5^+$ (41), $C_3H_3^+$ (39)

The fragment ions produced at m/z 43 by MVK and MACR are isobaric (which normally could provide information useful for quantification, CH_3CO^+ and $C_3H_7^+$ respectively). However, the fragment ions are not unique to the reaction of H_3O^+ with MVK and MACR and are produced by many common VOCs on fragmentation and therefore these ions are not useful for quantitative analysis in most matrices. In addition, the fragment ions produced at m/z 41 and m/z 39 are also common to many ions and as a result are not unique to the isomers. This contributes to a large background signal observed at these masses.

5.4.3 Product ion fragmentation for quantification

The major product ion (m/z 71, $C_4H_7O^+$) for both MVK and MACR is formed at all E/n values investigated (80-220Td). However, the relative change in the ion fragmentation is different between the two compounds (due to the structure of the ions). Therefore, it may be feasible to use the rate of change of the parent ion as a function of reduced electric field strength to determine how much of each compound is present in a mixture. This method was examined using calibrated diffusion tubes to create accurate mixtures.

5.4.4 Determination of accuracy and precision of methods

Mixtures of MVK and MACR were prepared using calibrated diffusion tubes. Due to the difference in vapour pressure between the two compounds, different bore diffusion tubes were selected for use at different temperatures. For MVK, a 0.5mm/2cm diffusion tube was used in a Kintek thermostat unit at 30°C and for MACR, a 0.2mm/2cm diffusion tube was used at 45°C. Regular weighing's over

12 days were recorded in order, firstly to optimise the temperature (to achieve similar emission rates) and secondly to provide weight loss data in order to determine the emission rate.

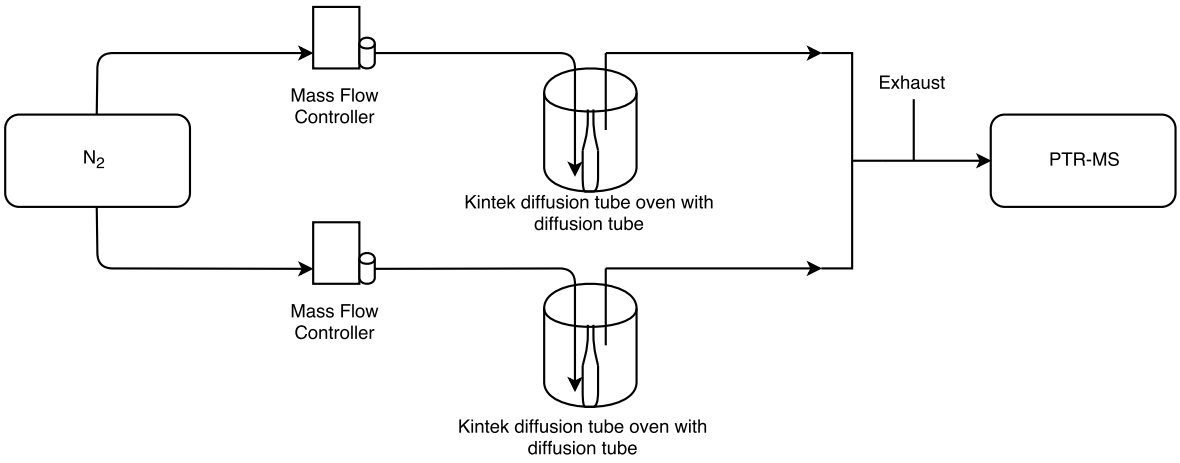

Figure 60 - Instrumental setup for the MVK/MACR diffusion tube evaluation of the isomeric quantification showing the mixing of the two dynamically generated gas standards. For measurement of the single compounds, the output of one of the diffusion tube ovens was sent to the exhaust.

Linear regression analysis on the weight loss data was performed, with 95% confidence interval and prediction interval plotted. The slope of the regression fit gives the emission rate in g/day, which using equation 22 (page 54) with a specified flow rate can be converted into a concentration.

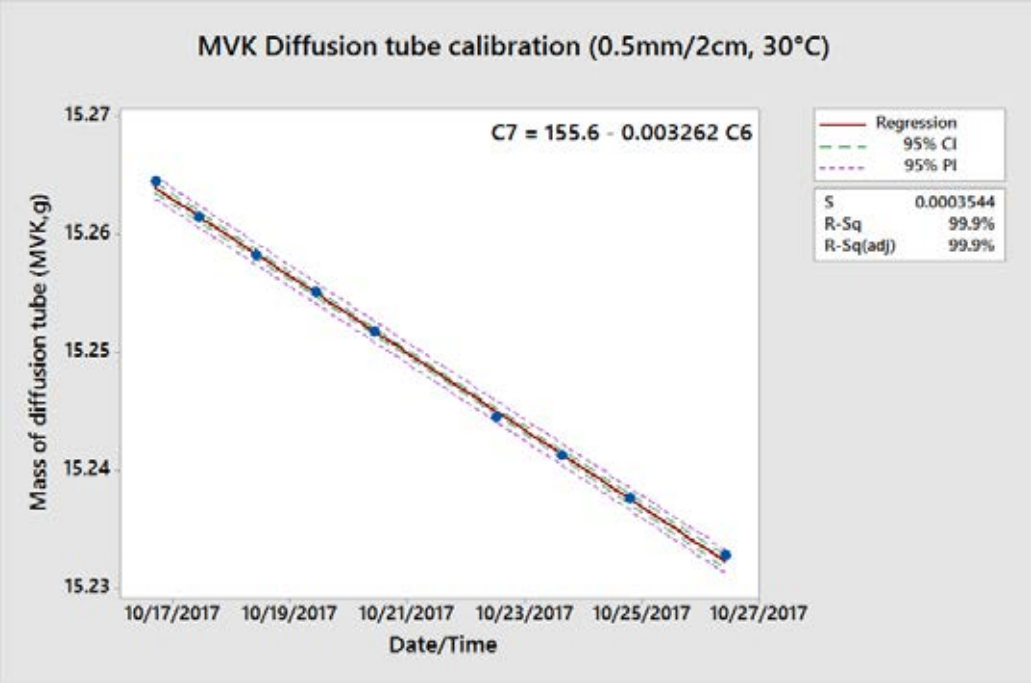

Figure 61 - Regression analysis of an MVK diffusion tube at 30℃ with a 100 ml/min flow of N_2. The emission rate of the tube is 2665 ng/min.

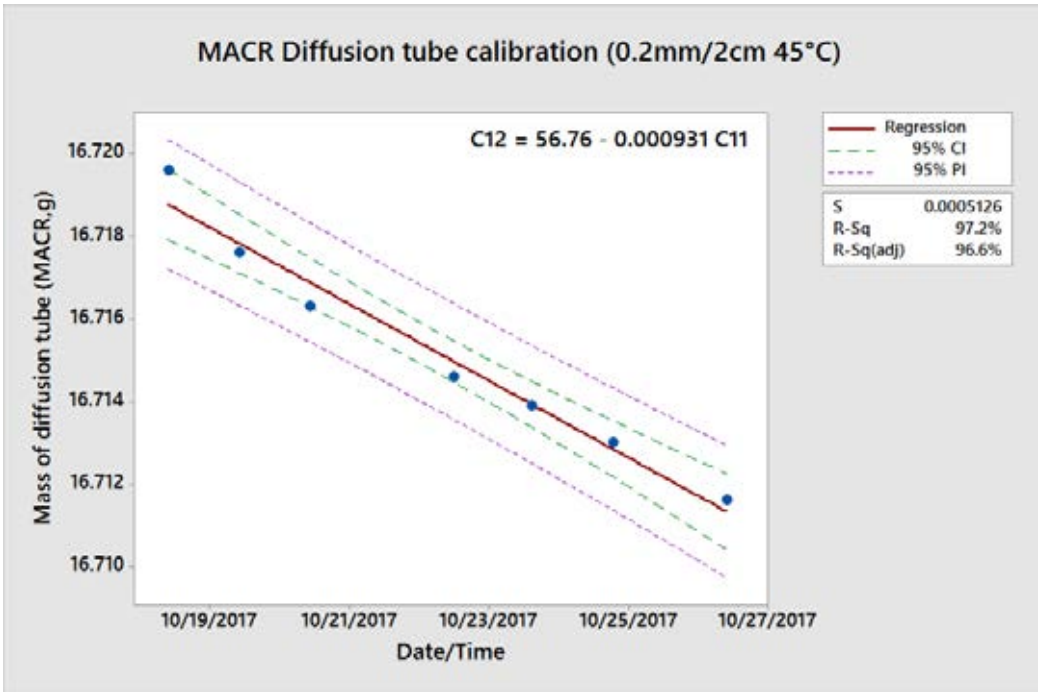

Figure 62 - Regression analysis of an MACR diffusion tube at 45℃ with a 100 ml/min flow of N_2. The emission rate of the tube is 646.5 ng/min.

The accuracy and precision of the methods were determined using mixtures of MVK and MACR prepared by dilution of each compound in a N_2 gas stream. MVK and MACR diffusion tubes were prepared separately using individual flow control to achieve a combined mixing ratio of 436ppb (1888ml/min and 500ml/min respectively) in order to quantify the differences in the fragmentation of the parent ion.

The reduction of the protonated parent ion can be used to quantify the isomers within a mixture, however the isomers have different relative sensitivity factors (MVK = 4cps/ppbv, MACR = 2.6cps/ppbv). Rather than comparing the intensity of the ions at each E/n, it is useful to consider the gradient of the reduction in m/z 71 across a range of E/n values.

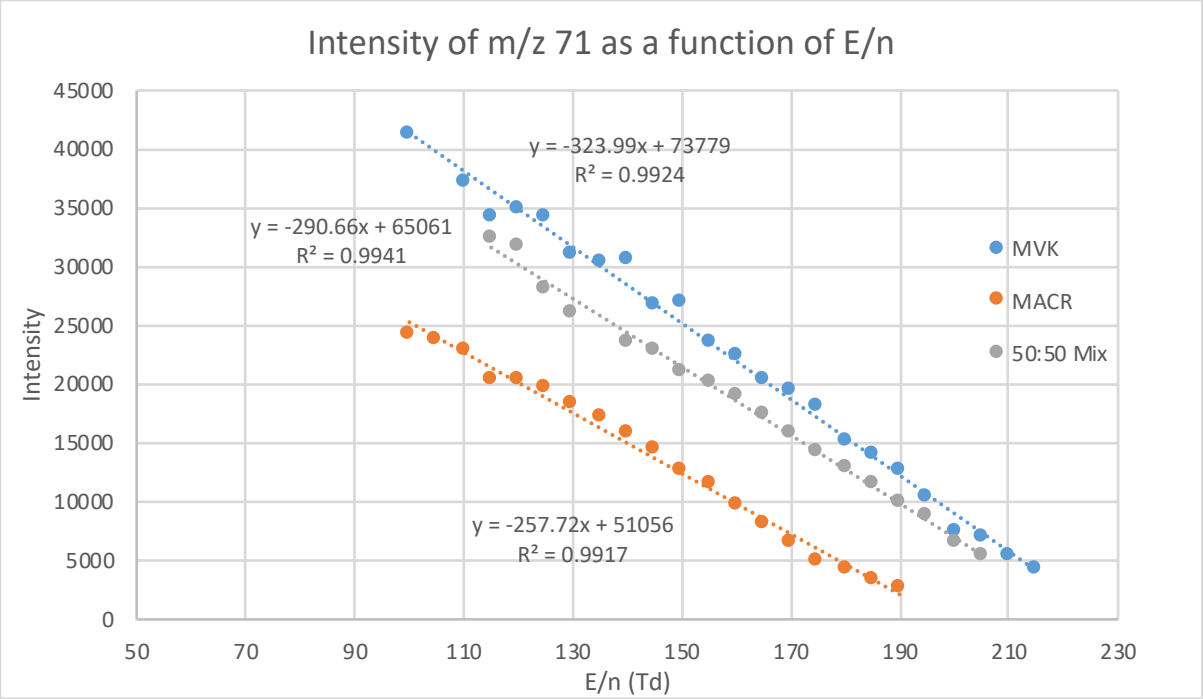

Figure 63 - Intensity of m/z 71 for 436 ppb MVK (blue), 436 ppb MACR (orange) and a mixture of 218 ppb MVK and 218 ppb MACR (grey). The gradient of the slope over the range of 100-190 Td for MVK and MACR allows a mixture to be quantified.

This can be represented mathematically by equations 30-32.

$$X_1 = \frac{\Delta\, Gradient}{100} \tag{30}$$

$$\%\, MVK = \frac{(Grad\ MVK - Grad\ Unknown)}{X_1} \tag{31}$$

$$\%\, MACR = \frac{(Grad\ Unknown - \ Grad\ MACR)}{X_1} \tag{32}$$

Where X_1 is the change in gradient expected for a 1% change in composition of the mixture, Δ Gradient is the difference in gradient of the fitted line between MVK and MACR (in figure 63, the Δ gradient would be 66.3). The %MVK and %MACR give the percentage of each compound measured in the mixture and will sum to give 100%.

Table 17 - Results of MVK/MACR quantification using the gradient of the fitted line for a series of reduced electric field experiments. Sample number 1 and 2 are pure samples of MVK and MACR respectively which were used for determination of gradient of fitted line for each compound.

Sample Number	**% MVK in mixture**	**% MACR in mixture**	**Gradient of unknown**	**% MVK in mixture**	**% MACR in mixture**
1	100	0	-324.0	100	0
2	0	100	-257.7	0	100
3	50	50	-290.7	50	50

5.4.5 Conclusion

The method developed here can be used to determine the composition of a mixture of MVK and MACR with an uncertainty of 5%. This has been demonstrated with a dynamic calibrated gas standard mixture.

The method used, the change in transmission/intensity of the parent ion, does not utilise all of the information available in the mass spectra, specifically the fragment ions. Theoretically the use of all product ions, including the fragment ions (m/z 39/41/43) in quantification of MVK and MACR is possible. However, this is difficult due to interferences from the fragmentation of other compounds, some of which are ubiquitous even in an instrument background when measuring zero air. The low mass ions could be used if all the VOC fragmentation patterns for any compound that may be in the air sample are investigated for a given set of conditions (this could be thousands of VOCs). However, the method using the parent ion fragmentation could be implemented into atmospheric measurements.

5.5 BTEX

5.5.1 Introduction

Benzene, Toluene, Ethyl benzene and Xylenes (BTEX) are important industrial compounds that have many modern-day applications [14, 107]. BTEX is used to produce many important compounds. In addition to this, BTEX is present in percent levels in fuel and often exists in urban atmospheres as a result of incomplete combustion. The composition of fuel (and BTEX contained within it) varies with location, usually due to the composition of the crude oil used for production of the fuel and regulations for the country in which the fuel is sold. For these reasons, urban concentrations of BTEX are significantly higher than rural concentrations.

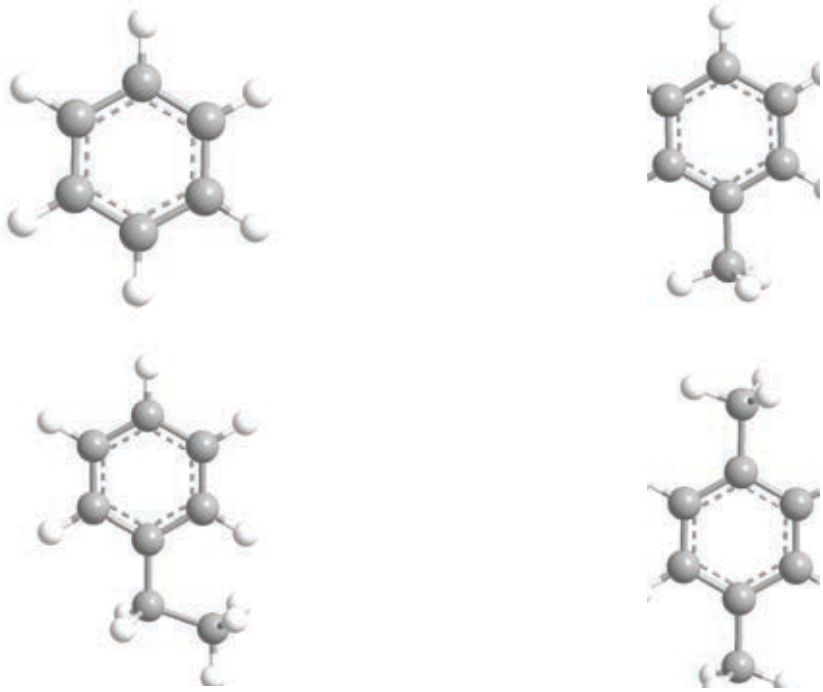

64 - Ball and stick structures (left to right and clockwise) of benzene, toluene, p-xylene and enzene

Ethyl benzene and the three xylene isomers (*o/m/p*) are C8 structural isomers (C_8H_{10}) and therefore appear as a single peak in a PTR-MS mass spectrum. Within the literature is well understood that the C8 compounds produce fragment ions that interfere with benzene measurements in PTR-MS [107, 108]. Toluene, a C7 compound, produces an ion at m/z 93 from the non-dissociative proton transfer, which does not interfere with the other compounds in the BTEX group.

Some studies have derived 'correction factors' that can be applied for a given E/n and specific set of experimental conditions to account for the contribution of fragmented C8 and C9 aromatics to the benzene signal at m/z 79 [39]. The approach used by Rogers (2006) had been detailed in equation 33 [39].

$$[Benz] = [M79] - 0.092 \times [C2\ Benz] - 0.065 \times [C3\ Benz] \qquad (33)$$

Where the contribution of C2 benzene compounds (0.092 x [C2 Benz]) and C3 benzene compounds (0.065 x [C3 Benz]) are subtracted from the measured intensity at M79.

This approach worked well for these studies, demonstrating good agreement between corrected benzene VMR with GC-FID VMR measurements [39]. The study unfortunately gives no quantifiable information about the individual C8 aromatics in BTEX using PTR-MS due to the isomeric interferences at m/z 107 and relies on the assumption that the relative proportions of the C8 aromatics (ethylbenzene, *o,m,p*-xylene) in the mixture analysed are fixed throughout the

duration of the measurement, restricting the experimental scenarios for which the correction is valid. This assumption was verified by GC-FID which allows validation that under these conditions, the benzene signal can be quantified from the C8 interference [39].

5.5.2 Motivation

The primary motivation behind the investigations into BTEX was to determine if quantifiable information about the C8 aromatics can be gained from modifying drift tube parameters, in a controlled, but high time resolution PTR-MS system.

The issue with using an experimental setup with a fixed E/n and parent ions only is that the discriminating power is low. For a mixture with some concentration of benzene, ethylbenzene and xylene, with the product ion distributions as shown in table 18. The mixture has 3 unknowns at 2 ions and most importantly, has 2 compounds which produce a single product ion at both m/z 79 and m/z 107. This means that any mathematical solution will be unable to fit the data based on the product ion distributions as the contribution of ethylbenzene to the ion intensity at m/z 79 and m/z 107 cannot be determined under these conditions.

Table 18 - Example product ion distributions for benzene, ethylbenzene and xylene for which a mathematical solution cannot be found

	m/z 79	**m/z 107**
Benzene	100	0
Ethylbenzene	50	50
Xylene	0	100

The branching ratios of benzene, toluene, ethylbenzene and the 3 xylene isomers were investigated to determine and quantify the interferences between compounds and the fragment ions formed.

5.5.3 Sample Preparation

For each individual compound, calibrated diffusion tubes were used to introduce the sample into the PTR-MS. The thermostat was first analysed at each E/n to characterise the background signal from the experimental setup, taking care to look at any interfering signals that appear at expected parent and fragment masses. The diffusion tubes were then inserted, allowed to equilibrate in a flow of N_2 and checked for saturation. Once signal saturation had been ruled out, an E/n study was performed, taking data for 20 seconds at each E/n in order to gain significant statistics on the count rate. The data was then processed by identifying parent and fragment ion signals, normalising these to the reagent ion signal (calculated m/z 19) and then subtracting the normalised background ion signal for the bag. The branching ratios for ethylbenzene and the 3 xylene isomers were then calculated.

5.5.4 Experimental results

The product ion distribution graphs for benzene, ethylbenzene and p-xylene are shown in figures 65-67.

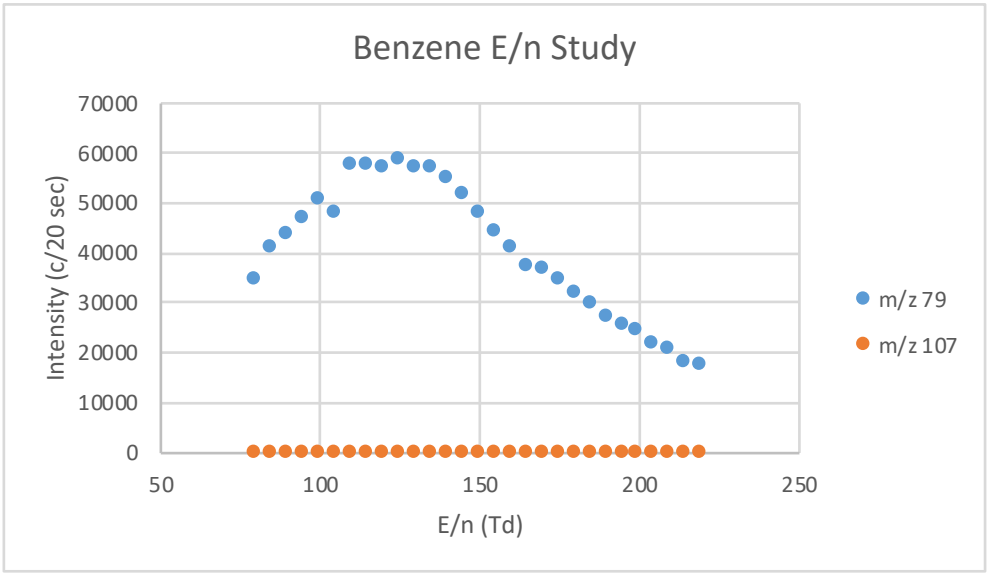

Figure 65 - Benzene E/n study over the E/n range 80-220 Td

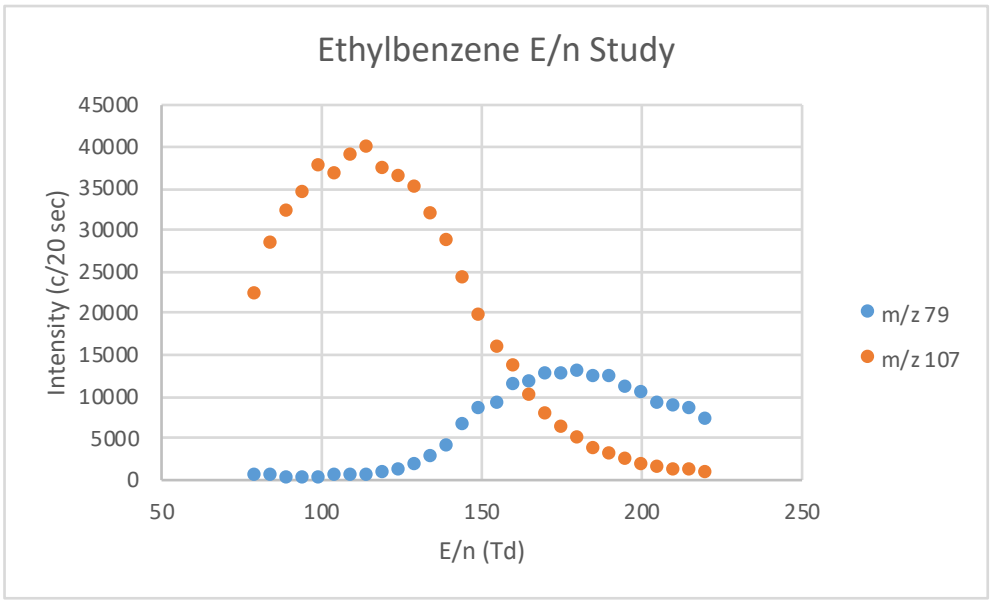

Figure 66 - Ethylbenzene E/n study over the E/n range 80-220 Td

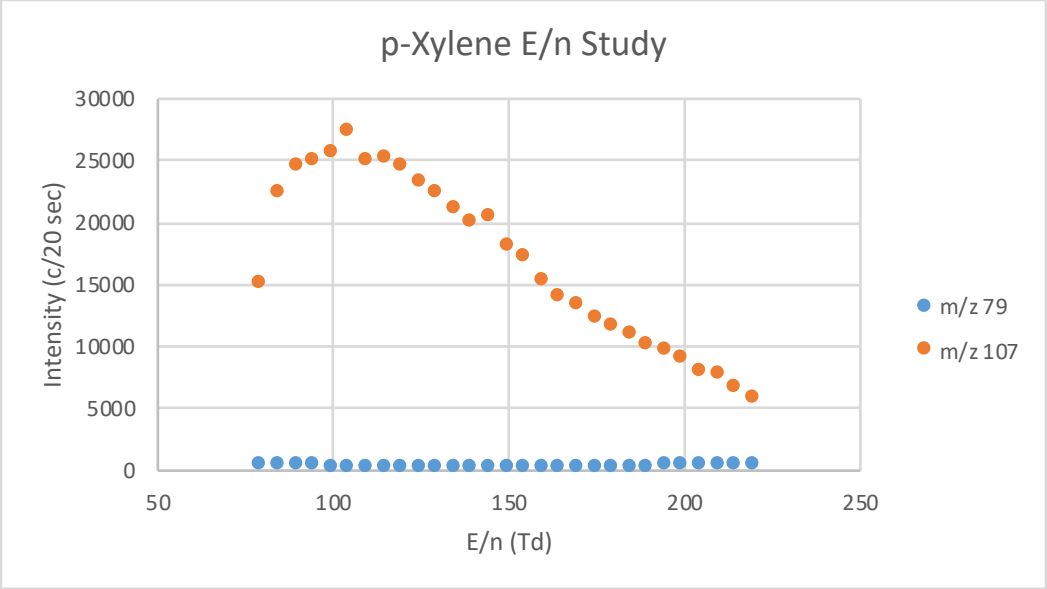

Figure 67 - p-xylene E/n study over the E/n range 80-220 Td

The fragmentation of the three xylene isomers (*o/m/p*) is minimal, shown in the branching ratio graphs in figures 68-70.

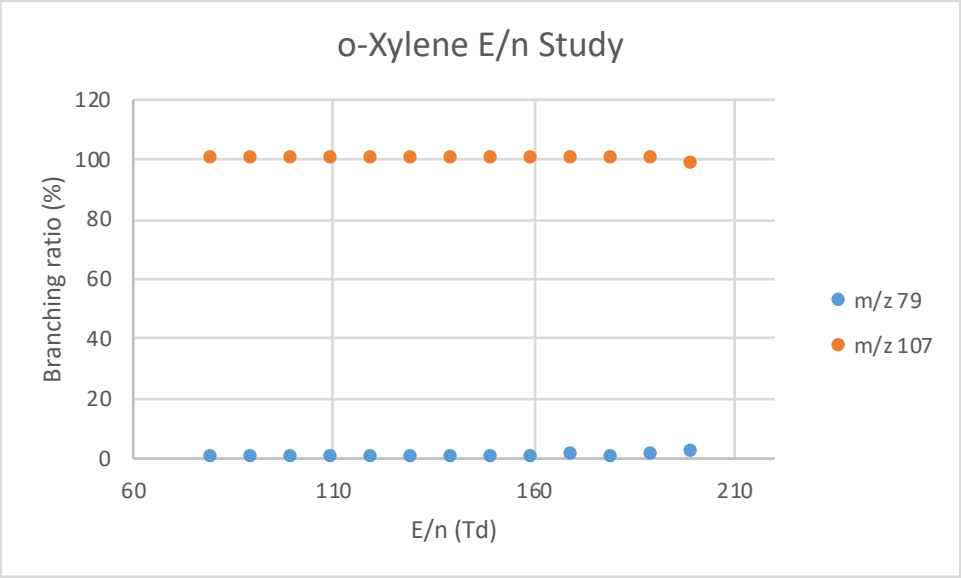

Figure 68 - Branching ratio graph for o-xylene over the range 80-200 Td.

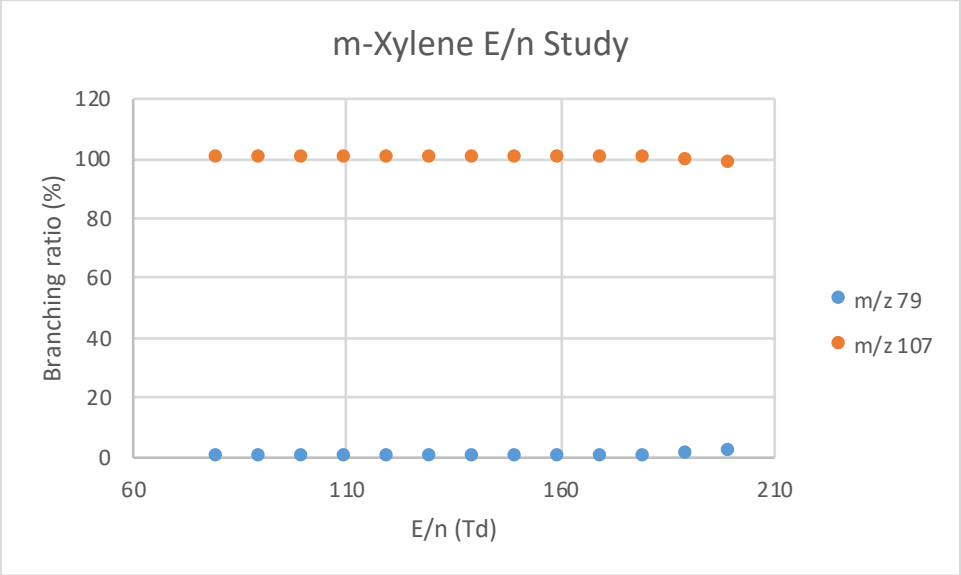

Figure 69 - Branching ratio graph for m-xylene over the range 80-200 Td.

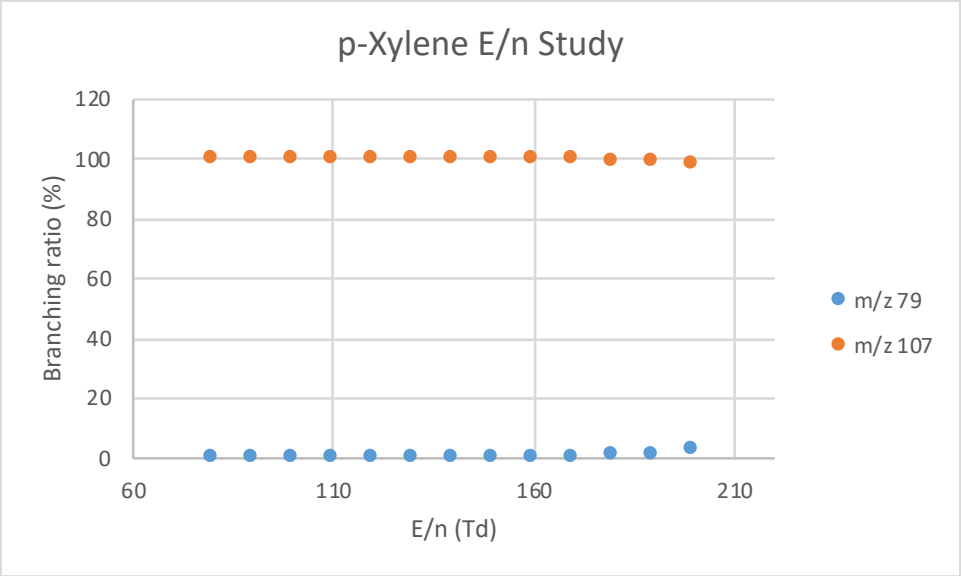

Figure 70- Branching ratio graph for p-xylene over the range 80-200 Td.

The branching ratio graphs demonstrate that for the isomeric C8 aromatics, the fragmentation is different between the *o/m/p*-xylene and ethylbenzene and it is this difference in fragmentation which may be manipulated in order to extract information about the VMRs of the individual compounds. Unfortunately, the only

product ion observed at the E/n values studied here for the 3 xylene isomers over the reduced electric field strength range of 80-180 Td is the protonated parent ion, produced as a result of non-dissociative proton transfer from H_3O^+. At reduced electric field strengths > 180 Td, some products of fragmentation are observed at m/z 79, however the transmission of the ions is poor as shown in figure 67 for p-xylene. This would make quantifying the individual xylene isomers difficult using the experimental conditions in this study.

The approach for development of an algorithm for quantification is based on the product ion distribution of the C8 aromatics. Whilst ethylbenzene produces a fragment ion at m/z 79 at E/n > 110 Td, the 3 xylene isomers do not fragment across the E/n range investigated (80-200Td).

The algorithm developed here for quantification of the individual components relies upon using the differences in product ions between measurements at different E/n values. The following sections explain the method for determining the concentration (VMR) of each compound in a mixture followed by the equations to solve for the quantification of each compound

5.5.4.1 Quantification of Benzene

From the data presented in figure 65 and 66, the quantification of benzene is relatively simple, even whilst avoiding interferences from the fragmentation of C8 aromatic species. The interferences in the benzene signal at m/z 79 from the C8 aromatics can be avoided by operating at an E/n of around 120Td. At 120Td, the C8 aromatics undergo very little fragmentation (<1%), the sensitivity of benzene is optimal for maximum sensitivity and similar to the E/n values which researchers often operate PTR-MS instrumentation.

5.4.4.2 Quantification of Ethylbenzene

Ethylbenzene is a C8 aromatic studied here that produces a significant fragment ion at m/z 79, which interferes with the benzene signal at E/n >120Td. Therefore, if a measurement is made at 180Td, a significant proportion of the signal intensity at m/z 79 will be from the fragmentation of ethylbenzene. Using a measurement of a mass spectrum at 2 different electric field strengths, where the behaviour of ethylbenzene is different would allow the quantification of the isomers.

Knowing the VMR of benzene from the measurement made at 120Td and the relative transmission factors for benzene and ethylbenzene in the PTR-MS at 120Td and 180Td (which are experimentally determined to take account for change in transmission of the ions and sensitivity at different reduced electric field strengths), the benzene signal at 180Td can be subtracted from the total signal at 180Td for m/z 79. This gives the signal intensity for the ethylbenzene fragment,

which using an appropriate RSF can be used to calculate the VMR of ethylbenzene.

5.5.4.3 Quantification of o/m/p-Xylene

The three xylene isomers are relatively stable and undergo very little fragmentation in the E/n range investigated here (80-200Td), producing the non-dissociative proton transfer product ion at m/z 107. As the xylene isomers exhibit very little fragmentation (<1%), the product ion distributions of the 3 xylene isomers are almost identical and therefore means quantifying them individually would be challenging with the current system. However, it would still be desirable to know the sum of the xylene isomers without the interference from ethylbenzene.

At E/n values > 120Td, ethylbenzene fragments to form an ion at m/z 79, however also forms a product ion from non-dissociative proton transfer at m/z 107 at all electric field strengths. At a carefully selected E/n, a multiplication factor can be used to determine the percentage of ethylbenzene signal at m/z 79 and m/z 107 (based on experimental lab data). This can then be used to determine the expected count rate at m/z 107 from ethylbenzene. Subtracting this from the total signal at m/z 107, in order to leave the signal associated with xylene.

The quantification and processing of the data can be displayed as the data processing flow chart as shown in figure 71.

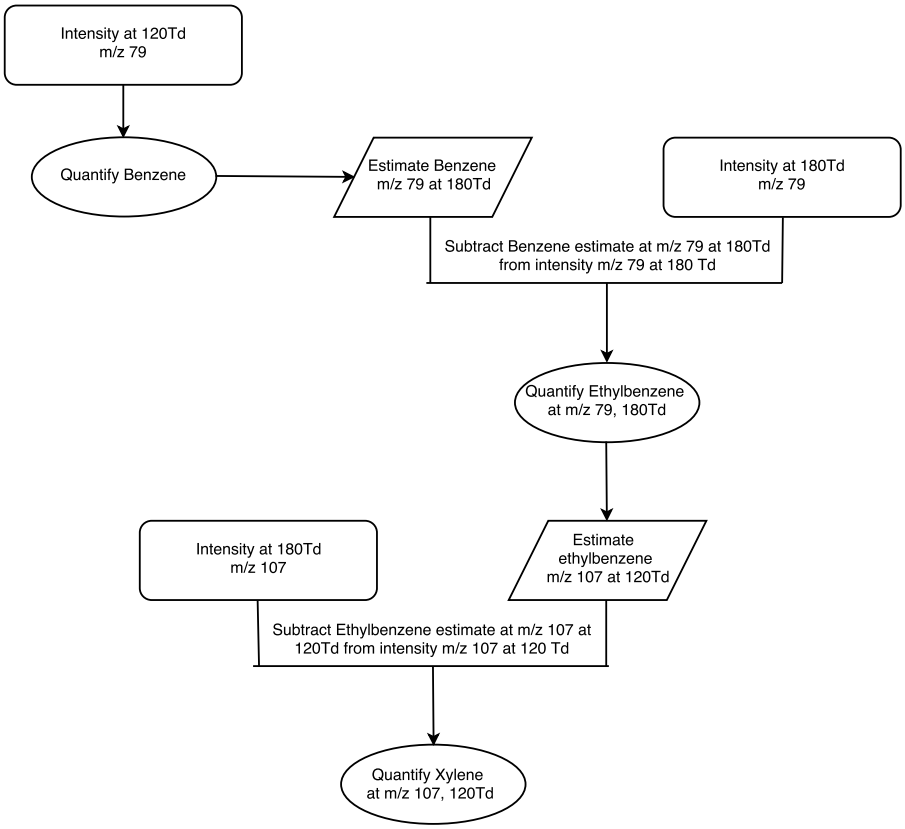

Figure 71 - Data processing diagram showing input values from mass spectra (rounded rectangles), estimates of signal intensity based on input data and product ion distribution of compounds (parallelograms) and signal intensity to quantify a given compound (ellipse).

5.5.5 Algorithm Development

Using multiple E/n values gives discriminating power to the mass spectral analysis that using a single E/n cannot. Many field campaigns and laboratory studies use a single fixed E/n, often a compromise between minimising water clusters and maximising protonated parent ion production leading to optimum sensitivity for VOCs [109, 110]. With the commercialisation of fast switching E/n power supplies,

the difficulty of using multiple E/n values can be overcome and may be useful, offering more discriminating power.

For a general case of three compounds, which can interfere with each other in 2 mass channels, the signal intensity which can be converted into a concentration with a suitable RSF, can be described in equations 34-37.

$$Int\ m/z_{1\ (Low\frac{E}{n})} = A_1 + B_2 + C_3 \quad (34)$$

$$Int\ m/z_{1\ (High\frac{E}{n})} = A_4 + B_5 + C_6 \quad (35)$$

$$Int\ m/z_{2\left(Low\frac{E}{n}\right)} = A_7 + B_8 + C_9 \quad (36)$$

$$Int\ m/z_{2\left(High\frac{E}{n}\right)} = A_{10} + B_{11} + C_{12} \quad (37)$$

There may not be a contribution for each compound (A, B, C) at each mass channel and reduced electric field strength, but this can be considered as the general case.

Equations produced for the quantification of BTEX can be solved for the concentration of benzene, ethylbenzene and xylene (equations 38-40).

$$Int_{79\ (120\ Td)} = [Benzene] \quad (38)$$

$$Int_{79\ (180\ Td)} = ([Benzene] \times A) + [Ethylbenzene] \quad (39)$$

$$Int_{107\ (120\ Td)} = ([Ethylbenzene] \times B) + [Xylene] \quad (40)$$

Where:

[Benzene] is the count rate for benzene at m/z 79 and 120Td

[Ethylbenzene] is the count rate for ethylbenzene at m/z 79 and 180Td

[Xylene] is the count rate for xylene at m/z 107 and 120Td

A is the transmission factor for benzene at m/z 79

B is the transformation from ethylbenzene count rate at m/z 79 at 180Td to m/z 107 at 120Td

The result of the equations gives the count rate for one of the compounds (BTX) at the specified mass channel and given E/n. These values can be converted into a concentration given a suitable instrument determined relative sensitivity factors (RSF). The average of the concentrations calculated for ethylbenzene and xylene should give a more accurate estimation of the real concentration as using multiple E/n values should give more confidence for the mixture analysis.

Each of the measurements, either of a count rate or individual compound for determination of an RSF are subject to errors. In solving these equations, there is a cumulative error which has been calculated and included in the mixture analysis results.

The main limitation of the method is in the use of factors A and B. For specified E/n values, these factors should be relatively reproducible within a specific instrument. However, there may be inter instrument variations in these factors, so they would have to be determined for specific instrumentation. The error in the

measurement of E/n and small variations in temperature, pressure and voltage should also be considered. For this reason, it is important to ensure that the instrumental factors A, B are as accurate as possible with the errors sufficiently represented.

When testing the method, the most important error to consider is the error in the preparation of the test mixtures. Regardless of how the mixtures are prepared, there is an inherent error. If using Teflon® bags or syringes, there could be a significant human error in the transfer of analytes. If the mixtures are prepared by combining gas cylinders, there is error in not just the stated concentration, but also the equipment used for mixing (such as mass flow controller).

This method to quantify isomers is dependent on several conditions being met. The first is that the concentration or composition of the mixture does not change significantly between the 2 E/n measurements. This can be ensured by reducing the measurement time and thus switching between the two reduced electric field strengths at a higher frequency (e.g. 1Hz). The second condition is that the RSFs and product ion branching ratios are accurately characterised for the specific PTR-MS under the operating conditions used in the sample measurements.

5.5.6 Determination of accuracy and precision of method

5.5.6.1 Preparing the standards and mixtures

In order to determine the accuracy and precision of the algorithm developed in this study, an experiment to test the method was devised. By using diffusion tubes, each filled with a different component of BTEX, accurate standards can be produced for validation of the method. Mixtures of these tubes can be used to validate if the method performs well for different scenarios.

Due to the vapour pressures of ethylbenzene and xylene relative to each other, the same size tubes and thermostat temperatures were used for ethylbenzene and xylene. A benzene standard (1ppm in nitrogen, BOC, UK) was used for determination of the benzene sensitivity and for creating mixtures.

Tubes were filled with 200μL of one of the compounds (ethylbenzene, xylene) (99+% purity, Sigma Aldrich) and weighed periodically. Throughout the calibration, the tubes were kept in a thermostatically controlled diffusion tube oven with a flow of 0.5 Lpm nitrogen (BOC, UK). The tubes were weighed periodically with the mass loss plotted vs time. Linear regression analysis was performed using Minitab and the 95% confidence internal and 95% prediction interval plotted. The slope of the linear trend line is equal to the mass loss for each tube and therefore the emission rate of the compound. Knowing the molecular mass of the compound and the dilution flow, the concentration of each compound standard can be calculated.

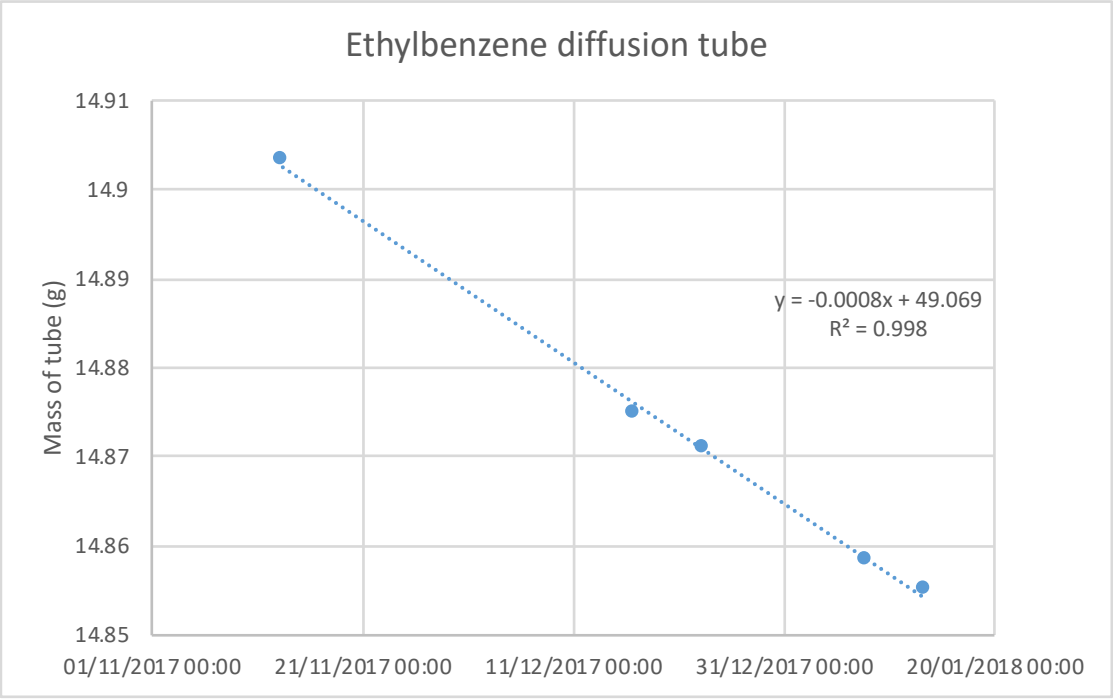

Figure 72 - Ethylbenzene diffusion tube calibration, using a 0.5mm/2cm capillary bore diffusion tube at 40℃. The emission rate from the slope of the linear regression gives a diffusion tube output of 793600ng/day.

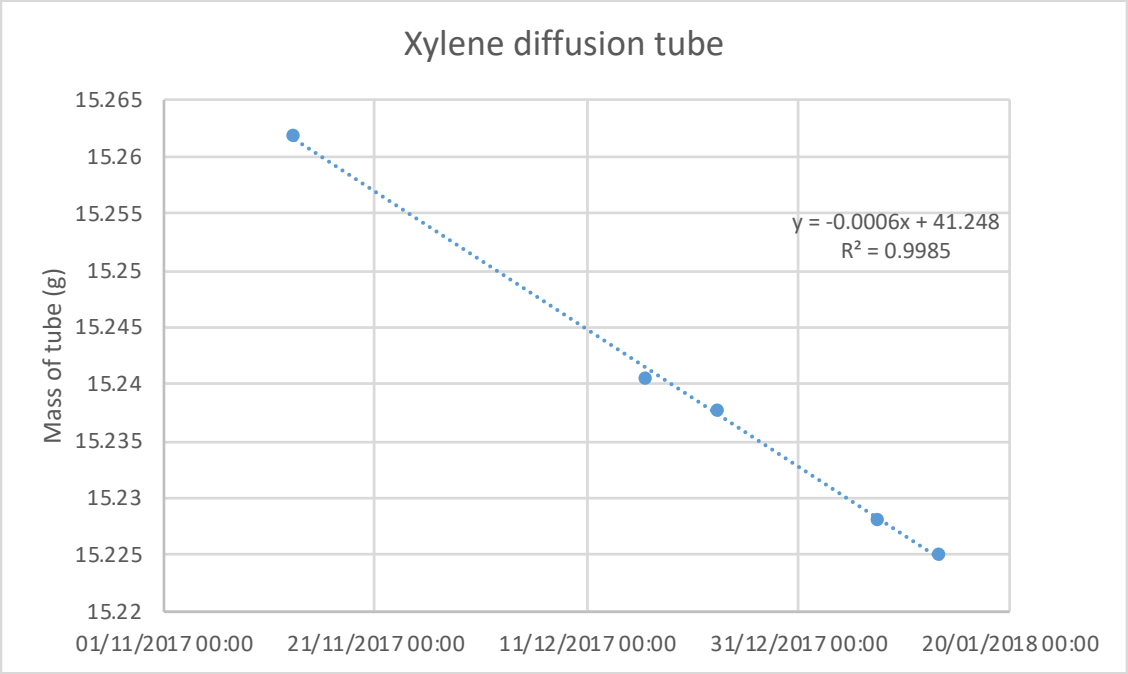

Figure 73 – Xylene diffusion tube calibration, using a 0.5mm/2cm capillary bore diffusion tube at 40℃. The emission rate from the slope of the linear regression gives a diffusion tube output of 603600ng/day.

The calibration graphs shown in figures 72 and 73 show the weighing's which produce a linear regression, where the diffusion tube is emitting at a constant rate. When showing all the weighing data, it is observed that the regression is not linear from the first weighing and indeed can take 1-7 days to show linearity. This is from the loss of volatile impurities present in the sample when purchased (as described in chapter 3).

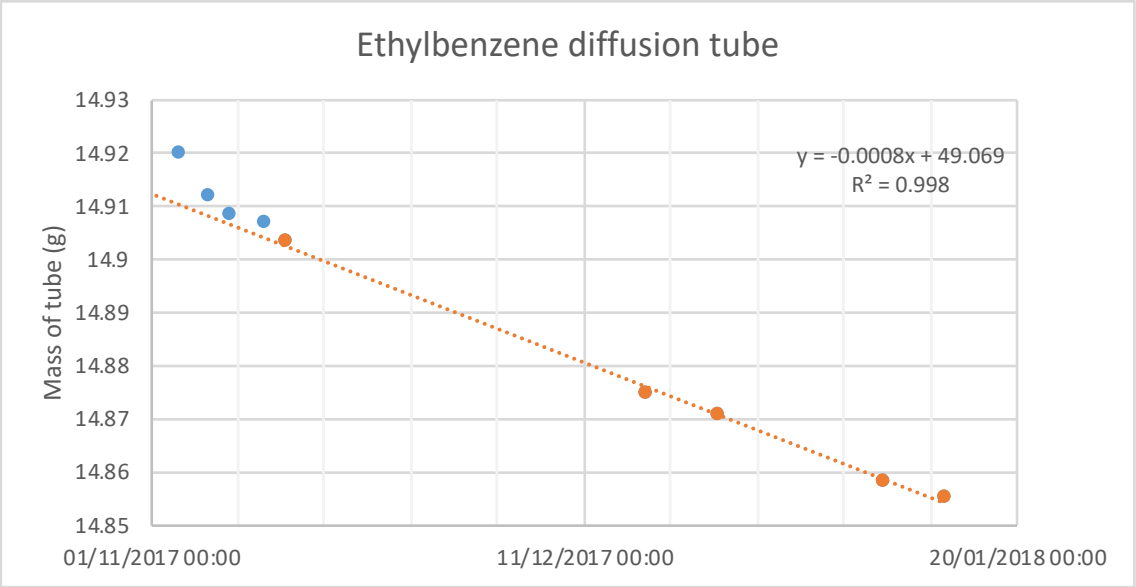

Figure 74 - Ethylbenzene diffusion tube, showing the increased rate of mass loss of volatile impurities between points 1-4.

In the case of ethylbenzene, it is assumed that benzene may also be present and due to the order of magnitude difference in vapour pressures (benzene 12.6 kPa at 25°C [73], ethylbenzene 1.28 kPa at 25°C [73]), benzene is emitted from the tube at a much quicker rate than ethylbenzene, resulting in a larger mass loss initially. This is difficult to quantify from a mass spectrum before gaining knowledge of the product ion distributions as benzene and ethylbenzene both contribute to an ion at m/z 79 ($C_6H_7^+$).

Using the linear regression line and extrapolating, it is possible to calculate the mass loss due to volatile impurities and whether this is consistent with the stated purity based on the total mass of compound used in the tube.

Equally if the impurities are less volatile than the compound in the diffusion tube, they will contribute a small percentage (>0.5%) to the mass loss of the compound filled tube and introduce a systematic error. This error is unavoidable without further purification of the compound as supplied and mitigation measures such as purchasing high purity analytical standards to reduce the systematic error can be used.

5.5.6.2 Measurement of standards and mixtures

In order to determine the algorithm accuracy and precision, specific measurements at predetermined reduced electric field strengths were needed in order to characterise the instrument sensitivity and fragmentation response to the compounds in the BTEX mixture. Each measurement was for a 60 second experiment time and 3 replicates analysed. The measurement was normalised to the reagent ion signal and the 3 replicates averaged, with a standard deviation of the mean calculated.

5 different mixtures were analysed, varying the flow through each of the thermostats (with a diffusion tube in each) and the flow of 1ppm benzene standard

to achieve different mixtures of BEX. The basic setup of the apparatus is shown in figure 75. A modification of the experiment setup to achieve different concentrations of the individual components of BTEX, where each thermostat was exhausted separately, was used for mixtures 4 and 5.

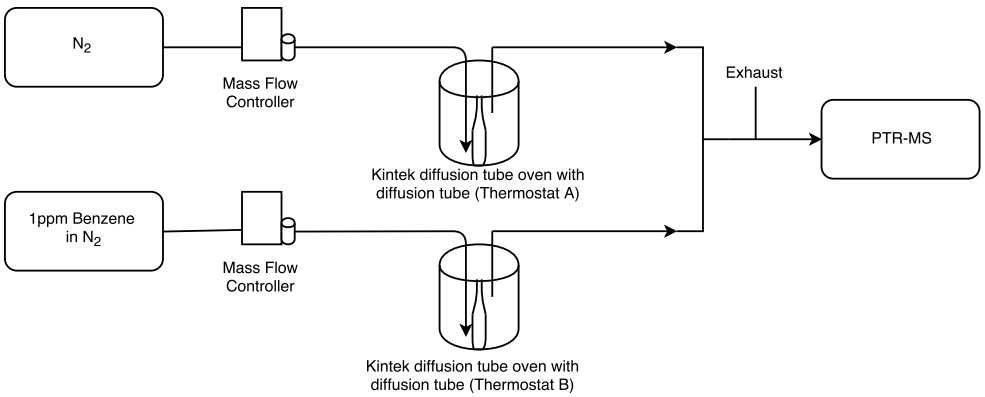

Figure 75 - Schematic of experimental setup for analysing BTEX mixtures

5.5.6.3 Results of standards and mixtures

The results of the mixtures are summarised in table 19, with the intensity of each of the product ions, the calculated concentration from the RSFs for each compound and the concentration of the compounds in the gas mixture.

Table 19 - Results from the analysis of 5 mixtures of BEX. The concentration of benzene (gas standard), ethylbenzene and xylene (diffusion tubes) were calculated along with uncertainties from the gradient of the slope at the 95% confidence interval for ethylbenzene and xylene and the stated uncertainty for the benzene gas standard.

	BEX used in the mixture			**Calculated BEX**		
Mixture	**Benzene (ppb)**	**Ethylbenzene (ppb)**	**Xylene (ppb)**	**Benzene (ppb)**	**Ethylbenzene (ppb)**	**Xylene (ppb)**
1	500 ± 50	318 ± 25	241.5 ± 17.5	492 ± 28	305.4 ± 34.5	273 ± 15
2	250 ± 25	318 ± 25	241.5 ± 17.5	219 ± 19	304.5 ± 34.5	205 ± 15
3	125 ± 12.5	318 ± 25	241.5 ± 17.5	96.5 ± 12.5	276.6 ± 34.5	268 ± 15
4	500 ± 50	635 ± 52	241.5 ± 17.5	428 ± 28	501 ± 31	258.5 ± 15
5	500 ± 50	318 ± 25	483 ± 35.5	422 ± 28	327 ± 34.5	422 ± 19

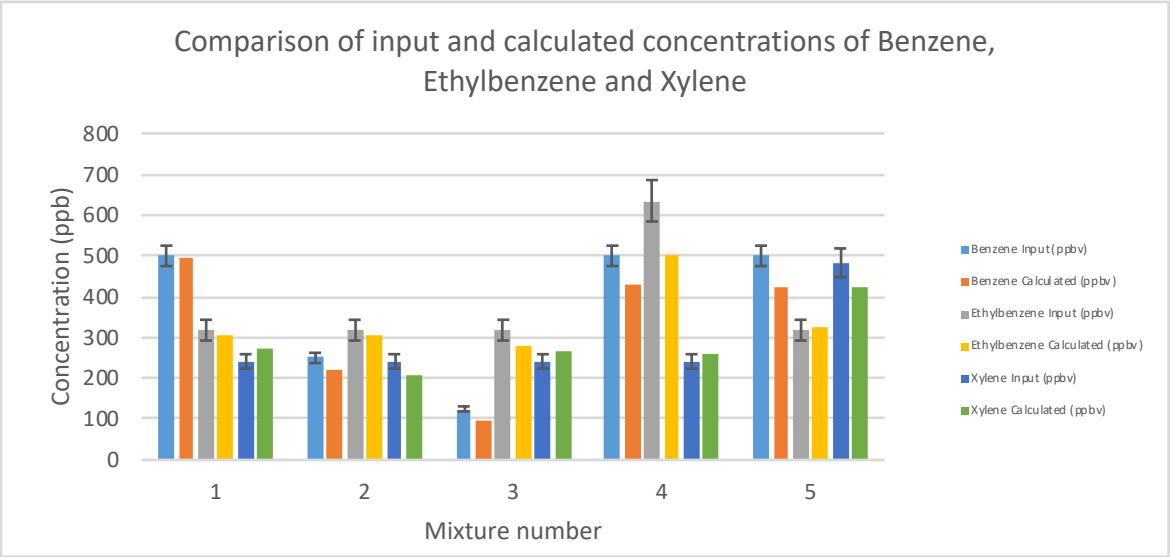

Figure 76 - Comparison of the input concentrations (calculated from the emission and flow rate for each compound) and the calculated concentration of each species in the 5 mixtures using the method detailed in this chapter with RSF.

For most of the mixtures analysed, the calculated values for each of the individual components are in agreement with the calculated concentrations from the output of the mixture analysis. There are however, some discrepancies between the input and calculated concentrations for BEX in a mixture and the most likely cause of these discrepancies is from poor mixing of the input gas streams, leading to the incorrect calculation and reporting of the concentration of each component in the gas mixture. This demonstrates the suitability of the method for analysis of mixtures of BEX.

5.5.7 Fast switching E/n

Switching of the electric field can be used to provide multiple data sets at a high frequency for use in differentiating isomers. This is useful for monitoring changing environments, as a condition of the method is for the concentration and

composition of the analyte gas to be relatively constant. In switching between 2 E/n values quickly, this can reduce the analysis time and allow the use of the method in more applications, such as flux measurements where the requirement of data at 1 Hz or better is required.

The equipment used for the fast switching relies on a secondary PTR reactor power supply (with control electronics) which allow for switching between the two supplies at up to 5 Hz. For routine analysis it is more useful to operate at a frequency of 1 Hz, to allow the most useable data to be extracted at each E/n. This is due to a short switching time of around 150 ms, associated with the electronics and the residence time of ions in the reactor. For this reason, operating at frequencies higher than 1 Hz reduces the amount of useable data.

The data can be extracted by specifying a switching time, removing these sections and combining the sections of the mass spectra taken at each E/n to produce 2 output files. An example of BTEX data, switched at 0.5 Hz is shown in figure 78, with the data plotted every 100 ms.

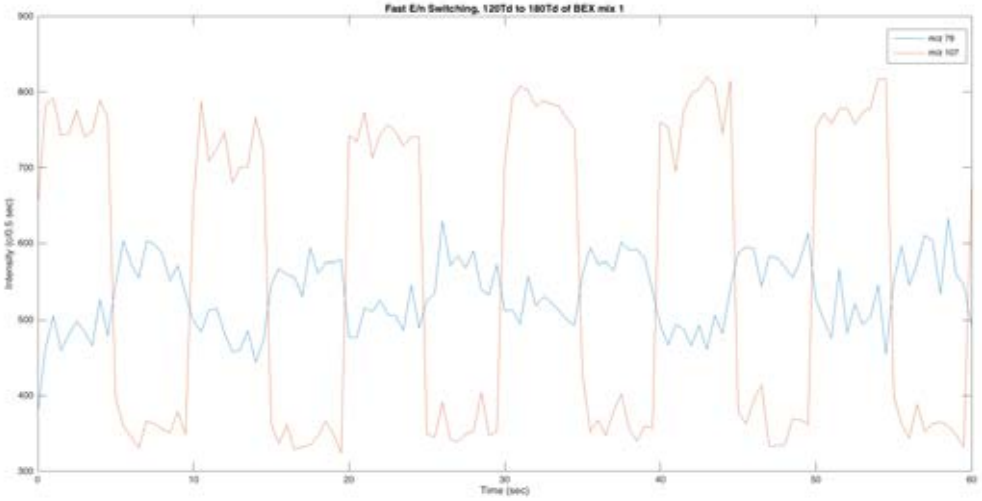

Figure 77 - E/n switching at 0.2Hz of mix 1 containing BEX plotted at 0.5 second resolution. At low E/n (120Td), the m/z 107 intensity is high, as the xylene and ethylbenzene produce significant amounts of this ion. At 180 Td, the ethylbenzene fragments to form an ion at m/z 79, decreasing the measured intensity. The other point to note is that the transmission efficiency of BEX decreases at higher E/n, reducing the measured signal at high E/n.

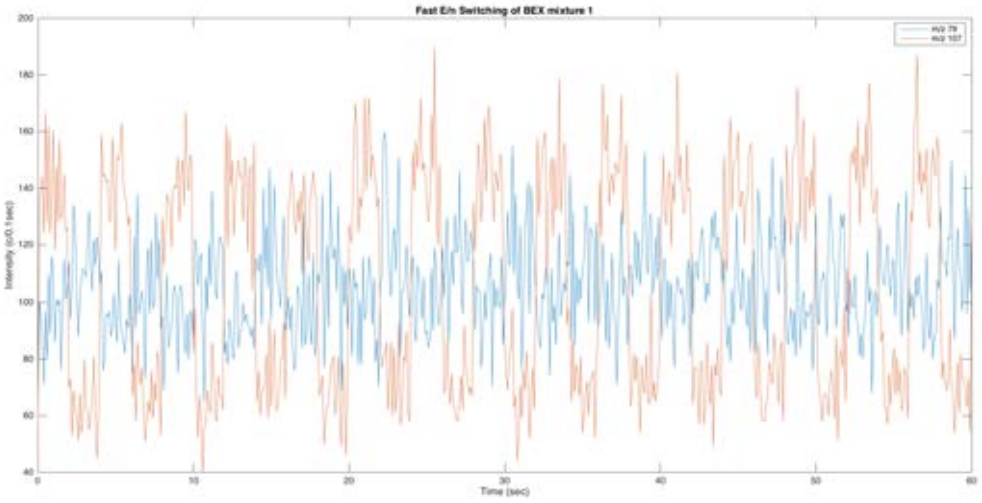

Figure 78 - E/n switching at 0.5 Hz of BEX mixture 1, plotted at 0.1 second resolution.

The implementation of the fast switching E/n and the analysis using the BEX method allows BEX mixtures to be quantified in changing environments.

5.6 Conclusion

This chapter demonstrates the practical use of modifying drift tube parameters in order to provide quantitative information on mixtures containing isomeric or interfering compounds. This includes compounds commonly measured in atmospheric chemistry, including isoprene and 2,3,2-MBO, MVK and MACR and BTEX. The method allows changes in concentration of individual compounds to be accurately accounted for at a high precision within complex atmospheric mixtures.

The implementation of a fast switching E/n power supply system has been demonstrated for a PTR-MS, allowing the automated measurement of the compounds at 2 different E/n values for use in the methods detailed in the chapter.

There are 3 main methods conceived here for the quantification of compounds in a mixture.

1) A method using the subtraction of one ion signal from another, in order to determine the concentration of both species. This has been demonstrated with isoprene and 232MBO.
2) A method using the change in the protonated parent ion as a function of E/n in order to determine the composition of a sample with 2 isomeric compounds. This method has been demonstrated with the isomers MVK and MACR.
3) A method to utilise several reduced electric field settings to quantify a BTEX mixture with multiple unknowns.

These methods could be used for other sets of compounds for which quantification due to interfering peaks is an issue in PTR-MS. Some *a priori* knowledge is required to use these methods

To use a more general method for analysis of unknowns, theoretically it would be possible to create a product ion distribution matrix for all VOCs measurable by PTR-MS in order to create a fitting algorithm to solve for all VOC present in a real air sample. This would involve significant analysis of individual compounds to build up a library file and is beyond the scope of the work in this thesis.
The implementation of this method to measurement of VOC mixtures would produce 3 main outcomes.

1) The proportions of individual isomers in VOC mixtures can be quantified, which can be important for determination of the VOC source or for monitoring purposes.
2) To provide information on the composition of VOC mixtures in air samples, reducing the requirement of confirmatory GC-MS analysis of isomers in complex VOC mixtures.
3) To expand the range of compounds for which soft chemical ionisation (specifically PTR-MS) can be used for during field studies.

6 - Measurement of Polycyclic Aromatic Hydrocarbons by PTR-MS

6.1 Introduction and motivation

Polycyclic aromatic hydrocarbons (PAHs) are molecules, released by industry and formed during incomplete hydrocarbon combustion, that have a wide range of health effects [111-113]. Some common PAHs are known to be toxic and carcinogenic, forming mutations in DNA which may lead to cancer [113]. Many countries have established limits for the atmospheric concentration of PAHs using benzo[a]pyrene (BaP) as a marker, especially in polluted inner city and industrial areas[111]. Within Europe, the atmospheric concentration of BaP is often well below the EU legal limit of 1ng/m^3 and monitored to ensure compliance with EU law [114]. However, the real concern is the air quality of rapidly industrialising cities, such as Beijing and New Dehli, with China and India accounting for over 38% of the estimated global total PAH emission (16 PAHs listed as US EPA priority pollutants) [115]. In these more polluted areas, the requirement to monitor PAHs frequently may be of benefit in tracking sources of PAHs, pollution events and deposition and reactions of PAHs.

Much of the routine analysis of atmospheric PAHs is currently achieved through trapping the PAHs on a filter, which can be thermally desorbed into a GC-MS [46] or extracted using a suitable solvent for HPLC or LC-MS [116]. These techniques both provide sensitive analysis at the picogram level [116], but suffer from time

averaged sampling, long analysis times and significant sample preparation requirements. This leads to a low sample throughput which may not be desirable if whole air samplers are drawing polluted air through the filters for short time periods.

In the UK, PAHs are currently monitored at 31 sites with each sample collected for a 24-hour period, producing a time averaged daily concentration [117]. In more polluted environments, the sampling period used is often much shorter, for example in China, where a 2-hour sampling period is sufficient [46]. Using a PTR-MS for the measurements of PAHs including benzo[a]pyrene at a higher frequency than currently used, or even on-line, would allow scientists to study the reactions of PAHs in the gas phase and the emissions from particular sources. This may be achievable as the measurement of SVOCs by PTR-MS has recently been demonstrated for several different classes of low volatility compounds, including explosives [42], narcotic substances and drugs [118].

This chapter was motivated by the requirement to determine if it would be feasible to measure PAHs using a PTR-MS, with little mechanical modification, with the aim to enhance the capability of PTR-MS for existing users and establish new instrument protocols for the analysis of SVOCs. The application of the RF ion funnel would also be investigated to determine if there are any selectivity/sensitivity enhancements for isomers and if controlled fragmentation could be used to quantify isomeric species. More specifically to environmental analysis, PTR-MS would provide an alternative technique for the measurement of

PAHs, with a rapid measurement time and higher sample throughput than existing techniques which would be beneficial for studying plumes or rapidly changing PAH concentrations.

6.2 PTR-MS for PAH measurement

At present, the literature available for the detection of PAHs by PTR-MS is limited to studies on the smallest and most volatile PAHs, naphthalene [43, 87], acenapthalene [119], acenaphthylene [119] and anthracene [120]. The chemical and physical properties of some common PAHs of interest (including those on the US EPA priority pollutants list) are shown in table 20. The vapour pressure of the PAHs is much lower than many of the common VOCs for which PTR-MS is commonly used by researchers.

Table 20 – Chemical and physical properties of some common PAHs, including the formula, structure, molecular weight, melting point, boiling point and vapour pressure [45, 55]

Compound	Formula	Structure	MW (g/mol)	MP (°C)	BP (°C)	Vp (Pa at 25°C)
Napthalene	$C_{10}H_8$	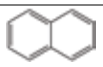	128.19	81	218	10.4
Acenapthalene	$C_{12}H_{10}$		154.21	96	278	0.3
Phenanthrene	$C_{14}H_{10}$	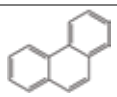	178.2	101	339	0.02
Anthracene	$C_{14}H_{10}$	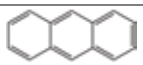	178.2	216	340	0.001
Pyrene	$C_{16}H_{10}$	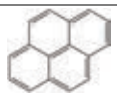	202.3	156	360	0.0006
Fluoranthene	$C_{16}H_{10}$	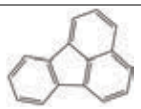	202.3	111	375	1.2×10^{-3}
Benzo[a]pyrene	$C_{20}H_{12}$	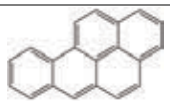	252.3	175	495	7×10^{-7}
Benzo[k]flouranthene	$C_{20}H_{12}$	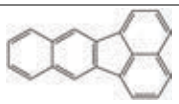	252.3	217	480	---

Much of the work on measurement of the most volatile PAHs (where the number of C<14) by PTR-MS is focused on the reactions of PAHs deposited on a Teflon surface with other species in the gas phase, such as chlorine atoms [119].

6.3 Sampling protocol

In order to develop a useful method for the detection of PAHs in the atmosphere, the sampling methods currently used need to be considered so that any development for detection of PAHs by PTR-MS can fit into existing monitoring regimes. As much of the current PAH measurement is by chromatographic methods such as LC and GC-MS, an offline trapping medium is used at the measurement site in order to adsorb VOCs and SVOCs for thermal desorption GC-MS [117] (usually at a later date).

The different methods of measuring PAHs are discussed in this section, with offline concentrating methods such as sorbent tubes and filter desorption and a comparison to direct air PAH sampling, including the use of dynamically generated PAH standards for PTR-MS.

6.3.1 Sorbent tubes

A common method of air sampling involves drawing air through a tube containing a sorbent material, which adsorbs compounds within the molecular structure of the sorbent. The choice of sorbent material is important for the absorption efficiency for specific compounds. There are many different types of porous adsorbent, some that can be general use, such as Tenax TA (a porous polymer for adsorption of a wide range of compounds), to more specific sorbents such as Tenax GR for PAHs (a 30% graphite carbon, 70% Tenax TA).

A benefit of sorbent tubes is that provided the compound isn't reactive or degrades quickly, they can be sealed and stored for moderate periods of time under the right conditions. This means that the sample can be analysed at a different time and location to where the sample was collected, which is beneficial if the sampling site is remote or particularly difficult to operate analytical instrumentation in. Typically, a thermal desorber is used to introduce the collected analyte to the inlet of an analytical instrument, such as a GC-MS or PTR-MS. Knowing the volume of air drawn through the tube and the adsorption efficiency of the compound to the sorbent allows a concentration of the PAH to be calculated from the quantitative measurement.

6.3.2 Swab/filter desorber

Within the UK monitoring network, the most common sampling technique for PAH measurement is to use filter samples, which are then extracted into a suitable solvent and analysed. The 31 UK network sites use automated Digitel DHA-80 air samplers, which draw air through a Teflon filter for a 24-hour period [117]. The instrument collects information on the volume of air sampled and stores the filter samples in a holder, ready to be collected and analysed. The samples are then extracted into an organic solvent, cleaned up and analysed by GC-MS.

Other commercialised methods of thermal desorption use a swab, similar in design to those seen at airport security, usually made of a material such as Teflon, that SVOCs and particular matter can adsorb onto.

Figure 79 - Image of a Teflon swab used for the work in this chapter, which has been clamped in the swab desorber

This produces a similar sampling method to the filters already commonplace in UK PAH sampling, but with some benefits. Dependant on the analytical technique used, the filter can be thermally desorbed directly into the analytical instrument, avoiding significant sample preparation. The card surround provides a physical support to the Teflon surface and with commercial desorbers, an air tight seal is created during desorption by plastic deformation of the Teflon surface.

6.3.3 Direct air sampling

It is theoretically possible to sample air directly using PTR-MS, provided that the instrumental conditions allow for the efficient transfer of PAHs. However, the current UK regulations stipulate a limit of 1ng/m^3 of Benzo[a]pyrene, equivalent to an atmospheric concentration of 0.1ppt. This is far below the current detection limit of the PTR-MS instrumentation used in this study.

As a result, for routine environmental measurements, it is preferential to have a preconcentration step such as sorbent tubes and filter samples discussed in 6.3.1 and 6.3.2.

Direct air sampling of PAHs using PTR-MS may have a role in monitoring polluted environments, such as in China, where the Benzo[a]pyrene concentration in urban air may be up to 500ng/m^3 [46] and in laboratory-based simulations, where a PAH can be introduced into a reaction chamber (such as Teflon, FEP or glass) in order to study reaction kinetics. Using a higher concentration of PAH than is usually found in the environment may help in studying the gas phase reactions, as the high time resolution measurement capability of the PTR-MS can be utilised.

6.4 Determination of experimental parameters

When measuring SVOCs, the temperature of the inlet and transfer system is important to carry the analyte from the source to the PTR-MS drift tube. The increase in temperature means that the compound has a higher vapour pressure and can more easily transported in the gas phase. The desorption time of a PAH sample from the swab desorber to the inlet line must be relatively quick (as the full desorption profile as measured using the PTR-MS is 3-20 seconds), but difficult to determine individually due to the combined effect of desorber, inlet and PTR-MS temperatures. In these sections, the effect of temperature on the inlet system was investigated, to give an optimum set of conditions for the detection and quantification of PAH samples.

6.4.1 Heating

The detection of SVOCs, such as PAHs, requires careful heating of the instrument, inlet and desorption sections. Heating a SVOC sample raises the vapour pressure of the compound and allows it to more easily partition in the vapour phase. This is especially important in the case of PAHs, where the vapour pressure is typically $10^{-1}/10^{-2}$ Pa at 100 °C but increases exponentially with temperature (an example of the vapour pressure of a PAH, benzo[a]pyrene as a function of temperature is shown in figure 80). The loss of PAHs to exposed surfaces in the inlet system will decrease with increasing temperature, hence the reason for using high temperatures. It is therefore important to heat these sections as much as is practicable, so the following sections detail experiments to determine which sections require heating and the temperature that is feasible for this PTR-MS.

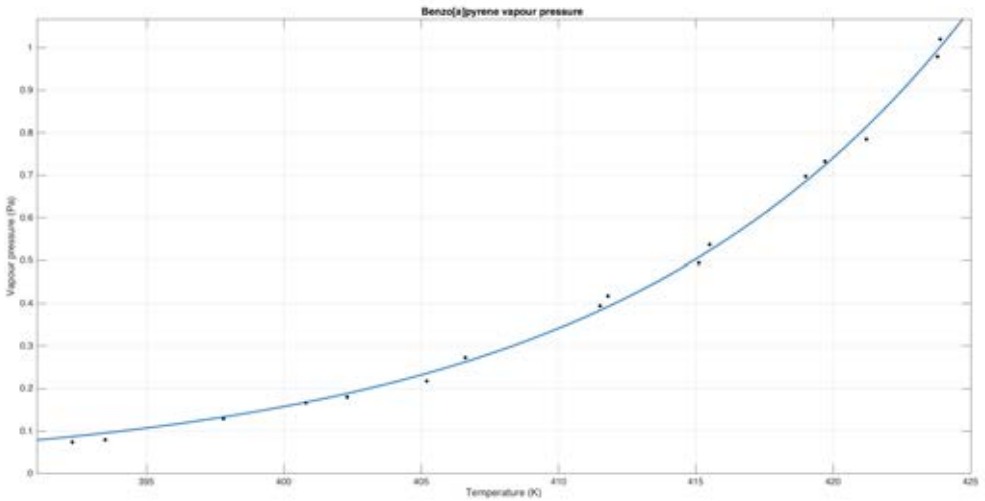

Figure 80 - Vapour pressure curve for Benzo[a]pyrene. Data taken from Goldfarb et al [121]

It is crucial to determine if the desorption and transfer heating is the important stage, or if the drift tube needs to be at high temperature also. The reasoning behind this is that in the silco steel coated pipe section from the desorber to the inlet valve, the analyte gas is at near atmospheric pressure and the analyte gas can freely interact with the surfaces of the inlet pipe. The surface effects for an analyte gas are reduced when at lower pressure, as the analyte gas has a higher velocity through the pipe and less collisions with the walls than at atmospheric pressure, resulting in lower adsorption of a sample of the walls of the pipe. If it is possible to operate the piping and drift tube at a lower temperature because they are at a lower pressure (≈ 2 mbar), this would allow existing instruments to be easily modified to measure PAHs. The only modification would be to introduce the sample by way of a thermal desorber, with a heated transfer line to the inlet valve.

6.4.1.1 – Effect of transfer line heating

In addition to the heating of the desorber and transfer lines, it is also important to consider the length of the transfer line on the desorption profile of the PAHs. As the analyte moves through the transfer line, the analyte will be in equilibrium between the mobile phase (gas) and stationary phase (inlet line). Increasing the proportion in the gas phase should decrease the spread of the analyte giving a sharper, better defined peak shape.

The length of the transfer line may also have an impact on the sensitivity through tailing of the desorption peak, as material may adsorb to the inlet line and be released slowly, causing a decrease in sensitivity of the desorption event.

6.4.1.2 Effect of inlet valve heating

The effect of inlet valve heating was determined using benzo[k]fluoranthene as a SVOC probe. The inlet valve and inlet line connectors (T2 and T3) were at atmospheric pressure and were heated using resistive nichrome wire heaters with an external power supply. The heating setup for the experiments are shown in figure 81 and summarised in table 21.

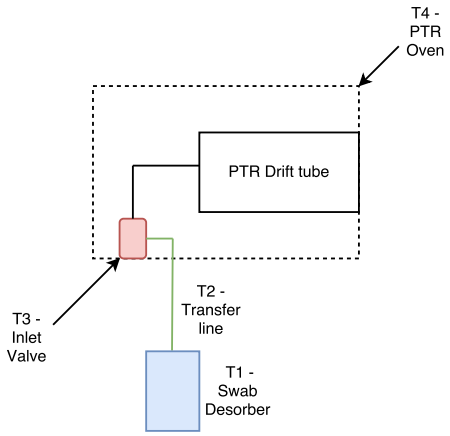

Figure 81 - Schematic of the different heating zones in the high temperature PTR-MS

The section of transfer line between the inlet valve and the PTR drift tube was passively heated by the PTR oven heaters to the temperature of the PTR oven. Between the inlet valve and the PTR drift tube the pressure is around that of the drift tube (≈ 1mbar) resulting in less interaction of the gas and the wall of the silco tubing.

Table 21 - Summary of the different heating zones in the PTR-MS and the method of heating for each section

Temperature control zone	Method of heating	Temperature range (°C)
T1 – Swab desorber	Internal resistive heating feedback loop control	20-200
T2 – 1/16" Silco transfer line	Nichrome resistive heating wire – external power supply	20-200
T3 – Silco inlet valve	Nichrome resistive heating wire – external power supply	20-200
T4 – PTR Oven	Fan oven heater and anode flange cartridge heater	20-200

The effect of heating the inlet valve to 200 °C was investigated using the PTR-MS. Both the swab desorber (T1) and transfer line (T2) were heated to 200 °C and the PTR oven (T4) was heated to 100 °C. Measurements of a 10ng swab of benzo[k]fluoranthene were taken with the inlet valve (T3) passively heated by the oven to 90°C and then resistively heated to 200 °C. The desorption profiles for the measurement are shown in figure 82 and summarised in table 22.

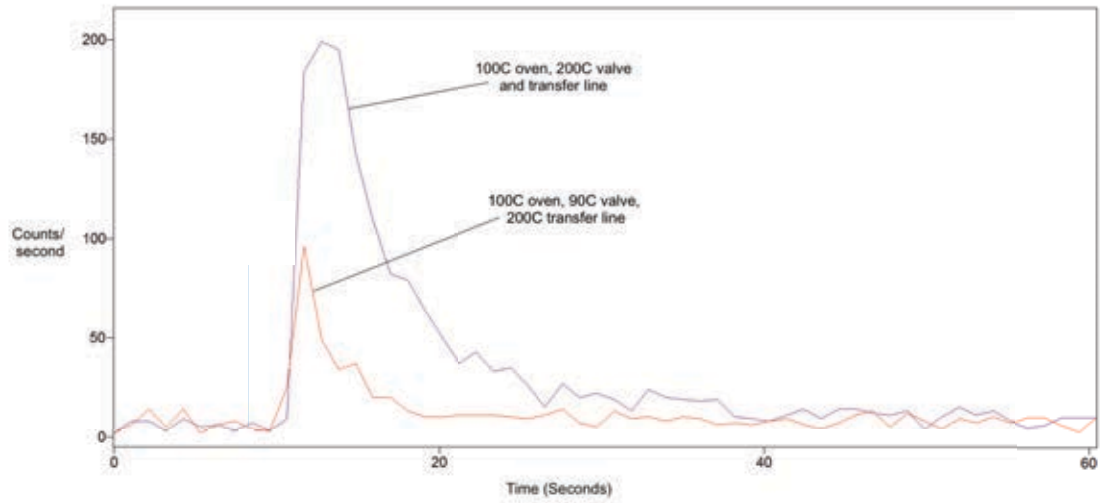

Table 22 – Results of the investigation into the optimum temperature settings for each of the temperature control regions in the PTR-MS. Three replicate desorption's of 10ng benzo[k]fluoranthene for each temperature setting were analysed in DC mode at 1 mbar drift tube pressure and 1.3mbar hollow cathode pressure with a reduced electric field setting of 140 Td.

Temperature setting	**ɔ ırber**	**T3 – I valve (°C)**	**T4 – P oven (°C)**	**Peak Area (Counts**	**RSD (%)**
2		200	100	1459	3.4

Figure 82 and the results in table 22 demonstrate the importance of heating the valve and all sections of the inlet which transfer the analyte at atmospheric pressure to a temperature as high as practicably possible. The upper working limit of the transfer line is around 200 °C and at temperatures above this, the materials used such as silicone cord insulation and the glass fibre heating cord have a reduced lifetime and are damaged during long term use (> 6 months).

6.4.1.3 Effect of oven temperature on sensitivity

The final section of the PTR-MS that requires elevated temperatures is the PTR oven, which directly influences the thermal energy contribution to the ions in the drift tube. The parameter space around the oven temperature is investigated, changing the oven temperature whilst maintaining 200 °C for the swab desorber, transfer line and inlet valve (which is known to give the best sensitivity from sections 6.4.1.1 and 6.4.1.2, see table 22). The result of changing the PTR oven temperature is shown in figure 83.

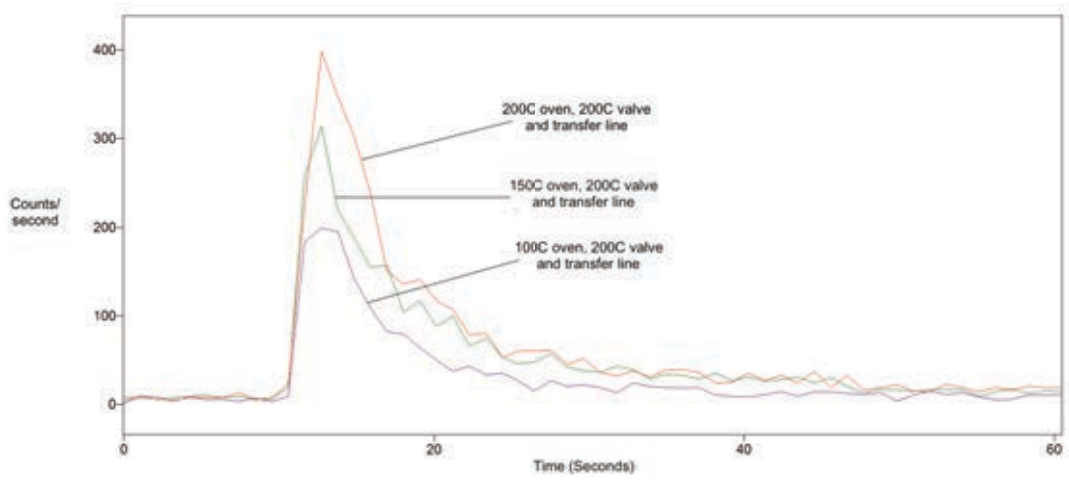

Figure 83 - Desorption of 10ng benzo[k]fluoranthene as a function of oven/drift tube temperature

In order to increase the efficient transfer of PAH into and through the mass spectrometer, it is desirable to increase the oven temperature. The sensitivity increase observed is explained by the more efficient transfer of PAH molecules at higher temperature.

6.5 Investigation into DC vs RF sensitivity

In order to optimise the instrumental parameters for increased sensitivity, the PTR drift tube pressure and PTR entry voltage were mapped when using the RF ion funnel and compared to the DC conditions that provided maximum sensitivity.

The optimum conditions for DC operation were found by comparing the mean of 3 normalised and background subtracted replicate desorption's at E/n values between 100 and 250 Td (at 20 Td intervals). The results for DC mode detection benzo[k]fluoranthene are shown in figure 84.

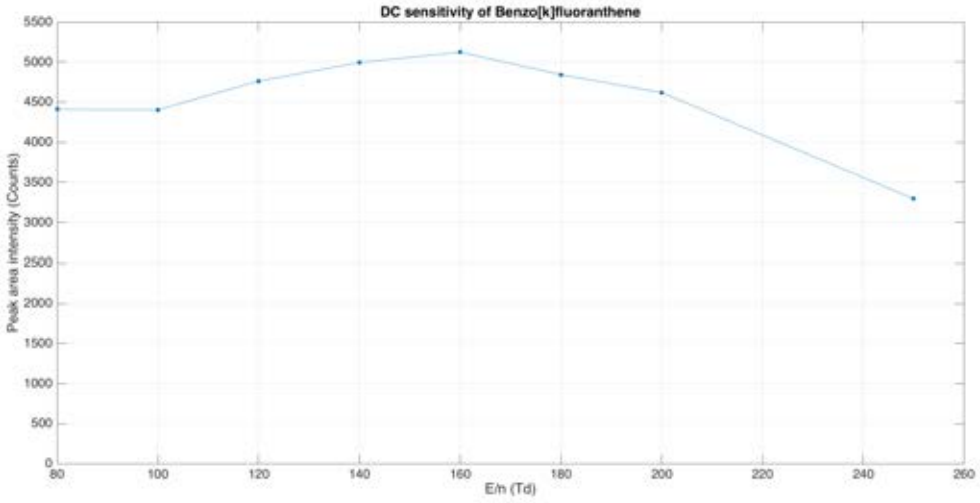

Figure 84 – DC mode sensitivity of benzo[k]fluoranthene as a function of reduced electric field strength (E/n). 10ng desorption's of benzo[k]fluoranthene were analysed at 1mbar drift tube pressure and 1.3 mbar hollow cathode pressure. All temperatures (swab desorber, transfer line, PTR oven) were at 200℃.

The RF measurements were made for multiple drift tube pressures between 1 and 3 mbar and between 15-50 V DC (at 5 V intervals). The background subtracted sensitivity for the RF mode operation was compared to the maximum DC mode sensitivity, with at least a 48-fold increase for the PAHs measured as standards, (these are discussed further in section 6.6). For the PAH standards investigated in this chapter, there is little difference in DC sensitivity across most of the E/n range investigated (100-200 Td).

6.5.1 RF Funnel transmission

From the investigation of the literature on RF ion funnels and experimental evidence of the behaviour of ions in the RF ion funnel, it has been hypothesised that when using the RF ion funnel, the ions 'bounce' along the electrodes of decreasing diameter in the second half of the drift tube, along with random

collisions with the gas molecules in the drift tube. For VOCs (m/z < 100 Da) at low drift tube pressure (and therefore a higher mean free path) and lower DC voltage (which reduces the axial velocity of the ions), the ions can be deflected further into the centre axis of the drift tube, at which point more of the ions can exit the drift tube through the central 400 μm aperture, resulting in an increase in sensitivity. However, for larger ions such as PAHs, the sensitivity increases with lower drift tube voltage and increasing drift tube pressure. The transmission of ions through the exit aperture during RF operation is pressure and mass dependent.

The pressure and mass dependence of ion transmission is also observed for the reagent ion. When using the RF ion funnel with very low DC fields (< 50 V), the measured reagent ion signal at the detector is often very low (m/z 21 = 20-40 cps), corresponding to a reagent ion signal at m/z 19 of 10,000-20,000 cps. The actual reagent ion signal must be much higher than this, otherwise the introduction of an analyte in a pulse would cause depletion of the reagent ion, which is not observed. When measuring the ion current at the exit plate for the above conditions (which is expected to be > 99 % reagent ion), the current measured is approximately 100 pA. This ion current corresponds to approximately $1x10^{11}$ ion collisions per second, significantly more than the 20,000 that pass through the exit orifice. The transmission of the low mass ions in these conditions is very poor, less than 0.001 % for m/z 19. The corresponding currents on the transfer lens electrodes are also increased during RF ion funnel usage.

6.5.2.2 Normalising data using RF ion funnel

In order to account for any changes in the reagent ion signal, sensitivity of the instrument and comparison between different instruments, the data must be normalised in order to allow comparison. However, in this case when using the RF ion funnel, the reduced transmission of the reagent ion limits the effectiveness of normalising the data. In the case of using the RF ion funnel, it would be normalising to a small reagent ion signal, subject to significant counting error causing low precision and this increases the potential error in the measurement of the PAHs. In order to address the issues of changing instrument sensitivity, the instrument was checked with a 1 ppm benzene gas standard periodically and for any changes in instrument sensitivity with benzo[a]pyrene. During the measurements for the PAHs (which occurred over a 6-month period), the low usage of the instrument was such that no change in detector gain was required, as there was no measurable change in sensitivity.

6.6 Standards experiments

It was important to determine practically that a range of PAHs can be detected using PTR-MS and for this, thermally desorbing certified reference standards allowed the simplest transfer of PAH into the PTR-MS. Using the thermal desorption of reference standards also allows the determination of the limit of detection and quantification for the method.

6.6.1 Operational parameters (Instrumental conditions)

In order to determine the sensitivity of the instrument using the certified reference standards, thermal desorption via a swab desorber was used as the method of sample introduction. The swab desorber is used to thermally desorb the PAH sample from the swab using an electronically controlled mechanically repeatable compression. The temperature control of the internal compression system and process gas pipe is accurate to ± 2 °C. Prior to the start of this study, the swab desorber used for this work had been compressed >2000 times without incident.

Figure 85 - Image of the swab desorber used in this study. The swab is inserted in the slot on the top of the unit, the N_2 gas supply is inserted on the Swagelok connector on the right of the unit and the process gas containing the analyte from the swab desorber comes out the Swagelok connection on the left of the unit.

PAH standards purchased in acetone, methanol or toluene were diluted to 1 µg/ml using the same HPLC grade solvent the PAH was supplied in. For each desorption experiment, an appropriate volume of this solution (<5 µL) was deposited on the Teflon swab surface in order to give the correct swab loading. The swab was left for 5 minutes for the solvent to evaporate and then desorbed into the PTR-MS using the swab desorber and heated transfer line.

The instrument was operated in RF mode to increase the transmission of PAH molecules, leading to a better sensitivity and lower limit of detection. For each of the compounds, the optimum pressure and DC voltage for maximum transmission was investigated within the range known to provide the best sensitivity to benzo[a]pyrene. Using the optimum conditions, 6 PAH standards were measured using PTR-MS to determine the limit of detection, limit of quantification, repeatability and reproducibility.

6.6.2 Analytical measurement parameters

6.6.2.1 LOD and LOQ

The definitions of limit of detection (LOD) and limit of quantification (LOQ) used in this study are commonly used in analytical science for establishing the lowest quantity of material that can be measured and quantified, using the confidence factors of 3 and 10 respectively.

$$\mathrm{LOD} = \mathrm{Mean} + 3 \text{ x } \mathrm{SD} \quad (41)$$

$$\mathrm{LOQ} = \mathrm{Mean} + 10 \text{ x } \mathrm{SD} \quad (42)$$

The LOD and LOQ from equations 41 and 42 can be converted to a mass of material using a suitable sensitivity factor derived experimentally from a background subtracted swab desorption's of PAH.

6.6.2.2 Linear dynamic range

The linear dynamic range was determined for the poly aromatic hydrocarbons investigated along with the r^2 value as metric for the linearity of the fit. The linear dynamic range for PAHs measured by PTR-MS typically extends for a couple of orders of magnitude. However, because of the high sensitivity of the PTR-MS using the ion funnel, the pulse counting saturation effects discussed in chapter 2 are significant and limit the upper bounds of the linear dynamic range. The linear dynamic range can be extended by the use of the ^{13}C isotope. As the PAHs measured in this study are C14-C22, the first ^{13}C isotope is 15.4-24.2 % of the

molecular ion peak and using this strong isotope peak can extend the LDR by an order of magnitude.

6.6.2.3 Repeatability

The repeatability was assessed by calculation of the relative standard deviations of 5 consecutive samples (with blank solvent desorption's in between) of a suitable PAH swab loading (between 0.2 and 1ng depending on the LDR).

6.6.2.4 Definition of peak limits

The desorption produces a peak as shown in figure 86, which is the response of the instrument to 2ng of Benzo[a]pyrene. In order to determine the sensitivity (number of counts/second/ng), the blank swab background peak area is subtracted from the signal peak area, with the limits of the peak defined using the limit of quantification. This is important because the desorption peak is not symmetrical or Gaussian and like a chromatographic peak, has a tail. Using the point at which the background subtracted signal is below the limit of quantification (10 x SD) gives a repeatable method of defining the peak limits to determine signal intensity and desorption time from the peak. Without this definition, the intensity of the peak can be incorrect by ± 10 %.

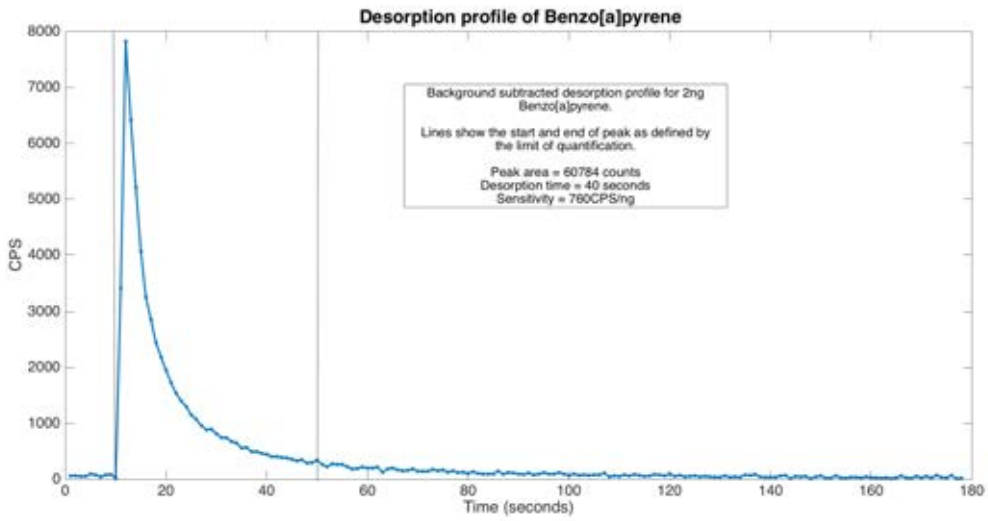

Figure 86 – Desorption profile of 2ng benzo[a]pyrene using a drift tube pressure of 1.7 mbar at 15 V DC with the RF ion funnel.

6.6.2.5 Instrument conditions

In order to determine the optimum conditions for the detection of PAHs using the RF ion funnel, the tuneable parameters of the drift tube should be investigated. For this, replicate 2ng desorption's of benzo[a]pyrene were used to determine the sensitivity of the instrument at different settings of drift tube pressure and drift tube DC voltage. The resulting desorption profiles were used to produce the response surface shown in figure 87.

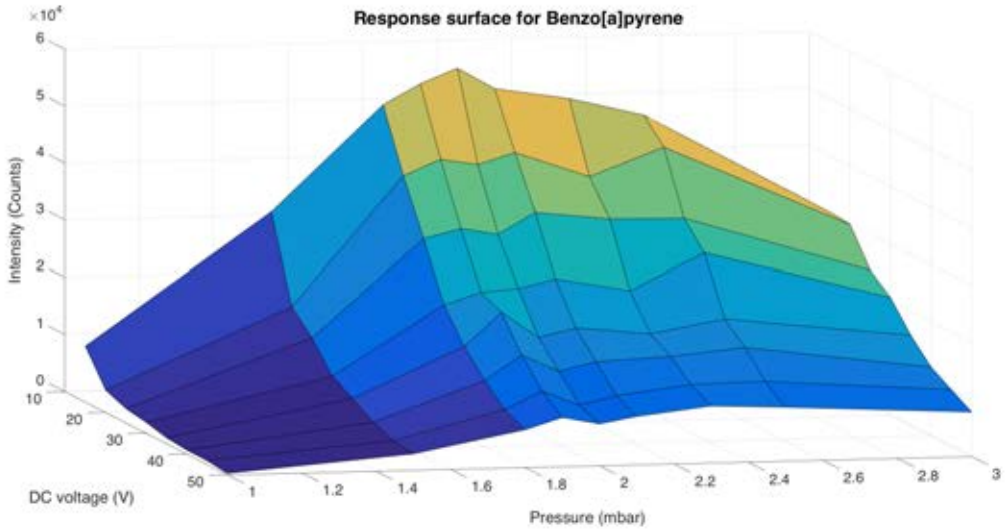

Figure 87 – Response surface showing the response of benzo[a]pyrene (in counts/ng) using the RF ion funnel as a function of drift tube pressure and DC entry voltage.

The response surface shows that the optimum conditions for the thermal desorption of benzo[a]pyrene using the RF ion funnel is at 2 mbar drift tube pressure and a drift tube voltage of 15 V. For the power supplies on this instrument, 15 V is the minimum voltage which can be applied to the PTR entry electrode as it is the lowest available output from the printed circuit board (PCB) from which the PTR entry supply is taken from. The surface seems to suggest that at pressures around 2 mbar, increasing the PTR entry voltage causes a large reduction of the transmission of PAHs and for this reason, the analysis of the PAH standards were investigated using a pressure of 2 mbar and a PTR entry voltage of 15 V DC.

After determining that the optimum DC voltage for the effective transmission of Benzo[a]pyrene was 15 V, the pressure dependence of the other PAHs was investigated in order to determine if the mass dependency previously observed for

VOCs using the RF ion funnel was significant for the PAH standards, shown in figure 88. This also determined the pressure at which each PAH has the maximum transmission.

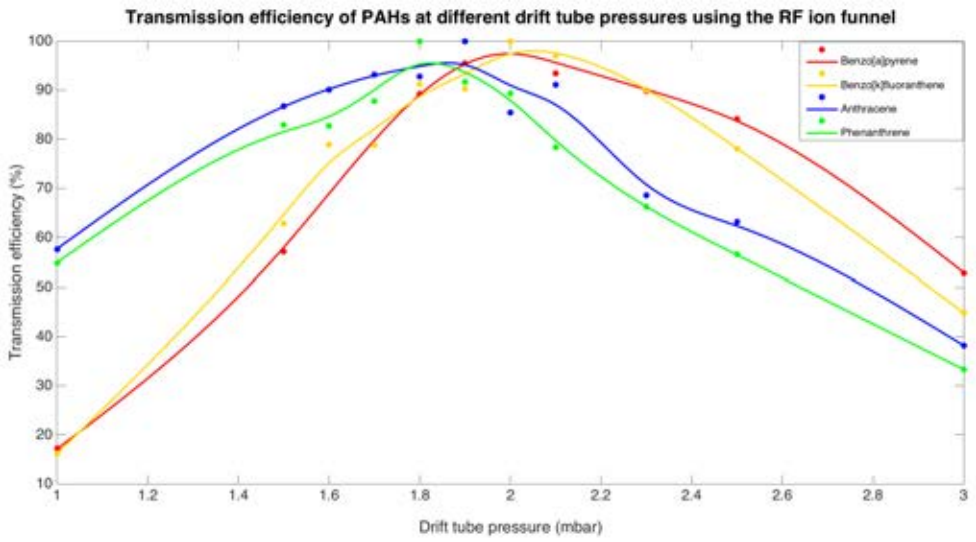

Figure 88 - Transmission efficiency of 4 PAH standards at different drift tube pressures, whilst maintaining 15V DC on PTR Entry

Small differences between the PAH curves exist, however the 2 pairs of isomers behave in broadly the same way (blue/green, yellow/red). Importantly despite the difference in mass between the C14 and C20 PAHs (74 Da), the pressure dependence is less important than expected and lower than observed for other compounds (non-PAHs). The difference in pressure at which they show the maximum sensitivity is only 0.2 mbar and at 2 mbar drift tube pressure, the transmission for all PAHs investigated is at least 80 % of the maximum measured. This demonstrates that 2 mbar is an ideal drift tube pressure to operate at, providing high transmission efficiency for a range of PAHs.

6.6.3 Results

The PAHs standards, deposited on swabs and thermally desorbed using the optimum instrument conditions found in chapter 6.6.2.5 were analysed in order to determine the product ions, limit of detection and limit of quantification for each of the compounds. The results from the analysis of the PAH standards, extracted and background subtracted as shown are reported in table 23.

Table 23 - Results of the analysis of PAH standards, including literature values for the vapour pressure at 25 °C and product ions observed at 15 V DC for analysis when using the RF ion funnel PTR-MS. The calculated linear dynamic range (which is low due to high sensitivity and therefore detector saturation), limit of detection (defined as 3σ), limit of quantification (defined as 10σ) and the repeatability expressed as %RSD for 5 replicate desorption's. The RF enhancement of the signal intensity vs DC operation is shown.

Compound	Vapour pressure (Pa at 25°C) [45]	Product ion mass	Linear dynamic range (ng)	R^2	Counts / ng (background subtracted)	RF enhancement (RF/DC)	Limit of detection (ng)	Limit of Quantification (ng)	Repeatability (%RSD, n=5)
Anthracene	0.001	179	0.05-1.2	0.993	31146	55	0.01 ± 0.003	0.03 ± 0.01	3.2
Phenanthrene	0.02	179	0.05-0.6	0.992	40133	90	0.008 ± 0.002	0.028 ± 0.005	5.5
Fluoranthene	0.001	203	0.1-0.6	0.989	33449	76	0.004 ± 0.003	0.04 ± 0.007	7.1
Pyrene	$6x10^{-4}$	203	0.1-1	0.988	27713	58	0.008 ± 0.003	0.026 ± 0.009	7.3
Benzo[a]pyrene	$7x10^{-7}$	253	0.2-10	0.997	25513	72	0.16 ± 0.03	0.58 ± 0.1	5
Benzo[k]fluoranthene	$1.3x10^{-7}$	253	0.2-9	0.996	15502	52	0.20 ± 0.03	0.65 ± 0.11	5.1

6.6.4 Discussion

The dominant product ion produced from the ionisation of PAHs with hydronium is predominantly the protonated parent, with very little fragmentation (<1%). This is to be expected on comparison with the electron impact mass spectra from the NIST database of electron impact mass spectra [122]. The production of a single molecular ion simplifies the quantification of PAHs but limits the ability to use changes in voltage or pressure (E/n) in order to quantify isomers based on the fragmentation of the molecular ion.

The linear dynamic range of the PAHs tested are typically an order of magnitude using pulse counting PTR-MS, which is less than other comparable techniques. However, when considering the ^{13}C isotope peak this can be extended by another order of magnitude. Operational parameters have been optimised to reduce the desorption time as much as is feasibly possible and therefore during a desorption, the pulse counting saturation is significant when using lower swab loadings. To avoid the pulse counting saturation effects and to extend the linear dynamic range, a PTR-MS system with analogue to digital converter could be used, allowing multiple ions to be counted at the same time and therefore giving the ability to measure higher concentrations without pulse counting saturation.

The limit of detection for the PAHs analysed are low with respect to typical PTR-MS sensitivities, with a sub nanogram LOD and LOQ for the least volatile compounds.

The low levels of sample variation as shown in the RSD measurements for repeatability also demonstrate that the technique could be used for routine analysis for atmospheric samples with a sufficiently high PAH concentration. For an atmospheric abundance of 1 ng m^{-3} benzo[a]pyrene (equivalent to 0.1 ppt) and with typical sampling flow rates through a Teflon filter of 0.5 and 60 m^3, the amount deposited on the swab for an hour sampling period is 0.5 and 60 ng respectively. These samples could be desorbed and quantified using PTR-MS by the method established in this chapter.

6.6.5 Nitroarenes

Nitroarenes are of importance in atmospheric chemistry, especially in determining the fate of PAHs that have reacted with OH radicals, NO_2 and O_3. Many PAHs have atmospheric lifetimes in the order of hours with respect to OH radicals, with much of the data produced from estimated rate coefficients [45]. The products of the reactions of PAHs with OH radicals can then go on to react with NO_2, forming amongst other things, nitroarenes. Nitroarenes can also be formed in vehicle exhausts at high temperature from the electrophilic addition of NO_2 to certain PAHs.

Detecting the nitroarenes formed in both ambient air and vehicle exhausts would give information as to the reaction rates. In addition, the ability to use PTR-MS would provide a tool to monitor real time changes in the composition of the reaction products, in either a real-world scenario or simulated experiments.

Two nitroarenes, 1-nitropyrene and 6-nitrochrysene were analysed using the same method as for the PAHs in section 6.6.3, using analytical standards deposited onto swabs, with the results shown in table 24.

Table 24 -- Results of the analysis of nitroarene standards, including literature values for the vapour pressure at 25℃ and product ions observed at 15V DC for analysis when using the RF ion funnel PTR-MS. The calculated linear dynamic range, limit of detection, limit of quantification and the repeatability expressed as %RSD for 5 replicate desorption's.

Compound	Vapour pressure (Pa at 25°C) [123, 124]	Product ion mass	Linear dynamic range (ng)	R^2	Counts/ng (background subtracted)	RF enhancement (RF/DC)	Limit of detection (ng)	Limit of Quantification (ng)	Repeatability (%RSD, n=5)
1-Nitropyrene	4.4 x 10^{-6}	248	0.1-1	0.992	47058	76	0.025 ± 0.004	0.08 ± 0.01	7.7
6-Nitrochrysene	1.0 x 10^{-6} (est)	274	0.1-4	0.993	21218	48	0.057 ± 0.01	0.18 ± 0.04	3.9

The nitroarene results are similar to those of the PAH standards, which also demonstrate the ability to use PTR-MS to detect derivatives and reaction products of PAHs from static standards.

6.7 Real time whole air sampling

Two methods of sampling air containing PAHs are detailed here, trapping gas phase PAHs present in the atmosphere on a Teflon filter surface, and generation of a standard PAH atmosphere, simulating on-line whole air measurement using a high temperature thermostat and diffusion tube.

6.7.1 Filter sampling

The current method of PAH sampling requires the analysis of PAH filters, collected over a sampling period of 24 hours. Within this study, the analysis of such filter samples was attempted using the thermal desorption.

UK samples were collected close to an existing local air quality monitoring site (Bristol Road Observation Site, BROS, Birmingham, UK) by drawing air through a Teflon ‘swab’ filter for 90 minutes at a flow rate of 6 LPM (equating to a total volume of 540 L).

Chinese air samples were collected onto Teflon filters from a campaign in Beijing in 2017. The sample was taken on 22/05/2017 in Beijing by drawing 5 LPM of air through the filter for 19 hours and 30 minutes using a minivol sampler onto an active area of 3.8 cm diameter, stored in airtight filter holder containers, shipped and stored at -20 °C until analysis. For analysis, a measured ‘strip’ of the Teflon sample was inserted into a Teflon swab to provide stability during desorption.

Figure 89 - Left image shows the filter sample as received from China, right image is the section of cut filter woven into the swab through 2 slots. The 'clean' side was instrument facing to avoid introducing large particulates into the PTR-MS which can block apertures and become charged, changing the electric field and causing adverse ion beam steering.

All Teflon filter samples were analysed using the optimum conditions found for the analysis of PAHs (oven/transfer line/swab desorber temperature 200 °C, drift tube pressure of 2 mbar, glow discharge pressure of 2.5 mbar, RF on, 15 V dc entry voltage, 4 V exit voltage). Spectra were measured across the mass range 15-300 Da for 3 minutes (although the compounds were typically fully desorbed and analysed by the PTR-MS within 30 seconds of inserting the swab).

6.7.1.1 UK sample

The UK sample was analysed within 5 minutes of removal from the sampler, using the conditions described, with the ions of interest shown in figure 90.

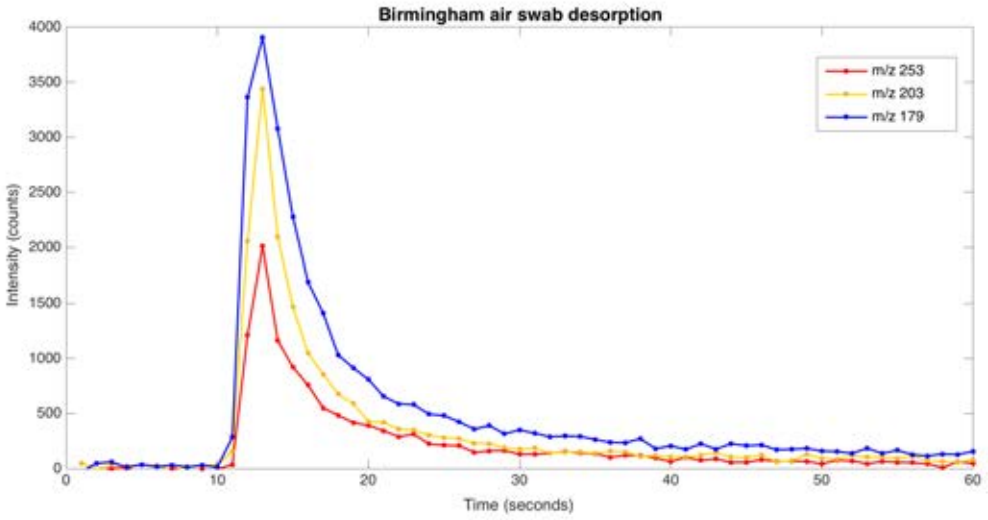

Figure 90 - Desorption of swab with Birmingham air collected onto the surface. The total volume sampled onto the filter was 540L.

Knowing the sensitivity of the instrument to benzo[a]pyrene determined using the analytical standard in table 23, the concentration of benzo[a]pyrene in ambient air can be calculated to be 0.41 ng/m^3, which is below the legal limit of 1 ng/m^3 [114]. This compares well with Benzo[a]pyrene measured by Defra at the Birmingham Tyburn measurement site, which states a verified measurement of 0.45 ng/m^3 (for the same month which the measurement was taken) [117].

6.7.1.2 China sample

The method has been tested further using a filter sample of air from Beijing, China which is visibly discoloured from the trapping or particulate matter on the Teflon surface. As the sample is discoloured, this suggested a high concentration of desorbed compounds and therefore the sample had to be analysed in sections as

to avoid saturation of the PTR-MS through the pulse counting system. The filter was cut and analysed as shown in figure 89, with 6 replicate sections analysed.

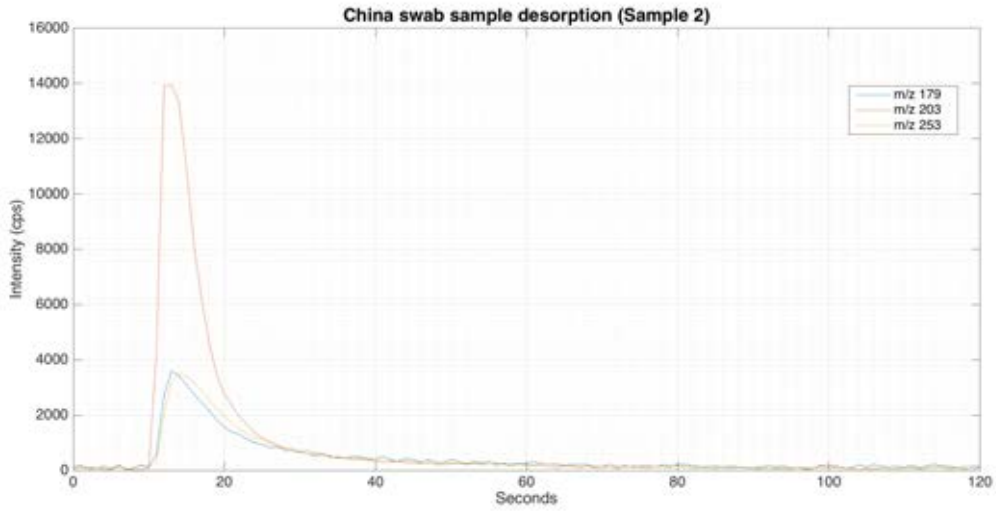

Figure 91 - Desorption of a sample of Beijing air from 22/05/2017 using a 12.5 mm by 4 mm section of filter sample. The area of the sample used was 0.5 cm^2 and resulted in 4.4 % of the total filter sample area, equivalent to sampling 258 L of air.

Table 25 - Results of replicate desorption's of a China swab filter sample, with the signal intensity at m/z 179, m/z 203 and m/z 253 displayed normalised to a 1 cm^2 sample area.

Sample number	Sample dimensions (cm)	Sample area (cm^2)	Intensity m/z 179 per cm^2 filter	Intensity m/z 203 per cm^2 filter	Intensity m/z 253 per cm^2 filter
1	1.25 x 0.41	0.51	51424	240271	108529
2	1.25 x 0.40	0.5	57038	214538	96114
3	1.42 x 0.34	0.48	60313	233358	96992
4	1.31 x 0.37	0.48	58710	227146	111317
5	1.32 x 0.34	0.44	55805	247391	102027
6	1.27 x 0.36	0.45	53364	245900	113060

The low RSDs in table 26 demonstrate that the variation from the mean is low for

the signal intensity normalised to a 1 cm^2 area and that therefore the technique is suitable for analysis of real air filter samples.

Table 26 - Mean signal intensity of three PAH ion species measured on the China filter sample normalised to a cm^2 of filter sample, RSD of the measurements (n=6) and calculated PAH concentrations of the air in ng/m3, based on the sensitivity of the instrument to the measured PAH standard.

m/z (Potential PAHs at this m/z)	**Mean signal intensity (c/cm^2)**	**RSD (%)**	**Counts/ filter**	**M^3 of air sampled**	**Concentration of PAH (ng/m^3)**
179 (Anthracene/ Phenanthene)	56109	5.9	6.36×10^5	5.85	3.05
203 (Fluoranthene/ Pyrene)	234767	5.3	2.66×10^6	5.85	14.88
253 (Benzo[a]pyrene/ Benzo[k]fluoranthene)	104673	7.0	1.19×10^6	5.85	6.55

Using the mean signal intensity measured for each of the m/z values and assuming the composition of the PAH species at each mass is equally split between the compounds measured using PTR-MS as analytical standards in table 21, the concentration of PAHs in the ambient air can be determined to be much higher than the limit of 1 ng/m^3, specified as a target for in both the UK and China. The data presented here agrees with the literature on the measurement of PAHs in China [125, 126]. The most important conclusion from this analysis is that this method of thermal desorption for filter samples can be used for quantitative

analysis of PAHs using PTR-MS, although further work is required to build on this exploratory study in order to show the suitability of the technique and provide full validation against GC-MS.

6.7.2 Sampling of dynamically prepared standards

Although being able to measure PAHs desorbed in the gas phase as a pulse of material is useful, especially for the analysis of swabs or filter samples, the real benefit of using PTR-MS is the real-time capability of the technique. With a suitable method of generating PAH standards in the gas phase, then it would be possible for real time measurements of PAHs in the gas phase.

In order to test this, thermostatted diffusion tubes were used in order to generate a PAH gas standard and develop the real-time measurement of PAHs by PTR-MS. The PAH chosen for this was fluoranthene, as it has a reasonably low vapour pressure at room temperature ($1x10^{-3}$ Pa at 25 °C) and that it can be easily prepared as a diffusion tube due to the availability of the compound (as a pure solid).

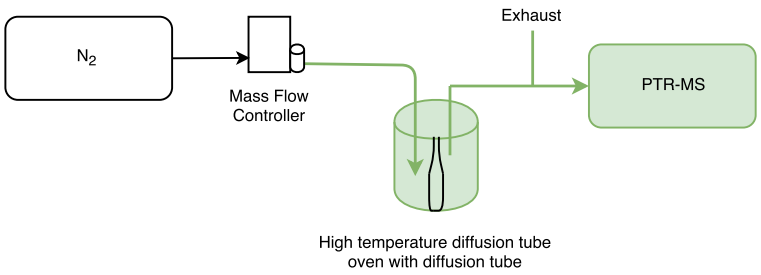

Figure 92 - Schematic of experimental setup for PAH generation unit, using a diffusion tube incubated in a high temperature thermostat. All heated sections of the experimental apparatus are shown in green. The high temperature thermostat was set at 177℃ ± 0.1℃ and transfer lines were heated to 200℃. The PTR-MS oven, valve and transfer lines were all 200℃.

The inlet lines and PTR-MS were heated to at least the temperature of the diffusion tube oven (in this case thermostat was 177 °C, all transfer lines and PTR-MS were 200°C) to avoid losses during transfer. The output of a 0.1mm/8cm diffusion tube containing fluoranthene was used to calibrate the PTR-MS and show the ability to make real-time measurements.

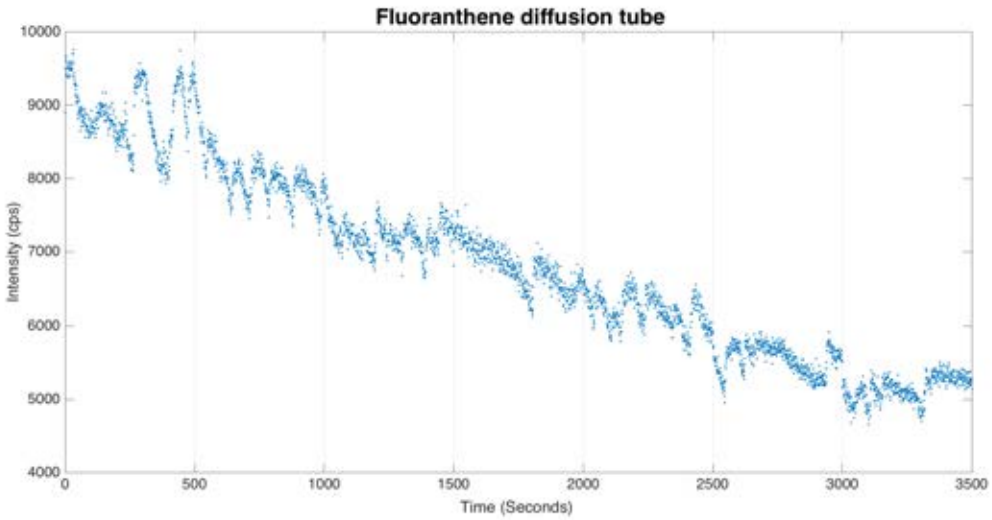

Figure 93 - Graph showing the raw data from the calibration of the PTR-MS using the fluoranthene diffusion tube. The flow rate of N_2 was increased every 500 seconds where the signal intensity was allowed to stabilise.

From the data shown in figure 93, the background signal at m/z 203 for each flow rate was subtracted, allowing the linear calibration response shown in figure 94.

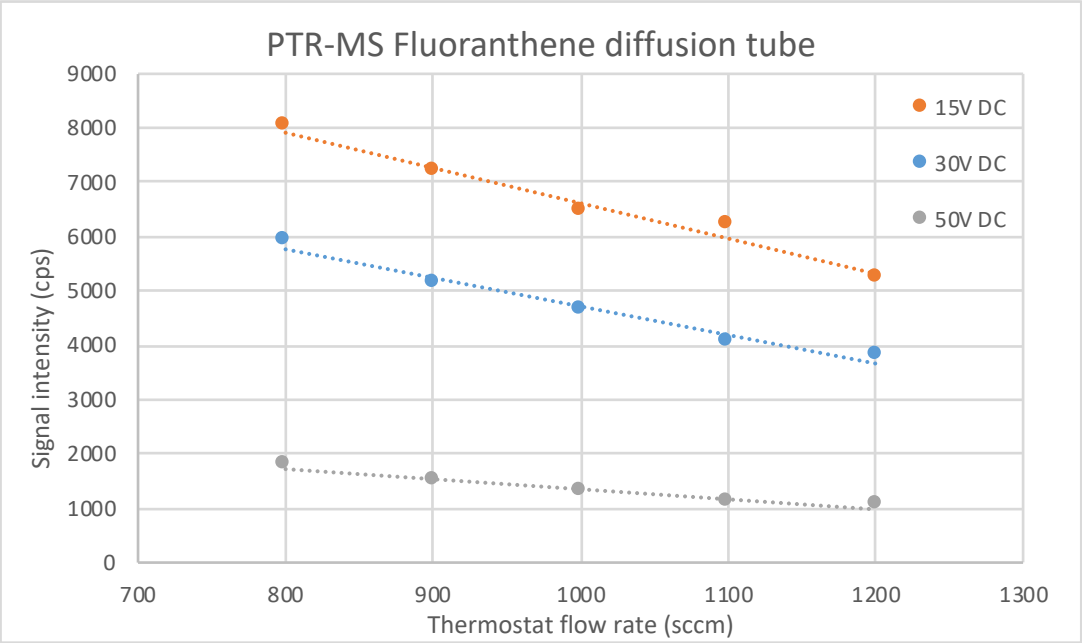

Figure 94 - Measured signal intensity (in cps) as a function of flow rate through the super ambient thermostat at three different instrumental conditions (Entry voltage grey 15V, blue 30V and orange 50V).

6.7.2.1 Discussion

For the dilutions at each of the PTR-MS instrumental conditions, the resulting fit is linear for a moderate range of flows. The volume of the glass thermostat section which contains the diffusion tube was approximately 550 cm^3 and therefore at the flow rates used in this experiment, the thermostat was completely flushed of air every 30 seconds. This is not ideal when changing flow rates as the change in flow rate may take up to 3 minutes to stabilise, however an equilibrium is established under the new flow conditions whereby the emission from the thermostat is constant and this was the time from which the data was taken.

Future improvements include a redesign of the glass thermostat to reduce the volume of the thermostat (whilst still maintaining a suitable size opening for inserting tubes and suitable high temperature heating arrangements).

The results of this experiment show that the method developed for generating low concentration standard atmospheres can be used for both calibration and generating a dynamic standard atmosphere for reaction studies.

6.8 Conclusions

This chapter demonstrates the practical application of PTR-MS to the measurement of polycyclic aromatic hydrocarbons, both from static and dynamic samples. Use of high temperature inlet lines and drift tube oven systems allows efficient transfer of analyte from sample to detection system, with high sensitivity and low detection limits (as low as 180 pg for benzo[a]pyrene deposited on swab, equivalent to adsorption of $1m^3$ of 0.18 ng m^{-3} ambient air onto a swab).

The application of PTR-MS to the detection of PAHs was demonstrated for both static samples, including analytical standards in solution and ambient air samples trapped on Teflon filters and on dynamic samples, created as a standard atmosphere by diffusion tube.

However, as is the case for most compounds in PTR-MS, quantification of isomeric and isobaric compounds is difficult unless they demonstrate any fragmentation or differences in ionisation mechanisms. This issue is also the case for PAHs, which do not exhibit any significant fragmentation at any of the PTR-MS conditions examined and are therefore difficult to quantify separately. With some prior knowledge of the typical composition of PAH isomers, then estimates for isomer concentrations could be determined.

7 Future Work

The experimental results contained within this thesis have demonstrated the ability to use PTR-MS for many new analyses and in the detection of molecules which have previously been detected using other techniques through advanced understanding of the ionisation mechanisms.

In chapter 3, the calibration of PTR-MS instruments was investigated, including the mechanism of storing oxygen sensitive VOCs for use in the generation of dynamic calibration standards for PTR-MS instruments. The expansion of the capabilities of dynamic calibration technology in order to produce dynamic standards for SVOCs was optimised, with a standard atmosphere of fluoranthene generated as a dynamic SVOC standard.

The experimental work in chapter 4 has developed the understanding of the ionisation mechanisms of the hydronium and oxygen reagent ions with chloroalkanes and chloroalkenes, determining general ionisation mechanism rules based on structure and the bond dissociation energy of the compounds which can be used in atmospheric measurements. This ionisation mechanism data can be used for both current and historical datasets and can be incorporated into automated analysis protocols.

In chapter 5, the measurement methods and data analysis protocols which allow the maximum amount of information to be extracted from a mass spectrum are

investigated. These methods are investigated with respect to commonly measured atmospheric compounds which are isomeric, or are difficult to distinguish in a PTR-MS mass spectrum. Methods to determine individual compound concentrations in a mixture were explored, along with the potential sources of error in a measurement.

The experimental work in chapter 6 investigates the capability of PTR-MS to measure SVOCs of atmospheric importance, most importantly PAHs. Initially this was with PAH standards in solvents, desorbed into the PTR-MS through a thermal desorber, but then using the dynamic fluoranthene standard prepared in chapter 3 in order to assess the capability of PTR-MS to be used from online, real-time PAH analysis.

The experimental results contained within this thesis have opened up many possibilities for future work related to the continued implementation of soft chemical ionisation to the detection and quantification of complex atmospheric VOC mixtures. Although significant progress in the investigation of novel approaches to the measurement of complex VOC systems has been detailed in the experimental sections of chapters 4-6, the opportunity for future work would allow more general implementation of this to field and chamber measurements often taken by researchers. For each chapter of results, a discussion of the potential for future work will be given.

7.1 Calibration techniques

The methodologies developed and presented in this thesis are useful for both researchers requiring accurate gas standards and mixtures for investigation of the ion molecule reactions of compounds and also for calibration of analytical instrumentation for measurement of VOCs and SVOCs.

Further work for the generation of VOC standards using diffusion tubes would be to take the methodology for the storage and calibration of oxygen sensitive VOCs developed in this thesis in order to prepare a standard procedure for analysts to conform to in order to reduce the error caused by oxidation of VOCs. A storage procedure may involve sealing aliquots of a liquid under nitrogen or argon in sealed ampoules, until required for use.

As PTR-MS becomes routinely used for on-line air quality monitoring and research into the sources and fluxes of SVOCs, then further development of the high temperature thermostat and a standard method for dynamic SVOC calibration would be required.

Ongoing work is continuing beyond the conclusion of the PhD in order to inform the analyst community of the issues with oxidation of VOCs used for dynamic calibration (and for creating static standards) and the requirement of a rigorous storage procedure to maintain high quality control. Naturally this would progress to a standardised method of VOC storage, especially for those compounds which are reactive in air.

7.2 Chlorocarbon analysis

Although this chapter of the thesis specifically focuses on the mechanisms of the ion-molecule reactions of H_3O^+ and O_2^+ with small organochlorides, there is scope to expand this study to include larger organochlorides and looking further forward, all halocarbons, including those with mixtures of group 7 atoms.

There are many other halocarbons which may display similar ionisation to the organochlorides, especially if they contain different halide substituents (fluorine, bromine, iodine etc) and a chlorine atom. Unfortunately, many of the CFCs that have been identified and restricted by the Montreal protocol have proton affinities much less than that of water and as a result, ionisation by proton transfer is inefficient due to the quick reverse reaction. The potential to use O_2^+ for these compounds could be further explored. This is important in atmospheric chemistry, including those that are included in the Montreal protocol and contribute to global warming and halocarbons which must be measured for workplace exposures and control measures.

From the work with the TO-15 mixture, it was tentatively identified that dibromochloromethane produces the product ion resulting from the loss of HCl. Further work on these compounds would allow the ionisation mechanism of the halocarbons to be determined, possibly allowing detection of many compounds previously not known to be ionised in PTR-MS. Understanding the ionisation mechanisms for halocarbons would allow the isobaric and isomeric interferences

to be mapped, with the information used to develop an algorithm for quantitation and quantification of halocarbons amongst a mixture of other common VOCs.

As a consequence of the results presented in this chapter, a commercial software package has been developed by Kore Technology for the analysis and quantification of the compounds in the TO-15 related gas standard, TO-14. This software uses the product ion distribution data developed throughout chapter 4 in order to fit the mass spectrum of an unknown sample to the expected product ion data. This can be primarily used for atmospheric measurement of VOCs and industrial monitoring for the toxic TO-14 compounds, with the ability for researchers to add product ion distribution data to analyse any compound ionisable by PTR-MS.

7.3 Isomeric separation

The generic methods developed and examined using the three exemplar systems in this thesis allow isomeric separation to be implemented for isomeric mixtures with some *a priori* knowledge of the compounds present in the process gas. For measurements of these compounds, the methods could be directly incorporated into measurement campaigns and post processing of data.

An addition to this work would be for a generalised analysis / fitting mechanism to be designed, using knowledge of the PTR-MS product ion distributions for the common VOCs encountered in a given sample at multiple reduced electric field

strengths, to deconvolute a PTR-MS mass spectrum containing isomers and overlapping product ion distributions. This may use a common mathematical fitting model, such as a least squares fit, which minimises the square of the residuals, or a novel fitting method. This fitting method would be implemented on a data set produced using fast E/n switching though addition of a secondary power supply, which would be optimised to produce multiple datasets at different reduced electric field strengths for analysis of different VOCs. In addition to this, the full set of fragmentation data for all reduced electric field strengths could be used to inform models on the optimum method for quantification.

As a result of the work in this chapter, efforts are being made to produce libraries of product ion distributions for quantification of mixtures of species, such as TO-14 and TO-15. This work is being continued at Kore Technology Ltd as a response to significant commercial interest in this area of analysis. The work contained within this experimental chapter has allowed the progression of the isomer quantification using PTR-MS, hopefully to encourage the further investigation into a general method for quantification of compounds in complex matrices.

7.4 PAH detection

From the PAH detection demonstrated in chapter 6, both using static (thermal desorption) and dynamic (diffusion tube, on-line sampling), several potential avenues for future work have presented themselves.

One strategy would be to develop the method for on-line PAH measurements further, applying this methodology to other PAHs of interest, namely benzo[a]pyrene, in order to determine the suitability of the PTR-MS for field deployment for the measurement of PAHs. Although more sensitive instrumentation would be required for detection of PAHs (such as benzo[a]pyrene) at ambient levels in the UK, instrumentation of sufficient sensitivity is commercially available and would only require modification to allow high temperature operation. This would allow real time measurement of PAHs, either to monitor sources and emission rates, or for monitoring a static atmosphere such as a smog chamber.

If further investigation confirms the suitability of the method and instrument for the on-line detection of PAHs, a second stage would be to take the 200°C instrument on a field campaign where it may be possible to take on-line PAH measurements (where the atmospheric concentrations are typically above the instrumental limit of quantification), such as China or India. This would assess the practical suitability of using PTR-MS as an on-line measurement technique for PAHs.

Another strategy would be to further assess the feasibility of using the instrument as a method of thermal desorption mass spectrometry for samples trapped on Teflon filters.

8 - References

1. Alam, M.S. and R.M. Harrison, *Recent advances in the application of 2-dimensional gas chromatography with soft and hard ionisation time-of-flight mass spectrometry in environmental analysis.* Chemical Science, 2016. **7**(7): p. 3968-3977.
2. Laothawornkitkul, J., et al., *Biogenic volatile organic compounds in the Earth system.* New Phytol, 2009. **183**(1): p. 27-51.
3. Guenther, A., et al., *A global model of natural volatile organic compound emissions.* Journal of Geophysical Research, 1995. **100**: p. 8873-8892.
4. Arneth, A., et al., *Why are estimates of global terrestrial isoprene emissions so similar (and why is this not so for monoterpenes)?* Atmos Chem Phys, 2008. **8**: p. 4605-4620.
5. Pyle, J.A., et al., *The impact of local surface changes in Borneo on atmospheric composition at wider spatial scales: coastal processes, land-use change and air quality.* Philos Trans R Soc Lond B Biol Sci, 2011. **366**(1582): p. 3210-24.
6. Pugh, T.A., et al., *Simulating atmospheric composition over a South-East Asian tropical rainforest: performance of a chemistry box model.* Atmos Chem Phys, 2010. **10**: p. 279-298.
7. Hewitt, C.N., et al., *Ground-level ozone influenced by circadian control of isoprene emissions.* Nature Geoscience, 2011. **4**(10): p. 671-674.
8. Holloway, A. and R. Wayne, *Atmospheric Chemistry*. 2010: RSC Publishing.
9. Aumont, B., S. Szopa, and S. Madronich, *Modelling the evolution of organic carbon during its gas-phase tropospheric oxidation: development of an explicit model based on a self generating approach.* Atmos Chem Phys, 2005. **5**: p. 2497-2517.

10. Morfopoulos, C., et al., *A model of plant isoprene emission based on available reducing power captures responses to atmospheric CO(2).* New Phytol, 2014. **203**(1): p. 125-39.
11. Sharkey, T.D., A.E. Wiberley, and A.R. Donohue, *Isoprene emission from plants: why and how.* Ann Bot, 2008. **101**(1): p. 5-18.
12. Mellouki, A., T.J. Wallington, and J. Chen, *Atmospheric chemistry of oxygenated volatile organic compounds: impacts on air quality and climate.* Chem Rev, 2015. **115**(10): p. 3984-4014.
13. Sindelarova, K., et al., *Global data set of biogenic VOC emissions calculated by the MEGAN model over the last 30 years.* Atmospheric Chemistry and Physics, 2014. **14**(17): p. 9317-9341.
14. Seinfeld, J.H. and S.N. Pandis, *Atmospheric Chemistry and Physics - From Air Pollution to Climate Change*. 1998: Wiley.
15. von Schneidemesser, E., et al., *How important is biogenic isoprene in an urban environment? A study in London and Paris.* Geophysical Research Letters, 2011. **38**(19): p. n/a-n/a.
16. MacKenzie, A.R. and F.D. Pope, *Pollution: causes, effects and control*. 5th ed, ed. R.M. Harrison. 2014: Roy. Soc. Chem.
17. Government, E.A.-U. *Using persistent organic pollutants (POPs)*. 2018 08/08/16 [cited 2018 28/04/2018]; Available from: https://www.gov.uk/guidance/using-persistent-organic-pollutants-pops#list-of-pops.
18. Union, E., *Limitation of emissions of volatile organic compounds due to the use of organic solvents in certain paints and varnishes and vehicle refinishing products and amending Directive 1999/13/EC*, E. Union, Editor. 2004.
19. Salthammer, T., *Very volatile organic compounds: an understudied class of indoor air pollutants.* Indoor Air, 2016. **26**(1): p. 25-38.

20. Lichtfouse, E., J. Schwarzbauer, and D. Robert, *Pollutant Diseases, Remediation and Recycling: 4 (Environmental Chemistry for a Sustainable World)*. 2013: Springer.
21. Pankow, J.F., *An absorption model of gas/particle partitioning of organic compounds in the atmosphere.* Atmospheric Environment, 1994. **28**: p. 185-188.
22. Lucattini, L., et al., *A review of semi-volatile organic compounds (SVOCs) in the indoor environment: occurrence in consumer products, indoor air and dust.* Chemosphere, 2018. **201**: p. 466-482.
23. Poschl, U., *Atmospheric aerosols: composition, transformation, climate and health effects.* Angew Chem Int Ed Engl, 2005. **44**(46): p. 7520-40.
24. Lindinger, W. and A. Jordan, *Proton-transfer-reaction mass spectrometry (PTR–MS): on-line monitoring of volatile organic compounds at pptv levels.* Chemical Society Reviews, 1998. **27**(5): p. 347.
25. Blake, R.S., P.S. Monks, and A.M. Ellis, *Proton-Transfer Reaction Mass Spectrometry.* Chemical Reviews, 2009. **109**: p. 861-896.
26. Ellis, A. and C. Mayhew, *Proton Transfer Reaction Mass Spectrometry - Principles and applications*. 1st ed. 2014: Wiley.
27. Barber, S., et al., *Increased sensitivity in proton transfer reaction mass spectrometry by incorporation of a radio frequency ion funnel.* Anal Chem, 2012. **84**(12): p. 5387-91.
28. Sinha, V., et al., *The effect of relative humidity on the detection of pyrrole by PTR-MS for OH reactivity measurements.* International Journal of Mass Spectrometry, 2009. **282**(3): p. 108-111.
29. Langford, B., et al., *Fluxes and concentrations of volatile organic compounds from a South-East Asian tropical rainforest.* Atmospheric Chemistry and Physics, 2010. **10**(17): p. 8391-8412.

30. Müller, K., et al., *Biogenic carbonyl compounds within and above a coniferous forest in Germany.* Atmospheric Environment, 2006. **40**: p. 81-91.
31. Rinne, J., et al., *On-line PTR-MS measurements of atmospheric concentrations of volatile organic compounds in a European boreal forest ecosystem.* Boreal Environment Research, 2005. **10**: p. 425-436.
32. Williams, J., et al., *Measurements of organic species in air and seawater from the tropical Atlantic.* Geophysical Research Letters, 2004. **31**(23): p. n/a-n/a.
33. Warneke, C. and J. de Gouw, *Organic trace gas composition of the marine boundary layer over the north west Indian Ocean in April 2000.* Atmospheric Environment, 2001. **35**: p. 5923-5933.
34. Colomb, A., et al., *Variation of atmospheric volatile organic compounds over the Southern Indian Ocean (30–49°S).* Environmental Chemistry, 2009. **6**(1): p. 70.
35. Capes, G., et al., *Secondary organic aerosol from biogenic VOCs over West Africa during AMMA.* Atmos Chem Phys, 2009. **9**: p. 3841-3850.
36. Murphy, J.G., D.E. Oram, and C.E. Reeves, *Measurements of volatile organic compounds over West Africa.* Atmospheric Chemistry and Physics, 2010. **10**(12): p. 5281-5294.
37. Robinson, N.H., et al., *Evidence for a significant proportion of Secondary Organic Aerosol from isoprene above a maritime tropical forest.* Atmospheric Chemistry and Physics, 2011. **11**(3): p. 1039-1050.
38. Borbon, A., et al., *Emission ratios of anthropogenic volatile organic compounds in northern mid-latitude megacities: Observations versus emission inventories in Los Angeles and Paris.* Journal of Geophysical Research: Atmospheres, 2013. **118**(4): p. 2041-2057.
39. Rogers, T.M., et al., *On-road measurements of volatile organic compounds in the Mexico City metropolitan area using proton*

transfer reaction mass spectrometry. International Journal of Mass Spectrometry, 2006. **252**(1): p. 26-37.
40. Materic, D., et al., *Monoterpene separation by coupling proton transfer reaction time-of-flight mass spectrometry with fastGC.* Anal Bioanal Chem, 2015. **407**(25): p. 7757-63.
41. Pallozzi, E., et al., *Does the novel fast-GC coupled with PTR-TOF-MS allow a significant advancement in detecting VOC emissions from plants?* Agricultural and Forest Meteorology, 2016. **216**: p. 232-240.
42. González-Méndez, R., et al., *Development and use of a thermal desorption unit and proton transfer reaction mass spectrometry for trace explosive detection: Determination of the instrumental limits of detection and an investigation of memory effects.* International Journal of Mass Spectrometry, 2015. **385**: p. 13-18.
43. Jobson, B.T., et al., *Comparison of aromatic hydrocarbon measurements made by PTR-MS, DOAS and GC-FID during the MCMA 2003 Field Experiment.* Atmos Chem Phys, 2010. **10**: p. 1989-2005.
44. Spanel, P. and D. Smith, *Selected ion flow tube studies of the reactions of H3O, NO , and O2 with some chloroalkanes and chloroalkenes.* International Journal of Mass Spectrometry, 1999. **184**: p. 175-181.
45. *PAHs and Related Compounds - Chemistry*. The Handbook of Environmental Chemistry, ed. A. H.Neilson. 1998: Springer.
46. Lv, J., et al., *Indoor and outdoor air pollution of polycyclic aromatic hydrocarbons (PAHs) in Xuanwei and Fuyuan, China.* J Environ Monit, 2009. **11**(7): p. 1368-74.
47. Lagg, A., et al., *Applications of proton transfer reactions to gas analysis.* International Journal of Mass Spectrometry and Ion Processes, 1994. **134**: p. 55-66.
48. Adams, N.G. and D. Smith, *THE SELECTED ION FLOW TUBE (SIFT); A TECHNIQUE FOR STUDYING ION-NEUTRAL*

REACTIONS. International Journal of Mass Spectrometry, 1976. 21: p. 349-359.
49. Francis, G.J., et al., *Real-Time Monitoring of Hazardous Air Pollutants.* Anal Chem, 2009. 81: p. 1595-1599.
50. Blake, R.S., et al., *Demonstration of Proton-Transfer Reaction Time-of-Flight Mass Spectrometry for Real-Time Analysis of Trace Volatile Organic Compounds.* Analytical Chemistry, 2004. 76: p. 3841-3845.
51. Gross, J.H., *Mass Spectrometry - A textbook*. 2004: Springer.
52. Fridman, A. and L.A. Kennedy, *Plasma Physics and Engineering*. 2nd ed. 2011: CRC Press.
53. Lieberman, M.A. and A.J. Lichtenberg, *Principles of Plasma Discharges and Materials Processing*. 2nd ed. 2005: Wiley.
54. Skoro, N., et al., *Electrical breakdown in water vapor.* Phys Rev E Stat Nonlin Soft Matter Phys, 2011. 84(5 Pt 2): p. 055401.
55. *CRC Handbook of Chemistry and Physics, 96th Edition*. 96th ed. Handbook of Chemistry and Physics, ed. W.M.Haynes. 2015.
56. Rajopadhye, N.R., et al., *Ion Secondary Electron Emission from Al2O3 and MgO films.* Solid State Communications, 1985. 60(8): p. 675-679.
57. Hunter, E.P.L. and S.G. Lias, *Evaluated gas phase basicities and proton affinities of molecules: An update.* 1998.
58. Goebbert, D.J. and P.G. Wentold, *Water dimer proton affinity from the kinetic method: dissociation energy of the water dimer.* Eur J Mass Spectrom (Chichester), 2004. 10(6): p. 837-46.
59. Lindinger, W., A. Hansel, and A. Jordan, *On-line monitoring of volatile organic compounds at pptv levels by means of Proton-Transfer-Reaction Mass Spectrometry (PTR-MS) Medical application, food control and environmental research.* International Journal of Mass Spectrometry and Ion Processes, 1998. 173: p. 191-241.

60. Blake, R.S., et al., *Chemical ionization reaction time-of-flight mass spectrometry: Multi-reagent analysis for determination of trace gas composition.* International Journal of Mass Spectrometry, 2006. **254**(1-2): p. 85-93.
61. Norman, M., A. Hansel, and A. Wisthaler, *O2+ as reagent ion in the PTR-MS instrument: Detection of gas-phase ammonia.* International Journal of Mass Spectrometry, 2007. **265**(2-3): p. 382-387.
62. Sulzer, P., et al., *From conventional proton-transfer-reaction mass spectrometry (PTR-MS) to universal trace gas analysis.* International Journal of Mass Spectrometry, 2012. **321-322**: p. 66-70.
63. Steinbacher, M., et al., *Performance characteristics of a proton-transfer-reaction mass spectrometer (PTR-MS) derived from laboratory and field measurements.* International Journal of Mass Spectrometry, 2004. **239**(2-3): p. 117-128.
64. de Gouw, J.A., *Validation of proton transfer reaction-mass spectrometry (PTR-MS) measurements of gas-phase organic compounds in the atmosphere during the New England Air Quality Study (NEAQS) in 2002.* Journal of Geophysical Research, 2003. **108**(D21).
65. La Lau, C., *Mass Discrimination caused by Electron-Multiplier Detectors.* Adv. Anal. Chem. Instrum, 1970. **8**.
66. Mitchell, G.D., *A Review of Permeation Tubes and Permeators.* Separation and Purification Methods, 2011. **29**(1): p. 119-128.
67. BSi, *Gas analysis — Preparation of calibration gas mixtures using dynamic volumetric methods — Part 10: Permeation method*, in *6145-10:2008*, BSi, Editor. 2008, BSi.
68. Metronics, V., *Generating Calibration Gas Standards.*
69. Kintek. *Permeation tube compund list*. 2018 [cited 2018 25/04/2018]; Available from: http://kin-tek.com/chemical-compound-list/.
70. Galloway, M.M., et al., *Yields of oxidized volatile organic compounds during the OH radical initiated oxidation of*

isoprene, methyl vinyl ketone, and methacrolein under high-NOx conditions. Atmospheric Chemistry and Physics, 2011. **11**(21): p. 10779-10790.
71. Pang, X., et al., *A smog chamber comparison of a microfluidic derivatisation measurement of gas-phase glyoxal and methylglyoxal with other analytical techniques.* Atmospheric Measurement Techniques, 2014. **7**(2): p. 373-389.
72. Fu, T.-M., et al., *Global budgets of atmospheric glyoxal and methylglyoxal, and implications for formation of secondary organic aerosols.* Journal of Geophysical Research, 2008. **113**(D15).
73. Daubert, T.E. and R.P. Danner, *Physical and Thermodynaic Properties of Pure Chemicals Data Compilation*. 1989, Taylor and Francis: Washington, D.C.
74. Pubchem. *Methyl Vinyl Ketone*. 2018 [cited 2018 08/04/2018]; Methyl Vinyl Ketone Chemical and Physical properties]. Available from: https://pubchem.ncbi.nlm.nih.gov/compound/6570.
75. Pubchem. *Pyruvaldehyde*. 2018 [cited 2018 08/04/2018]; Pyruvaldehyde Chemical and Physical properties]. Available from: https://pubchem.ncbi.nlm.nih.gov/compound/880#section=Top.
76. Petitjean, M., et al., *Vapor Pressure Measurements of Hydroxyacetaldehyde and Hydroxyacetone in the Temperature Range (273 to 356) K.* J. Chem. Eng. Data, 2010. **55**: p. 852-855.
77. Newman, P.A., et al., *A new formulation of equivalent effective stratospheric chlorine (EESC).* Atmos Chem Phys, 2007. **7**: p. 4537-4552.
78. Ullmans, *Ullman's Encyclopedia of Industrial Compounds - Chlorinated Hydrocarbons*, in *Ullman's Encyclopedia of Industrial Compounds*. 2006, Wiley.

79. Forster, P.M.D.F. and M. Joshi, *The Role Of Halocarbons In The Climate Change Of The Troposphere And Stratosphere.* Climatic Change, 2005. **71**(1-2): p. 249-266.
80. Khalil, M.A.K. and R.A. Rasmussen, *Atmospheric Methyl Chloride.* Atmospheric Environment, 1999. **33**: p. 1305-1321.
81. NOAA, *NOAA 20 questions - Q16 CFCs.* 2010.
82. UNEP, *The Montreal Protocol on Substances that Deplete the Ozone Layer.* 2000.
83. Laube, J.C., et al., *Tropospheric observations of CFC-114 and CFC-114a with a focus on long-term trends and emissions.* Atmospheric Chemistry and Physics, 2016. **16**(23): p. 15347-15358.
84. WHO, *The use of DDT in malaria vector control.* 2011.
85. *Reactive halogen compounds in the atmosphere*. The handbook of environmental chemistry 4E, ed. P. Fabien and O.N. Singh. 1999: Springer.
86. Khalil, M.A.K., et al., *Natural emissions of chlorine-containing gases: Reactive Chlorine Emissions Inventory.* Journal of Geophysical Research: Atmospheres, 1999. **104**(D7): p. 8333-8346.
87. Brilli, F., et al., *Proton Transfer Reaction Time-of-Flight Mass Spectrometric (PTR-TOF-MS) determination of volatile organic compounds (VOCs) emitted from a biomass fire developed under stable nocturnal conditions.* Atmospheric Environment, 2014. **97**: p. 54-67.
88. Sarkar, C., et al., *Overview of VOC emissions and chemistry from PTR-TOF-MS measurements during the SusKat-ABC campaign: high acetaldehyde, isoprene and isocyanic acid in wintertime air of the Kathmandu Valley.* Atmospheric Chemistry and Physics, 2016. **16**(6): p. 3979-4003.
89. Ionicon. *H3O+, NO+ and O2+ as precursor ions in PTR-MS: isomeric VOC compounds and reactions with different chemical groups*. Feb 2017 [cited 2017 02/02/2017]; Available from:

http://www.ionicon.com/sites/default/files/uploads/doc/poster_ionicon_dgms_sri.pdf.
90. Spanel, P. and D. Smith, *Selected ion flow tube studies of the reactions of H3O , NO , and O2 with several aromatic and aliphatic monosubstituted halocarbons.* International Journal of Mass Spectrometry, 1999. **189**: p. 213-223.
91. *Ion/Molecule Attachment Reactions: Mass Spectrometry*, ed. T. Fujii. Springer.
92. Budzikiewicz, H., C. Djerassi, and D.H. Williams, *Mass spectrometry of organic compounds*. 1967: Holden-Day.
93. Mikhailov, V.A., et al., *Isomeric Effects in the Gas-Phase Reactions of Dichloroethene, C2H2Cl2, with a Series of Cations.* J. Phys. Chem. A, 2006. **110**: p. 5760-5771.
94. Frash, M.V., A.C. Hopkinson, and D.K. Bohme, *A Quantum-Chemical Study of the C2H3F2+ and C2H3Cl2+ Isomers and Their Interconversion. CBS-QB3 Proton Affinities of Difluoroethenes and Dichloroethenes.* J Phys Chem A, 1999. **103**: p. 7872-7882.
95. Xu, S., J. Pavlov, and A.B. Attygalle, *Collision-induced dissociation processes of protonated benzoic acid and related compounds: competitive generation of protonated carbon dioxide or protonated benzene.* J Mass Spectrom, 2017. **52**(4): p. 230-238.
96. Smith, D., A. Pysanenko, and P. Spanel, *The quantification of carbon dioxide in humid air and exhaled breath by selected ion flow tube mass spectrometry.* Rapid Commun Mass Spectrom, 2009. **23**(10): p. 1419-25.
97. Brown, P., et al., *Proton transfer reaction mass spectrometry investigations on the effects of reduced electric field and reagent ion internal energy on product ion branching ratios for a series of saturated alcohols.* International Journal of Mass Spectrometry, 2010. **294**(2-3): p. 103-111.
98. Yu-Ran, L., *Handbook of Bond Dissociation Energies in Organic Compounds*. 2003, USA: CRC Press.

99. Riahi, K. and N. Sellier, *Separation of Isomeric Polycyclic Aromatic Hydrocarbons by GC-MS: Differentiation Between Isomers by Positive Chemical Ionization with Ammonia and Dimethyl Ether as Reagent Gases.* Chromatographia, 1998. **47**: p. 309-312.
100. Romano, A., et al., *Wine analysis by FastGC proton-transfer reaction-time-of-flight-mass spectrometry.* International Journal of Mass Spectrometry, 2014. **369**: p. 81-86.
101. Misztal, P.K., et al., *Development of PTR-MS selectivity for structural isomers: Monoterpenes as a case study.* International Journal of Mass Spectrometry, 2012. **310**: p. 10-19.
102. McLafferty, F.W. and F. Turecek, *Interpretation of Mass Spectra*. 1993: University Science Books.
103. Guenther, A., et al., *Estimates of global terrestrial isoprene emissions using MEGAN (Model of Emissions of Gases and Aerosols from Nature).* Atmos Chem Phys, 2006. **6**: p. 3181-3210.
104. Karl, T., L. Kaser, and A. Turnipseed, *Eddy covariance measurements of isoprene and 232-MBO based on NO+ time-of-flight mass spectrometry.* International Journal of Mass Spectrometry, 2014. **365-366**: p. 15-19.
105. Goldan, P., W. Kuster, and F.C. Fehsenfeld, *The observation of a C5 alcohol emission in a north american pine forest.* Geophysical Research Letters, 1993. **20**: p. 1039-1042.
106. Aschmann, S.M. and R. Atkinson, *Formation Yields of Methyl Vinyl Ketone and Methacrolein from the Gas-Phase Reaction of O3 with Isoprene.* Environ Sci Technol, 1994. **28**: p. 1539-1542.
107. Karl, T., et al., *Emissions of volatile organic compounds inferred from airborne flux measurements over a megacity.* Atmos Chem Phys, 2009. **9**: p. 271-285.
108. Jobson, B.T., et al., *On-line analysis of organic compounds in diesel exhaust using a proton transfer reaction mass*

spectrometer (PTR-MS). International Journal of Mass Spectrometry, 2005. **245**(1-3): p. 78-89.
109. Ammann, C., et al., *Application of PTR-MS for measurements of biogenic VOC in a deciduous forest.* International Journal of Mass Spectrometry, 2004. **239**(2-3): p. 87-101.
110. Ammann, C., et al., *Technical note: Water vapour concentration and flux measurements with PTR-MS.* Atmos Chem Phys, 2006. **6**: p. 4643-4651.
111. Mari, M., et al., *Inferences over the sources and processes affecting polycyclic aromatic hydrocarbons in the atmosphere derived from measured data.* Sci Total Environ, 2010. **408**(11): p. 2387-93.
112. Alam, M.S., et al., *Using atmospheric measurements of PAH and quinone compounds at roadside and urban background sites to assess sources and reactivity.* Atmospheric Environment, 2013. **77**: p. 24-35.
113. Ma, Y. and S. Harrad, *Spatiotemporal analysis and human exposure assessment on polycyclic aromatic hydrocarbons in indoor air, settled house dust, and diet: A review.* Environ Int, 2015. **84**: p. 7-16.
114. Garrido, A., P. Jiménez-Guerrero, and N. Ratola, *Levels, trends and health concerns of atmospheric PAHs in Europe.* Atmospheric Environment, 2014. **99**: p. 474-484.
115. Zhang, Y. and S. Tao, *Global atmospheric emission inventory of polycyclic aromatic hydrocarbons (PAHs) for 2004.* Atmospheric Environment, 2009. **43**(4): p. 812-819.
116. Lung, S.C. and C.H. Liu, *Fast analysis of 29 polycyclic aromatic hydrocarbons (PAHs) and nitro-PAHs with ultra-high performance liquid chromatography-atmospheric pressure photoionization-tandem mass spectrometry.* Sci Rep, 2015. **5**: p. 12992.
117. DEFRA. *Polycyclic Aromatic Hydrocarbons (PAH)* 2018 05.02.2018]; Available from: https://uk-air.defra.gov.uk/networks/network-info?view=pah.

118. Agarwal, B., et al., *Use of proton transfer reaction time-of-flight mass spectrometry for the analytical detection of illicit and controlled prescription drugs at room temperature via direct headspace sampling.* Anal Bioanal Chem, 2011. **400**(8): p. 2631-9.
119. Riva, M., et al., *Kinetics of the gas-phase reactions of chlorine atoms with naphthalene, acenaphthene, and acenaphthylene.* J Phys Chem A, 2014. **118**(20): p. 3535-40.
120. Bruns, E.A., et al., *Characterization of gas-phase organics using proton transfer reaction time-of-flight mass spectrometry: fresh and aged residential wood combustion emissions.* Atmospheric Chemistry and Physics, 2017. **17**(1): p. 705-720.
121. Goldfarb, J.L. and E.M. Suuberg, *Vapor Pressures and Enthalpies of Sublimation of Ten Polycyclic Aromatic Hydrocarbons Determined via the Knudsen Effusion Method.* J. Chem. Eng. Data, 2008. **53**: p. 670-676.
122. NIST. *Benzo[a]pyrene NIST chemistry webbook*. 2018 [cited 2018 24/02/2018]; Available from: http://webbook.nist.gov/cgi/cbook.cgi?ID=C50328&Mask=200#Mass-Spec.
123. Yaffe, D., et al., *Multimedia Analysis of PAHs and Nitro-PAH Daughter Products in the Los Angeles Basin.* Risk Analysis, 2001. **21**.
124. PubChem. *6-Nitrochrysene*. [cited 2018 26.02.2018]; Available from: https://pubchem.ncbi.nlm.nih.gov/compound/6-nitrochrysene#section=Solubility.
125. Zhai, Y., et al., *Polycyclic aromatic hydrocarbons (PAHs) in the environment of Beijing, China: Levels, distribution, trends and sources.* Human and Ecological Risk Assessment: An International Journal, 2017. **24**(1): p. 137-157.

126. Xu, S., W. Liu, and S. Tao, *Emission of Polycyclic Aromatic Hydrocarbons in China.* Environ Sci Technol, 2006. **40**: p. 702-708.
127. Liquide, A. *TO-15 Method gas standard compound list*. 2018 [cited 2018 21/04/2018]; Available from: https://industry.airliquide.us/sites/activity_us/files/2015/10/21/method_to_standards_1516.2.pdf.

Appendix A

Compound list of TO-15 standard (all 1ppm in balance nitrogen). Gas supplied by Air Liquide for Scott gas method TO-15 [127].

Compound	CAS number	Compound	CAS Number
Acetone	67-64-1	Ethylbenzene	100-41-4
Acrolein	107-028	4-Ethyltoluene	622-96-8
Benzene	71-43-2	Halocarbon 11 (Trichlorofluoromethane)	75-69-4
Benzyl Chloride	100-44-7	Halocarbon 12 (Dichlorodifluoromethane)	75-71-8
Bromoform	75-25-2	Halocarbon 113 (1,1,2-Trichlorotrifluoroethane)	76-13-1
Bromomethane	74-83-9	Halocarbon 114 (1,2-Dichlorotetrafluoroethane)	76-14-2
Bromodichloromethane	75-27-4	Heptane	142-82-5
1,3-Butadiene	106-99-0	Hexachloro-1,3-butadiene	87-68-3
2-Butanone (MEK)	78-93-3	Hexane	110-54-3
Carbon Disulphide	75-15-0	2-Hexanone (MBK)	591-78-6
Carbon Tetrachloride	56-23-5	4-Methyl-2-Pentanone (MIBK)	108-10-1
Chlorobenzene	108-90-7	Methylene Chloride	75-09-2
Chloroethane	75-00-3	Methyl Methacrylate	80-62-6
Chloroform	67-66-3	Methyl-tert-butyl ether (MTBE)	1634-04-4
Chloromethane	74-87-3	2-Propanol	67-63-0
Cyclohexane	110-82-7	Propylene	115-07-1
Dibromochloromethane	124-48-1	Styrene	100-42-5
1,2-Dibromoethane	106-93-4	1,1,2,2-Tetrachloroethane	79-34-5
1,2-Dichlorobenzene	95-50-1	1,1,1-Trichloroethane	71-55-6
1,3-Dichlorobenzene	541-73-1	1,1,2-Trichloroethane	79-00-5
1,4-Dichlorobenzene	106-46-7	1,2,4-Trichlorobenzene	120-82-1
1,1-Dichloroethane	75-35-3	1,2,4-Trimethylbenzene	95-63-6
1,2-Dichloroethane	107-06-2	1,3,5-Trimethylbeznene	108-67-8
1,1-Dichloroethene	75-35-4	Tetrachloroethene	127-18-4
cis-1,2-Dichloroethene	156-59-2	Tetrahydrofuran	109-99-9
trans-1,2-Dichloroethene	156-60-5	Toluene	108-88-3
1,2-Dichloropropane	78-87-5	Trichloroethylene	79-01-6
cis-1,3-Dichloropropene	10061-01-5	Vinyl Acetate	108-05-4
trans-1,3-Dichloropropene	10061-02-6	Vinyl Chloride	75-01-4
1,4-Dioxane	123-91-1	m-Xylene	108-38-3
Ethanol	64-17-5	o-Xylene	95-47-6
Ethyl Acetate	141-78-6	p-Xylene	106-42-3

Appendix B

The following graphs show the product ions of the ion-molecule reactions of the chloroalkenes and chloroalkanes investigated in chapter 4 with the hydronium ion as a function of reduced electric field strength.

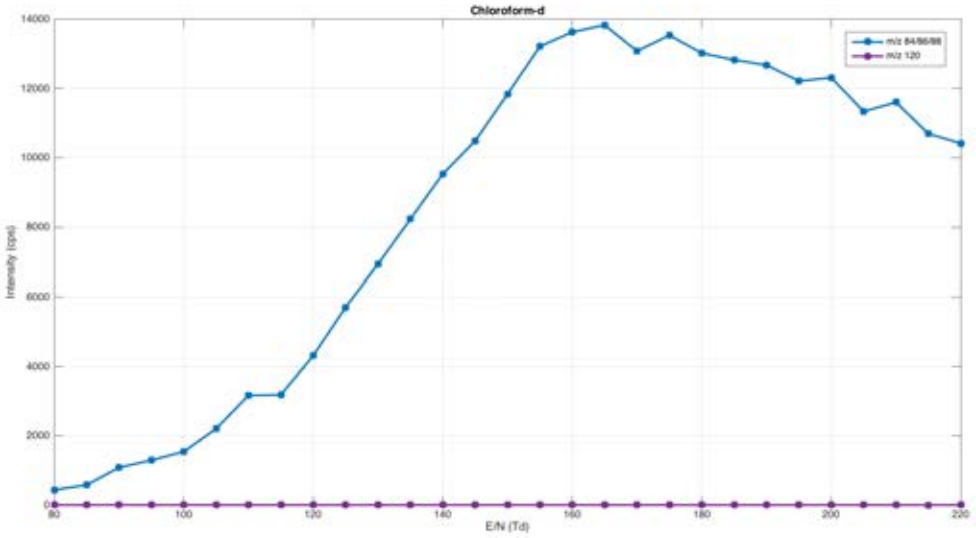

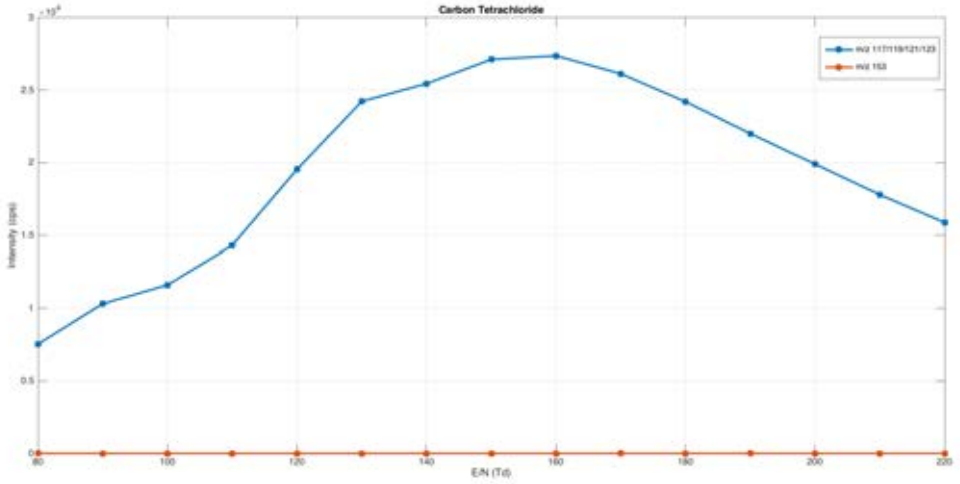

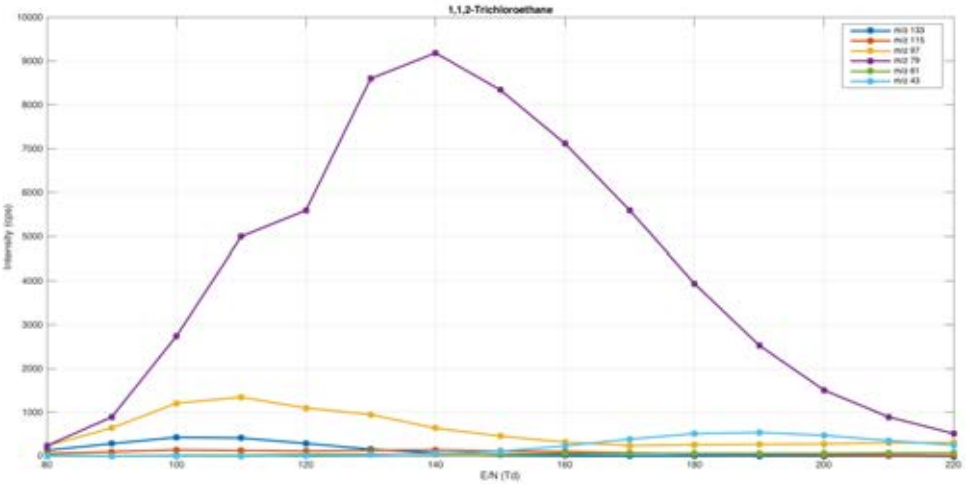
1,1,2-Trichloroethane
Intensity (cps)
E/N (Td)

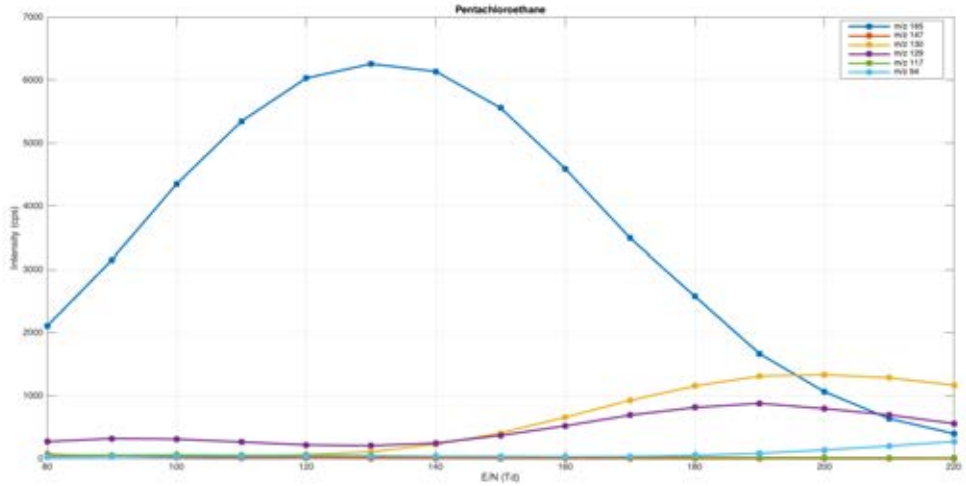
Pentachloroethane
Intensity (cps)
E/N (Td)

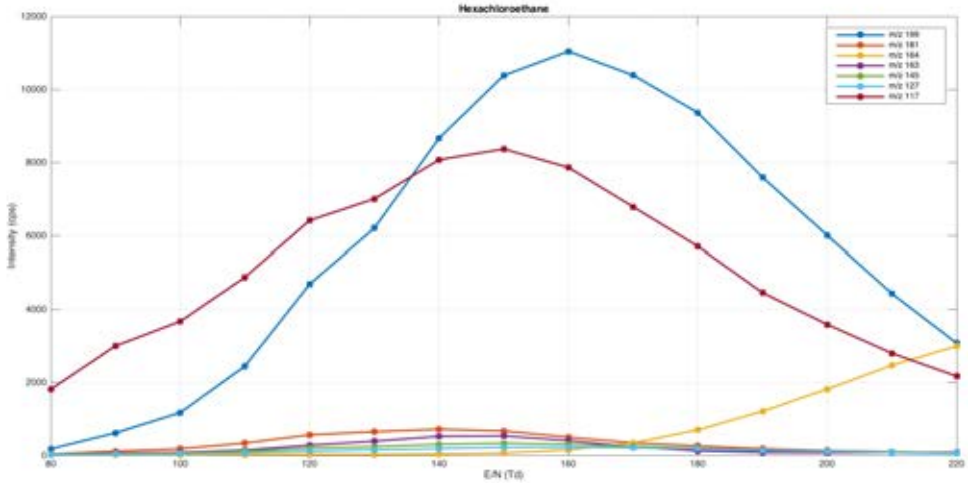
Hexachloroethane
Intensity (cps)
E/N (Td)

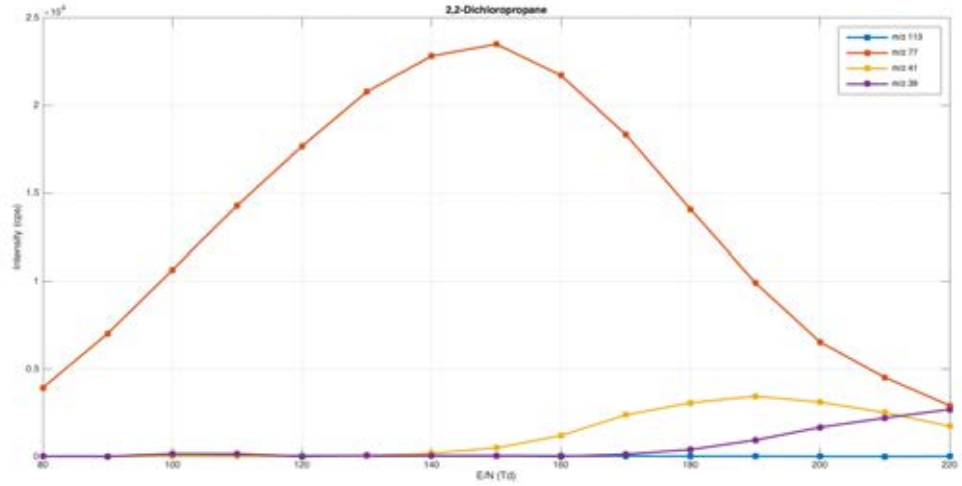
2,2-Dichloropropane
m/z 113
m/z 77
m/z 41
m/z 39
Intensity (cps)
E/N (Td)

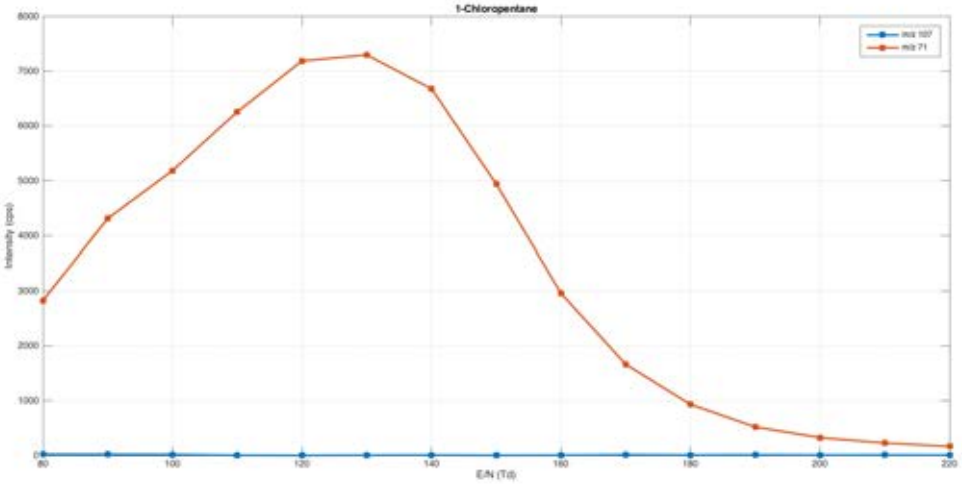
1-Chloropentane
m/z 107
m/z 71
Intensity (cps)
E/N (Td)

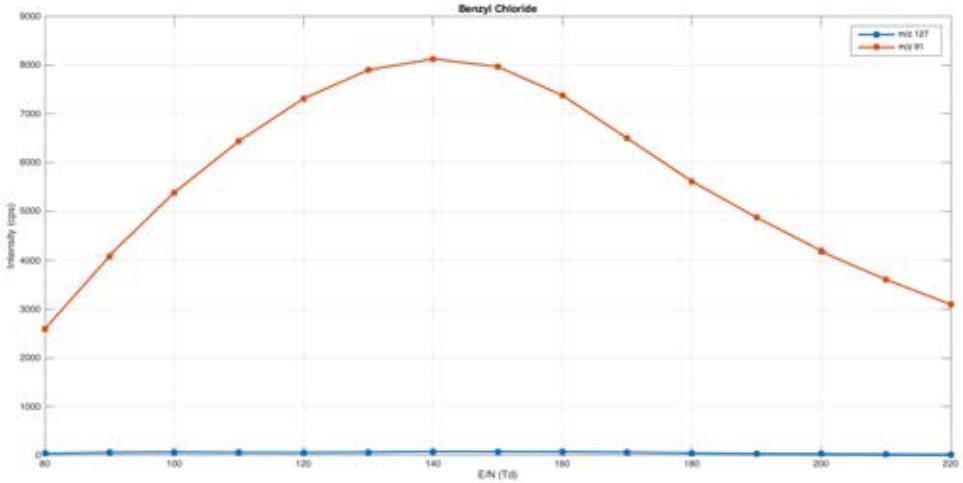
Benzyl Chloride
m/z 127
m/z 91
Intensity (cps)
E/N (Td)

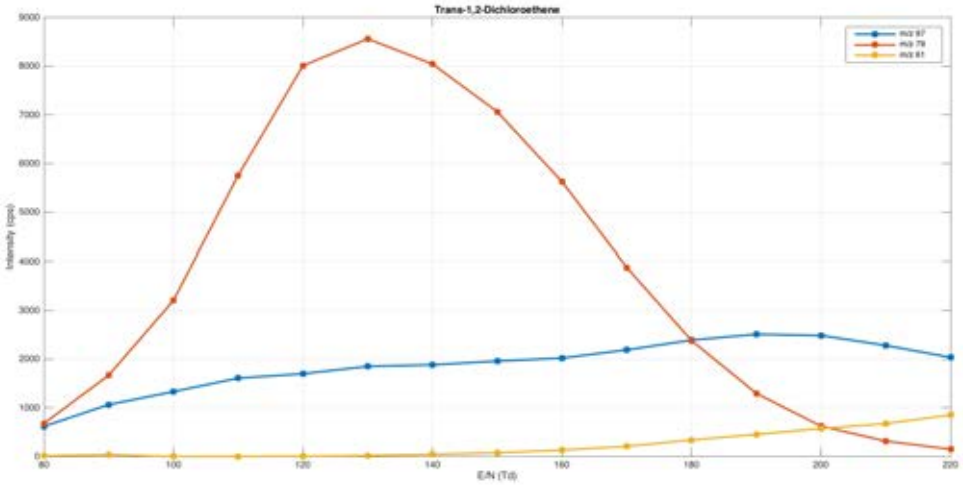
Trans-1,2-Dichloroethene
m/z 97
m/z 79
m/z 61
Intensity (cps)
E/N (Td)

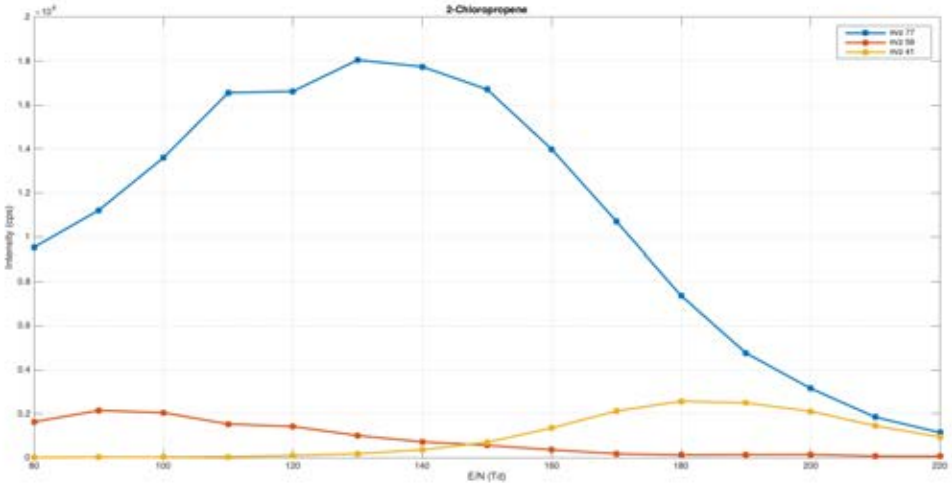
2-Chloropropene
m/z 77
m/z 59
m/z 41
Intensity (cps)
E/N (Td)

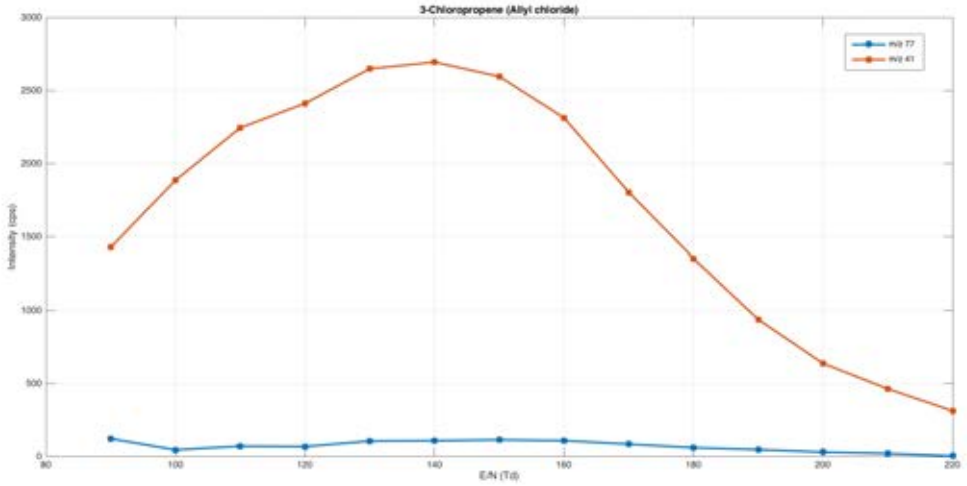
3-Chloropropene (Allyl chloride)
m/z 77
m/z 41
Intensity (cps)
E/N (Td)

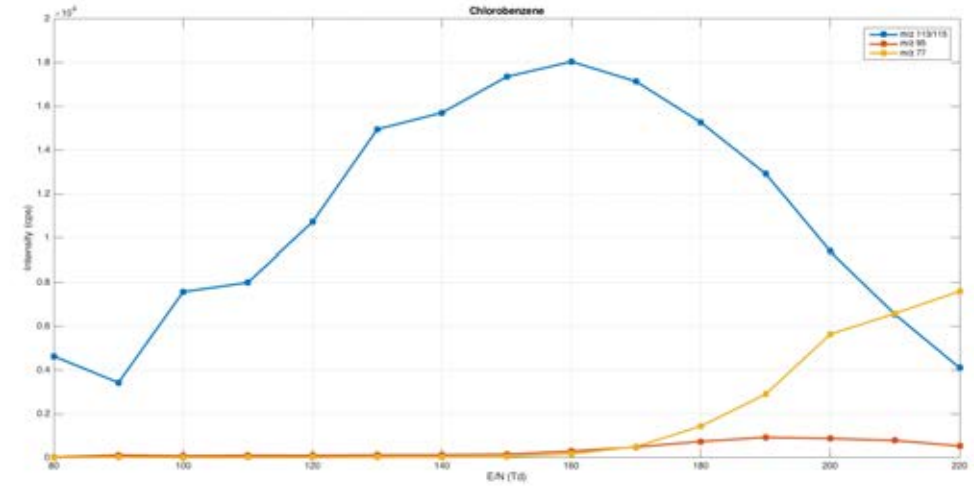
Chlorobenzene
m/z 113/115
m/z 95
m/z 77
Intensity (cps)
E/N (Td)

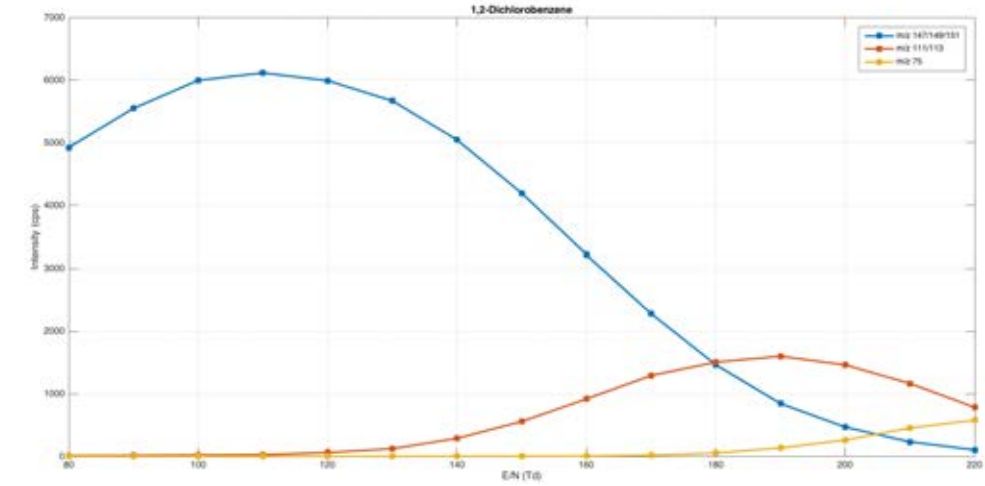
1,2-Dichlorobenzene
m/z 147/149/151
m/z 111/113
m/z 75
Intensity (cps)
E/N (Td)

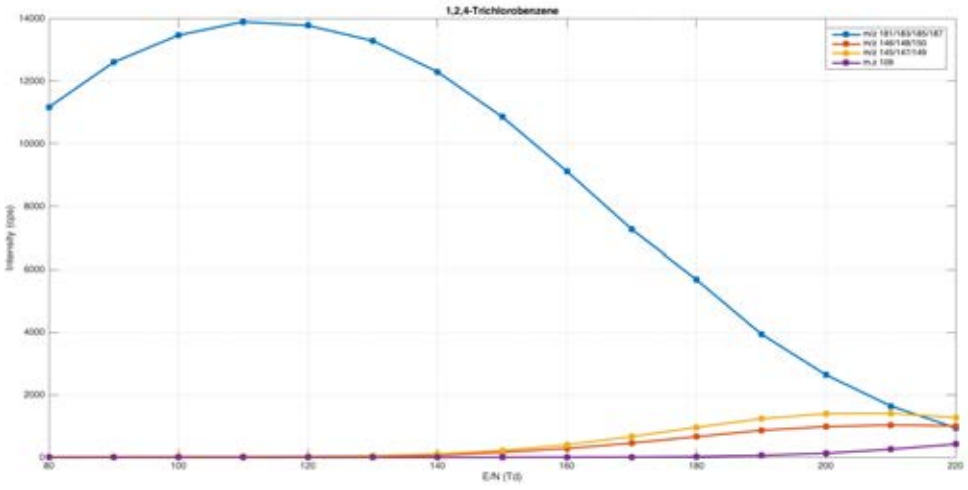
1,2,4-Trichlorobenzene
m/z 181/183/185/187
m/z 146/148/150
m/z 145/147/149
m/z 109
Intensity (cps)
E/N (Td)